Modeling and design of a photovoltaic infrastructure based on a microgrid and dedicated to electromobility

Saleh Cheikh Mohamad

Par **Saleh CHEIKH MOHAMAD**

Modeling and design of a photovoltaic infrastructure based on a microgrid and dedicated to electromobility

Thèse présentée
pour l'obtention du grade
de Docteur de l'UTC

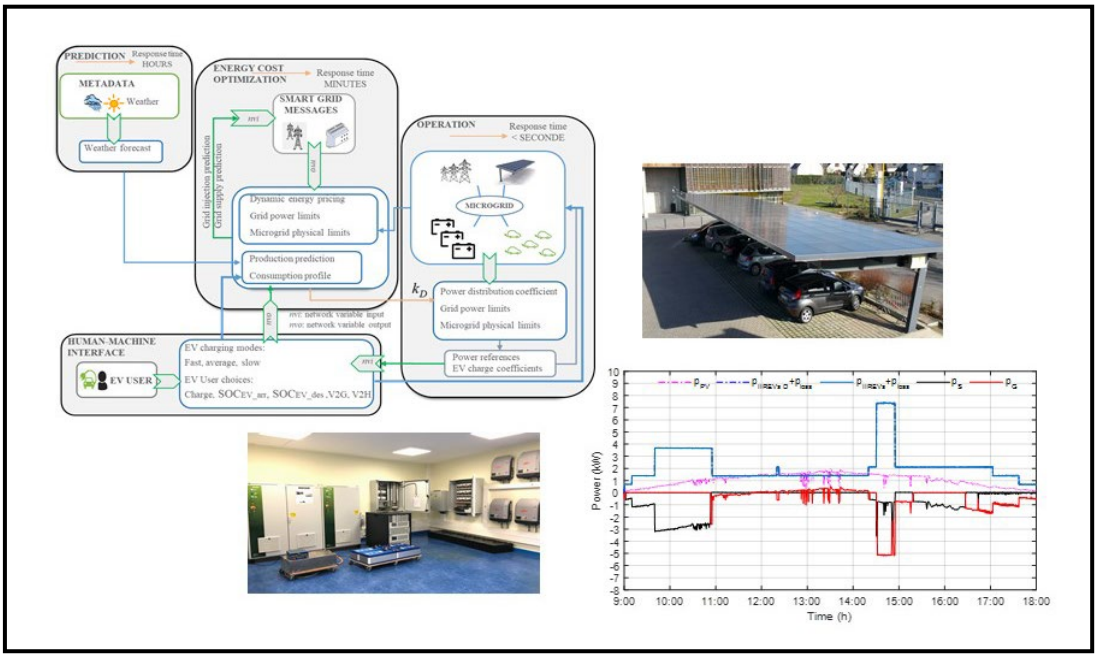

Soutenue le 4 octobre 2022
Spécialité : Génie Électrique : Laboratoire Avenues – (EA-7284)

D2700

UNIVERSITÉ DE TECHNOLOGIE DE COMPIÈGNE

THESE

Pour obtenir le grade de

DOCTEUR

Spécialité : Génie Électrique

Saleh CHEIKH MOHAMAD

Modeling and design of a photovoltaic infrastructure based on a microgrid and dedicated to electromobility

Laboratoire AVENUES, EA 7284

Soutenue le 04 Octobre 2022 devant le jury composé de :

Rapporteurs :	Prof. Seddik BACHA	G2Elab, Université Grenoble Alpes
	Prof. Jean-Paul GAUBERT	LIAS, Université de Poitiers
Examinateurs :	Prof. Bruno FRANCOIS	L2EP, Ecole Centrale de Lille
	Prof. Vincent LANFRANCHI	Roberval, UTC Compiègne
Directeur de these :	Prof. Manuela SECHILARIU	Avenues, UTC Compiègne
Co-Directeur de these :	Prof. Fabrice LOCMENT	Avenues, UTC Compiègne

Université de Technologie de Compiègne – Avenues
Rue du docteur Schweitzer, 60203 Compiègne

Abstract

Environmental benefits lie in reducing direct air pollution and greenhouse gas emissions. In contrast to thermal vehicles, electric vehicles (EVs) have zero tailpipe emissions, but their contribution in reducing global air pollution is highly dependent on the energy source they have been charged with. Thus, the energy system depicted in this manuscript is a photovoltaic (PV)-powered charging station (PVCS) based on a DC microgrid and includes stationary storage and public grid connection as power source backups. The goal is to identify the preliminary requirements and feasibility conditions for PV-powered EV charging stations leading to PV benefits growth. Simulation results of different scenarios prove that slow charging with long park time could increase PV benefits for EVs and may reduce the charging price, therefore, EV users should be more willing to stay at charging stations. Whereas, for fast charging, EV users should accept the high charging price since it depends on the public energy grid. For all these scenarios, the energy system distribution and EV's energy distribution regarding its charge are well presented.

On the other hand, the PVCS has to control the whole system considering the energy cost optimization; so, that it becomes an intelligent infrastructure for recharging EVs. The energy cost optimization problem is studied taking into account the intermittent arrival and departure of each EV, meaning that the energy optimization is operated in real-time power management. For this, a mixed-integer linear programming is formulated as an optimization problem to minimize the total energy cost, taking into consideration the physical limitations of the system. The interaction with the human-machine interface provides EV data in real-time operation, Regarding the prediction data, only PV power profile is required; the interface communicates the PV power prediction based on the solar irradiation prediction provided by the national meteorological institute in France. The optimization is executed at each EV arrival, with the actualized data in the DC microgrid. Simulation and real-time experimental results of different meteorological conditions show that the EV user demands are satisfied while the PV benefits grow and the energy cost is minimized, proving the feasibility of the proposed optimization problem for real-time power management.

Furthermore, the deployment of EVs in a large scale will increase load demand and the burden on the public grid. However, vehicle-to-grid (V2G) service is promising and can bring benefits to the public grid operators and to the EV users, who will be rewarded. The goal is to study the energy management and to analyze the energy cost of the PVCS with the implementation of V2G service, taking into account the interaction of EV users with the human-machine interface. Simulation results show that the proposed energy management satisfies the EV user demands under V2G service, proving its feasibility. The energy cost analysis highlights the benefits of the V2G service, where the variable power scenario can make profits and the energy discharged of EVs into the grid is 75% of the total energy injected into the grid in peak hours.

Lastly, based on a life cycle assessment mixed with carbon impact methodology, the carbon impact of the PVCS is studied and then compared with a grid-powered charging station. The obtained results show that

the carbon impact of the PVCS is highly dependent on the PV system, thus levers action are proposed with recent data and recycled materials. The proposed scenarios show a reduction in the carbon impact of a PVCS, as for the grid-connected charging station, the carbon impact is highly dependent on the electricity mix of energy.

Keywords: carbon impact; charging station; electric vehicle; energy distribution; energy management; feasibility conditions; human-machine interface; microgrid; energy cost optimization; photovoltaic energy; power flow management; real-time experiment; vehicle-to-grid.

Résumé

Les bénéfices environnementaux résident dans la diminution de la pollution atmosphérique directe et la réduction des émissions de gaz à effet de serre. Contrairement aux véhicules thermiques, les véhicules électriques (VEs) n'ont aucune émission d'échappement, mais leur contribution à la réduction de la pollution atmosphérique mondiale dépend fortement de la source d'énergie avec laquelle ils ont été chargés. Ainsi, le système énergétique décrit dans ce manuscrit est une station de recharge photovoltaïque (PV) (PVCS en anglais) basée sur un micro-réseau DC et comprend un stockage stationnaire et une connexion au réseau public comme sources d'alimentation de secours. L'objectif est d'identifier les exigences préliminaires et les conditions de faisabilité pour les stations de recharge de VE alimentées par PV menant à la croissance des avantages PV. Les résultats de simulation de différents scénarios prouvent qu'une charge lente avec une longue durée de stationnement pourrait augmenter les avantages du PV pour les VEs et réduire le prix de la charge. Par conséquent, les utilisateurs de VE devraient être plus disposés à rester à la station de recharge, alors que pour une recharge rapide, les utilisateurs de VE doivent accepter le prix de recharge élevé puisqu'il dépend du réseau électrique public. Pour tous ces scénarios, la distribution des énergies du système et la distribution des énergies dans la recharge des véhicules électriques sont bien présentées.

De l'autre part, la PVCS doit contrôler l'ensemble du système en tenant compte de l'optimisation des coûts énergétiques afin qu'il devienne une infrastructure intelligente pour recharger les VEs. Le problème d'optimisation des coûts énergétiques est étudié en tenant compte de l'arrivée et du départ intermittents de chaque VE, ce qui signifie que l'optimisation énergétique est opérée en gestion de la puissance en temps réel. Pour cela, une programmation linéaire en nombres entiers mixtes est formulée comme un problème d'optimisation pour minimiser le coût énergétique total, en tenant compte des limitations physiques du système. L'interaction avec l'interface homme-machine fournit des données des VEs en temps réel. En ce qui concerne les données de prédiction, seul le profil de puissance PV est requis ; l'interface communique la prévision de puissance PV basée sur la prévision d'irradiation solaire fournie par l'institut national de météorologie en France. L'optimisation est exécutée à chaque arrivée d'un VE, avec les données actualisées dans le micro-réseau DC. La simulation et les résultats expérimentaux en temps réel de différentes conditions météorologiques montrent que les demandes des utilisateurs de VE sont satisfaites, tandis que les avantages du PV augmentent et que le coût de l'énergie est minimisé, prouvant la faisabilité du problème d'optimisation proposé pour la gestion de l'énergie en temps réel.

De plus, le déploiement des VEs à grande échelle augmentera la demande de la recharge et l'impact sur le réseau public. Cependant, le service véhicule-vers-réseau (V2G) est prometteur et peut apporter des avantages aux opérateurs de réseaux publics et aux utilisateurs de VE, qui seront récompensés. L'objectif est d'étudier la gestion de l'énergie et d'analyser le coût énergétique du PVCS avec la mise en œuvre du service V2G, en tenant compte de l'interaction des utilisateurs de VE avec l'interface homme-machine. Les résultats de la simulation montrent que la gestion de l'énergie proposée répond aux demandes des

utilisateurs de VE sous le service V2G, prouvant sa faisabilité. L'analyse des coûts énergétiques met en évidence les avantages du service V2G, où le scénario de puissance variable peut générer des bénéfices et où l'énergie rejetée par les VE dans le réseau représente 75% de l'énergie totale injectée dans le réseau aux heures de pointe.

Enfin, sur la base d'une analyse de cycle de vie couplée à une méthodologie d'impact carbone, l'impact carbone du PVCS est étudié puis comparé à une borne de recharge alimentée uniquement par le réseau. Les résultats obtenus montrent que l'impact carbone du PVCS est fortement dépendant de l'impact carbone du système PV, ainsi des leviers d'action sont proposés avec des données récentes et des matériaux recyclés. Les scénarios proposés montrent une réduction de l'impact carbone d'un PVCS. Toutefois, l'étude met en exergue que l'impact carbone des stations de recharge, alimentées par le réseau et/ou un micro-réseau basé sur de l'énergie PV, est fortement dépendant du mix énergétique électrique du pays où la station est implantée et où les composants du système ont été fabriqués.

Mot-clés : conditions de faisabilité ; distribution d'énergie ; énergie photovoltaïque ; essais expérimentaux en temps réel ; gestion d'énergie ; gestion des flux de puissance ; interface homme-machine ; impact carbone ; micro-réseau ; optimisation des coûts énergétiques ; station de charge ; véhicule électrique ; V2G (véhicule-vers-réseau).

Acknowledgement

My first appreciations goes to my thesis directors, Manuela Sechilariu, and Fabrice Locment. Thank you Manuela for your dedicated time, encouragement, inspiration, and critics that helped me completing this thesis. Thank you Fabrice for always being there when needed, for your dedicated time, continuous support, assistance that have been of a great interest. Thank you both for your valuable trust, precious critics, wise advices and for our fruitful discussions in which I was able to progress and move forward. I would like also to express how much I appreciated your considerable time, presence, for your commitment and respect for deadlines in reviewing the documents and articles sent. Lastly, I was touched by your morality, personality, leadership, and for your listening and understanding throughout my thesis.

I would like to thank the reporters, Seddik Bacha and Jean-Paul Gaubert, as well as the examiners, Bruno François and Vincent Lanfranchi, for accepting to take part in my thesis jury.

Thank you again Manuela for giving me the opportunity to teach and explore the role of being *enseignant-chercheur* in the University of Technology of Compiegne. Thanks for the students and their questions in which I was able to develop my skills.

I would like to thank the other members of the Urban Engineering department in the UTC for providing a good ambiance for my years spend among them. So, thank you to Jean-Louis Batoz, Jean-Pascal Foucault, Fabien Lamarque, Nassima Mouhous-Voyneau, Nathalie Molines, Carine Henriot, Eduard Antaluca, Justin Emery, Berk Celik, Gilles Morel, Hipolito Martell-Flores, Josiane Gilles, Nancy Dobaire. I want also to thank my colleagues, Ghada Tay, Dian Wang, Wenshuai Bai, Jamila Aourir-Mezian, Hongwei Wu, Saray Chavez, Soelarso, Jules Boulet for the shared moments and cultures throughout my thesis.

Many thanks for my second family (my friends): Fadi Agha Kassab, Amalie Alchamie, Nathanael Dougier, Ali Hamdan, Inass Soukarieh, Mohamad Albilani, Karl Abdallah, Sarah-Joe Salame, Valentin Kerskens, Khalil Aroua, Mohamad Wahba, Julia Zeaiter, Hussein Issa, Wassim Jouni, Abdallah Said, for the daily life and activities together, and for the Lebanese community in Compiegne, you are so many.

Finally, at the end of this work, I would like to express my deepest gratitude to those who have supported and encouraged me throughout these years. I would like to express my love for my family, especially my mother for her love and support, my brother for his advices, sharing moments together. Thanks for supporting me in my decisions and encourage me to continue my studies in France, their presence and encouragement are the cornerstones of who I am and what I do. Father, your memory is always present.

Table of content

List of figures

Liste of tables

Abbreviations

AC	Alternative Current
BEV	Battery Electric Vehicle
CO_2	Carbon dioxide
CTs	Charging Terminals
DC	Direct Current
DER	Distributed Energy Resources
DP	Dynamic Programming
EU	European Union
EV	Electric Vehicle
GHG	Greenhouse Gases
HEV	Hybrid Electric Vehicle
HMI	Human-Machine Interface
ICE	Internal Combustion Engine
ICEV	Internal Combustion Engine Vehicle
IEA	International Energy Agency
IIREV	Intelligent Infrastructure for recharging electric vehicle
I2H	Infrastructure-to-Home
LCA	Life Cycle Assessment
LP	Linear Programming
MG	Microgrid
MPPT	Maximum Power Point Tracking
MILP	Mixed-Integer Linear Programming
PHEV	Plug-in Hybrid Electric Vehicle
PV	Photovoltaic
PVCS	PV-powered Charging Station
PGCS	Grid-powered Charging Station

LP	Linear Programming
QP	Quadratic Programming
RC	Reinforced Concrete
RES	Renewable Energy Sources
SOC	State of Charge
STC	Standard Test Conditions
UK	United Kingdom
USA	United States of America
V2H	Vehicle-to-Home
V2G	Vehicle-to-Grid

Nomenclature

Δt	Time interval between two samples
ρ_c	Density of concrete
γ	Power temperature coefficient
C_{Li-Ion}	Li-Ion batteries' capacity
$CO_{2,n}$	Carbon emission coefficient of n component
$CO_{2,PV}$	Carbon emission coefficient of PV system
$CO_{2,PV\ panels}$	Carbon emission coefficient of PV panels
$CO_{2,inv,a}$	Carbon emission coefficient of inverter a
$CO_{2,inv,b}$	Carbon emission coefficient of inverter b
$CO_{2,supp}$	Carbon emission coefficient of PV panels support
$CO_{2,wiring}$	Carbon emission coefficient of wiring connections
$CO_{2,instal}$	Carbon emission coefficient of PV system installation
$CO_{2,uninstal}$	Carbon emission coefficient of PV system uninstallation
$CO_{2,clean}$	Carbon emission coefficient of PV system cleaning
$CO_{2,servicing}$	Carbon emission coefficient of transport of agents for PV system maintenance
$CO_{2,Li-Ion}$	Carbon emission coefficient of Li-Ion
$CO_{2,Li-Ion,man}$	Carbon emission coefficient of Li-Ion maintenance
$CO_{2,Li-Ion,recy}$	Carbon emission coefficient of Li-Ion recycling
$CO_{2,CT,sus}$	Carbon emission coefficient of suspended CT
$CO_{2,CT,gnd}$	Carbon emission coefficient of grounded CT
$CO_{2,cc}$	Carbon emission coefficient of the concrete cement
$CO_{2,RC}$	Carbon emission coefficient of the RC

$CO_{2,Steel}$	Carbon emission coefficient of the steel used
$CO_{2,shade}$	Carbon emission coefficient of one parking shade
$CO_{2,PG}$	Carbon emission coefficient of the public grid
c_{EV_p}	EV penalty tariff
c_G	Grid energy tariff
c_{G_NH}	Grid energy tariff in normal hours
c_{G_PH}	Grid energy tariff in peak hours
c_S	Storage energy tariff
c_{PVS}	PV shedding energy tariff
$C_{EV\_penalty}$	EV penalty energy cost
C_G	Grid energy cost
C_S	Storage energy cost
C_{PVS}	PV shedding energy cost
C_P	Controller proportional gain
d	Annual distance travelled by the maintenance agents
E_{Bat}	Energy capacity of the stationary storage (kWh)
E_{G_v}	Public grid energy consumed by *v* vehicle
E_{PV_v}	PV energy consumed by *v* vehicle
E_{S_v}	Stationary storage energy consumed by *v* vehicle
E_v	Energy capacity of the *v* vehicle (kWh)
E_{PV}	Energy produced by PV
E_{PG}	Energy supplied by the public grid
G_{test}	Fixed solar irradiation for testing
g	Solar irradiations (W/m²)

H_{found}	Height of the RC foundation
i	Index of time
Imp_n	Carbon impact of component n
Imp_{PV}	Carbon impact of PV system
$Imp_{Infra,\ PV}$	Carbon impact of PV infrastructure
Imp_{mtn}	Carbon impact of the maintenance
Imp_{site}	Carbon impact of PV construction site
$Imp_{PV\ panels}$	Carbon impact of PV panels
Imp_{inv}	Carbon impact of the inverters
Imp_{supp}	Carbon impact of PV panels support
Imp_{wiring}	Carbon impact of wiring connections
Imp_{instal}	Carbon impact of PV system installation
$Imp_{uninstal}$	Carbon impact of PV system uninstallation
Imp_{clean}	Carbon impact of PV system cleaning
$Imp_{servicing}$	Carbon impact of transport of agents for PV system maintenance
Imp_{Li-Ion}	Carbon impact of Li-Ion batteries
$Imp_{CT,sus}$	Carbon impact of the suspended CT
$Imp_{CT,mtn}$	Carbon impact of the suspended CT maintenance
Imp_{CE}	Carbon impact of the civil engineering for the installation of CTs
Imp_{infra}	Carbon impact of the infrastructure
$Imp_{RC,\ found}$	Carbon impact of the RC foundation
Imp_{Steel}	Carbon impact of the stell
Imp_{m_shades}	Carbon impact of m car parking shades
Imp_{PG}	Carbon impact of the public grid

Imp_{PVCS}	Carbon impact of the PVCS
Imp_{PGCS}	Carbon impact of the PGCS
k_D	Power distribution coefficient
L_{found}	Length of the RC foundation
M_v	Charging mode of vehicle *v*
m	Number of car parking shades
$m_{CT,gnd}$	Weight of the grounded CT
$m_{CT,sus}$	Weight of the suspended CT
m_{Steel}	Weight of the steel used
$NOCT$	Nominal Operating Cell Temperature
N_{PV}	Number of PV panels
N_v	EVs total number
$N_{CT,sus}$	Number of suspended CT
N_{CT}	Number of CT
N_{poles}	Number of poles
N_{places}	Number of parking places
$P_{EV\_max_v}$	Maximum charging power of *v* vehicle
$P_{EV\_aver\_max}$	Maximum average charging power
$P_{EV\_fast\_max}$	Maximum fast charging power
$P_{EV\_slow\_max}$	Maximum slow charging power
p_{EV_v}	EV charging power of *v* vehicle
$p_{EVs\ D}$	EVs total demand power
p_{EVs}	Total EVs power
p_G	Grid power

p_{G_I}	Grid injection power
p_{G_S}	Grid supply power
p_{G_ref}	Grid power reference
$P_{G\_I\_max}$	Maximum grid injection limit
$P_{G\_S\_max}$	Maximum grid supply limit
$p_{IIREVs\ D}$	IIREVs total demand power
p_{IIREVs}	IIREVs total power
$p_{IIREVs\ S}$	IIREVs shed power
$p_{PV\ MPPT}$	PV MPPT power
$p_{PV\ MPPT\ pred}$	PV power prediction in MPPT mode
p_{PV}	PV power
p_{PV_S}	PV shed power
P_{PV_STC}	PV power under STC
P_{S_max}	Stationary storage power limit
p_S	Stationary storage power
p_{S_C}	Stationary storage charging power
p_{S_D}	Stationary storage discharging power
p_{S_ref}	Stationary storage power reference
p_{ref}	Reference power
P_{inv}	Inverter power
P_p	PV pic power
q	Lifetime of PV panels
Q_n	Component n
r_{Li-Ion}	Number of Li-Ion replacement

r_{CT}	Number of CT replacement
S_{PV}	PV surface area
soc_{EV_v}	SOC of vehicle *v*
$SOC_{EV\_arr_v}$	SOC of vehicle *v* at arrival
$SOC_{EV\_dep_v}$	SOC of vehicle *v* at departure
$SOC_{EV\_des_v}$	Desired SOC of vehicle *v* at departure
SOC_{EV_max}	Maximum state of charge of electric vehicle
SOC_{EV_min}	Minimum state of charge of electric vehicle
SOC_{S_max}	Maximum state of charge of stationary storage
SOC_{S_min}	Minimum state of charge of stationary storage
SOC_{S_0}	Initial SOC of stationary storage
soc_S	State of charge of stationary storage
t_0	Initial time instant
$T_{air-test}$	Fixed air temperature
T_{amb}	Ambient temperature
t_{arr_v}	Arrival time of *v* vehicle
t_{dep_v}	Departure time of *v* vehicle
$t_{est\_ch_v}$	Estimated charging time of vehicle *v*
t_F	Time instant at the end of time operation
t_i	Continuous time
T_{PV}	PV cell temperature
v	Index of EV number
$v_{DC\ bus}$	Voltage of the DC bus
V_{ref}	Reference voltage of the DC bus

V_c	Concrete volume
V_{RC}	Reinforced concrete volume
W_{found}	Width of the RC foundation

Publications associated with this PhD thesis

The most of the works presented in this thesis have been published in various international journals and conferences. The details of them are listed as following:

Publications:

Articles in international journals with peer review and indexed in Scopus and / or ISI WoS

- **S. Cheikh-Mohamad**, M. Sechilariu, F. Locment, Y. Krim: "PV-Powered Electric Vehicle Charging Stations: Preliminary Requirements and Feasibility Conditions", Applied Sciences, vol. 11, no.4, pp 1770, MDPI Ed., 2021, Impact Factor 2.679, WoS, Scopus, https://doi.org/10.3390/app11041770
- **S. Cheikh-Mohamad**, M. Sechilariu, F. Locment: "Real-Time Power Management Including an Optimization Problem for PV-Powered Electric Vehicle Charging Stations", Applied Sciences, vol. 12, no.9, pp 4323, MDPI Ed., 2022, Impact Factor 2.679, WoS, Scopus, https://doi.org/10.3390/app12094323

Communications with selection committee and proceedings published in international congresses

1. **S. Cheikh-Mohamad**, M. Sechilariu, F. Locment: "PV-Powered Charging Station: Energy Management and Cost Optimization", IEEE 30th International Symposium on Industrial Electronics (ISIE) ISIE21 (virtual), Kyoto 20-23 June 2021, pp. 1-6, https://doi.org/10.1109/isie45552.2021.9576324
2. **S. Cheikh-Mohamad**, M. Sechilariu, F. Locment: "Carbon Impact Methodology for PV-powered Infrastructure for Recharging Electric Vehicles", 2021 IEEE Vehicle Power and Propulsion Conference (VPPC) (virtual), Gijon 25-28 October 2021, pp. 1-6, https://doi.org/10.1109/VPPC53923.2021.9699192
3. **S. Cheikh-Mohamad**, M. Sechilariu, F. Locment: "PV-Powered Charging Station: Energy Management with V2G Operation and Energy Cost Analysis", 7th International Conference on Smart and Sustainable Technologies 2022 (in person) Bol 05-08 July 2022, DOI coming soon

International project report

"PV-Powered Electric Vehicle Charging Stations: Preliminary Requirements and Feasibility Conditions", IEA PVPS TCP (Ed.), ISBN: 978-0-12-803736-2, 145 pages, Dec. 2021. Author of chapter 2.2 of this scientific work accepted after reviewing. ISBN: 978-3-907281-26-0, https://iea-pvps.org/key-topics/pv-powered-electric-vehicle-charging-stations/

Communications with selection committee and proceedings published in national congresses

1. **S. Cheikh-Mohamad**, M. Sechilariu, F. Locment "Station de Recharge Alimentée par le Photovoltaïque pour les Véhicules Électriques", JCGE 2022 Conférence des Jeunes Chercheurs en Génie Électrique, Le Croisic, 14-17 juin 2022.

Oral communications without acts in a (inter) national congress, GDR,…

1. M. Sechilariu, **S. Cheikh-Mohamad**: "PV-powered EV charging stations: requirements and feasibility conditions considering grid interactions", Solar in Mobility and Transport Systems, organized by ASOM (NL) et TNO (NL), 15 Oct 2020 (web conference). Public: researchers, industrialists, institutions, http://asom.solar/
2. M. Sechilariu, **S. Cheikh-Mohamad**: "Preliminary requirements and feasibility conditions for PV-powered charging stations for low-duty vehicles", conference 30 min, Virtual Workshop IEA PVPS T17 PV&Transport, 2 nov 2020 (web conference). Public: researchers, industrialists, institutions.
3. **S. Cheikh-Mohamad**, M. Sechilariu, F. Locment: "Preliminary requirements and feasibility conditions for PV-powered charging stations", presentation 20 min, Journée scientifique du GT Micro-réseaux (GDR SEEDS), 2 fév. 2021, web conference. Public: researchers, PhD students.
4. **S. Cheikh-Mohamad**, M. Sechilariu, F. Locment: "Preliminary requirements and feasibility conditions for PV-powered charging stations", conference 30 min, Virtual Workshop IEA PVPS T17 PV&Transport, 25 mars 2021 (web conference). Public: researchers, industrialists, institutions.
5. **S. Cheikh-Mohamad**, M. Sechilariu, F. Locment: "Cost Optimization for PV-powered intelligent infrastructures for recharging electric vehicles", conference 30 min, International WebConf Sustainable Transport & Sustainable Cities, 18 feb 2021, Public: researchers, industrialists, institutions, https://avenues.utc.fr/vie-du-laboratoire/agenda.html
6. **S. Cheikh-Mohamad**, M. Sechilariu, F. Locment: "Power optimization algorithm for PV-Powered Charging Station", conference 30 min, Virtual Workshop IEA PVPS T17 PV&Transport, 27 mai 2021 (web conference). Public: researchers, industrialists, institutions.
7. **S. Cheikh-Mohamad**, M. Sechilariu, F. Locment: "Human-System Interfaces for PV-powered Electric Vehicles Charging Station", conference 30 min, Virtual Workshop IEA PVPS T17 PV&Transport, 17 Nov 2021 (web conference). Public: researchers, industrialists, institutions.
8. **S. Cheikh-Mohamad**, M. Sechilariu, F. Locment: "Real time power management including optimization algorithm", conference 30 min, Virtual Workshop IEA PVPS T17 PV&Transport, 1 April 2022 (web conference). Public: researchers, industrialists, institutions.
9. **S. Cheikh-Mohamad**, M. Sechilariu, F. Locment: "Human-System Interfaces for PVCS", conference 30 min, Virtual Workshop IEA PVPS T17 PV&Transport, 1 April 2022 (web conference). Public: researchers, industrialists, institutions.

10. **S. Cheikh-Mohamad**, M. Sechilariu, F. Locment: “Experimental results for PVCS optimization algorithm”, conference 30 min, Workshop IEA PVPS T17 PV&Transport, 12 Mai 2022 (CEA INES). Public: researchers, industrialists, institutions.

11. **S. Cheikh-Mohamad**, M. Sechilariu, F. Locment: “PV-Powered electric Vehicle Charging Stations”, Round Table 20 min, Next generation mobility – supporting sustainable Urban Mobility & Local Public Transport, (virtual), 03-05 Mai 2022 Turin. Public: researchers, industrialists, institutions. https://www.linkedin.com/feed/update/urn:li:activity:6927660254184779776/.

General introduction

The world's population is rapidly growing, in addition to the advancement in civilization, has led to a massive increase in energy demand. Despite the fact that fossil fuels are not sustainable, which have significant health and environmental impacts, they remain the largest source to the energy sector [1], [2]. During the combustion process of fossil fuel, greenhouse gases (GHG), as methane, carbon dioxide (CO_2), and nitrous oxide are released in big quantities, which it also expected to increase over the time. These emissions will cause serious health problems, ice melting and rising sea level, climate change [3], which will endanger the human beings, their public health, and the food supply chain [4], [5]. The Paris agreement on climate change aims to limit the global warming to 1.5°C by 2050 [3], [6]. With the increasing concern of climate change, most countries have started implementing different strategies to avoid such scenarios. The Paris agreement sets a path to limit global rise in temperature by adopting bold steps to reduce GHG and enhance resilience to climate change's irreversible effects [7]. Various strategies have been proposed to mitigate GHG emissions, such as improving the efficiency of existing technologies [8], [9], introducing new devices more efficient and have greater impact on the environment [10], [11], and increasing the penetration level of renewable energy sources (RES), which seems to be the most promising strategy to replace fossil fuels [12], [13]. RES are reliable, environmental friendly as they can produce energy with a nearly zero emissions of GHG [14].

However, RES have to get over many barriers and challenges, as infrastructure, feasibility, availability, sustainability, capacity, connectivity, and technical experience and skills of human labor. Among the most difficult challenges of RES is their grid integration, due to their intermittency [15]. Therefore, storage systems has long been recognized as an ideal solution to mitigate the intermittency of RES [16]. The transport industry is the origin for a large part of pollution [17], with a 56% of GHG emissions in Europe [18]. Therefore, the transition towards electromobility could be a promising solution. Electric vehicle (EV) is defined as a vehicle powered by electric motor, it could be a car, a bus, a scooter, a bus, etc... In this section, EV is narrowed to hybrid EV (HEV), plug-in hybrid EV (PHEV), and battery EV (BEV) [19]. HEV has an internal combustion engine (ICE) with a small electric battery pack, recharged by ICE and regenerative braking. PHEV is a HEV with higher electric battery capacity and can be recharged by plug it in. BEV has only an electric battery pack, it must be recharged by plug it in. EV has many advantages as it has no noise, no vibration, no smell, and easy gear transmission relatively to ICE vehicle (ICEV).

In the recent report [20] about energy pathways to 2050, the French transmission system operator "RTE" has discussed the strategies to abandon fossil fuel and reach carbon neutrality in 2050 as of Paris agreement. The pathway will imply major changes on the economy and other sectors heavily dependent on fossil fuels. Despite the low carbon emission of the French power grid, however, it remains higher than world average when considering the carbon impact of imports. Alternatives are proposed as reducing energy consumption, increase in the share of electricity mix, and increase the reliance on RES. Many scenarios were studied and

analyzed based on four axes: technical, economic, environmental, and societal. The scenarios for the consumption trajectories as cited in the report are: sufficiency, extensive reindustrialization, rapid electrification, less electrification, less energy efficiency, and hydrogen. As for the scenarios for the generation mix are: 100% RES in 2050, distributed, large RES, RES and new nuclear level 1, RES and new nuclear level 2, RES and new nuclear level 3. They concluded that by 2030, France must develop more RES and extend the lifetime of the existing nuclear reactor to reduce the carbon emission by 55%. By 2050, it is possible to reach carbon neutrality with cost-effective but most importantly action should be taken immediately. It is worth mentioning that the baseline projection regarding the energy consumption for the transport section goes from 15 TWh nowadays to 100 TWh in 2050. Moreover, the 100% RES needs a massive increase in development rates to phase out nuclear plants by 2050, thus solar capacity should be increased from 30 GW to 70 GW or 200 GW in the highest projection, which is costly.

As for the French distribution network operator "ENEDIS" in its report [21] shows no difficulties in the integration of electromobility into the French grid, yet the growth of EV charging infrastructure remains slow. As per ENEDIS, in 2020, there were 70 k EVs sold which is the double of EVs sold in 2019 despite the COVID pandemic and around 30 k public charging stations. In 2021, there are around 500 k EVs on the roads in France. Moreover, optimizing the charging of EVs could bring savings to the user and reduce the negative impact of the public grid. Three possibilities to optimize the charging management: shifting the charging time where the energy tariff is advantageous, adjusting the charging power to reduce the charging demand, and management to maximize photovoltaic (PV) benefits during the day. Furthermore, a fleet of EVs could offer flexibility by discharging the stored energy in the EVs' batteries to the public grid when needed.

In light of growing concerns of global warming and pollution from fossil-fuel power plants, renewable energies can therefore reduce carbon emissions and GHG. Furthermore, the energy transition promotes the growth of renewable energy sources, but these can involve the complexity of the electrical grid, in the sake of reliability and quality. Thus, the concept of microgrid (MG), which is based on RES, storage devices, load and a public grid connection, could solve these problems, balance the production and consumption of energy, and bring benefits to the end user by reducing electricity costs, transmission costs as well as lower distribution, and also less energy loss for long transmission lines.

Moreover, electromobility related to the emergence of EVs in cities will no longer be a complexity to the power grid but will instead involve providing services associated with the grid such as flexibility and multi-energy resources. In this context, the following issues are discussed: renewable energy, design and sizing of the energy system, charging EVs, power grid availability, load stations analysis. An advanced search in Scopus with a filter on microgrid in the abstracts, titles, keywords, and specifically searching within EV charging station from 2010 to 2021 shows an increasing interest in this field, as illustrated in Figure 1, yet still not a lot of research as the number of publications is not significant.

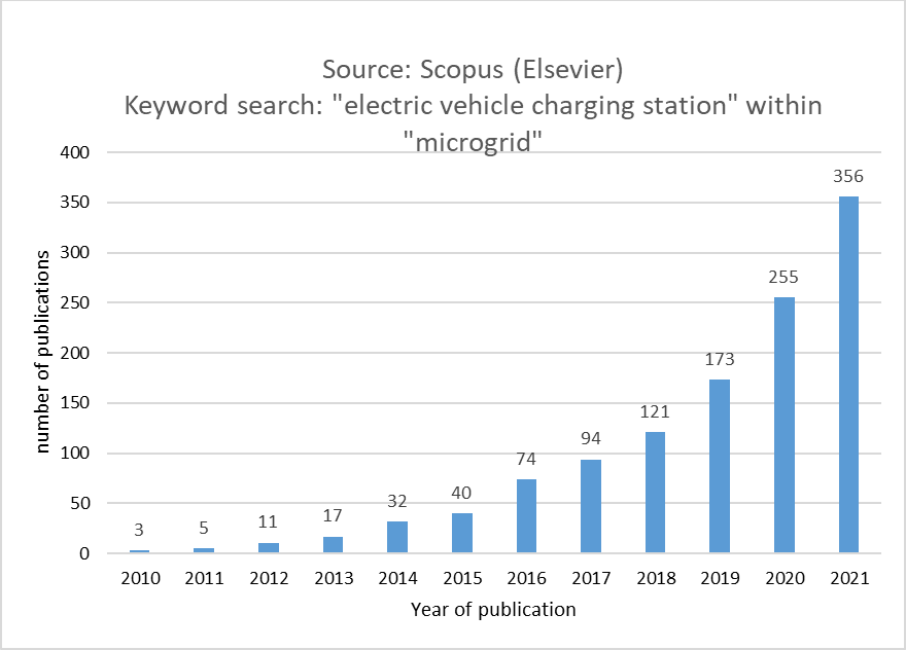

Figure 1: Electric vehicle charging station publications with the microgrid context.

Therefore, this thesis aims to investigate an energy system capable of optimizing energy flows and facilitating interaction between an intelligent infrastructure for recharging EVs (IIREVs), EVs, and a connection to a nearby building, as shown in Figure 2.

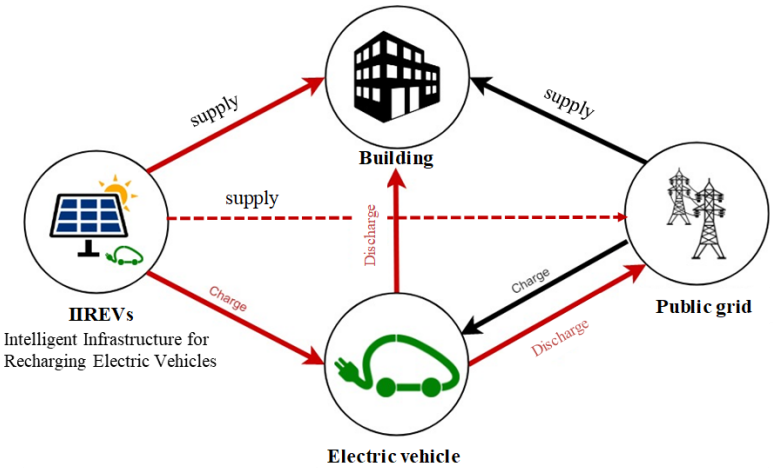

Figure 2: Innovative energy system [22].

This IIREVs is conceived as MG that considers the vehicle-to-grid (V2G), which is the discharge of EV batteries in the public grid, vehicle-to-home (V2H), which is the discharge of EV batteries in the building, and infrastructure-to-home (I2H), where the energy produced by the IIREVs but not used by EVs feeds directly into the building appliances, as shown in Figure 3. The research work aims at developing the MG and facilitate the interaction between the IIREVs, the public grid, EV users and the nearby building.

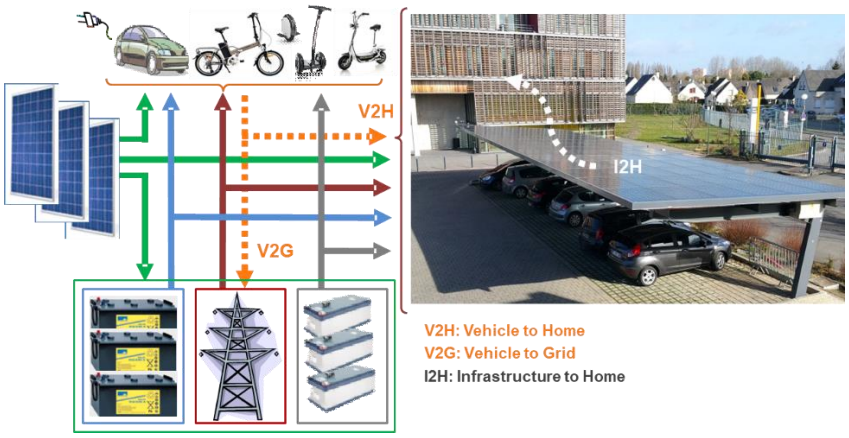

Figure 3: Strategies proposed by the IIREVs [22].

The research work aims at developing a technical-economic optimization methodology and tool that take into account the intermittent arrival of EVs and the services mentioned above for the IIREVs, with respect to various constraints. The simulation is operated under Matlab/Simulink environment, the optimization problem is solved by CPLEX in C++, and then the real-time experiments are conducted in different meteorological conditions in the experimental platform STELLA, as shown in Figure 4.

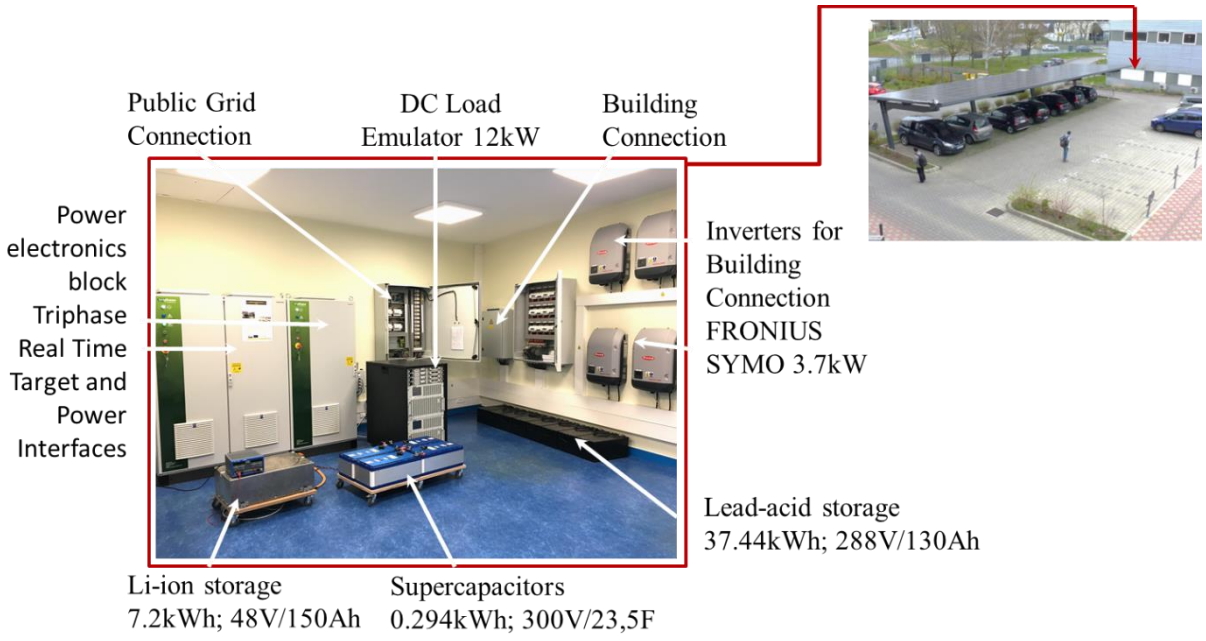

Figure 4: Experimental platform–STELLA.

The goal of this thesis is to design and develop an intelligent energy management system that optimizes power transfer in the IIRVEs, adapts to limits imposed by the grid, considers the various constraints imposed by users, and minimizes both the final energy cost for the EV user and the negative impact on the public grid.

To accomplish these objectives, this thesis is structured into six chapters as shown in Figure 5.

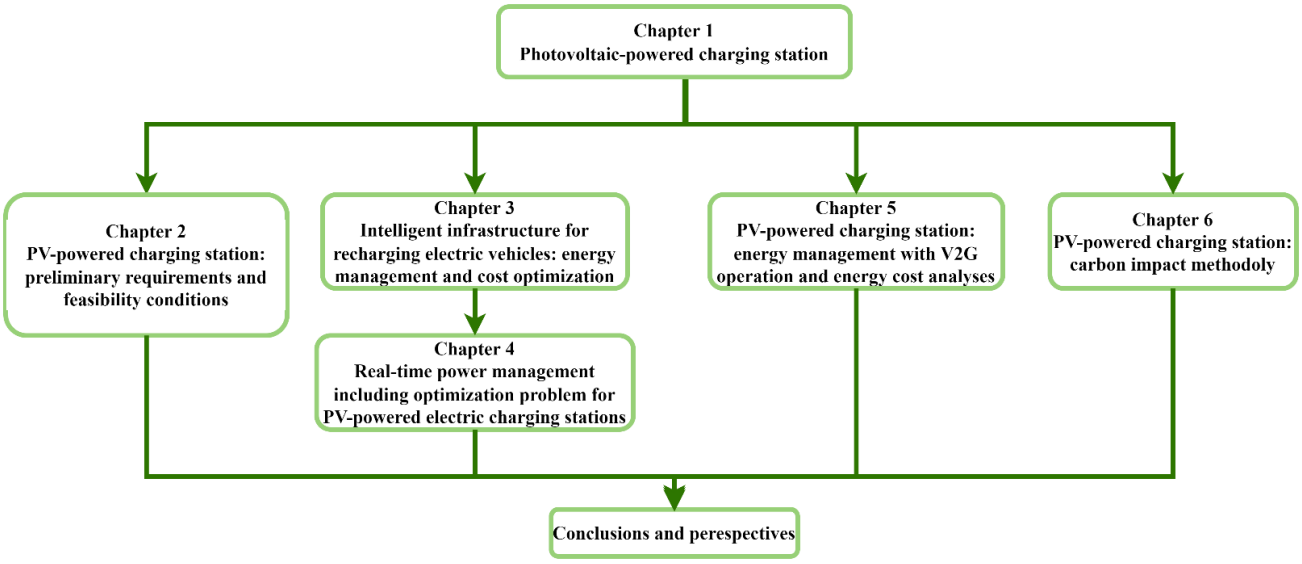

Figure 5: Thesis outline.

Chapter one 'Photovoltaic-powered charging station' gives a general overview of the electromobility transition in order to combat the climate change. Then, it introduces the EV charging station that is powered by PV sources and it is called PV-powered charging station (PVCS), giving an overview of EV charging station over the world. Literature review and the status in France are presented. Later on, the positioning of this manuscript is compared with the previous work at Avenues and the literature review and the main contribution is this thesis.

Chapter two 'PV-powered charging station: preliminary requirements and feasibility conditions' introduces the driving characteristics, the charging profiles, and the PVCS in order to identify the preliminary requirements and feasibility conditions. On this basis, simulation tests are conducted, for several scenarios, taking into account various EV charging profiles and the data of the least monthly PV energy production in Compiegne, France. The goal is to identify the conditions to maximize PV benefits while charging the EVs.

Chapter three 'Intelligent infrastructure for recharging electric vehicles: energy management and cost optimization' presents the IIREVs that is a PVCS but with an intelligent energy management system to optimize the power flow, aiming at PV benefits growth, and minimize the energy cost. The supervisory control system is introduced that includes four layers: prediction, human-machine interface (HMI), energy cost optimization, and operation layer. The optimization problem formulation is presented with its constraints and simulation cases, conducted in different weather conditions, prove the effectiveness of the proposed optimization algorithm.

Chapter four 'Real-time power management including optimization problem for PV-powered electric vehicle charging station' describes the experimental platform STELLA, where real-time experimental tests are conducted. Various cases are studied; different EV power profiles interacting with HMI and in different weather conditions to prove the superiority of the proposed optimization algorithm.

Chapter five ‘PV-powered charging station: energy management with V2G operation and energy cost analyses’ investigates the implementation of V2G operation in the PVCS. The energy management is presented, simulation cases are conducted with different EV power profiles and weather conditions and their results are analyzed.

Chapter six ‘PV-powered charging station: carbon impact methodology’ presents the carbon impact methodology for a PVCS. The carbon impact is detailed for each component in the PVCS. Then, the carbon impact of the PVCS is compared with the charging station only powered by the public grid in France and other countries.

Lastly, general conclusion and the perspectives of this research are given.

Chapitre I. *Photovoltaic-powered charging station*

This chapter gives a general overview of the electromobility, the description on the charging EV and its characteristics, and introduces the PVCS that is powered by PV sources presenting some existing PVCS over the world. Literature review and the current status in France regarding the PVCS are presented. Later on, the positioning of this manuscript is compared with the literature review and previous work at Avenues laboratory. This chapter is constructed as follows: Section I.1 introduces the transition towards electromobility. Section I.2 presents the PVCS. Section I.3 is a literature review on the PVCS. Section I.4 presents the EV and PVCS research work in France. Section I.5 outlines the previous research work in Avenues laboratory and the main contributions in this thesis. Section I.6 concludes the chapter.

I.1. Electromobility

The section is based on the recent report of Global EV Outlook 2021 [23] of the International Energy Agency (IEA) stated that despite the pandemic, there are 10 M EVs, deployed worldwide by the end of 2020, as shown in Figure 6. A 43% increase to 2019, after a decade of fast growth, due to national policies and international efforts. The expansion of EVs fleet will keep reducing GHG emissions, with the net saving over ICEVs increasing with the time, depending on how fast the power production decarbonizes. Although the current success of EV penetration, achieving the climate targets is still challenging and needs further actions and policies from all governments to promote EV charging infrastructure. The cost of EVs will keep decreasing manufacturing materials and battery technology improve.

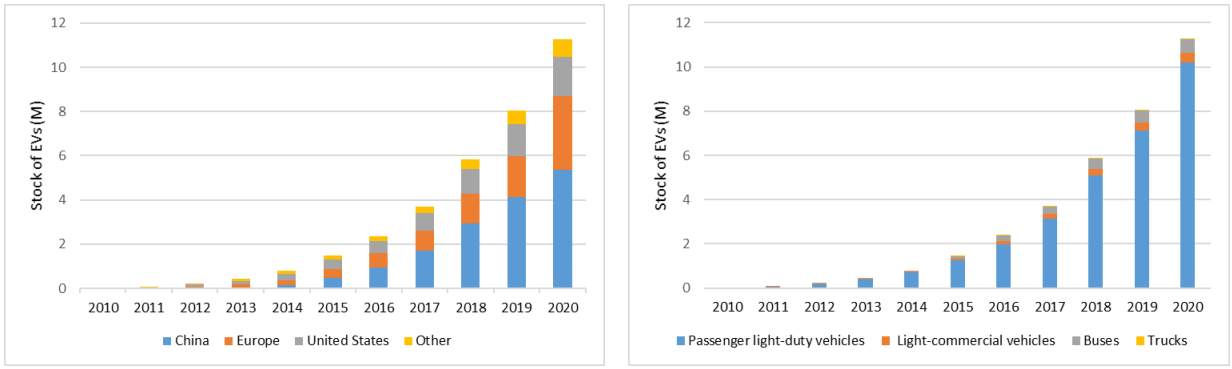

(a) **(b)**

Figure 6: Stock of EVs in the market by (a) region and (b) transport mode, based on [23].

In Europe, the car market has dropped by 22% in 2020. However, new EV registrations has increased to 1.4 M, representing 10% of car sales. The highest registration of EVs was in Germany with 395 k, followed by France with 185 k, and the United Kingdom (UK) with 176 k. Whereas, in Norway, 75% of car sales were EVs, followed by 50% in Iceland, 30% in Sweden, and 25% in the Netherlands. BEVs represent 54%

of EVs registered in 2020, exceeding the PHEVs. The highest share of BEVs registered was 82% in the Netherlands, followed by 73% in Norway, 62% in UK, and 60% in France.

In China, the car market has dropped by only 9% as they were less impacted by the pandemic. However, new EV registrations have increased from 4.8% in 2019 to 5.7% of car sales. BEVs represent 80% of EVs registered in 2020. In the United States of America (USA), the car market has dropped by 23%. However, new EV registrations has increased 2% of car sales, to register 295 k new EVs. BEVs represent 78% of EVs registered in 2020.

Fuel cell EVs are zero-emission vehicles, using fuel cell to convert hydrogen stored onboard into power. Fuel cell EVs were available on the market in 2014, their registrations still are 3 times lower than EVs due to the lack of hydrogen recharging stations among others. The Fuel cell EV stock has increased 40% in 2020, where Korea leads the way with 29% of fuel cell EV stock, followed by 27% in the USA, 24% in China, and 12% in Japan.

Although most EV charging is performed at home and at workplace, installing public chargers will be crucial for leading countries in EV adoption to make it simpler and provide autonomy for EV users. In 2020, there were 1.3 M public chargers deployed, 30% were fast chargers. The deployment of these public chargers has increased by 45% over 2018, but had a slower rate by 85% over 2019 due to the pandemic. China leads with the most public available chargers in slow and fast modes.

In 2020, the deployment of slow chargers (charging power less than 22 kW) has increased in China by 65% to reach 500 k public slow charger, which represents more than half of the globe's stock of slow chargers. While, Europe comes in second place with 250 k public slow chargers, and increase of a third by 2020. In the USA, the deployment of public slow chargers has increased by 28% to reach 82 k by 2020. Whereas, the deployment of fast chargers (charging power greater than 22 kW) has increased in China by 44% to reach 310 k public fast charger. Whilst, Europe increased the rate of deployment of fast chargers more than slow chargers by 38 k public fast chargers, and increase of a 55% by 2020. In France, there are only 2 k public fast chargers. In the USA, the deployment of public fast chargers has increased to reach 17 k by 2020, 60% are Tesla superchargers. As for private chargers, there are 9.5 M chargers for low duty vehicles in 2020, where 7 M chargers are deployed at homes.

In 2020, EVs helped in reducing GHG emissions worldwide by more than 50 Mt $CO_{2,\,eq}$. Yet, to reduce even more GHG emissions, EV deployment should be accompanied by decarbonizing the power grid. BEVs have 20-30% lower GHG emissions over ICEVs, throughout their manufacturing, use, and end of life. This advantage is more evident in countries where their grid energy mix is more decarbonized, as in European Union (EU) and especially France. As EV fleet is growing and expanding rapidly, it is expected to increase significantly the charging load on the grid over the years. Therefore, ensuring security and reliability of the grid is critical and possible solutions could be investing in smart charging, or charging EVs with renewable energies to reduce the burden on the grid.

I.2. PV-powered charging stations

The following subsections describe the type of charging process, type of EV charger, charging levels, microgrid based charging station architecture, hierarchical control and overview of PVCS.

I.2.1. Type of charging process

The types of charging process of EV batteries are conductive charging, wireless charging, and battery swapping [24], shown in Figure 7. Conductive charging requires an electrical outlet having two connectors, one is plugged in the charging terminal to transmit power and the other is plugged in the EV to receive power. This charging is suitable for slow and fast charging as well as the efficiency is high. Wireless charging can be either inductive or capacitive coupling, where no standard cables and connectors are required. The wireless charging can be dynamic, yet the losses increase and the cost of coils will increase also the price of the EV. Moreover, as wireless charging is slow and the efficiency is low, the charging process will take longer time than if it is conductive charging with the same charging power. Therefore, the CO_2 emissions will increase. Electronic devices in the charging device will increase also its complexity. In the static wireless charging, the device can not be displaced and must be left on a surface, therefore the charging area is limited. Battery swapping is based on battery replacement, which is done in less than a minute. Standard battery size and type are required and charging stations should be able to handle many batteries. In this research work, conductive charging is the type of charging applied.

(a)

(b)

(c)

Figure 7: (a) Conductive charging, (b) Battery swapping [25], and (c) Wireless charging [26].

I.2.2. Type of EV chargers

There is two types of EV chargers [24], shown in Figure 8, on-board charger, where the charger is inside the EV, and off-board charger, where the charger is outside the EV and its weight is reduced. On-board charging is dedicated for slow charging power and EVs are charged with AC sources, whereas, off-board charging is dedicated for fast DC charging and the possibility to participate in V2G. The main disadvantage of on-board charger is the maximum power charging and it does not offer the possibility of vehicle-to-x; on the other hand, off-board charger has to face challenges of battery heating and the cost of charging is therefore high.

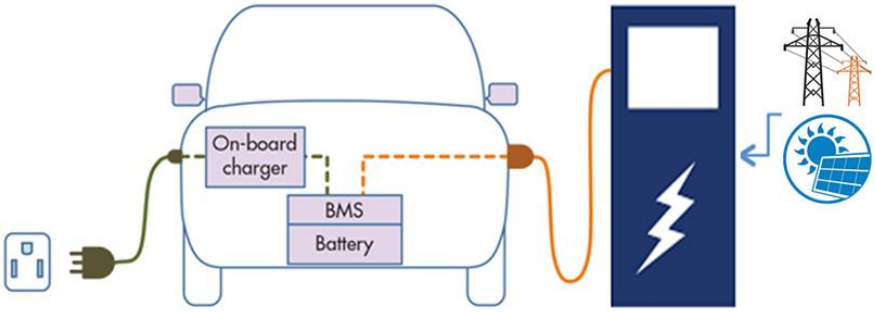

Figure 8: On-board and off-board chargers.

I.2.3. Charging levels

The charging stations are classed based on the voltage level that correspond to the power rating, where level 1 and level 2 corresponds mostly to the on-board charging and level 3 corresponds to the off-board charging. The charging rate determine the charging time, charging cost, charging equipment, and public grid utilization. The different levels of charging stations are presented in Table 1 [24].

Table 1: Charging station levels.

Supply type	Levels	Voltage range	Current range	Power rating	Charger type
Single phase AC	Level 1	120 V 240 V	16 A 13-16 A	1.9 kW 3 kW	On-board
Single/three phase AC	Level 2	208-240 V	80 A	20 kW	On-board
Three phase / combo charging	Level 3	300-600 V	400 A max	120-240 kW	Off-board
DC	Level 1	200-500 V	<80 A	40 kW	Off-board
DC	Level 2	200-500 V	<200 A	100 kW	Off-board
DC	Level 3	200-600 V	<400 A	240 kW	Off-board

The DC charging is preferred over AC charging as the PV and stationary storage are DC sources, the energy flow in EVs is DC, easier implementation of V2G with DC charging.

I.2.4. Microgrid-based charging station architecture

A MG-based charging station could have three architectures based on the type of the common bus [24], AC MG, DC MG, and hybrid MG.

In the AC MG-based charging station architecture, as shown in Figure 9, all the sources and loads are connected through their dedicated converters to the common AC bus. PV sources are connected to a DC/AC inverter including maximum power point tracking (MPPT), the stationary storage is connected to a bidirectional DC/AC converter. Whereas, wind turbines are connected to AC/AC converters, the EV

chargers are connected to AC/DC inverters and the grid connection does not require any inverter where it can provide more flexibility for charging/discharging the stationary storage but it requires power compensation to measure the active power at the point of common coupling. This architecture gives an option for sizing independently each component, and by controlling reactive and active power separately can yield to stabilize the bus voltage. In case of fault or grid failure, the MG is isolated by switching off the point of common coupling on the AC bus and it continues supplying the loads.

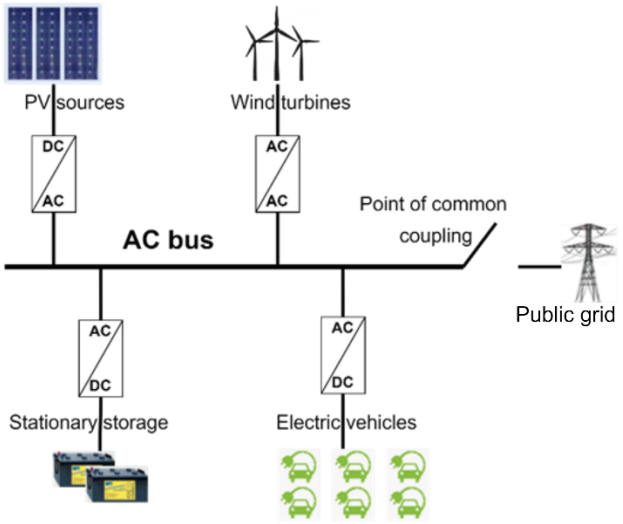

Figure 9: AC microgrid-based charging station architecture.

In the DC MG-based charging station architecture, as shown in Figure 10, all the sources and loads are connected through their dedicated converters to the common DC bus.

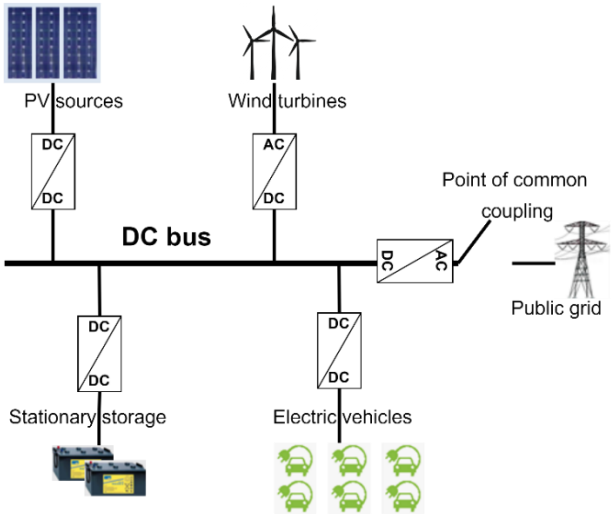

Figure 10: DC microgrid-based charging station architecture.

The PV sources are connected to a DC/DC converter working with the MPPT, the stationary storage is connected to a bidirectional DC/DC converter, and the EV chargers are connected to DC/DC converters, they could be bidirectional if V2G is applicable. Whereas, wind turbines are connected to AC/AC converters, and the grid connection requires a bidirectional AC/DC inverter, which is essential to ensure

the continuity of the charging as the PV source is intermittent. As EV charging is DC, thus DC MG architecture is more efficient due to lower conversion stages. Usually, the droop control is used to maintain the stability of the bus voltage.

Hybrid MG-based charging station architecture, as shown in Figure 11, combines both AC and DC MG where there are two buses feeding AC and DC loads. It combines the advantages of both AC and DC MG, where DC sources are connected to a DC/DC converter as PV sources and the stationary storage are connected to DC/DC converters, and the EV chargers are connected to DC/DC buck converters. Whereas, the grid connection does not require any inverter and maintains its AC voltage to supply AC loads. The interlinked converter is essential to link AC and DC parts, it transmits power in both directions, and can work in both modes to ensure the power balance between the two parts based on the actual demands.

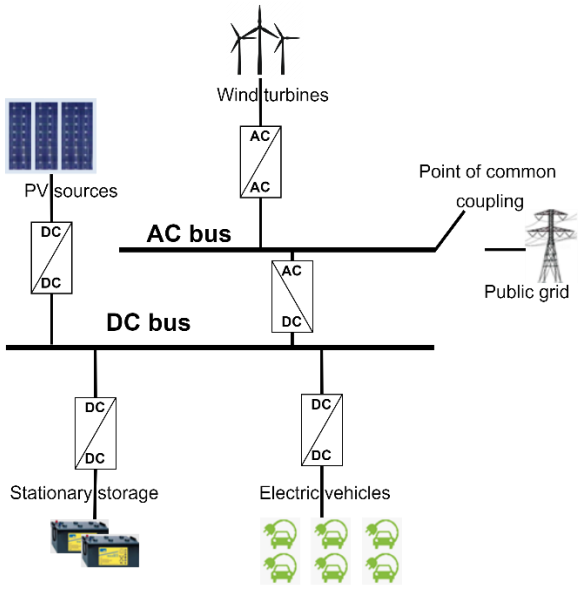

Figure 11: Hybrid microgrid-based charging station architecture.

DC MGs have become recently more attractive and popular than AC MG in industrial sites, commercial buildings and households as the difficulty for AC MGs lie in stabilizing the bus voltage and the frequency. The following are the main advantages of the DC MG:

- DC based RES need only one stage conversion to be connected to the DC bus, while, they need single or three phase inverters to be connected to the AC bus. Whereas, AC based RES need two stage conversions to be connected to the AC bus. This reduction in conversion stages can result in system cost reduction;
- DC sources are highly reliable and efficient;
- No reactive power in DC sources, therefore, low power loss and high transmission capacity are attained;
- Controlling DC MG can be simply done by controlling the power source on the DC bus.

I.2.5. Hierarchical control

The hierarchical control is also an important subject to evoke for MGs. There are three control levels; primary control, secondary control, and tertiary control, which are depicted in this section.

The primary control is the primary level of the control structure, which includes the current and voltage droop controllers, and proportional-integral controllers. The primary level is driven by reference signals generated by the secondary control level, which is represented by the energy management system. It regulates the dynamic response of each component connected through their dedicated converters. The main goal of the energy management system is to maximize RES utilization, minimize the energy cost with respect to imposed constraints, and reduce the negative impact on the stationary storage and public grid. The main concern is the economic operation, where dynamic electricity tariffs, ancillary services, and controllable EV charging could be the main parameters to be used to minimize the operation cost. Moreover, energy management system can offer possible revenues in case of extra power generation of RES. The tertiary control is the upper level that gives reference signals to the secondary control considering the state of the public grid. This level should coordinate the global power management between different charging stations. The main goal is to plan the charging of EVs in a smart way, which depends on various parameters and characteristics of the EVs, to provide some merits to the public grid as peak load reduction.

I.2.6. PV-powered charging stations overview

Therefore, charging EVs with RES, especially with PV sources, help increasing the environmental benefits of EVs and is a key element in reducing their GHG emissions [27]. PV systems can be installed on car parking shades or building rooftops and dedicated for EV charging, where they are called by PVCS and they can operate in island mode or grid-connected mode. Figure 12 shows a typical PVCS, where they consist of:

- PV sources installed on the parking's area;
- Power electronic devices represented by dedicated converters as DC-DC converters including MPPT or DC-AC converters;
- Storage system used to compensate the difference of PV power production and charging load. lithium-ion batteries are widely used as well as lead acid batteries can also be used;
- EV supply equipment needed to connect EV to the charging terminal as power cable, connector plug-in, protection devices, and user interface of the charging station;
- Other materials as mounting structures for PV arrays, switches, and wires.

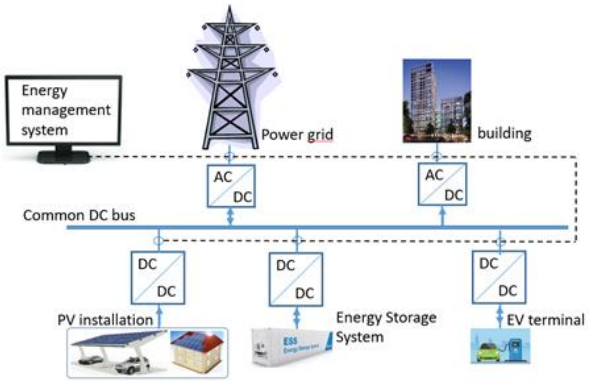

Figure 12: Typical PVCS [27].

Energy management system is needed to control and monitor the flows of energy in the PVCS to ensure a defined objective as minimize the charging cost and satisfy the EV user with full charging process. These PV-powered infrastructures are dedicated for charging EVs, or feeding energy to buildings, or injecting power into the grid. The following shows an overview and some existing infrastructures for PVCS in several countries.

Beam Global have installed EV ARC^{TM} 2020 [28] as a free public charging unit for EV in San Diego, USA, as shown in Figure 13. It is compact in area, sustainable, powered by PV, off-grid, and transportable, where it can be transported and installed anywhere in minutes, as it does not require any construction or electrical work.

Figure 13: EV ARC^{TM} 2020, Global Beam charging unit [28].

The PV arrays can reach 4.3 kWp, a storage system is integrated into the charging unit with an energy capacity up to 43 kWh, which allows EV to charge up to 426 km and in all circumstances, including nighttime and bad weather, and even blackout. It can charge any brand charger up to 4.3 kW and up to six EVs at a time, withstand wind speed up to 193 km/h and flood level up to 2.89 m. However, when the storage is empty, charging of EV will be limited to the PV power and will last long.

Fastned [29], a Dutch company, installs charging stations fully powered by PV sources and wind turbines, as shown in Figure 14. Their infrastructures are standalone, without storage systems, and their charging power can reach up to 350 kW in DC.

Figure 14: Fastned charging point [29].

Paired Power have their DC SEVO SunStation™ [30], as in Figure 15, fully powered by standalone PV sources that can provide up to 16.8 kWp with 48 PV panels and charge six EVs.

Figure 15: SEVO SunStation™ [30].

Secar Technologie have their E-port [31], which is made of carbon fiber and 360° bifacial PV cell technology, as shown in Figure 16. It can be connected to the grid and can have a storage system. It can provide up to 3.78 kWp and 5.67 kWp with 12 and 18 PV panels respectively and charging power of 22 kW with the assistance of the grid and the storage system.

Figure 16: Secar Technologie E-port [31].

MDT-tex presents the Solar Carport [32], which is made of PVC material covering two parking lots with a square of 5.3x5.3 m in two formats symmetrical and asymmetrical mast, as shown in Figure 17. These

shapes help storing rainwater in a covered water tank after going into the drainage pipes, and through the filtration system. It can provide up to 5.4 kWp with 15 PV panels and have lithium-ion as storage system with 8.5 kWh, it is grid-connected and can charge electric bikes and EVs with a maximum charging power of 22kW using Mennekes AMTRON Premium type 2.

Figure 17: MDT-tex Solar Carport [32].

Tesla have their new supercharger V3 [33], as shown in Figure 18, which can provide up to 250 kW. Their infrastructures have PV sources and lithium-ion batteries as powerpack [34], with up to 232 kWh AC as the grid charges them mainly.

Figure 18: Tesla Supercharger V3 [33].

IRISOLARIS has installed its FLEXSUN with mixed energy solutions as part of the renovation of the Gardanne's train station, offering free charging terminals for EVs in protected parking zones [35], as shown in Figure 19. The energetic renovation has started in February 2020, to be operational in summer 2020, undertaken by Aix-Marseille-Province metropolis. The park provides 352 parking places, where EV users can come to park and charge their EVs freely to encourage them to use public transport in favor of the environment, over an area of 950 m^2 covered by PV panels providing an energy of 130 kWp capable of charging 16 EVs and 56 electric bikes. EVs are charged mainly by the PV sources, and a storage system can store excess PV energy and may take over the EVs charging; also, part of PV energy is injected into the grid and sold.

Figure 19: PV-powered infrastructure at Gardanne's train station [35].

Transdev, the public transport operator in southeast Queensland, Australia, has announced that it will test a 39 seater electric bus charged only by PV sources [36], as shown in Figure 20.

Figure 20: Transdev electric bus PV-powered depot [36].

Two hundred and fifty PV panels, producing an average of 438 kWh/day, cover the depot, equipped with 10 Tesla Powerwall batteries with 135 kWh energy capacity. The stored energy is used to charge the electric buses, having 348 kWh battery capacity per bus and giving an average range up to 300 km per bus. Further improvements are desirable, as the storage system is only capable of charging around one third of an electric bus energy capacity.

A PVCS is implemented in SAP Labs in the south of France, where EVs can charge in workplace and it includes a power management system and parking time management [27], as shown in Figure 21. SAP Labs France are a subsidiary of SAP SE company, and are interested in the electromobility transition. In the context of energy transition and reducing GHG emissions, SAP Labs are installing PV sources to generate clean energy and reduce its dependency on the public, along with implementing software to optimize the peak load consumption. They are increasing the PV installation over the car parking as their EV fleet is expanding.

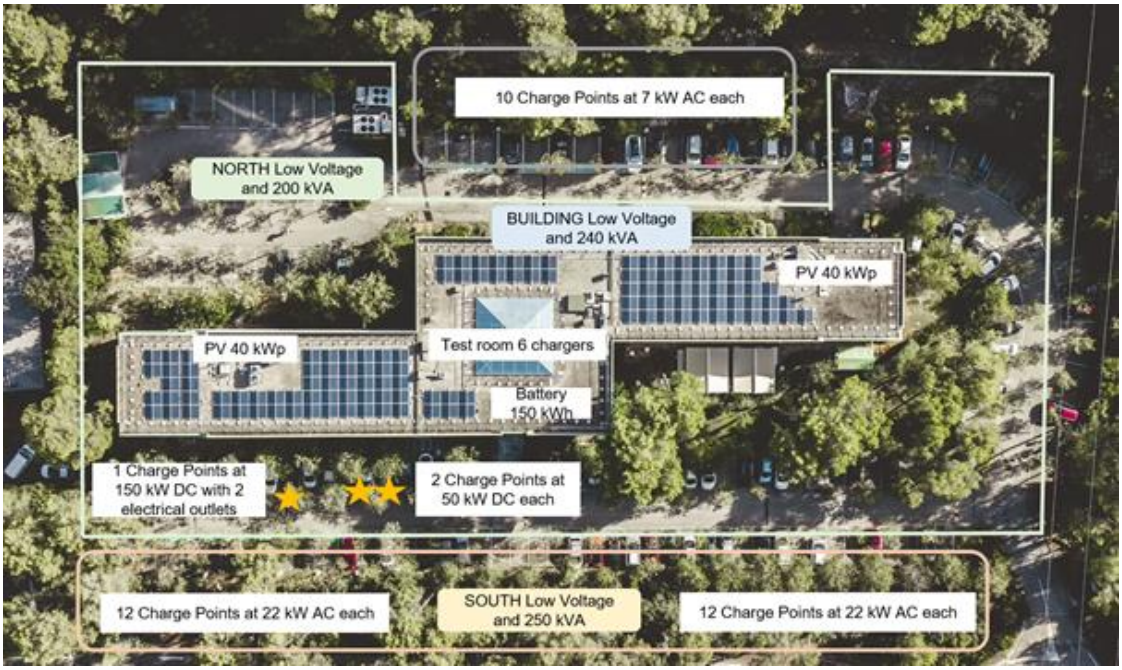

Figure 21: PVCS at SAP Labs Mougins, France [27].

There are 252 PV panels installed on the roof, occupying an area of 428 m^2, with an optimal inclination of 10° and oriented to the east west. They can produce around 80 kW and an estimated annual production of 78 080 kWh. A second-life batteries are used as storage system with an energy capacity of 150 kWh. The software, e-mobility, allows an intelligent communication between the operators and the EV users, as receiving information regarding the remaining charging time and notifications when charging is completed, it allows a better management and optimizes the energy costs. The charging stations is composed of three parts, classed by their location:

- North: it comprises ten charging terminals at 7 kW each;
- South: it comprises 24 charging terminals at 22 kW each;
- Building: it comprises two charging terminals at 50 kW each, and one charging terminal at 150 kW with two electrical outlets.

Most of these infrastructures have slow charging, whereas, Tesla and Fastned have ultra-fast chargers with 250 kW and 300 kW respectively. Only Fastned is grid independent, while the other infrastructures depend on the grid to either charge EVs or the storage system. Despite the fact that these EV charging stations are PV-powered, yet their PV power is limited even if they are equipped with stationary storage, they depend mainly on public grid power. Even more, there is no optimization of energy cost or power flow and no smart or intelligent charging based on algorithms to increase PV benefits or reduce the energy cost. Thereafter, this research work presents a PVCS, which is an intelligent infrastructure that optimizes the power flow of sources to minimize the energy cost.

I.3. Literature review

A feasibility study has been conducted in [37] for a PVCS, as shown in Figure 22, in a technical, economic, and environmental aspects in four cities in Australia, Brazil, Norway, and The Netherlands. They investigate how a PVCS can contribute in charging EVs with different grid energy mix, and compares the CO_2 emissions of charging EVs solely from the grid, with charging EVs from the PVCS, as well as ICEVs. Technically, in the countries with high irradiance over the year, PVCS performed more efficiently than in countries with high variability of irradiance over the year. Economically, PVCS still not feasible as the cost of storage system remains expensive. Environmentally, PVCS can reduce CO_2 emissions in countries where their grid CO_2 footprint is high, where it is significant with high annual average irradiance.

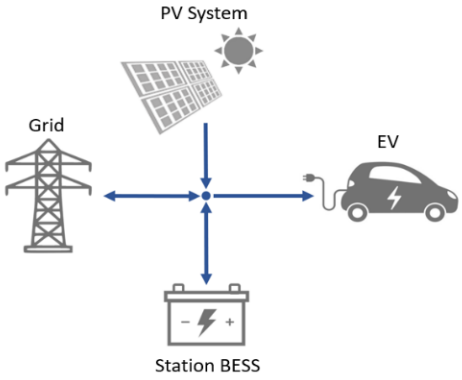

Figure 22: PVCS as proposed by [37].

In [38], a supervision control system has been studied for a smart charging of a fleet of EVs in a PVCS research based building. Their strategy is based on a real-time operation to satisfy EV users using PV forecast and EV charging historical records over 4 years in the research to predict the EV power profiles. A user-friendly smart charging has been developed in [39], where the EV user is a key player in the process of choosing the best scenario among uncoordinated charging, smart charging, and bidirectional smart charging control. The proposed methodology is based on a real-time rule-based controller and a linear optimization model predictive control. Different scenarios were examined, where input data are received for PV power prediction and electricity prices, as well as data received from the EV user. Afterwards, the EV user has to choose his final scenario after comparing the results of the scenarios presented. The results showed that bidirectional had the best cost reduction, then comes smart charging, compared to uncoordinated charging control. When the EV discharges into the grid, their user gain profits and considering the overall operation charging/discharging, it can reduce the charging bill up to 50% compared to uncoordinated charging. A novel linear technique has been presented in [40] to limit the number of discharging cycles of EVs in V2G operation using model predictive control based optimization. The proposed constraint was actually nonlinear, thus the used technique linearized the constraint. The simulation cases were considered for different values of discharging cycles, where it is supposed that the EV user will choose his discharging cycle, and the results showed that the novel linear technique performed

in all cases and is satisfied. The reward gained by V2G was high as the discharging cycles become bigger, however, even with one discharging cycle, the reward is still interesting as the discharging cycle was done during peak energy price. An overview in [41] has been given on the smart charging studies, taking into consideration PV power and electricity consumption. They have presented the different actors involved in the smart charging system, the interaction with the grid and its impact, the expected outcomes from the smart charging and the optimization algorithms applied to achieve these objectives, and the different spatial configurations applied for smart charging; in residential buildings, in non-residential buildings, and in charging stations.

A mixed integer linear programming (MILP) optimization problem has been presented in [42] to optimize the scheduling of charging/discharging of EVs in a charging station, which integrates PV sources and storage system, based on the EV user priorities and electricity tariff. The simulation results showed that the proposed optimization problem have maximized the satisfaction of EV users and minimized the operation cost of the charging station. An energy management system design has been proposed in [43] to predict PV power production, using autoregressive integrated moving average model, and to optimize the power flow between PV sources, grid, and EVs in a workplace. Moreover, a MILP has been presented in [43] to reduce charging costs, grid energy, increase PV self-consumption. An optimal energy management algorithm has been investigated in [44] to minimize the peak load consumption in a university campus, which integrates PV sources, storage system, and smart parking lot for EVs. They have proposed a time allocation method to prioritize the charging/discharging of EV based on priority and rules that take into account decision factors set by the user and EV data. Simulation results proved the efficiency of the proposed method and outperformed the conventional charging scheme, which has a significant impact on the peak load consumption. An EV aggregator optimization problem using the alternating direction method of multipliers has been proposed in [45], which is a scalable distributed convex optimization framework. This method allows evaluating up to 1 million EVs to solve the valley filling problem and minimize the charging cost. The results showed the computational time increases linearly with the number of EVs and performs better than the centralized optimization as the number of EVs increases. The authors in [46] have addressed a real-time charging scheme in an EV charging station for a demand response application. They have aimed to minimize the energy cost paid to the grid and to maximize the number of designated EVs for charging. They have also proposed a modified convex relaxation algorithm to solve the computational problem and to be appropriate for real-time calculations. Their results proved the efficiency of the proposed method and their goals are satisfied. Mixed integer programming has been studied in [47] to minimize the cost of energy traded to the PVCS, where the intermittency of PV power can be compensated and green classed EVs can discharge energy to the PVCS. The EVs were classed in three categories and the results showed that the increase of green EVs, only this category of EVs where their users can allow discharging of energy into the charging station, can reduce the total cost of the PVCS. MILP has been used in [48] to optimize the sizing of a PVCS, to minimize the investment cost and the operational cost, considering the uncertainties of PV and EV charging power profiles, in which it has been modeled using probability distribution function. The

results showed that EV charging station powered by PV are more cost-effective than EV charging station powered by the grid.

A fuzzy logic method has been described in [49] to arrange charging/discharging of EVs in a charging station with fair and optimal approach, based on the EV state of charge (SOC), charging time, electricity tariff. They have proposed also a scheduling optimization problem formulated as linear programming (LP) to optimize the charging/discharging level of the connected EVs. Their results proved the efficiency of the proposed method by introducing V2G service to reduce the charging cost. LP has been presented in [50] for static EV charging scenario, where the charging power is constant based on EV demands that are known in advance, and heuristic algorithm has been proposed for dynamic EV charging scenario where EV can leave anytime. The objective was to increase the revenue of the aggregator and reduce the charging cost for the EV users.

Dynamic programming (DP) has been formulated in [51] for a hierarchical management scheme in a distribution network to coordinate charging of EV fleet, to reduce peak loads and charging cost with respect to constraints. DP has been also proposed in [52] to reduce computational load of EV charging fleet, studied as an aggregate battery, than the results of the charging cost were compared to heuristic algorithm. An approximate DP based energy management system has been described in [53] to reduce the operation costs of an EV charging station with different types of chargers, then the DP algorithm is combined with evolution algorithm to find the ideal charging start time for each EV. DP has been investigated in [54] to find the optimal charging schedule as a smart charging for EVs in order to reduce the charging cost considering behavior of EV users.

Quadratic programming (QP) has been used in [55] for a distribution grid with a fully decentralized mode integrating vast PV sources and EVs to optimize the power flow, to reduce the losses in the distribution grid, to reduce PV curtailment, to provide high satisfaction for EV users. QP has been studied in [56] to reduce the total grid power for utilities, where PHEVs can operate in smart charging/discharging. In V2G mode, the PHEVs achieved peak load shaving and benefits to the power grid. QP has been introduced in [57] for a fleet of electric buses to optimize the charging based on scheduling charging, the objective was to reduce the charging cost and the load power variations. Robust optimization has been presented in [58] to schedule the EVs' regulation capacity while maximizing the profits, considering market rules of the independent system operator in the US, the random arrival and departure of EVs. Stochastic programming has been proposed in [59] to study the uncertainties of EVs and electricity tariffs for the optimal behavior of EVs in a parking lots and to optimize the participation level of each EV in demand response program. A game theoretical approach has been studied in [60] to solve the charging scheduling problem of EVs in a parking lot, considering transformer capacity constraints and other constraints. A genetic algorithm has been presented in [61] to optimize the charging time of PHEVs in a PVCS and to reduce the charging cost.

A MILP optimization problem has been proposed in [62] to find the optimal sizing of PV and storage system for an EV ultra-fast charging station. Simulation results proved that the proposed optimization

problem can reduce the annualized cost of the charging station, taking into consideration investment and maintenance cost of PV and storage system, and grid energy cost. A nonlinear programming optimization has been presented in [63] to minimize battery aging of electric bus by proposing overnight charging, taking into account grid power, electric vehicle supply equipment, and electric bus operating conditions as constraints. A dynamic wireless power transfer for charging EV has been described in [64], which consists of many stationary ground side coils and a moving vehicle side coil. The results showed that the dynamic wireless power transfer is equivalent to the stationary system. Solenoid coils were used instead of circular coils for better performance. An energy management architecture for PV battery charging station has been presented in [65], where individual and parallel charging are studied to reduce the charging cost and time. The proposed method prioritizes the charging depending on the highest SOC or a voltage threshold, then the next battery is charged to the same threshold, and in the final stage, all batteries are charged in parallel.

To sum up all the above cited references, despite the various optimization methods used in the literature such as MILP to minimize the charging cost of EVs, DP to coordinate the charging of EVs, QD to reduce the losses in the distribution grid, and other heuristic and stochastic algorithms, they did not evoke the real-time optimization for a PVCS. Firstly, preliminary requirements and feasibility conditions were not well identified for such PVCS in order to increase PV benefits. Secondly, the optimization problem formulated in the above references were based on EV prediction profiles, whereas, real-time optimization was not studied to extent to our knowledge and no human-machine interface existed to exchange and communicate information with the PVCS. Therefore, EV uncertainties such as time of arrival, time of departure, SOC of arrival, SOC at departure, charging power, were not well considered in most considered and they were predefined. Moreover, the real-time optimization will be validated in simulation and experimental test in the STELLA platform. In addition, V2G service is studied to reduce energy cost during peak periods. Lastly, the carbon impact methodology is presented and compared with a charging station powered by the grid.

I.4. EV and PVCS research work in France

In [66], Femto-ST laboratory has studied the system control and economic operation optimization of a charging station. The coordinated control techniques, for the primary control, has been addressed with implementation of PV sources and storage system to ensure the stability in real-time operation of an EV charging station. MPPT method is applied to extract maximum power from PV sources, which are modelled as an ideal diode, the stationary storage is connected to a bidirectional DC/DC converter, and the grid is connected to a 3-phase AC/DC converter, where all these components are connected to a DC bus. A phase lock loop is applied to synchronize the AC part with the public grid. An event-triggering-driven energy management has been proposed to perform coordinated control. The charging sport of each EV is allocated based on a fuzzy logic guiding system based on its urgency. Thereafter, an approximate DP based energy management system has been proposed to reduce the charging station operation costs, then the optimization

algorithm is combined with the evolution algorithm to find the optimal charging start time for each EV. Lastly, a finite-horizon Markov decision process has been presented for the optimal operation of the EV charging station powered by PV, using V2G service to provide ancillary services, considering uncertain behaviors of EV users and dynamic electricity tariffs. Their proposed DP method can reduce operational costs to 50% compared to the uncoordinated charging. Furthermore, as approximated DP only determines the charging start time of the EV, this has offered an autonomy to provide the optimal charging profile, which can improve battery lifetime. As for V2G operation, the total operation cost is reduced and the battery lifetime is considered as the charging/discharging cycles are reduced.

In [67], a literature review on installation frameworks, highlighting the key features, has been conducted in an non electrical perspective for EV charging station. In addition, it has identified the trade-offs between various power charging infrastructure and the BEV users demands, taking into account: BEV asset and range, private charging accessibility, public infrastructure accessibility, BEV adaptability with the charger in terms of technical limitations. Also, it has addressed the optimal BEV battery capacity for rural and urban usage, as well as the deployment of fast chargers. Furthermore, it has investigated, using mixed-effects regression, the impact of economic, socio-demographic, and technical aspects on EV penetration in France. The mixed-effects regression is an extension to linear models that considers time-variant and constant covariates to analyze EV adoption. As well, it has outlined the policy recommendations to hasten the transition towards electromobility.

In [68], Femto-ST laboratory has proposed an efficient hierarchical energy management strategy for a hybrid charging system that is based on PV sources, storage system, and grid connection to fulfill the demands of EVs. It has been implemented to maximize PV energy, to respond to the variable load of EVs, taking into account the fast response of the storage system, and to mitigate the stress on the grid. The PV sources are modelled using the ideal diode model, where MPPT is used to extract maximum power and applied to interleaved boost converter to regulate PV output voltage. The stationary storage and EV charger are interfaced with a 3-phase interleaved bidirectional converters. This strategy has improved the overall performance, the reliability, and the energy cost. Moreover, to enhance the power quality, an efficient energy conversion step has been proposed using interleaved buck-boost converters, and an extended Kalman filter has been studied to estimate the SOC of a lithium-ion stationary battery. Their proposed charging system with the interleaved converter has a high efficiency and improved power quality, as well as the extended Kalman filter helped estimated SOC value near real value.

I.5. Previous work in Avenues laboratory

The research unit Avenues, team of “Energy management and urban microgrid”, has more than 10 years of expertise in the fields of renewable energy, DC MG, and energy management. They have directed nine

PhDs until this day. This part shows the previous work done in Avenues laboratory that is only relevant to DC MG, optimization, and PVCS.

Issam Houssamo was the first PhD student who started working on DC MG. The objectives in his thesis [69] were to study, investigate, and implement a multisource system in a DC MG considering some aspects of power quality. He developed a purely experimental model of PV source and a classical MPPT algorithm was upgraded to obtain the maximum PV power. The storage priority was proposed as first energy management system, proved the technical feasibility of the DC MG PV based, where the appliances in a building were taken as the load, and experimental tests were realized. The main findings proved the applicability of the experimental model of the PV sources and the improved perturb and observe method to extract the maximum power. As for the stationary storage, the dynamic model, which depends on various parameters, was not the best model to use as the parameters change and the static model could be used as a simplified model of the stationary storage, which neglects the temperature and internal resistance. As for the grid connection, phase lock loop and resonant corrector were used to improve the quality of the DC bus voltage and to insure the synchronization of the AC part to the public grid.

Then, Baochao Wang in his thesis [70] has proposed a building integrated DC MG, for on-grid operating mode, and a multi-layer supervision system was developed to optimize the energy cost using prevision data. The supervision system provides power balance, and real-time experimental tests were conducted to prove the feasibility of the proposed system, considering uncertainties. The supervision system can interact with the end-users through an interface, exchange information with the smart grid, receive meteorological previsions, and perform day-ahead energy management. The proposed supervisory control can operate in on-grid and off-grid and the optimization problem was proved to be cost-effective for a building integrated DC MG in both simulation and experimental tests.

Later on, Leonardo Trigueiro Dos Santos continued in his thesis [71] the study of the energy management to keep the stability of the DC bus voltage, to optimize the energy cost using improved prediction methods to predict more accurately PV power. Moreover, he has proposed a demand side management by applying a knapsack method to maximize the use of electric appliances when load shedding is required to keep the DC bus voltage stable. The proposed methods were proven by real-time experimental tests. The proposed load shedding algorithm was validated in simulation and experimental tests as well as the supervisory control to operate and to optimize the energy cost for on-grid and off grid for a DC MG.

Furthermore, Changie Yie in his thesis [72] has studied the impact of diesel generation integration in a standalone DC MG with the application of supercapacitors to mitigate the slow startup of the diesel generator and to maintain the power quality. A control strategy has then been proposed to keep the DC bus stable of the MG and it is been validated in simulation and experimental tests. In addition, an optimization problem has been proposed to reduce the energy cost of the diesel generator, fuel cost, and the total energy cost of the DC MG. The results found have proved that supercapacitors mitigate the slow startup of the diesel generator and the proposed control strategy was able to maintain the stability of the DC MG bus and

to coordinate between the power sources. Even more, the optimization problem in comparison with the normal operation mode is proved cost-effective, which is validated in simulation and experimental tests.

More after, Hongwei Wu in his thesis [73] has focused on the study and analysis of the losses in the DC MG and energy models of converters were conceived to analyze the variation of losses in the different operating points. The implementation of models and the use of dynamic yields improve the overall performance of the MG. Real-time experimental tests were carried out to validate the application on the converters in the DC MG. The results found showed that the efficiency of the PV converter is in the range of 80-90%. The losses considered in the study are related to the conduction and commutation for the transistor, diode, and the copper losses in the inductance, thereafter, the estimated efficiency of each converter is acceptable. The dynamic converter efficiency method has improved the energy quality and the global efficiency of the DC MG, which has been validated in simulation and experimental tests.

Lastly, Wenshuai Bai in his thesis [74] continued the study of a building integrated DC MG in urban area in a full operation mode, combining the advantages of on-grid and off-grid modes. Therefore, the full DC MG integrates PV sources, stationary storage, grid connection, backup diesel generator, and supercapacitors to mitigate the slow startup of the diesel generator. Dynamic efficiency and power losses of the converters have been also considered in the full DC MG. The main results showed that the proposed supervisory control system for full MG performed better than on-grid or off-grid and has a lower load shedding cost.

Dian Wang in her thesis [75] has proposed an rule based algorithm for the PVCS that interacts with the human-machine interface, considering EV user uncertain behaviors and their random choices. Simulation results were conducted to prove the feasibility of the proposed algorithm along with a shedding and restoration algorithm where it is not possible to fully charge the EVs in the station. Then V2G service was proposed in the PVCS to reduce peak power problems during peak periods and to reduce the public grid energy cost. The proposed algorithm had a good performance and the PVCS can interact with EV users and satisfy their demands. In addition, V2G service can bring benefits to EV users in the meantime satisfying the users.

A survey on the social acceptance of an PVCS has been conducted in [22]; a case study in France. The results showed that vast majority accept the PVCS, yet have some concerns that have to be taken into consideration in the implementation of some urban cases. Youssef Krim, post-doctoral position, in his research work [76] has focused on a quantitative assessment of the PV benefits obtained from PVCS. A technical-economic tool based on Visual Basic for Applications on Excel has been developed for the proposed methodology in three phases to help PVCS owners in determining the preliminary requirements and feasibility conditions of a PVCS, considering local constraints.

In [75], a PVCS has been designed and modelled that interact with EV users and it was simulated with a proper power management, however, the real-time optimization was not a center of interest in the thesis. As for the prior theses done in Avenues laboratory and related to the optimization, neither the EVs nor the PVCS were evoked as their load was mainly on the building load. Therefore, this manuscript focus on

proposing a real-time optimization algorithm for a PVCS to minimize the total energy cost. As for the literature review, many papers have proposed optimization problem for charging stations, yet they have not highlighted the interaction with EV users in a user interface. Moreover, their optimization algorithm is based on EV prevision profiles. Our novelty lies in proposing an optimization problem that interacts with EV users using the HMI in a real-time operation and is validated in experimental tests.

In chapter two, the goal is to define the preliminary requirements and feasibility conditions for PVCS in an urban area and to emphasize the importance of a business model that can influence the EV users' behavior. The main contributions are:

- A PVCS model is proposed, which consists of PV sources, stationary storage system, public grid connection, and EVs. This model satisfies the EV user demands while improving PV-benefits for EVs if the following requirements and feasibility conditions are considered:
  - On user behavior/flexibility:
    a. Prefer daily charging over weekly charging;
    b. Accept long and slow charging when possible;
    c. Limit charging to the number of kWh required for the daily trip, or charge more when PV power is available;
  - On technical aspects:
    a. Limit charging power and stationary storage power to about 7 kW;
    b. Choose an optimal size for stationary storage;
    c. Give priority to charging stationary batteries by PV over charging from the grid.

In chapter three and four, the objective is to perform a real-time control under optimization for the minimum energy cost and the maximum PV energy for each EV for IIREVs considering the intermittent and random arrival of the EVs, featuring the EV users' interaction. The main contributions are:

- Proposing a new real-time power management, including energy cost and PV energy optimization for the IIREVs considering the intermittent and random arrival of EVs, where the optimization is performed at each EV arrival;
- The analysis of the energy distribution by source category for EV charging and the entire station energy system;
- The validation of the proposed control under optimization in simulation and real-time experimental tests in different weather conditions and different random EV power profiles.

Chapter five focuses on a PVCS equipped with five chargers that could support slow, average and fast charging. It highlights the importance of participating in V2G in peak hour in terms of energy share among other sources and the income in variable power charging/discharging. The main contributions are:

- An energy management system conceived so that the PVCS can operate to charge EVs as well as V2G service;

V2G service can bring benefits to the PVCS by either reducing its energy cost or by selling energy to the public grid; however, the energy discharged from EVs into the public grid is significant comparing to the PV energy injected into the public grid during peak periods.

In chapter six, the carbon impact estimation of PVCS is detailed; the PVCS is a car parking shade equipped with PV sources, stationary storage, and grid connection. Then, a comparison with a grid powered charging station (PGCS) is presented and analyzed. The main contributions in this chapter are:

- Presenting a methodology to calculate the carbon impact for PVCS;
- Comparing the results with a PGCS considering the electricity mix of several public grids.

I.6. Conclusions

The growing concerns on climate change and its repercussions on the planet has forced to act and find solutions to combat climate change. As transport sector is considered one of the major contributors to emit CO_2, therefore, the transition towards electromobility is seen as a promising path to reduce carbon emission. Even though when EVs are rolling on the roads emit zero or low carbon emissions, their global carbon emission throughout their life cycle depend highly on the production phase, power charging phase and end of life phase. Thus, combining zero-emission EVs with clean energy sources as PV can reduce the carbon emission compared to ICEVs. Thereafter, EV charging station powered by PV is a growing research topic.

This chapter has started with an overview on the electromobility and its recent outlook report that shows the expansion of EVs and its infrastructure over the world. Then, a description on the charging is evoked as type of charging process, type of chargers, level of charging, architecture of MG-based charging station and the hierarchical control. Later on, the PVCS is described, which is based on MG concept and some existing infrastructure has been addressed. A literature review about the PVCS has been presented in this chapter and the positioning of this thesis has been identified regarding the literature review and the previous work done in Avenues laboratory.

The next chapter will introduce the PVCS and the driving characteristics of the EV users. First, a Simulink model of the PVCS was developed and then case studies were realized in order to identify the preliminary requirements and feasibility conditions.

Chapitre II. *PV-powered charging station: preliminary requirements and feasibility conditions*

This chapter presents the preliminary requirements and feasibility conditions for a PVCS aiming at increasing PV benefits. Based on a DC MG, the charging station integrates PV sources, stationary storage, and public grid connection. Following the description and simulation validation, PV benefits increase for EVs charging when the park time for EVs is long, the charging mode is slow, and the charging power is variable. This chapter, presented in [77], is constructed as follows: Section II.1 gives an introduction. Section II.2 presents the literature review. Section II.3 describes the charging infrastructures for an electric vehicle. Section II.4 presents the driving characteristics and charging load profiles. Section II.5 represents the PVCS simulation results and discussion. Section II.6 concludes the chapter.

II.1. Introduction

Nowadays, the problems related to electrical energy are emerging worldwide and all countries are facing challenges, whether for its management, operation, production, or even transport. Fossil fuels are the major source of energy production. Therefore, electric-powered vehicles are a promising alternative to fossil-fuel-powered vehicles, in the automotive industry. EVs have been the center of attraction due to their environmental and health benefits.

The charging of EVs will become a serious issue and will increase the burden on the public grid, as EV stock continues to grow and expand. The charging of EVs during the day will increase the peak load, as shown in Figure 1a. However, EVs are considered a flexible load unlike uncontrollable loads; therefore, the charging of EVs can be controlled and shifted to other times to prevent the peak load by implementing a smart charging framework, for example, overnight charging as shown in Figure 23b. However, this can constrain EV users, whose behavior is hard to predict and control.

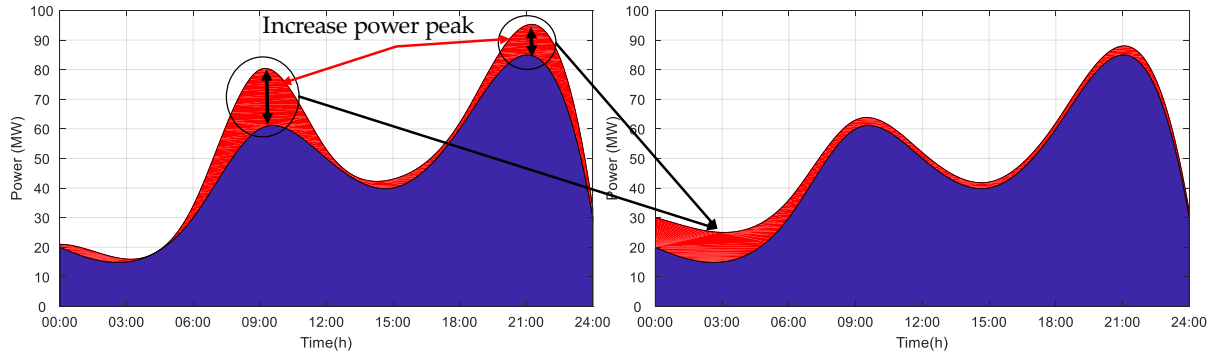

Figure 23: (a) EVs charging and peak load; (b) Shifted EVs charging to overnight.

To overcome this constraint, the EVs can charge with PV energy which is a reliable and effective option, to reduce the burden on the public grid [78]. Thus, while the EVs are being charged with green energy [79], [80], the EV market will be encouraged since EVs contribute to minimizing the impact of transportation on the environment [50], [79], [81].

Different charging/discharging frameworks of EVs exist [82]:

- Uncontrolled charging: the EV starts charging immediately until its battery is fully charged or the EV user unplugs their vehicle [83]. This framework can be expressed as uncoordinated charging or immediate charging where the EV is charged at maximum power with no restrictions [84], [85]. In this framework, there is not any interaction between the EV users and the electrical grid. This is the worst scenario since it charges the EV with the maximum power to be fully charged in the shortest time imposing difficulties on the grid and peak load [86].
- Delayed charging: when the park time (time duration for an EV parked in a station) is longer than the actual required time of charging, therefore, the EV charging can be delayed taking into account the time of use price and can be charged during the low-cost and off-peak energy period [83], [84].
- Average charging: the EV is charged at constant power depending on the park time in which the EV is able to meet the requested SOC or full SOC, where it is not necessary to charge with full power [84]–[86].
- Smart charging: the EV users provide the public grid with information regarding the park time and the requested charge that must be supplied before leaving the station. Therefore, renewable energies are used first to supply the load then the public grid will control and shape the EV charging profiles and minimize the charging costs [83].
- Smart discharging: known as V2G, the EVs act as stationary storage allowing to discharge power back to the public grid [83]. This will improve the electrical grid efficiency and reliability.

Delayed charging can be considered as a smart charging framework, since it changes the charging start time, charging end time, and charging power, yet most importantly delivering the requested energy to the

EV. Additionally, the average charging can be considered as an uncoordinated charging framework, since it starts charging immediately when the EV is plugged-in but with limited power [86]. The delayed charging profile is similar to the uncontrolled charging profile but the peak load is shifted to overnight/dawn (around 5:00 am and 9:00 am). Whereas, in average charging, the profile is flattened instead of having a peak [84].

Uncoordinated charging of EVs may increase the peak load, imposing a heavy burden on the public grid leading to more losses. Therefore, through smart charging or coordinated charging, EVs can be an asset for the grid by helping to increase penetration of renewable energies, balancing the energy system, and improving the efficiency of the system while satisfying EV user demands [87]. Coordinated charging is classified into two types, time coordinated charging and power coordinated charging as in [88]. In time coordinated charging, the number of EVs that can charge is controlled to ensure the total load demand is within the available power for EV charging. Whereas, in power coordinated charging, the power of EV charging is controlled to ensure the total load demand is within the available power for EV charging.

The most important parameters in EV modeling are the charging/discharging rate, initial SOC, battery capacity, charge depleting distance, and user behavior, which is hard to predict in advance. In addition, the arrival time at the charging station, the departure time, and the driving distance of the EV are variables, depending on user habits. They can, however, be assumed and follow probability distribution functions [85], [89]. For this purpose, probability distribution functions are generated to determine the arrival time at the charging station, the departure time, and the driving distance of the EV. Then, the energy needed to fully charge the EV is calculated and the total charging time of the EV is the energy needed to fully charge the EV over the charging rate [85], [89], [90].

II.2. Literature review

Since the EV market is growing vastly, many research studies are expanding, in this field, especially regarding the charging process for EVs. A home-scale EV charging station based on hydrogen has been proposed in [91]. They have compared, environmentally and financially, their scheme with a conventional vehicle, fossil fuel-based, having the same characteristics and with an EV charged directly from the public grid. They have shown that with the EV charged with hydrogen, no fossil fuel is required, it has zero carbon emissions, and the EV charged by hydrogen or electricity is cheaper than oil/petrol over a year. In [92], the minimum size and cost of a charging station for EV fleets has been studied in two urban areas in Europe, as well as the impact of the charging station on the electrical grid in terms of power and energy demand. Their analysis has identified some policies and highlighted that the critical barrier for charging station deployment in urban areas could be the time required to implement charging stations. In [93], the authors have proposed an EV charging control scheme from the grid operator perspective rather than the EV user. They have proposed a method to change indirectly the route of the EV using dynamic pricing to improve the system operation, keep the voltage stable, and meet charging demands. The optimal operation of a DC

MG-based EV charging station using mixed-integer linear programming has been studied in [94]. The operation aimed to optimize the daily operating cost, based on PV production forecast and EV needs. In [95], the authors have studied a bi-level planning model of charging stations, by establishing a travel pattern model based on a Monte Carlo simulation and driving data of EVs. They aimed at satisfying the needs of EV users and minimizing the total social cost. The authors of [96] have designed the aspects and presented the practical implementation of a solar-assisted EV charging station. A smart charging strategy has been presented in [97] for a plug-in EV network that provides different charging options; battery swapping facilities at the charging station, AC level 2 charging, and DC fast charging. The strategy aimed at finding the optimal charging station considering the minimum driving time, charging cost, and charging time. In [98], the authors have evaluated the factors affecting the EV charging demand and predicted the charging demand of various EVs under different circumstances; such factors are driver behavior, electricity pricing, location of charging stations, social characteristics of the EV user, and economic elements. Their results contributed to identifying optimal locations for charging stations to maximize their utilization. The authors of [99] have analyzed competitive interactions for different EV charging stations with renewable energy sources using a game-theoretical analysis. The objective is to maximize the revenue of each EV charging station, subject to physical constraints. Their results have shown that EV charging stations equipped with renewable energy sources decrease the electricity price and increase the revenue of the EV charging station. An EV charging station based on PV sources, stationary storage, diesel generator, and a public grid connection has been implemented in [100]; so it can operate in three modes: grid-connected, islanded operation, and diesel generator set connected. Their test results have proved the capability of the EV charging station under different conditions. In [101], a real-time rule-based algorithm has been proposed for the operation of a DC MG-based EV charging station with imposing charging power limit depending on power availability. They have focused on the management strategy for the EV charging station, highlighting the interaction with EV users. Their results have proved the feasibility of the intelligent management proposed, including EV shedding and EV restoration priority, and its efficiency in considering user choices.

In [102], the authors have proposed an optimization problem to reduce the stress on the grid and to reduce the cost of consumed energy. They have proposed a model predictive to forecast EV's power demand. They have proposed to charge the EVs by PV, storage, and grid instead of directly feeding the EVs from the grid. In [103], the authors have investigated peak load reduction using PV, storage, and a vehicle-to-grid strategy for EVs. They have focused on increasing the capacity of the storage to decrease the grid dependency. The authors of [104] have investigated the charging of EVs using PV energy in the workplace. They have studied the optimal sizing of storage to make the charging station grid-independent. However, these articles did not propose different charging modes for the EVs, they have focused on reducing peak load demand or reducing the cost of energy consumed by the grid rather than increasing the PV benefits for the EV users. Moreover, the energy distribution system and energy distribution for each EV are not depicted in these papers.

However, to the extent of our knowledge, the previously cited references have not discussed the preliminary requirements and feasibility conditions for an EV charging station, while satisfying EV user needs and the factors that can influence their choice to increase PV benefits and lower their charging cost from the public grid.

In previous studies, home charging represents 75% of EV charging time, the longest duration of vehicle dwelling time, and workplace charging represents 14% of EV charging time. These two locations have the largest opportunity for charging [84]. EV users tend to charge their EV based on their convenient time and place rather than what the public grid operators prefer and when the electricity price is cheap to prevent negative impact on the public grid [86]. In this chapter, the goal is to define the preliminary requirements and feasibility conditions for PV-powered EV charging stations in an urban area and to emphasize the importance of a business model that can influence the EV users' behavior.

II.3. Charging infrastructure for electric vehicle

The charging infrastructures rely on the relations between driving needs, charging equipment usage, EV stock, and technical capabilities. Population density, driving range, and charging behavior are specific factors that have direct implications on the geographical location of the EV supply equipment and on the charging rates, for electric low-duty vehicles. Two charging modes, slow and fast charging [105], [106], are presented in this paper, which denotes the charging rate for an EV.

Slow charging is mostly rated at 3 kW, but in reality, it is ranged between 1.8 kW and 6 kW. Charging time depends on the charging rate and the EV energy capacity, thus, a full charge takes 6–12 h for 3 kW. Slow chargers are common for most EVs, they can be found everywhere, e.g., at home, workplace, and public places. EV users tend to charge at home overnight for long charging.

Fast charging is typically rated from 7 kW up to 22 kW (single or three-phase 32A), where charging an EV with 40 kWh capacity takes 4–6 h with 7 kW and 1–2 h with 22 kW. The majority of fast chargers provide AC charging, however, some infrastructures are equipped with 25 kW DC chargers with CHAdeMO connectors. Fast chargers can be found in public places, such as shopping centers, car parks, workplaces, supermarkets, train stations, and airport parking.

The sizing and characteristics of PVCS depend on the PV installation (parking shade or building-integrated PV), solar irradiation potential, stationary storage, and the adopted business model. The viability of well-designed PV-powered EV charging stations depends on social acceptance, PV benefits, and the business model.

Private chargers stand for 90% of global EV chargers in 2019, as profitability, convenience, and various supports and incentives are the main motivations of the universality of private chargers [107]. The preferred locations are home and private workplaces to charge the EV. The infrastructure for home charging is a

compatible electric socket and charger plug, which already exists in homes. Nearly 60% of EV users have access to private chargers in China based on The China EV Charging Infrastructure Promotion Agency recent report published in 2019 [106]. The EVs consume approximately 75% of energy from private charging at home and at the workplace, in the United States, United Kingdom, and the European Union [108].

II.4. Driving characteristics and charging power profiles

People have different attitudes and living styles, and therefore, they differ in their driving patterns, which significantly affects the spatial-temporal distribution of the charging load (e.g., EV battery). However, the EV charging load profiles vary and depend mainly on the type of charging preferences, EV user habits, and energy consumption rates. In [109] the driving data for different users are analyzed in time and space dimensions to understand driving patterns of different populations, grouped by age as a demographic attribute. The daily driving distance is the factor to compare the behavior of different EV users. The U.S. National Household Travel Survey dataset, as in [109], shows the daily driving distance and where the elderly drive for a short distance.

Based on these data, the daily average urban/peri-urban trip can be deduced as 20–40 km. With two driving modes, normal drive with 15 kWh/100 km and eco-drive with 10 kWh/100 km, therefore, the daily energy consumption rate is 3–6 kWh for a normal drive and 2–4 kWh for an eco-drive. Considering the above and an average EV battery, e.g., 50 kWh, Figure 24 shows the required time for 80% of EV's SOC charging (green lines) and 10% of EV's SOC charging (orange lines), depending on power delivered by the terminal and accepted by the EV battery.

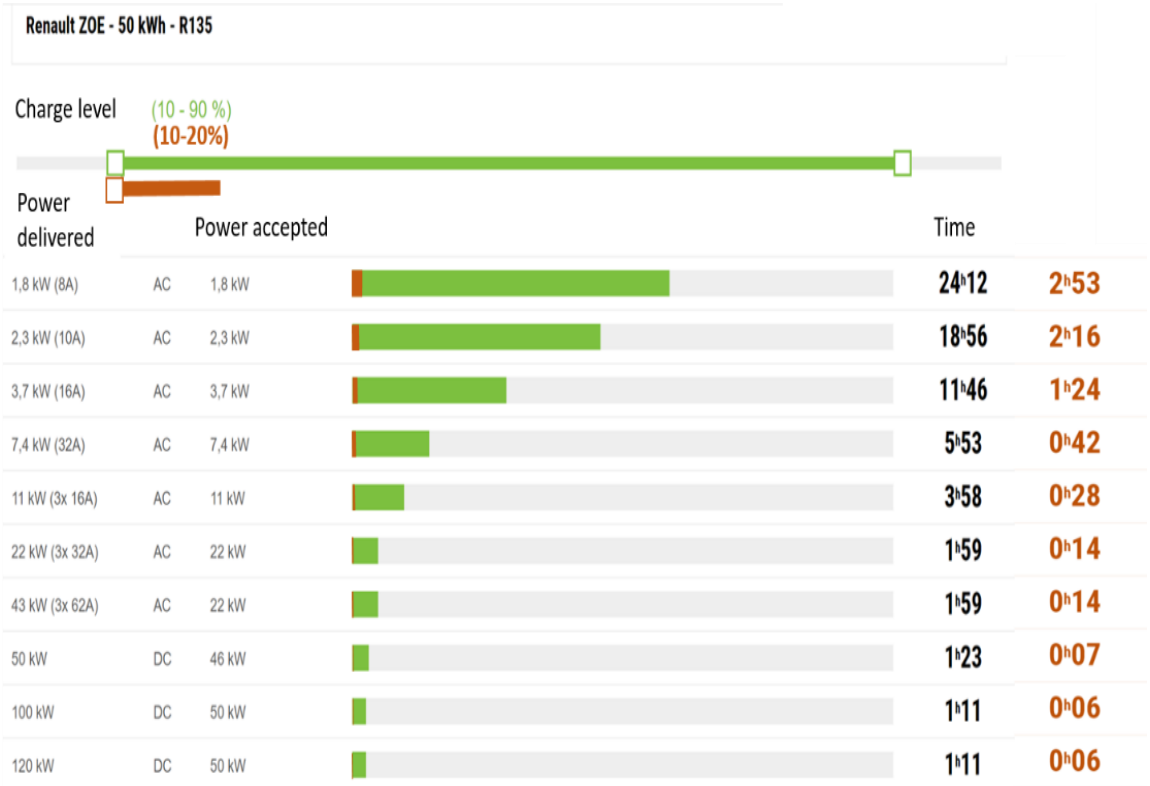

Figure 24: Required time for EV charging based on demand charge and delivered/accepted power.

For delivered and accepted power of 1.8 kW, the time required is more than 24 h to charge 80% and around 3 h to charge 10% of EV battery capacity. On the other hand, the time required is around 1 h to charge 80% and around 6 min to charge 10% of EV battery capacity, for delivered power of 100 kW and accepted power of 50 kW. Thus, a 10% increase of charge, e.g., 5 kWh, is possible with reasonable charging time depending on delivered/accepted power. Therefore, an EV charging load profile must be built to increase PV benefits for PVCS.

II.5. PV-powered charging station power flow management

The PVCS considered in this chapter and illustrated in Figure 25, includes stationary storage and public grid connection and is modeled using MATLAB/Simulink R2015b.

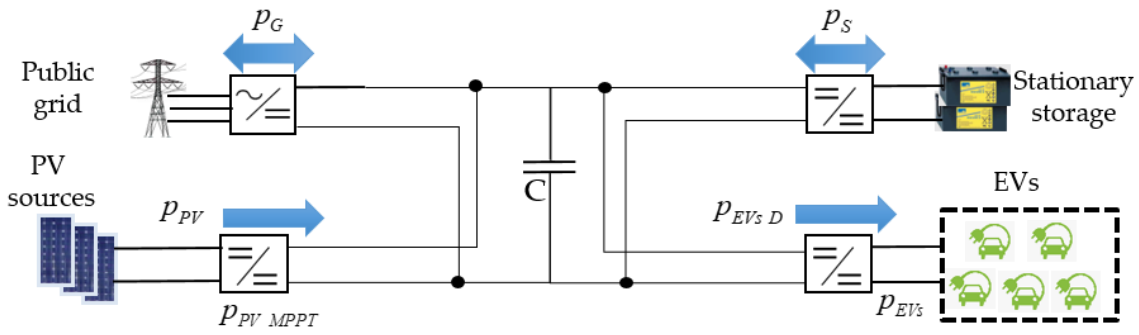

Figure 25: PVCS scheme.

In Figure 25 $p_{PV\ MPPT}$ is the PV power in maximum power point tracking (MPPT) mode, p_{PV} is the PV power, p_G is the public grid power, p_S is the stationary storage power, $p_{EVs\ D}$ the EVs total demand power, and p_{EVs} is the total EVs power.

The public grid can absorb or supply power. The capacitor C represents a common DC bus, where the components of the charging station are coupled through their dedicated converters. PV sources are connected to the DC bus through the DC/DC converter to extract the MPPT power.

The stationary storage is needed to construct the DC MG and it is connected through a reversible DC/DC converter. The DC load, represented by the EVs' batteries, is connected through the DC/DC converter. The public grid connection is required to ensure power at all times and mitigate the power difference between the power production and the load demand; it is connected through a three-phase bidirectional AC/DC converter. The stationary storage is charged by PV sources only and can discharge power to the DC common bus.

The energy management strategy, as shown in Figure 26, follows the priorities: PV is the first energy source to charge EVs, then stationary storage is the second energy source, and the public grid is the last energy source to charge EVs. Stationary storage is charged with excess energy produced by PV sources and the public grid by excessive energy from PV sources when the stationary storage reaches its maximum limits (power or state of charge).

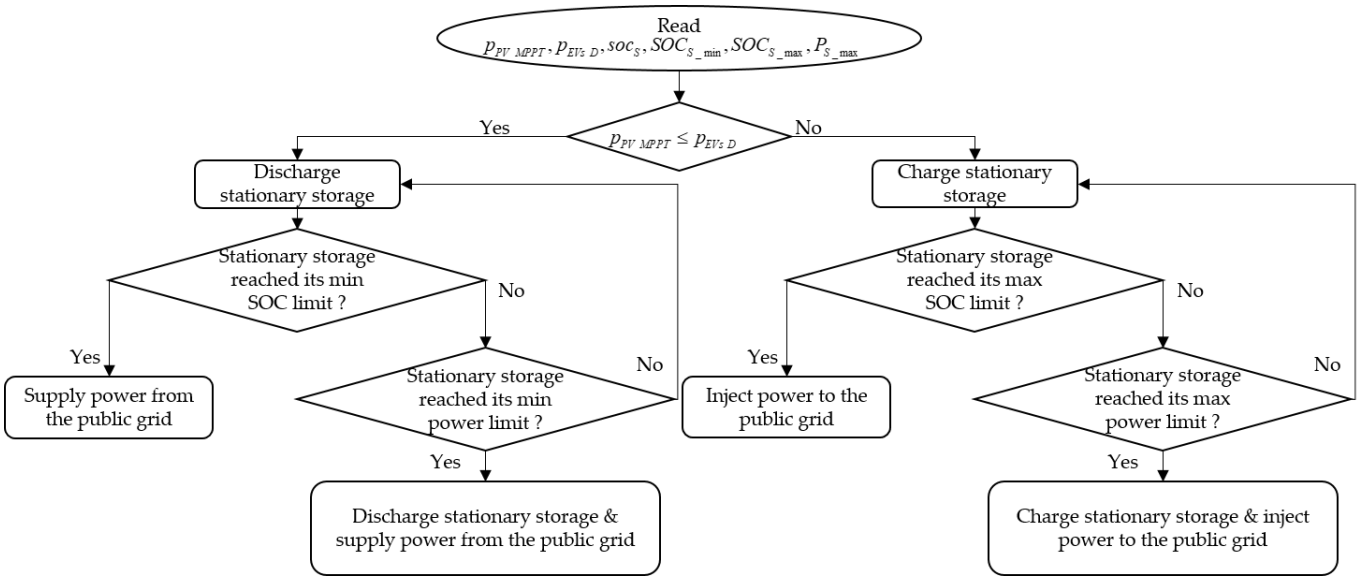

Figure 26: Flowchart for the power flow management of the PVCS.

The design of the PVCS is based on a DC MG, as shown in Figure 25. Therefore, it is required to keep the power balance [110] given by (2.1):

$$p_{PV}(t_i) = p_{EVs}(t_i) + p_S(t_i) + p_G(t_i),\ with\ t_i = \{t_0, t_0 + \Delta t, t_0 + 2\Delta t, ..., t_F\}, \tag{2.1}$$

where t_i, t_0, Δt, and t_F are continuous time, initial time instant, time interval between two samples, and time instant at the end of time operation respectively.

The PV power is calculated in MPPT mode, $p_{PV\ MPPT}$, [111] as given by (2.2) and (2.3):

$$p_{PV\ MPPT}(t_i) = P_{PV\_STC} \cdot \frac{g(t_i)}{1000} \cdot [1 + \gamma \cdot (T_{PV}(t_i) - 25)] \cdot N_{PV}, \tag{2.2}$$

$$T_{PV}(t_i) = T_{amb}(t_i) + g(t_i) \cdot \frac{NOCT - T_{air-test}}{G_{test}}, \tag{2.3}$$

where P_{PV_STC} is the PV power under standard test conditions (STC), g is the solar irradiation, $\gamma = -0.29\%/^{\circ}C$ is the power temperature coefficient, T_{PV} is the PV cell temperature, N_{PV} is the number of PV panels, T_{amb} is the ambient temperature, $NOCT = 41.5°C$ is the nominal operating cell temperature, $T_{air-test} = 20^{\circ}C$ is the fixed air temperature, and $G_{test} = 800W/m^2$ is the fixed solar irradiation for testing.

A simplified state of charge of the stationary storage [112], soc_S, is used as in (4) for its simplicity, where self-discharge and temperature are not taken into account, and the over-charging/discharging protections [35] are expressed by (2.5) and (2.6):

$$soc_S(t_i) = SOC_{S_0} + \frac{1}{3600 \cdot E_{Bat}} \int_{t_0}^{t} p_S(t_i) dt, \tag{2.4}$$

$$SOC_{S\_min} \le soc_S(t_i) \le SOC_{S\_max}, \tag{2.5}$$

$$-P_{S\_max} \le p_S(t_i) \le P_{S\_max}, \tag{2.6}$$

where SOC_{S_0} is the initial soc_S, E_S is the energy capacity (kWh) of the stationary storage, SOC_{S_max}, SOC_{S_min} are soc_S maximum and minimum limits, and P_{S_max} is the stationary storage power limit.

Regarding the EV battery, its dynamic state of charge, soc_{EV_v}, is given by (2.7):

$$soc_{EV_v}(t_{i+1}) = SOC_{EV\_arr_v}(t_i) + \frac{p_{EV_v}(t_i) \cdot \Delta t_i}{E_v} \; \forall t_i \in [t_{arr_v}, t_{dep_v}], \; with \; v = \{1, 2, ..., N_v\}, \tag{2.7}$$

where v is the index of the EV, soc_{EV_v} is the state of charge of v vehicle, $SOC_{EV\_arr_v}$ is arrival state of charge of v vehicle, N_v is the EVs total number, p_{EV_v} is the EV charging power of v vehicle, E_v is the energy capacity of v vehicle, t_{arr_v} and t_{dep_v} are the arrival and departure time of v vehicle respectively.

The EVs are charged using the PV energy, stationary storage energy, and grid energy. The distribution of these energies is calculated as follow by (2.8), (2.9), and (2.10) respectively:

$$E_{PV_v} = \int_{t_{arr_v}}^{t_{dep_v}} p_{PV}(t_i) \cdot \frac{p_{EV_v}(t_i)}{p_{EVs}(t_i)} \, dt_i \;\; \forall t_i \in [t_{arr_v}, \, t_{dep_v}], \tag{2.8}$$

$$E_{S_v} = \int_{t_{arr_v}}^{t_{dep_v}} p_S(t_i) \cdot \frac{p_{EV_v}(t_i)}{p_{EVs}(t_i)} \, dt_i \;\; \forall t_i \in [t_{arr_v}, \, t_{dep_v}], \tag{2.9}$$

$$E_{G_v} = \int_{t_{arr_v}}^{t_{dep_v}} p_G(t_i) \cdot \frac{p_{EV_v}(t_i)}{p_{EVs}(t_i)} \, dt_i \;\; \forall t_i \in [t_{arr_v}, \, t_{dep_v}], \tag{2.10}$$

where E_{PV_v}, E_{S_v}, and E_{G_v} are the PV energy, stationary storage energy, and public grid energy respectively consumed by v vehicle during the charging period.

II.6. PV-powered charging station power flow management simulation results and analyses

This paper presents two case studies for the PVCS: PV parking shade for one private charger and PV parking shade for nine chargers at the workplace. The two cases are simulated under the same solar irradiation profile. Regarding the EVs, lithium-ion batteries were considered and it was assumed they have

the same EV's battery capacity of 50 kWh, while the driving characteristics and charging profiles covered a daily needed charge of 2–6 kWh, as described in Section 3, but they are not exclusive.

For all scenarios, the following assumptions were considered:

- Charging station location is in Compiegne, France, where the yearly average solar irradiation is not very high;
- PV panel is Sunpower SPR X21-345 with 21% efficiency under STC;
- Mounting position is fixed and optimized as follows: slope angle 38° and azimuth angle −2°;
- System loss was estimated at 14% system loss;
- Lithium-ion batteries were considered for the stationary storage and its limits were chosen as 20% and 80% for SOC_{S_min} and SOC_{S_max} respectively.

With the objective of determining preliminary requirements and feasibility conditions of PVCS that may bring some PV benefits, the following subsections present and analyze several scenarios as well as simulation results.

II.6.1. Case 1—private charging station: PV parking shade for one private charger

Case 1 considered a PV parking shade of nine PV panels, i.e., 3.1 kWp, like the example illustrated in Figure 27.

Figure 27: PV parking shade.

In this case, the lowest monthly PV production is in December, as shown in Figure 28, with an average daily of 3.88 kWh. To reach 2–6 kWh, stationary storage and public grid connection are required for complementary energy. PV can either charge directly the EV or the stationary storage during the day and thereafter, the stationary storage can charge the EV during the evening/night. For this case, the public grid power limit was set to 9 kVA, the stationary storage capacity and its power limit were chosen 4 kWh and 5 kW respectively.

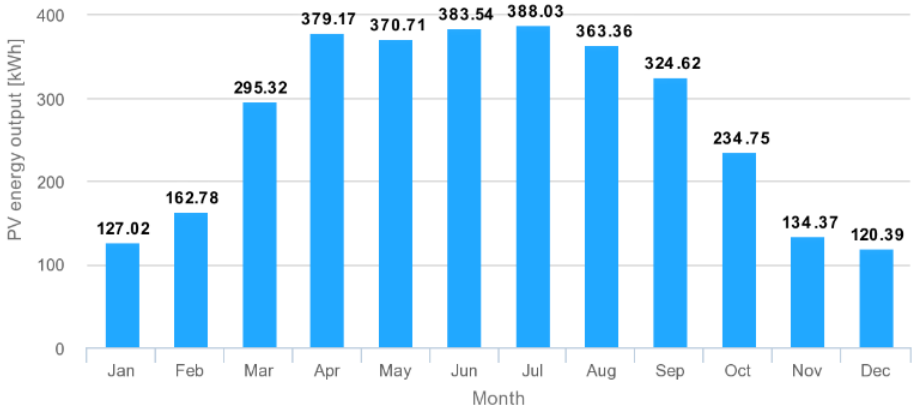

Figure 28: Monthly PV production - Case 1.

Figure 29 shows the solar irradiation g (W/m^2) and $p_{PV\ MPPT}$ for 24 December 2019 in Compiegne.

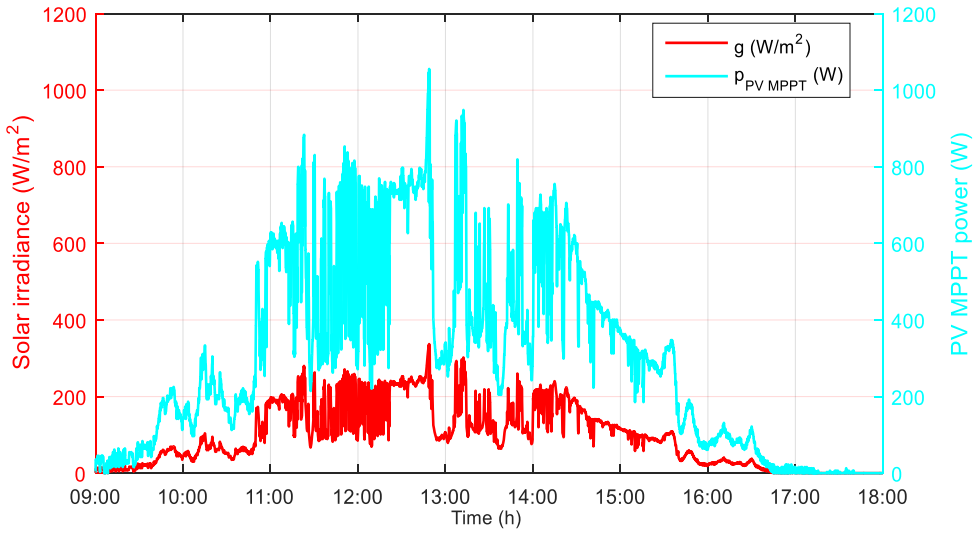

Figure 29: Solar irradiation and PV MPPT power - Case 1.

II.6.1.1. Scenario 1a

The hypotheses for the scenario 1a are shown in Table 2.

Table 2: Hypotheses for Scenario 1a.

EV number	Arrival time	SOC at arrival	Desired SOC at departure	Charging mode/Power
EV1	10:30	60%	68%	Slow/1.8 kW

Figure 30 shows the system power flows and the stationary storage SOC evolution.

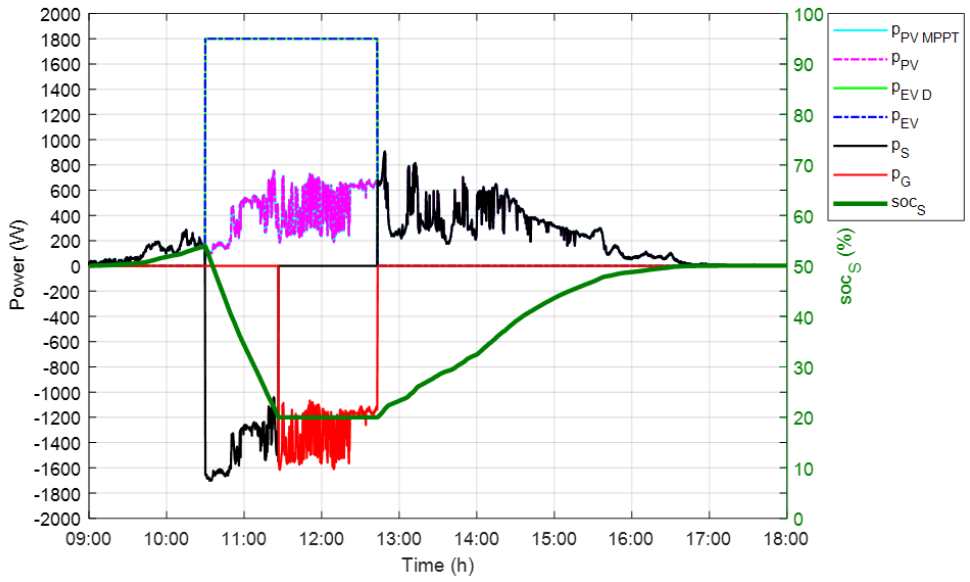

Figure 30: Scenario 1a, system power flows and stationary storage SOC evolution.

As PV power was insufficient to fully charge the EV with a constant power of 1.8 kW, the stationary storage charges the EV until it becomes empty, reaching its capacity limit around 11:30, and then the public grid supplies the EV from 11:30 until EV departure. In this scenario, PV energy is not invested well since it charges the EV for a period and the rest of the time, charges the stationary storage. Therefore, scenario 1b proposes a known parking time for the EV to see the impact of PV energy on the EV charging.

II.6.1.2. Scenario 1b

The hypotheses for scenario 1b is shown in Table 3. The parking time is the time when the EV is in the charging station.

Table 3: Hypotheses for Scenario 1b.

EV number	Arrival time	SOC at arrival	Desired SOC at departure	Park time	Charging mode/Power
EV1	10:30	60%	68%	06:30	Slow/0.615 kW

Based on the hypotheses presented in Table 3, including the parking time as a known variable, the charging power p_{EV_v} is calculated based on (7). Figure 31 shows the system power flows and the stationary storage SOC evolution.

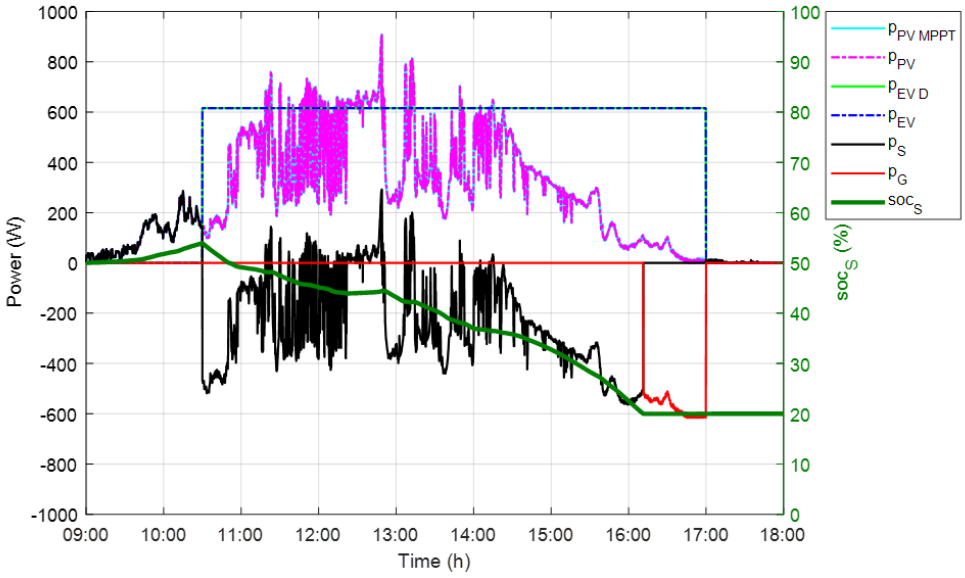

Figure 31: Scenario 1b, system power flows and stationary storage SOC evolution.

As the parking time is known and longer than in scenario 1a, the recharging portion from PV has increased, and the stationary storage lasts longer, preventing its fast discharge, thus the dependency on the public grid has reduced. The stationary storage becomes empty, reaching its capacity limit around 16:10 and then the public grid supplies the EV, from 16:10 until EV departure.

II.6.1.3. Scenario 1a versus scenario 1b

Figure 32 shows the EV charging power and EV SOC evolution for the two scenarios (a) and (b). It shows that the desired SOC at departure for the EV is respected in the two scenarios, while for scenario 1b the charging power is lower than in scenario 1a and the charging period is longer as well.

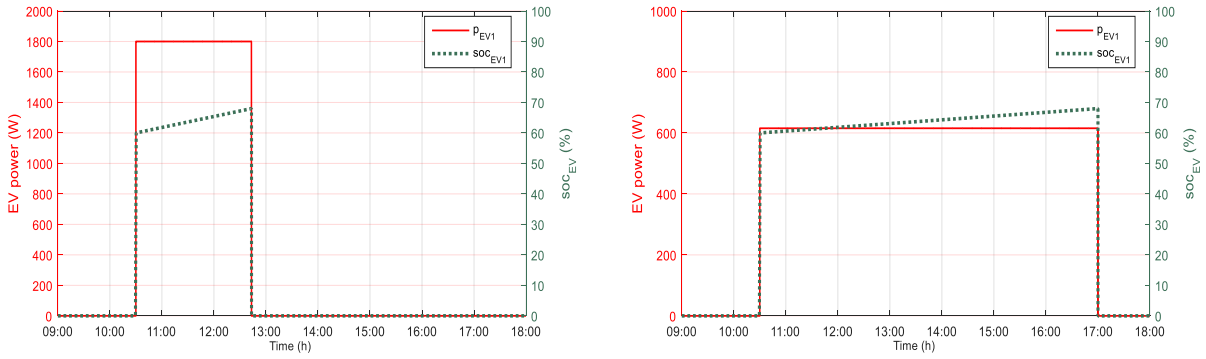

(a) **(b)**

Figure 32: (a) EV charging power and EV SOC evolution for scenario 1a; (b) EV charging power and EV SOC evolution for scenario 1b.

Figure 33 shows a comparison between the two scenarios and the superiority of scenario 1b, where the EV is charged with more than 50% of PV and only 11.50% of public grid power, whereas, in scenario 1a, the EV is charged with 24.50% of PV and more than 40% of public grid power.

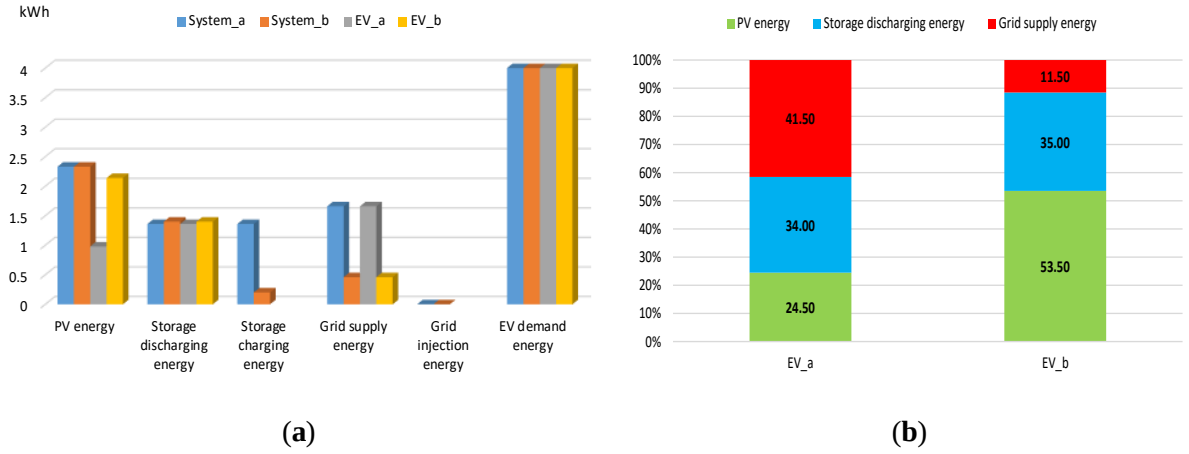

Figure 33: (a) Energy system distribution; (b) EV energy distribution for scenarios 1a and 1b.

In conclusion, when the park time is known and long, PV benefits increase for the EV charging and the dependency on the public grid is reduced.

II.6.2. Case2—publicly accessible charging station: PV parking shade with nine spots and nine chargers

Figure 34 shows the installation of the PV parking shade, which consisted of 84 PV panels in the Innovation Center of the Université de Technologie de Compiègne, i.e., 29.8 kWp.

Figure 34: PV parking shade installation for nine spots.

The stationary storage system has an energy capacity of 17.76 kWh, and the storage power limit was chosen at 7 kW to not exceed the maximum charging power in slow mode. However, no public grid power limit was set in this case. The lowest monthly PV production is in December, as shown in Figure 35, with an average daily of 36.22 kWh. If the nine EVs are connected, then one EV may receive 4.02 kWh, which represents the average energy needed to charge an EV with a daily trip of 20–40 km.

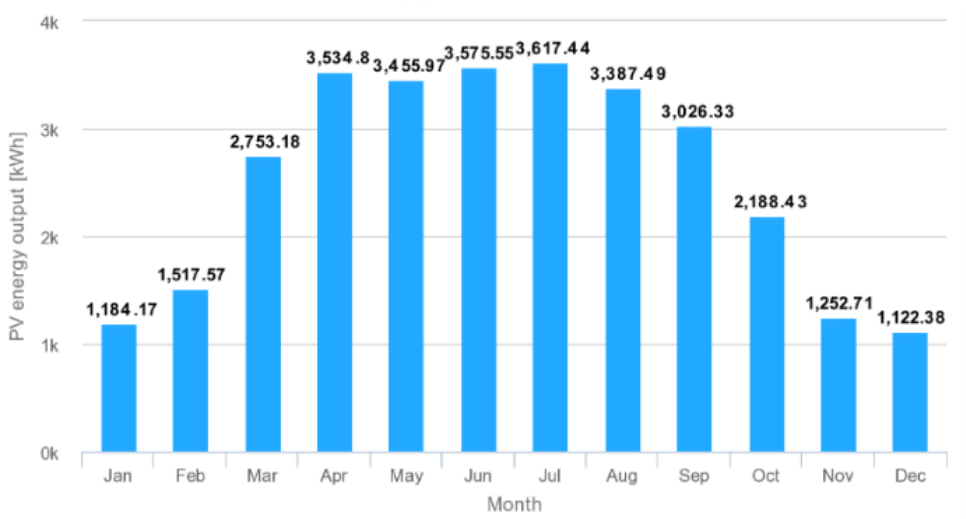

Figure 35: Monthly PV production - Case 2.

Figure 36 shows the solar irradiation g (W/m^2) and $p_{PV\ MPPT}$ for 24 December 2019 in Compiegne.

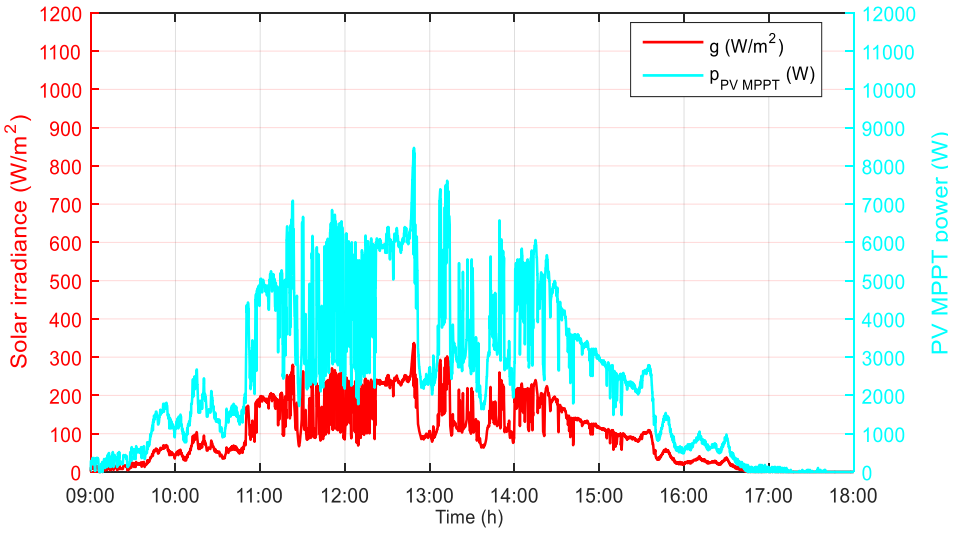

Figure 36: Solar irradiation and PV MPPT power - Case 2.

Different scenarios and simulation results are considered and analyzed to define the preliminary requirements and feasibility conditions for a PV-powered EV charging station with PV benefits increased in the following subsections.

II.6.2.1. Scenario 2a

The hypotheses for the scenario 2a are shown in Table 4.

Table 4: Hypotheses for Scenario 2a.

EV#	Arrival Time	SOC at Arrival	Desired SOC at Departure	Charging Mode/Power
EV1	09:30	65%	75%	Slow/1.8 kW
EV2	10:30	62%	70%	Slow/1.8 kW
EV3	12:00	61%	66%	Slow/1.8 kW
EV4	13:00	58%	66%	Slow/1.8 kW
EV5	14:30	57%	68%	Slow/1.8 kW

The total EVs demand energy is 21 kWh. Figure 37 shows the system power flows and the stationary storage SOC evolution. PV and stationary storage share power to charge the EVs, without the need for the public grid supply. When the PV production is higher than the EV's demand power, PV charges the stationary storage so it can supply further power afterward.

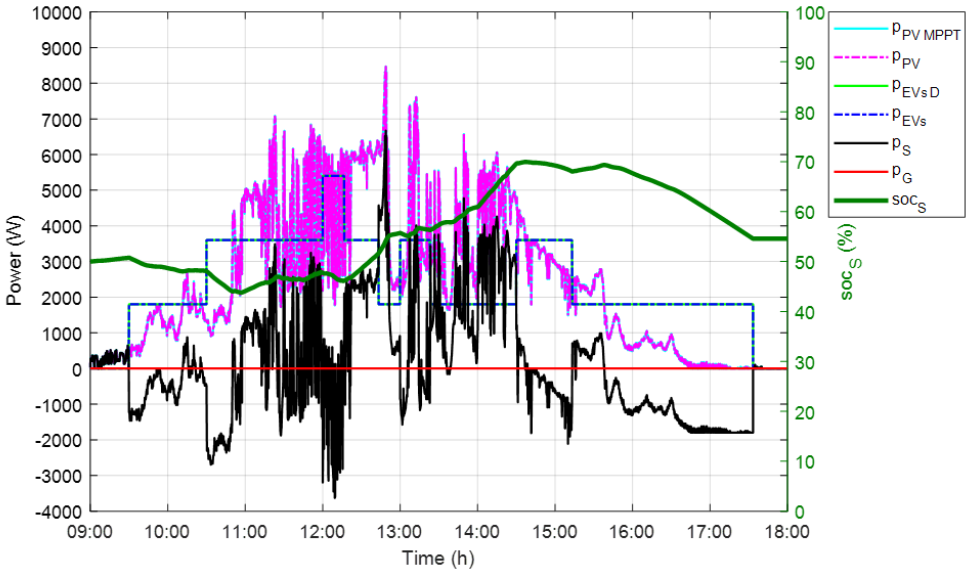

Figure 37: Scenario 2a, system power flows and stationary storage SOC evolution.

II.6.2.2. Scenario 2b

The hypotheses for the scenario 2b are shown in Table 5.

Table 5: Hypotheses for Scenario 2b.

EV#	Arrival time	SOC at arrival	Desired SOC at departure	Departure time	Charging Mode/Power
EV1	09:30	65%	75%	15:00	Slow/0.909 kW
EV2	10:30	62%	70%	16:00	Slow/0.727 kW
EV3	12:00	61%	66%	14:00	Slow/1.25 kW
EV4	13:00	58%	66%	14:30	Slow/2.66 kW
EV5	14:30	57%	68%	17:00	Slow/2.2 kW

Then, the total EVs demand energy is 21 kWh. Figure 38 shows the system power flows and the stationary storage SOC evolution.

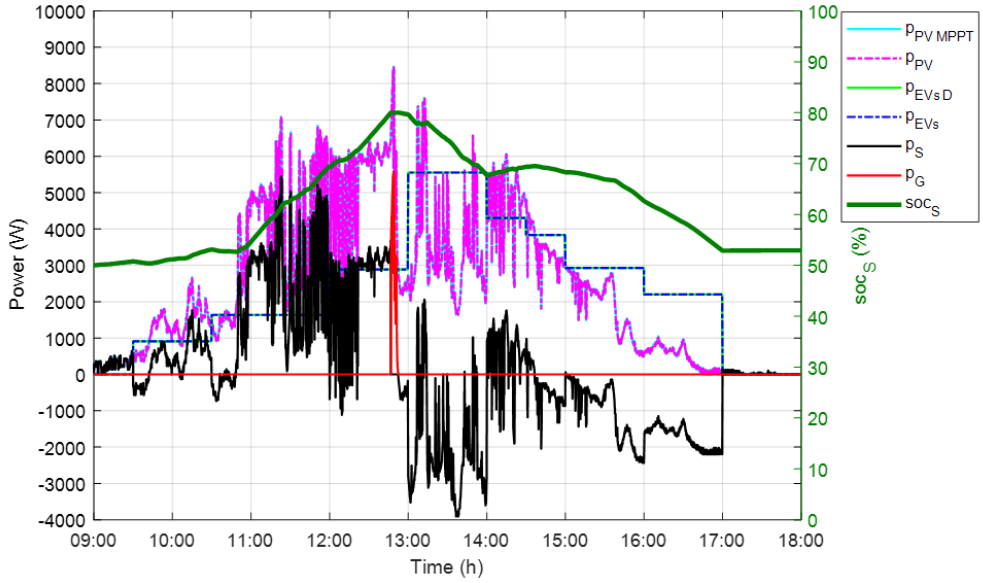

Figure 38: Scenario 2b, system power flows and stationary storage SOC evolution.

PV and stationary storage share power to charge the EVs, without the need for the public grid supply. When the PV production is higher than the EV's demand power, PV charges the stationary storage so it can supply further power afterward. The stationary storage becomes full, reaching its maximum capacity around 12:50, therefore, PV injects power into the public grid. The EVs charging power and EVs SOC evolution for the two scenarios 2a and 2b are shown in Figure 39.

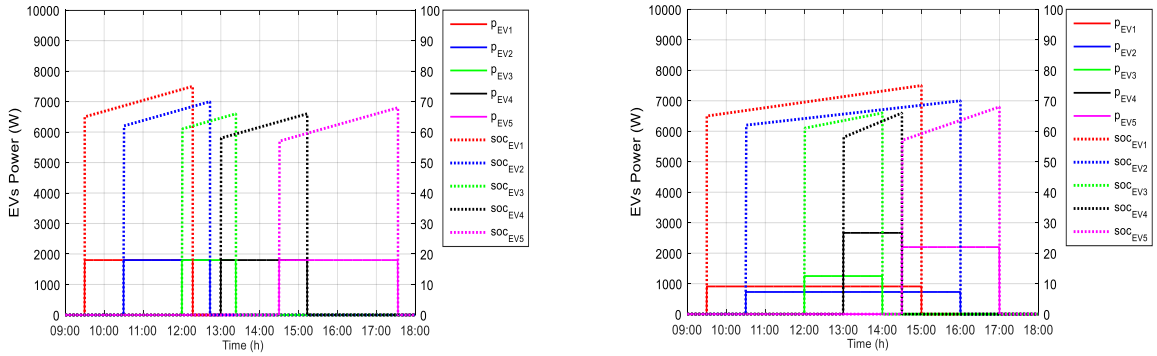

(a) **(b)**

Figure 39: (a) EVs charging power and EVs SOC evolution for Scenario 2a; (b) EVs charging power and EVs SOC evolution for Scenario 2b.

A comparison between the two scenarios is shown in Figure 40. All EVs are charged mainly with PV energy, except for the last EV, i.e., EV5, where it comes in the late afternoon and the PV production is low. As the charging mode is slow for all EVs, the public grid is not required.

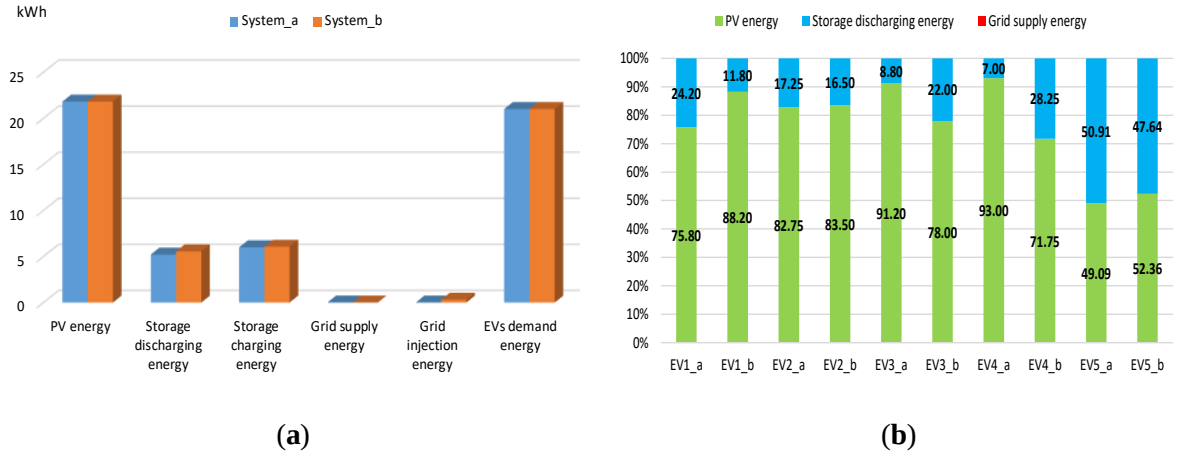

Figure 40: (a) Energy system distribution; (b) EVs energy distribution for Scenarios 2a and 2b.

In conclusion, scenario 2b may be superior to scenario 2a and may improve the PV benefits for the EVs when the park time is known and longer than the time actually needed for charging in scenario 2a. It should be noted that when the park time is longer, some EVs charge simultaneously so the PV production is shared between them thus reducing the portion of PV energy.

These two scenarios are focused on slow charging mode only. The next scenarios will consider slow and fast charging mode and more than 10% of energy charge to analyze the impact of fast charging on the EVs and their PV benefits.

II.6.2.3. Scenario 2c

The hypotheses for the scenario 2c are shown in Table 6.

Table 6: Hypotheses for Scenario 2c.

EV#	Arrival Time	SOC at Arrival	Desired SOC at Departure	Charging Mode/Power
EV1	09:40	64%	75%	Slow/1.8 kW
EV2	10:00	58%	65%	Fast/22 kW
EV3	10:50	57%	63%	Slow/1.8 kW
EV4	14:40	60%	66%	Slow/1.8 kW
EV5	15:00	57%	64%	Fast/22 kW

The total EVs energy demand is 18.50 kWh. Figure 41 shows the system power flows and the stationary storage SOC evolution.

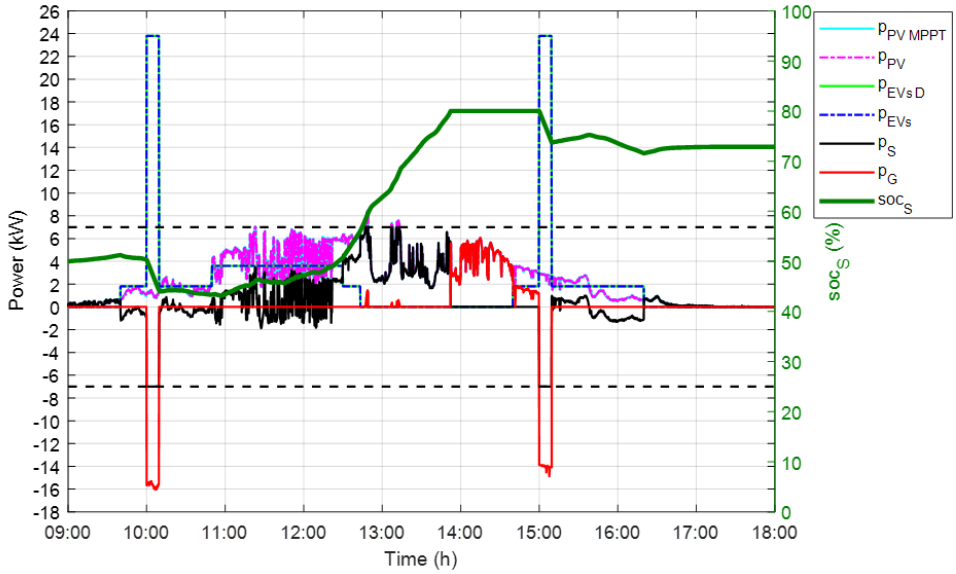

Figure 41: Scenario 2c, system power flows and stationary storage SOC evolution.

PV and stationary storage share power to charge the EVs in slow mode. However, when an EV comes to charge in fast mode and the stationary storage has reached the power limit of 7 kW, the public grid supplies the EVs, at 10:00–10:10 and 15:00–15:10. When the PV production is higher than the EV's power demand, PV charges the stationary storage so it can supply further power afterward. Moreover, PV injects power into the public grid, when the stationary storage reaches its capacity limit, a SOC of 80% around 13:50–15:00, and when it reaches the power limit, around 12:50 and 13:10.

II.6.2.4. Scenario 2d

The hypotheses for the scenario 2d are shown in Table 7.

Table 7: Hypotheses for Scenario 2d.

EV#	Arrival time	SOC at arrival	Desired SOC at departure	Departure time	Charging Mode/Power
EV1	09:40	64%	75%	13:00	Slow/1.65 kW
EV2	10:00	58%	65%	10:25	Fast/8.39 kW
EV3	10:50	57%	63%	11:50	Slow/2.99 kW
EV4	14:40	60%	66%	16:40	Slow/1.49 kW
EV5	15:00	57%	64%	15:20	Fast/10.49 kW

The total EV's energy demand is 18.50 kWh. Figure 42 shows the system power flows and the stationary storage SOC evolution. The stationary storage is charged only by PV energy, therefore, its power must be limited to not exceed the slow charging power of 7 kW.

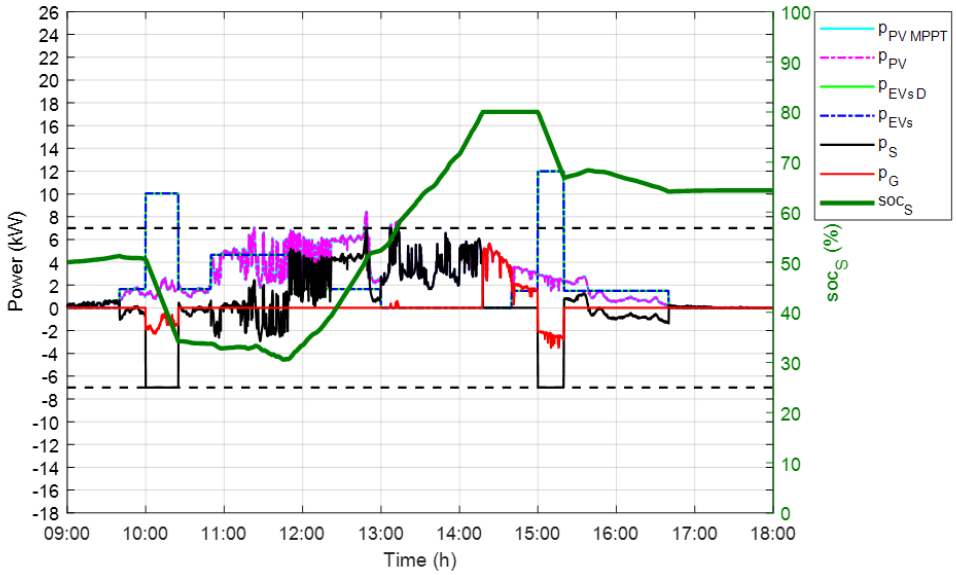

Figure 42: Scenario 2d, system power flows and stationary storage SOC evolution.

PV and stationary storage share power to charge the EVs in slow mode. However, when an EV comes to charge in fast mode and the stationary storage has reached the power limit of 7 kW, the grid supplies the EVs, at 10:00–10:10 and 15:00–15:10. When the PV production is higher than the EV's power demand, PV charges the stationary storage so it can supply further power afterward. Moreover, PV injects power into the grid when stationary storage reaches its capacity limit, SOC of 80% around 14:10–15:00, and when stationary storage reaches the power limit, around 13:10.

The EVs charging power and EVs SOC evolution for the two scenarios 2c and 2d are shown in Figure 43.

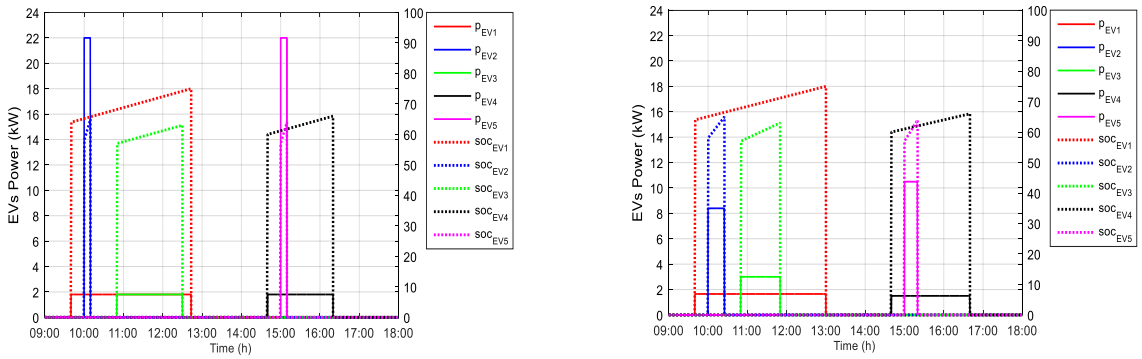

(a) **(b)**

Figure 43: (a) EVs charging power and EVs SOC evolution for Scenario 2c; (b) EVs charging power and EVs SOC evolution for Scenario 2d.

Figure 44 shows a comparison between the two scenarios. All EVs in slow mode are charged mainly with PV energy, except for EV4, where it comes in the late afternoon and the PV production is low. Whereas, EV2 and EV5 in fast mode are charged mainly with the public grid and a small portion with PV. Moreover, EV2 and EV5, since they charge in fast mode, will affect negatively EV1 and EV4 respectively.

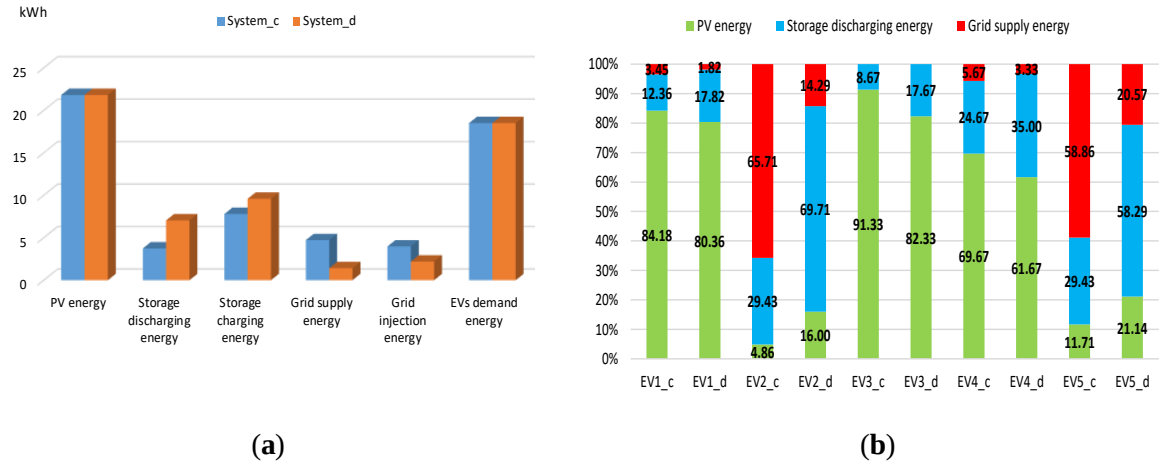

(**a**) (**b**)

Figure 44: (a) Energy system distribution; (b) EVs energy distribution for Scenarios 2c and 2d.

In conclusion, scenario 2d shows that EV2 and EV5 consume more PV energy than in scenario 2c and the public grid dependency has been reduced. This shows that the variable charging power based on time duration availability can improve the PV benefits and the EVs can depend more on PV and less on the public grid. The stationary storage could be emptied quickly, if its power is not limited, since for EVs charging in fast mode their charging power could reach up to 22 kW. Thus, in scenario 2c, EV2 and EV5 charge with a greater percentage of public grid energy. However, since the stationary storage is charged by PV sources only, as mentioned earlier, this could prove the superiority of scenario 2d over scenario 2c, as the PV energy and stationary storage energy combined are higher than scenario 2c, as shown in Figure 22d.

II.6.2.5. Scenario 2e

The hypotheses for scenario 2e are shown in Table 8.

Table 8: Hypotheses for Scenario 2e.

EV#	Arrival time	SOC at arrival	Desired SOC at departure	Charging Mode/Power
EV1	09:40	64%	75%	Slow/1.8 kW
EV2	10:00	58%	100%	Fast/22 kW
EV3	10:50	57%	63%	Slow/1.8 kW
EV4	14:40	60%	66%	Slow/1.8 kW
EV5	15:00	57%	64%	Fast/22 kW

The total EVs demand energy is 36 kWh. Figure 45 shows the system power flows and the stationary storage SOC evolution.

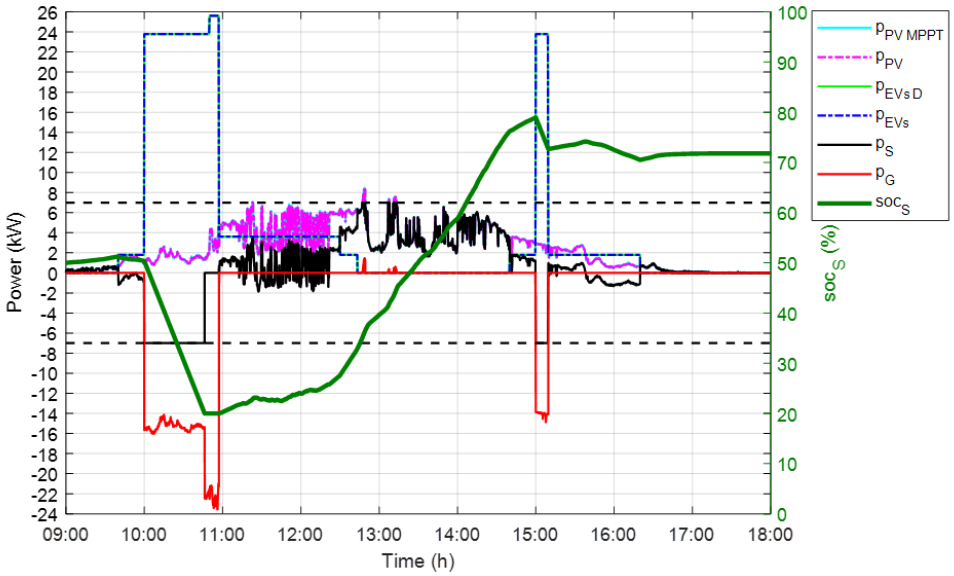

Figure 45: Scenario 2e, system power flows and stationary storage SOC evolution.

PV and stationary storage share power to charge the EVs in slow mode. However, when an EV comes to charge in fast mode and the stationary storage has reached the power limit of 7 kW, the grid supplies the EVs at 10:00–10:50 and 15:00–15:10. At 10:50, the stationary storage has reached its capacity limit, SOC of 20%, so the public grid supplies more power to the EVs since PV production is insufficient. When the PV production is higher than the EV's power demand, PV charges the stationary storage so it can supply further power afterward. Moreover, PV injects power into the grid when stationary storage has reached the power limit, around 12:50 and 13:10.

The EVs charging power and EVs SOC evolution for scenarios 2e is shown in Figure 46.

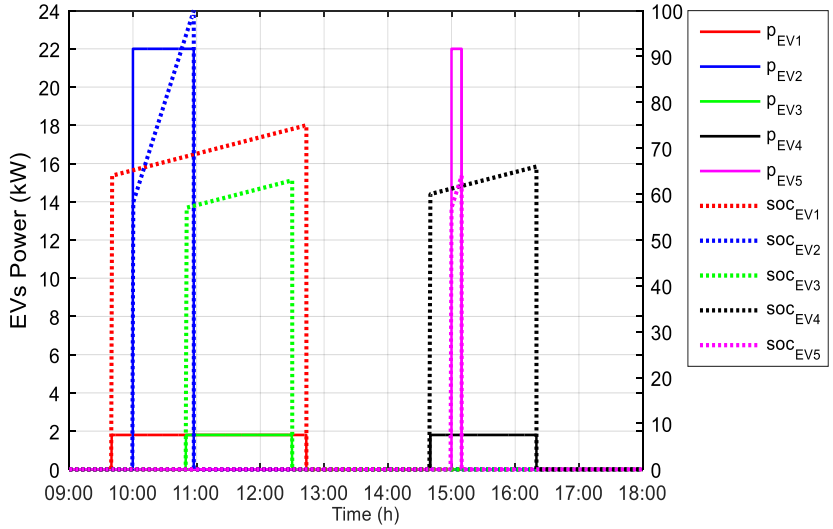

Figure 46: EVs charging power and EVs SOC evolution for Scenario 2e.

Figure 47 shows a comparison between the two scenarios. The difference in scenario 2e with scenario 2c is that EV2 wanted to charge 42% of its battery capacity in fast mode. Therefore, EV2 is charged mainly with the public grid and a small portion with PV. Moreover, EV2 will affect negatively EV1 and EV3 and,

therefore, the PV benefits for EV1 and EV3 have reduced since EV2 charges in fast mode for around 1 h and the three EVs charge simultaneously for a while.

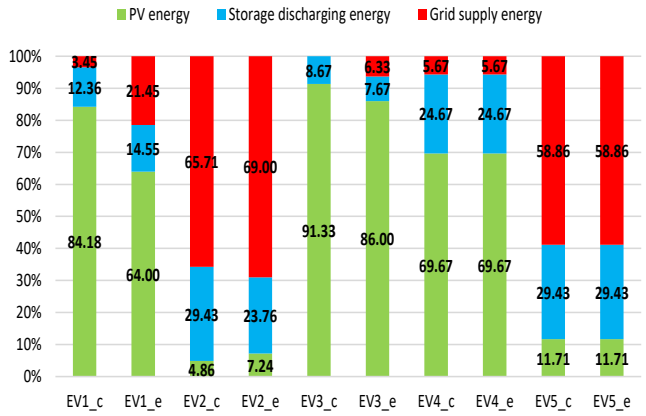

Figure 47: EVs energy distribution for Scenarios 2c and 2e.

In conclusion, scenario 2e shows how fast charging mode affects negatively the other EVs currently in charge and their dependency on the public grid. The stationary storage could be emptied quickly, if its power is not limited, since for EVs charging in fast mode their charging power could reach up to 22 kW. In contrast to scenario 2d, in scenario 2e, EV2 charges with 22 kW, and the requested SOC at departure is 100%. Therefore, the percentage of stationary storage energy remains low. So, the main issue for PV-powered EV charging stations, is how to increase PV penetration for EVs charging? In what conditions? What is the appropriate sizing of the system?

II.6.3. Discussion

In scenario 1, only one EV is charged in slow mode with a private charger. It is shown that the known park time could bring PV benefits and reduce public grid dependency, which will decrease the charging price for the EV user. In Scenario 2, there are five EVs that are charged with public chargers. Regarding scenario 2a versus 2b, where all EVs are charged in slow mode, it is shown that scenario 2b may be superior to scenario 2a, where PV benefits are greater since the park time is known for each EV. Regarding scenario 2c versus 2d, where three EVs are charged in slow mode and two EVs are charged in fast mode, it is shown that EVs charged in fast mode depend mainly on the public grid and stationary storage energy while EVs charged in slow mode depend on PV energy. However, when the park time is known and longer than the time actually needed to charge, PV benefits could increase and public grid dependency could be reduced. Regarding scenario 2e, the same conditions as for scenario 2c are applied but EV2 requests full charge (100%) in fast mode. It is shown that EV2 affects negatively EV1 and EV3 since they coincide some of the time, this will reduce PV benefits for EV1 and EV3. Moreover, EV2 is largely dependent on the public grid and stationary storage energy. The stationary storage power is limited to 7 kW, so it will not be emptied quickly if some EVs want to charge in fast mode.

The simulation results show, for fast charging mode, that EVs depend mainly on public grid energy. Moreover, the public grid energy tariff is dynamic in reality and it is high in peak times. Therefore, EV users who want to charge in fast mode are supposedly willing to pay higher bills. However, knowing that charging the EV in fast mode is costly, EV users will tend to change their behavior and choose to charge in slow mode since it is cheaper. Hence, an economic model is necessary for the PV-powered charging station to optimize the EV charging power, have the best power distribution for energy sources, and have the lowest cost for charging EVs, which is the key factor to influence EV users.

Nevertheless, uncertainties always exist in the real world. However, in the present study, the uncertainty of the demand profile by EVs is always ensured by first, the stationary storage and then by the public grid when there is uncertainty in PV generation to ensure power at all times. Regarding the EV's capacity, it is assumed that all EVs are the same. For EV's SOC and operating schedules, these are taken as hypotheses, where they represent the data and choices of EV users that they choose through the human-system interface. The demand profile of EVs is hard to predict as it depends on various factors (type of user, charging preference, and energy demand). Therefore, the arrival time of the EV, SOC of the EV at arrival, and its requested SOC at departure are assumed arbitrarily but cover many cases.

Finally, to increase PV benefits, the preliminary requirements and feasibility conditions for a PV-powered charging station may be summarized as follows:

Slow charging is characterized by:

- Charging power up to 7 kW;
- Based on PV energy and stationary storage, which is charged by PV sources only;
- Stationary storage should be well designed and its power should be limited;
- EV battery filling up to 6 kWh;
- User acceptance for long and slow charging.

For fast charging mode:

- Charging power from 7 kW up to 22 kW;
- Based on public grid energy;
- Stationary storage should be well designed and its power should be limited at 7 kW;
- User acceptance for high charging price.

Moreover, PV power generation depends on the geographical location and weather conditions, as solar irradiation and the temperature of the PV modules. Proper sizing of the stationary storage is required. A user interface is required to facilitate the interaction between the EV users and the charging station and to take into consideration EV user choices. The parking time, which is the time availability of the EV in the charging station, is better to be known and longer to increase PV benefits. The system limitations could be

presented as low PV energy production throughout the year due to geographical location for the scenarios taken into study. The stationary storage physical limits and proper sizing must be studied and well adjusted to fit the charging station dimensions. However, the public grid can always provide energy or can buy energy when there is an excess of PV production as for case 2 where no grid limits have been imposed.

II.7. Conclusions

This study focuses on the preliminary requirements, feasibility conditions, and business model of PV-powered EV charging stations in an urban area. The simulation results show that the EV charging demand are not constrained; the EV user can charge from slow to fast mode, and no restrictions for EV battery capacity ($10\% < soc_{EV_v} < 100\%$). However, the PV benefits have increased when the average daily urban/peri-urban trip of 20–40 km is considered, with an EV consumption of 10–15 kWh/km, which gives the daily charge needed of 2–6 kWh. In addition, the maximum PV benefits are proved for the daily EV charging instead of weekly and when the park time is known.

For the requirements and feasibility conditions, two charging modes are possible; slow mode up to 7 kW based mainly on PV energy and storage and EV filling capacity up to 6 kWh, fast mode from 7 kW and up to 22 kW based mainly on public grid energy. Proper sizing of the stationary storage system is required and social acceptance relative to longer charging duration for slow mode and higher charging price for fast mode, so a business model is important.

The two main concerns, highlighted in the case studies, are the control-command of the system, i.e., PVCS based on stationary storage and public grid, and the business model that is able to influence consumer behavior through price charging.

Chapitre III. *Intelligent infrastructure for recharging electric vehicles: energy management and cost optimization*

This chapter presents real-time power management including an optimization problem, formulated as MILP, for a MG-based intelligent infrastructure for recharging EVs (IIREVs). The IIREVs is a PVCS as described in the previous chapter, yet called intelligent as the optimization algorithm has the objective to minimize the total energy cost. Simulation results under different meteorological conditions prove the feasibility of the proposed control and its superiority over the storage priority strategy. This chapter, presented in [114], is constructed as follows: Section III.1 gives an introduction. Section III.2 presents the literature review. Section III.3 describes the control system for the IIREVs, then the MILP optimization problem is detailed with the constraints and the objective function. Section III.5 concludes the chapter.

III.1. Introduction

As EV stock continues to grow and expand, thus the charging of EVs will become a serious issue and will increase the burden on the public grid. Uncoordinated charging of EVs during the day will increase the peak load. However, as the preliminary requirements have been identified in the previous chapter in the context of PVCS, therefore, intelligent infrastructure, in which smart charging or optimization algorithms are implemented in the PVCS, could be a key element to manage EV charging and reduce the energy cost. These optimization algorithms are based on predictions, such as PV power prediction and EV charging prediction, and depend on energy tariffs. In this chapter, the optimization algorithm proposed is based only on PV power prediction, and EV charging profiles are communicated in real-time through an interface.

III.2. Literature review

Recent studies have aimed to design MGs for EV charging. The authors of [94] have proposed MILP for an EV charging station integrated into a DC MG to determine the optimal operation planning. They have focused on optimizing the daily operational costs based on forecasting PV production and EV operation. A hybrid optimization problem for energy storage management has been proposed in [115] to minimize the EV charging cost in a PVCS using time-of-use wholesale electricity pricing. The authors in [116] have presented meta-heuristic methods, such as binary particle swarm optimization and binary grey wolf optimization. They have studied an optimal charging coordination strategy for a random arrival of plug-in EVs. A MILP optimization has been proposed in [117] to minimize the MG operation cost by having an

aggregated EV charging station for an islanded MG and in [118] to minimize the energy generation cost and load shedding considering various constraints in a MG that integrates battery EV charging station. A heuristic operation problem has been proposed in [119] for a commercial building MG that integrates EVs and a PV system to study a strategy to acquire data in real-time rather than forecasting EV charging demand or PV production. A genetic algorithm optimization has been studied in [120] for the multi-criteria optimization problem to minimize the charging costs of the EV, maximize the use of PV and the storage device and minimize the degradation of the storage device. A MILP optimization has been proposed in [121] to solve the day-ahead optimization problem and to find the optimal scheduling and operation of a prosumer who owns renewable energy sources and a plugged-in EV. They have used a feed-forward artificial neural network for the weather prediction module in the energy management system. LP and QP optimization problems have been addressed in [122] to minimize the total operating costs for building a MG that integrates a heterogeneous fleet of EVs. A multi-objective scheduling optimization problem based on genetic algorithms has been presented in [123] for MGs including EVs to reduce grid loss and charging costs considering various constraints of the MG sources and EV charging characteristics. The authors in [124] have presented an optimal model for an energy management strategy in a real MG, which integrates a PV system with storage devices, smart buildings and a plug-in EV. They have minimized the total costs of energy consumption by reducing the power supplied from the grid. A robust optimization has been described in [125] and compared with stochastic optimization to minimize the economic and environmental costs of a MG, which integrates PV and EVs. They have proposed a mathematical model to study the uncertainty of EV charging behavior and PV power. A model predictive control has been depicted in [126] using a smart charging strategy that takes into account the future EV charging demand. Their goal is to reduce the peak energy demand for an EV parking lot with PV sources. A multi-objective evolutionary particle swarm optimization problem has been presented in [127] to minimize the costs and the overloading for high demands of grid energy for EV scheduling based on a day-ahead scenario.

A novel convex quadratic objective function has been proposed in [128] to minimize the power loss of a MG in a two-stage optimization method with different penetration levels of plug-in hybrid EVs, studying the behavior of the plug-in hybrid EVs. The authors of [129] have proposed a stochastic planning model as a convex programming problem to optimize the component sizes by minimizing the total cost of the EV charging station considering the uncertainties of PV production, EV charging demand, and different constraints. An improved optimal sizing methodology of a typical residential MG integrating RES and EVs has been proposed in [89] to lower greenhouse gases emissions and minimize the cost. An annealing mutation particle swarm optimization problem has been studied in [130] for MG optimal dispatching to minimize the environmental protection cost and the operation and maintenance cost of a MG in a multi-objective economic dispatch model. A multi-agent particle swarm optimization problem has been addressed in [131] for a grid-connected PV, energy storage system and EV charging station to size the PV and the energy storage system and to set the charging/discharging pattern of the energy storage system. The EV charging station integrates PV, an energy storage system and a grid connection. A machine learning-based

approach has been proposed in [132] for energy management in a MG, taking into account a reconfigurable structure based on remote switching of ties and sectionalizing. They have also proposed a new modified optimization problem based on dragonfly due to the complexity of the problem. An optimal configuration of PVCS in [133] has been studied economically and technically under different solar irradiation profiles in Vietnam using the HOMER Grid program. An optimization model based on a genetic algorithm has been proposed in [134] to optimize the use and scheduling of energy sources for an intelligent hybrid energy system, including EVs and a micro-combined heat and power system. In [135], a bi-level robust optimization has been proposed to optimize the design of an EV charging station with distributed energy resources. The authors of [136] have proposed an optimization model for a battery-swapping station to minimize the charging cost of EVs by optimizing the charging schedule for swapped EV batteries. An optimal charging profile has been proposed in [137] for EVs to minimize battery degradation and extend their lifetime.

A robust optimal power management system has been presented in [138] for a standalone hybrid AC/DC MG. The optimization problem, formulated as a MILP problem, is responsible for supervising the power flow in the hybrid MG, with the objective to satisfy the load demand while maximizing the usage of renewable sources (PV and wind), minimizing the usage of diesel generation, extending battery life, and limiting the utilization of the converter between the AC and DC MGs. An energy management system for a grid-connected MG has been addressed in [139] based on a MILP problem to minimize the total energy cost over 24 h, taking into account load demand, grid tariffs, and renewable energy sources production. A long short-term memory network has been proposed in their paper to deal with the power prediction of the renewable energy sources and the load demand, where each hour, it predicts the profiles for the next 24 h. Then, real-time implementation is enabled by the receding horizon strategy, which is used to minimize the prediction error and gives commands for the first hour; then, each hour, the data are actualized. The proposed strategy in [139] proved its cost reduction in comparison with an offline optimization after conducting simulation tests. In [140], a novel modular modeling method has been described for an energy management system for urban multi-energy sources, including cooling, heating and renewable sources, that allow complex system topologies to be modeled. They have conducted various case studies with different climate conditions and electrical loads. They have also compared the results with a rule-based algorithm to compare the annual cost reductions. In [141], the authors have investigated the technical, economic, and environmental aspects of renewable energy sources in a MG. An equilibrium optimization problem was developed to minimize the operational cost of the MG, which includes PV, wind turbines, and a biomass generator. The simulation results proved the benefits of using the proposed algorithm in reducing operational costs and emissions. An equilibrium optimization problem has been addressed in [142] for optimum PV-storage system integration in a radial distribution network. Multi-objective functions have been addressed to minimize the cost of investment in PV and storage system installations, their cost of operation, the cost of energy not supplied, the power losses in the distribution lines, and the CO_2 emissions by the PV and the grid. The proposed method is compared with various techniques to prove its effectiveness.

In [143], the authors have proposed an equilibrium algorithm to optimally find the lithium-ion battery parameters, formulated as a nonlinear optimization problem. The proposed method was compared with various recent techniques to prove its accuracy; also, it has proved its closeness to the experimental measurement. An artificial hummingbird optimization technique has been presented in [144] to find the unknown parameters of lithium-ion batteries used in EVs. The proposed method is compared with various recent techniques to prove its value and effectiveness. An experimental test was conducted, and the proposed technique had the highest degree of precision among the other techniques.

In the previously cited references, the optimization was performed knowing the EV charging prediction profile for the entire day as day-ahead planning. Knowing an EV charging prediction profile is based on contextual assumptions, e.g., schedule according to the occupancy of a car park or the average EV autonomy, which are not yet validated in the real world. In this work, the objective is to perform a real-time control under optimization for the minimum energy cost and the maximum PV energy for each EV for an IIREVs considering the intermittent and random arrival of the EVs, featuring the EV users' interaction. For the current work, the optimization is performed more realistically at every random arrival of an EV. Therefore, when a new EV comes to the station, the state of charge (soc_S) of the stationary storage and the current state of charge of EVs (soc_{EV_v}) in charge are actualized for suitable optimization.

III.3. Supervisory control system based on real-time power management

Figure 48 shows the DC MG, denoted as IIREVs, and includes PV sources, stationary storage, power grid connection, and EVs as DC loads. Two operation modes exist for the PV sources: MPPT, where maximum power is drawn using a perturb and observe algorithm, and PV power limitation, where PV power is limited in case of a surplus of PV power production [145] because the excess power can no longer be fully injected into the storage and/or into the grid. The stationary storage is a backup source acting as an energy reservoir when there is insufficient PV power to charge the EVs. When there is insufficient PV power to charge the EVs, the grid ensures the security of the system by injecting power to the EVs if the stationary storage has reached its lower limits (empty or minimum discharge power). On the other hand, the DC MG can sell power to the grid by injecting it when there is a surplus of PV power production and the stationary storage has reached its higher limits (full or maximum charging power) [146]. Regarding the EVs charging, they can operate in two modes: fully charging as requested by their users and EV shedding when it is not possible to fully supply the EVs.

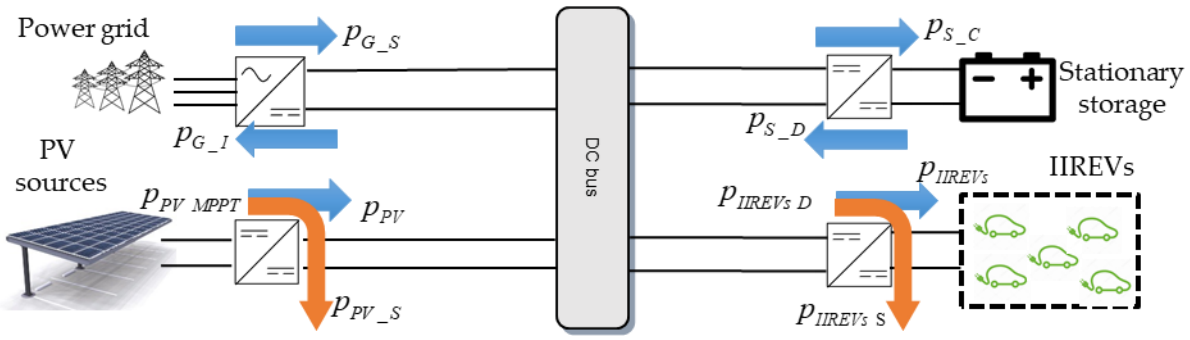

Figure 48: Power flow for the intelligent infrastructure for recharging EVs.

The power flow for IIREVs is shown in Figure 48, where $p_{PV\ MPPT}$ is the PV MPPT power, p_{PV} is the PV power, p_{PV_S} is the PV shed power, p_{G_I} is the grid injection power, p_{G_S} is the grid supply power, p_{S_C} is the stationary storage charging power, p_{S_D} is the stationary storage discharging power, $p_{IIREVs\ D}$ is the IIREVs' total demand power, p_{IIREVs} is the IIREVs' total power, and $p_{IIREVs\ S}$ is the IIREVs' shed power. The components of the IIREVs are coupled through their dedicated converters to the common DC bus. PV sources are connected to the DC bus through the DC/DC converter to draw the MPPT power. The stationary storage is connected through a reversible DC/DC converter. The EVs' batteries, as DC loads, are connected through the DC/DC converter. The grid is connected through a three-phase bidirectional AC/DC converter. It is necessary to ensure power at all times and mitigate the power difference between the power production and the EVs' demand.

The supervisory control system for the IIREVs is shown in Figure 49. The supervisory and control system consists of four layers: prediction, energy cost optimization, operation, and HMI. The design and implementation of the IIREVs' control are based on the interaction between the EV users and DC MG. Energy cost optimization and operation layers form the control block that should keep the power balanced.

The prediction layer is based on weather forecasts. The energy cost optimization is based on the production prediction and consumption profile. They are calculated based on data from the prediction layer and the interaction with the HMI. From the prediction layer, messages from the smart grid about energy system limits, grid power limits, and dynamic energy pricing are communicated. From the interaction with the HMI, the EV users choose their charging mode (M_v), desired state of charge of their EV at departure ($SOC_{EV\_des_v}$) in real-time, and get the state of charge of their EV at arrival ($SOC_{EV\_arr_v}$). MILP optimization is used for the technical-economic dispatching of the MG sources and load. This supervisory control has the advantage of interacting with the EV users to perform the optimization; however, if the choices of the EV users are not feasible, they have to change them in order to perform the optimization [147].

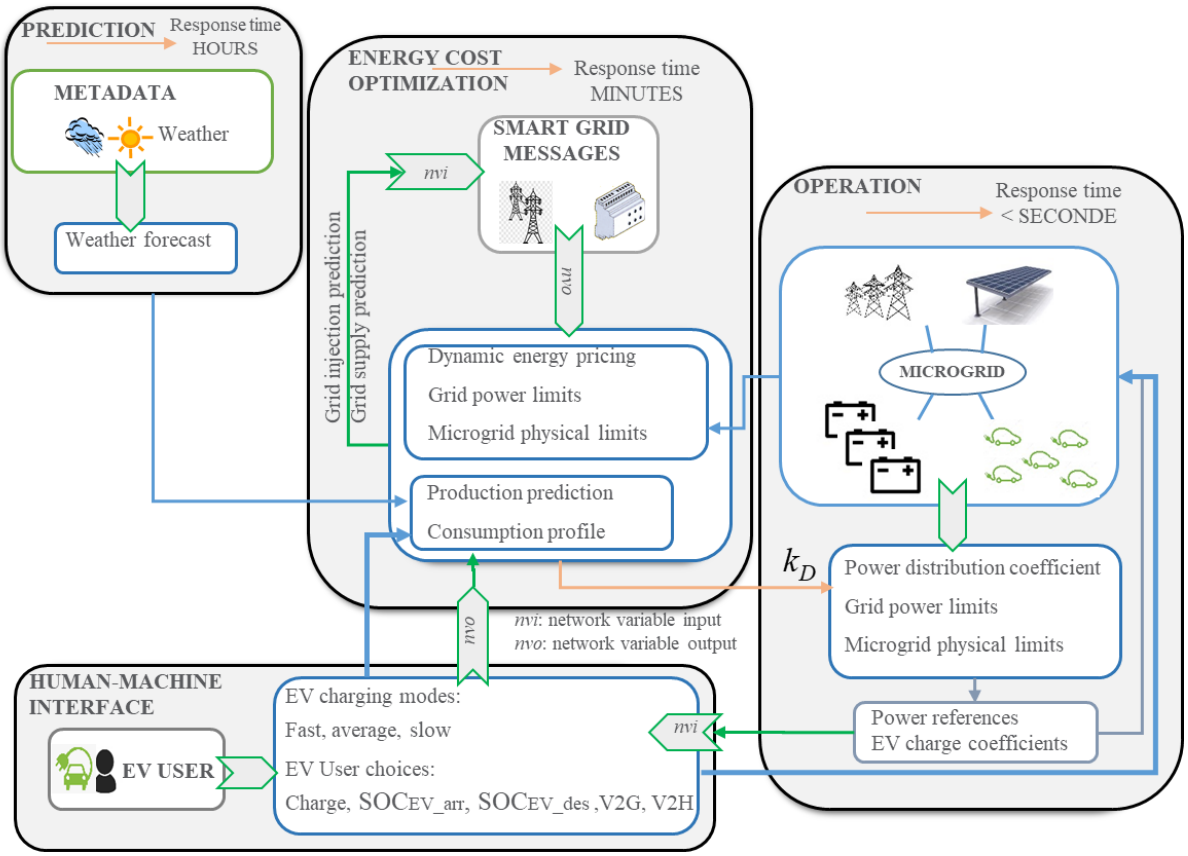

Figure 49: Supervisory control system for the IIREVs.

The main challenge lies in dealing with the discrete events coming from the HMI. The optimization results communicate the predictive control settings to the operation layer and update the smart grid about the power references of the stationary storage and the power grid. The operation layer holds the algorithm that keeps the power balanced with respect to the constraints of the system and its physical limits [148]; it sets the PV power limitation and performs EV shedding if needed.

III.3.1. Prediction layer

Météo France provides hourly predictions allowing the calculation of PV power prediction, which is based on solar irradiation (g) and ambient temperature (T_{amb}) forecast data [149]. The PV power prediction $p_{PV\ MPPT\ pred}$ is calculated in MPPT mode for each time instant t_i [150] as given in following equations (3.1) and (3.2):

$$p_{PV\ MPPT\ pred}(t_i) = P_{PV\_STC} \cdot \frac{g(t_i)}{1000} \cdot [1 + \gamma \cdot (T_{PV}(t_i) - 25)] \cdot N_{PV} \quad (3.1)$$
$$with\ t_i = \{t_0, t_0 + \Delta t, t_0 + 2\Delta t, \ldots, t_F\},$$

$$T_{PV}(t_i) = T_{amb}(t_i) + g(t_i) \cdot \frac{NOCT - T_{air-test}}{G_{test}}, \quad (3.2)$$

where P_{PV_STC} is the PV power under standard test conditions (STC), γ is the power temperature coefficient (−0.29%/°C), T_{PV} is the PV cell temperature, N_{PV} is the number of PV panels, t_0, Δt, and t_F are the initial time instant, time interval between two samples, and time instant at the end of time operation, respectively, $NOCT$ is the nominal operating cell temperature (41 °C), $T_{air-test}$ is the fixed air temperature (20 °C), and G_{test} is the fixed solar irradiation (800 W/m^2).

III.3.2. Human-machine interface

As for the EVs, it is possible to charge them in three modes: slow, average, and fast. All EVs can handle up to fast mode, and they are considered to have the same energy capacity. The HMI allows the EV users to set their $SOC_{EV\_arr_v}$, M_v, and $SOC_{EV\_des_v}$, and, therefore, the estimated charging time, $t_{est\_ch_v}$, which is the required time to reach $SOC_{EV\_des_v}$, is calculated as given in (3.3):

$$t_{est\_ch_v} = \frac{(SOC_{EV\_des_v} - SOC_{EV\_arr_v}) \cdot E}{P_{EV\_max_v}}, \tag{3.3}$$

where E is the EV's battery capacity, and $P_{EV\_max_v}$ is the maximum charging power based on the charging mode set by the EV user. The HMI for the IIREVs is shown in Figure 50 and is well explained in detail in [151].

Figure 50: Human-machine interface for the IIREVs [151].

III.3.3. Energy cost optimization

The energy cost optimization layer interacts with the prediction layer and the HMI to run the optimization. The objective of the optimization is to find the lowest energy cost and the maximum PV power for each EV. The sharing power between the stationary storage and the grid is represented by the power distribution coefficient k_D that is calculated from this layer using the power references obtained in the optimization. The benefits of optimization lie in many aspects: reducing the grid peak power consumption, minimizing the energy cost, deciding which of the stationary storage or grid may have the better contribution, and avoiding EV and PV shedding. The communication with the smart grid informs the system about grid power limits for injection and supply, which are set by a contract with the grid operators, and the energy pricing in real-time. Additionally, stationary storage physical limits should be known. The objective is to minimize the total energy cost with respect to different constraints [149].

The constraints and the objective function are represented in the following subsections.

III.3.3.1. PV sources

The two operation modes for the PV are MPPT and limited power. The PV power that must be shed is noted as p_{PV_S}. Therefore, p_{PV} is calculated [149] as given by (3.4):

$$p_{PV}(t_i) = p_{PV\ MPPT}(t_i) - p_{PV\_S}(t_i), \tag{3.4}$$

where $p_{PV\_S} = 0$ is in MPPT mode; it should not be negative in power limitation mode. Thus, constraints (3.5) and (3.6) are added as follows:

$$p_{PV}(t_i) \geq 0, \tag{3.5}$$

$$0 \leq p_{PV\_S}(t_i) \leq p_{PV\ MPPT}(t_i). \tag{3.6}$$

III.3.3.2. Stationary Storage

The stationary storage, represented by lithium-ion batteries, must be protected from overcharging and over-discharging; thus the maximum storage power P_{S_max} and the maximum and minimum state of charge of the storage SOC_{S_max} and SOC_{S_min} must be respected to extend the storage lifetime [149], [152] as given by (3.7) and (3.8). The simplified state of the charge of the storage soc_S evolution [146] is given by (3.9) for simplicity, where self-discharge and temperature are not considered:

$$-P_{S\_max} \leq p_S(t_i) \leq P_{S\_max}, \tag{3.7}$$

$$SOC_{S\_min} \leq soc_S(t_i) \leq SOC_{S\_max}, \tag{3.8}$$

$$soc_S(t_i) = SOC_{S_0} + \frac{1}{3600 \cdot E_{Bat}} \int_{t_0}^{t} p_S(t_i) dt, \tag{3.9}$$

where SOC_{S_0} is the initial soc_S, and E_{Bat} is the storage energy capacity (kWh) and the storage power $p_S(t_i) = p_{S\_C}(t_i) - p_{S\_D}(t_i)$. The PV power should not be limited if SOC_{S_max} is not reached; this constraint is given by (3.10):

$$p_{PV\_S}(t_i) = 0 \; if \; SOC_S(t_i) < SOC_{S\_max}. \tag{3.10}$$

III.3.3.3. Grid connection

The smart grid transmits messages to IIREVs to respect the maximum grid supply $P_{G\_S\_max}$ and injection $P_{G\_I\_max}$ limits set by the grid [149], as in (3.11), where $p_G(t_i) = p_{G\_I}(t_i) - p_{G\_S}(t_i)$:

$$-P_{G\_S\_max} \leq p_G(t_i) \leq P_{G\_I\_max}. \tag{3.11}$$

III.3.3.4. Electric vehicles

EV batteries, seen as the entire MG's load, can be shed, p_{IIREVs_S}, when $p_{IIREVs\ D}$ cannot be fully supplied due to deficient in power, e.g., the storage and grid have reached their limits [149]. Hence, p_{IIREVs} is given by Equation (3.12), and knowing that p_{IIREVs_S} should not be negative, thus, constraints Equations (3.13) and (3.14) are added as follows:

$$p_{IIREVs}(t_i) = p_{IIREVs\ D}(t_i) - p_{IIREVs\ S}(t_i), \tag{3.12}$$

$$p_{IIREVs}(t_i) \geq 0, \tag{3.13}$$

$$0 \leq p_{IIREVs\_S}(t_i) \leq p_{IIREVs\ D}(t_i). \tag{3.14}$$

No PV shedding power is required when PV power can be fully used, and no EV shedding power is imposed when EVs can be fully charged. Thus, the constraints of Equations (3.15) and (3.16) must be respected.

$$if \; p_{PV\ MPPT}(t_i) \geq p_{IIREVs\ D}(t_i) \; then \begin{cases} p_{IIREVs\ S}(t_i) = 0 \\ p_G(t_i) \geq 0 \\ p_S(t_i) \geq 0 \end{cases}, \tag{3.15}$$

$$if \; p_{PV\ MPPT}(t_i) \leq p_{IIREVs\ D}(t_i) \; then \begin{cases} p_{PV\_S}(t_i) = 0 \\ p_G(t_i) \leq 0 \\ p_S(t_i) \leq 0 \end{cases}. \tag{3.16}$$

The EV users can select their charging mode and other choices that are expressed in the IIREVs' interface. The following EV constraints given in (3.17)–(3.31) represent the EV users' interaction:

(a) EV charging mode:

$$if\ M_v = 1\ then\ 0 \le p_{EV_v}(t_i) \le P_{EV\_fast\_max}\ \forall t_i \in [t_{arr_v}, t_{dep_v}] \quad with\ v = \{1,2,...,N_v\}, \tag{3.17}$$

$$if\ M_v = 2\ then\ 0 \le p_{EV_v}(t_i) \le P_{EV\_aver\_max}\ \forall t_i \in [t_{arr_v}, t_{dep_v}], \tag{3.18}$$

$$if\ M_v = 3\ then\ 0 \le p_{EV_v}(t_i) \le P_{EV\_slow\_max}\ \forall t_i \in [t_{arr_v}, t_{dep_v}], \tag{3.19}$$

$$p_{EV_v}(t_i) = 0\ \forall t_i \notin [t_{arr_v}, t_{dep_v}], \tag{3.20}$$

where v is the index of the EV, p_{EV_v} is the EV charging power of v vehicle, t_{arr_v} and are the arrival and departure time of v vehicle, respectively, and N_v is t_{dep_v} the total number of EVs.

(b) Total EV charging power:

$$p_{IIREVs\ D}(t_i) = \sum_{v}^{N_v} p_{EV_v}(t_i)\ \forall t_i \in [t_{arr_v}, t_{dep_v}]. \tag{3.21}$$

(c) EV state of charge:

$$SOC_{EV\_min} \le soc_{EV_v}(t_i) \le SOC_{EV\_max}\ \forall t_i \in [t_{arr_v}, t_{dep_v}], \tag{3.22}$$

$$soc_{EV_v}(t_i) = 0\ \forall t_i \notin [t_{arr_v}, t_{dep_v}], \tag{3.23}$$

$$soc_{EV_v}(t_i) = SOC_{EV\_arr_v}(t_i)\ \forall t_i = t_{arr_v}, \tag{3.24}$$

$$SOC_{EV\_arr_v}(t_i) \ge SOC_{EV\_min}\ \forall t_i = t_{arr_v}, \tag{3.25}$$

$$soc_{EV_v}(t_i) \ge SOC_{EV\_arr_v}(t_i)\ \forall t_i \in [t_{arr_v}, t_{dep_v}], \tag{3.26}$$

$$SOC_{EV\_dep_v}(t_i) \le SOC_{EV\_des_v}(t_i)\ \forall t_i = t_{dep_v}, \tag{3.27}$$

$$soc_{EV_v}(t_{i+1}) = soc_{EV\_arr_v}(t_i) + \frac{p_{EV_v}(t_i).\Delta t_i}{E}\ \forall t_i \in [t_{arr_v}, t_{dep_v}], \tag{3.28}$$

$$SOC_{EV\_dep_v}(t_i) = soc_{EV_v}(t_i)\ \forall t_i = t_{dep_v}, \tag{3.29}$$

where SOC_{EV_v} is the state of charge of v vehicle, SOC_{EV_min}, SOC_{EV_max}, and $SOC_{EV\_dep_v}$ are the minimum, maximum, and departure state of charge of v vehicle, respectively;

(d) Acceptance criteria:

The estimated charging time of the EV set by the user is t_{ch_v}, given by (3.30).

$$t_{ch_v} = t_{dep_v} - t_{arr_v}, \tag{3.30}$$

$$\frac{(SOC_{EV\_des_v} - SOC_{EV\_arr_v}(t_i)).E}{p_{EV_v}} \le t_{ch_v} \ \forall t_i \in [t_{arr_v}, t_{dep_v}]. \tag{3.31}$$

If the constraints defined by (3.30) and (3.31) are not qualified, then the EV user must change their choices, e.g., estimated charging time and/or desired soc of EV at the departure time and charging mode. It is worth mentioning that $t_{est\_ch_v}$ is the minimum charging time imposed by the IIREVs, which is calculated based on the choices of the EV user. t_{ch_v} is the time of the EV spent at the IIREVs, which is set by its user. Therefore, t_{ch_v} should be equal to or greater than $t_{est\_ch_v}$. The dynamic soc evolution of v vehicle, SOC_{EV_v}, is given by (3.28).

III.3.3.5. Power balancing

All power signs are assigned positives, and the physical law of power balancing [149] can be given by (3.32):

$$p_{PV}(t_i) + p_{S\_D}(t_i) + p_{G\_S}(t_i) = p_{IIREVs}(t_i) + p_{S\_C}(t_i) + p_{G\_I}(t_i). \tag{3.32}$$

As previously noted, k_D is the coefficient representing the sharing power between the stationary storage and the grid, given by (3.33):

$$k_D(t_i) = \frac{p_{S\_C}(t_i) + p_{S\_D}(t_i)}{p_{S\_C}(t_i) + p_{S\_D}(t_i) + p_{G\_I}(t_i) + p_{G\_S}(t_i)}. \tag{3.33}$$

III.3.3.6. Objective function

The total energy cost, C_{total}, takes into account the cost of the supplied power from the grid, the profit of injected power into the grid, the cost of the storage degradation when operating, the penalty cost if the EV at departure has not reached its desired SOC, and the cost of the PV shedding power, which represents the PV power that has not taken advantage of it. Therefore, the objective function is to minimize C_{total}, given by Equations (3.34)–(3.38):

$$C_{total} = C_G + C_S + C_{PVS} + C_{EV\_penalty}, \tag{3.34}$$

$$C_G = \sum_{t_i=t_0}^{t_F} [c_G(t_i) \cdot \Delta t \cdot (-p_{G\_I}(t_i) + p_{G\_S}(t_i))]$$
$$c_G(t_i) = \begin{cases} c_{G\_NH} & \text{for } t \in \text{normal hours} \\ c_{G\_PH} & \text{for } t \in \text{peak hours} \end{cases}, \quad (3.35)$$

$$C_S = \sum_{t_i=t_0}^{t_F} [c_S(t_i) \cdot \Delta t \cdot (p_{S\_C}(t_i) + p_{S\_D}(t_i))], \quad (3.36)$$

$$C_{PVS} = \sum_{t_i=t_0}^{t_F} [c_{PVS}(t_i) \cdot \Delta t \cdot p_{PVS}(t_i)], \quad (3.37)$$

$$C_{EV\_penalty} = \sum_{v}^{N_v} [c_{EV\_p} \cdot (SOC_{EV\_des_v} - SOC_{EV\_dep_v}) \cdot E], \quad (3.38)$$

where C_G, C_S, C_{PVS}, and $C_{EV\_penalty}$ are the grid, storage, PV shedding energy costs, and EV penalty cost, respectively, and c_G, c_S, c_{PVS}, and c_{EV_p} are the grid, storage, PV shedding energy tariffs, and EV penalty tariff, respectively. Lastly, the final optimization problem is given by (3.39):

$$
\begin{aligned}
&\textit{min } C_{total} = C_G + C_S + C_{PVS} + C_{EV\_penalty} \\
&\textit{with respect to:} \\
&\begin{cases}
p_{PV}(t_i) + p_{S\_D}(t_i) + p_{G\_S}(t_i) = p_{S\_C}(t_i) + p_{G\_I}(t_i) + p_{IIREVs}(t_i) \\
p_S(t_i) = p_{S\_C}(t_i) - p_{S\_D}(t_i) \\
p_G(t_i) = p_{G\_I}(t_i) - p_{G\_S}(t_i) \\
p_{PV}(t_i) = p_{PV\_MPPT}(t_i) - p_{PV\_S}(t_i) \\
p_{IIREVs}(t_i) = p_{IIREVs\ D}(t_i) - p_{IIREVs\ S}(t_i) \\
\textit{if } p_{PV\_MPPT}(t_i) \geq p_{IIREVs\ D}(t_i) \ \textit{ then } \begin{cases} p_{IIREVs\ S}(t_i) = 0 \\ p_G(t_i) \geq 0 \\ p_S(t_i) \geq 0 \end{cases} \\
\textit{if } p_{PV\_MPPT}(t_i) \leq p_{IIREVs\ D}(t_i) \textit{ then } \begin{cases} p_{PV\_S}(t_i) = 0 \\ p_G(t_i) \leq 0 \\ p_S(t_i) \leq 0 \end{cases} \\
SOC_{S\_\min} \leq soc_S(t_i) \leq SOC_{S\_\max} \\
soc_S(t_i) = SOC_{S_0} + \dfrac{1}{3600 \times E_{Bat}} \int_{t_0}^{t} p_S(t_i) \Delta t \\
p_{PV}(t_i) \geq 0 \\
p_{IIREVs}(t_i) \geq 0 \\
0 \leq p_{IIREVs\ S}(t_i) \leq p_{IIREVs\ D}(t_i) \\
0 \leq p_{PV\_S}(t_i) \leq p_{PV\_MPPT}(t_i) \\
-P_{G\_S\_\max} \leq p_G(t_i) \leq P_{G\_I\_\max} \\
-P_{S\_\max} \leq p_S(t_i) \leq P_{S\_\max} \\
p_{PV\_S}(t_i) = 0 \textit{ if } SOC_S(t_i) \leq SOC_{S\_\max} \\
\textit{if } M_v = 1 \textit{ then } 0 \leq p_{EV_v}(t_i) \leq P_{EV\_fast\_\max} \ \forall t_i \in [t_{arr_v}, t_{dep_v}] \\
\textit{if } M_v = 2 \textit{ then } 0 \leq p_{EV_v}(t_i) \leq P_{EV\_aver\_\max} \ \forall t_i \in [t_{arr_v}, t_{dep_v}] \\
\textit{if } M_v = 3 \textit{ then } 0 \leq p_{EV_v}(t_i) \leq P_{EV\_slow\_\max} \ \forall t_i \in [t_{arr_v}, t_{dep_v}] \\
p_{EV_v}(t_i) = 0 \ \forall t_i \notin [t_{arr_v}, t_{dep_v}] \\
p_{IIREVs\ D}(t_i) = \sum_{v}^{N_v} p_{EV_v}(t_i) \ \forall t_i \in [t_{arr_v}, t_{dep_v}] \\
SOC_{EV\_\min} \leq soc_{EV_v}(t_i) \leq SOC_{EV\_\max} \ \forall t_i \in [t_{arr_v}, t_{dep_v}] \\
soc_{EV_v}(t_i) = 0 \ \forall t_i \notin [t_{arr_v}, t_{dep_v}] \\
soc_{EV_v}(t_i) = SOC_{EV\_arr_v}(t_i) \ \forall t_i = t_{arr_v} \\
SOC_{EV\_arr_v}(t_i) \geq SOC_{EV\_\min} \ \forall t_i = t_{arr_v} \\
soc_{EV_v}(t_i) \geq SOC_{EV\_arr_v}(t_i) \ \forall t_i \in [t_{arr_v}, t_{dep_v}] \\
SOC_{EV\_dep_v}(t_i) \leq SOC_{EV\_des_v} \ \forall t_i = t_{dep_v} \\
soc_{EV_v}(t_{i+1}) = SOC_{EV\_arr_v}(t_i) + \dfrac{p_{EV_v}(t_i) \cdot \Delta t}{E} \ \forall t_i \in [t_{arr_v}, t_{dep_v}] \\
SOC_{EV\_dep_v}(t_i) = soc_{EV_v}(t_i) \ \forall t_i = t_{dep_v} \\
t_{ch_v} = t_{dep_v} - t_{arr_v} \\
\dfrac{(SOC_{EV\_des_v} - SOC_{EV\_arr_v}(t_i)) \cdot E}{p_{EV_v}(t_i)} \leq t_{ch_v} \ \forall t_i \in [t_{arr_v}, t_{dep_v}] \\
t_i = \{t_0, t_0 + \Delta t, t_0 + 2\Delta t, ..., t_F\} \\
v = \{1, 2, ..., N_v\}
\end{cases}
\end{aligned}
\tag{3.39}
$$

The decision variables in this optimization problem are p_{EV_v}, $p_{IIREVs\,S}$, p_G, p_{PV_S}, p_S, soc_S, and soc_{EV_v}, in which they are continuous variables. As the decision variables are continuous and the constraints are linear, therefore, the optimization problem as MILP over any other optimization techniques [153].

III.3.4. Operation layer

The energy optimization layer finds the optimal power flow of the sources and the EVs based on $p_{PV\ MPPT\ pred}$ and $p_{IIREVs\,D}$. The coefficient k_D is calculated based on the optimized power flow obtained by CPLEX [154]. This coefficient controls the operational layer for the IIREVs in real-time operation. The advantage of k_D is balancing the power flows, coupling the energy management easily while respecting all constraints [149].

The operational layer must consider optimized power flow in real operating conditions, $p_{PV\ MPPT}$ and $p_{IIREVs\,D}$. In addition, the operation management must ensure robustness and withstand uncertainties in the forecast data. Then, this layer calculates the power references and performs PV shedding or EV shedding when necessary. The actual operating conditions lead to a reference power p_{ref} to stabilize the DC bus voltage, defined by (3.40) and (3.41):

$$p_{ref}(t_i) = p_{PV\ MPPT}(t_i) - p_{IIREVs\,D}(t_i) - C_P(V_{ref} - v_{DC\,bus}), \tag{3.40}$$

$$p_{ref}(t_i) = p_{G\_ref}(t_i) + p_{S\_ref}(t_i), \tag{3.41}$$

where C_P, V_{ref} and $v_{DC\,bus}$ are the proportional controller gain, reference voltage, and the actual voltage of the DC bus, respectively. The stationary storage power reference can be calculated as in (3.42):

$$p_{S\_ref}(t_i) = k_D(t_i) \cdot p_{ref}(t_i), \tag{3.42}$$

where k_D is defined in the interval [0, 1].

The grid power reference p_{G_ref} is calculated taking into account the stationary storage physical limit, which means $p_{S\_ref} = 0$ if the storage reaches its maximum $SOC_{S\_\max}$ or minimum $SOC_{S\_\min}$ limits or its maximum power $P_{S\_\max}$, and the grid power reference becomes $p_{G\_ref} = p_{ref}$. Figure 51 shows the control algorithm of the power balancing strategy for the IIREVs.

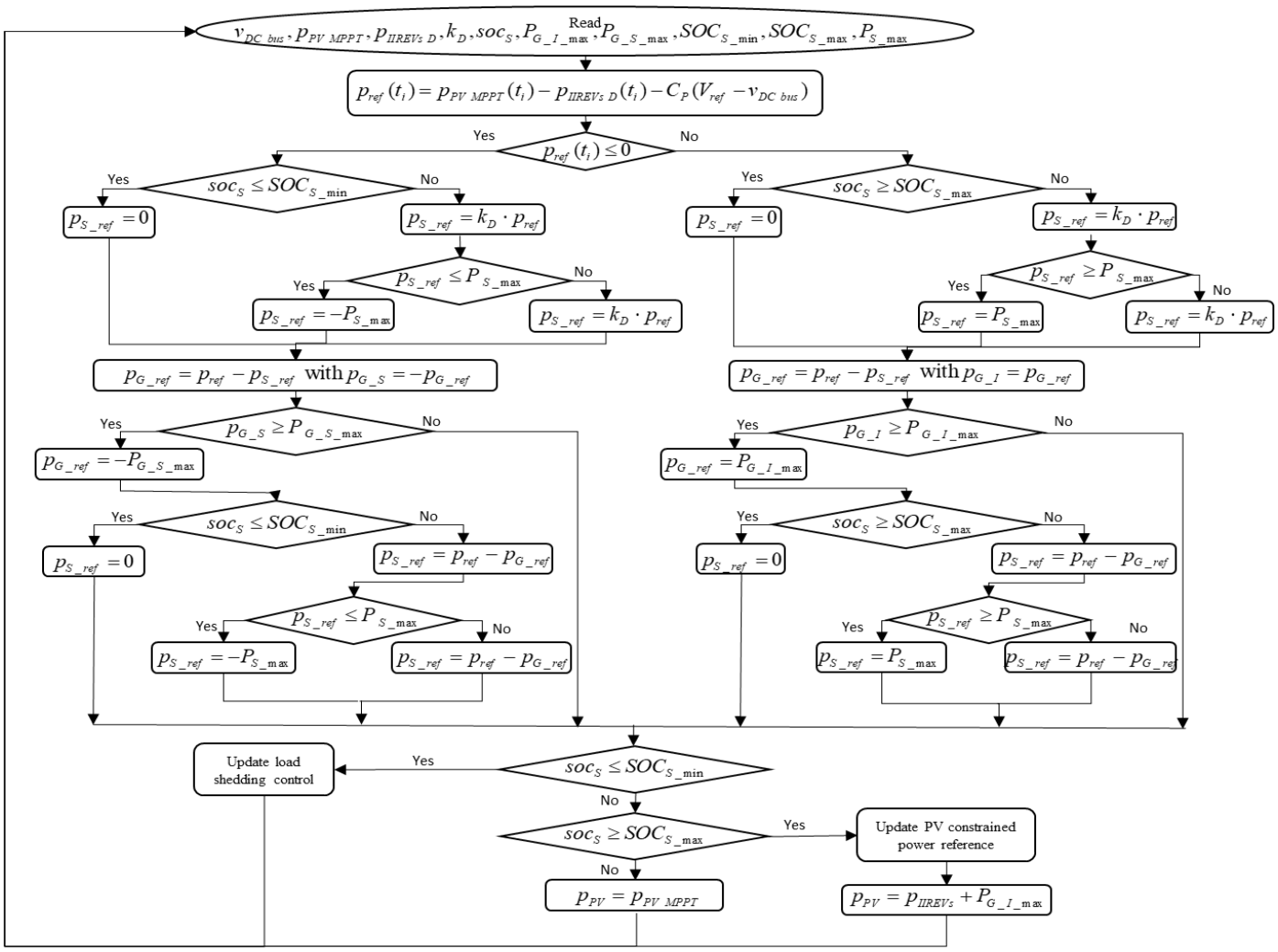

Figure 51: Control algorithm for IIREVs.

To prove the feasibility of the optimization problem, it is compared with a storage priority algorithm simulation without optimization "Sim w/o opt", where k_D is one in this operation mode. Moreover, these operation modes are compared with an ideal case, "Opt for real conditions", which is based on real PV MPPT and IIREV powers.

III.4. Simulation results and analyses

A Simulink model is developed to simulate the IIREVs with a step time of 0.01 s, which contains five chargers with three charging modes in real-time operation and balances the power of DC bus. M_v, $SOC_{EV\_arr_v}$, $SOC_{EV\_des_v}$, and t_{arr_v} are randomly generated. $SOC_{EV\_arr_v}$ and $SOC_{EV\_des_v}$ are generated in the interval (20%, 50%) and (70%, 100%), respectively. Regarding the EV batteries, lithium-ion batteries were considered, and their capacities are assumed to be capable of handling up to fast charge. Sunpower SPR X21-345 with 21% efficiency under STC is considered as PV panels, and the system loss was estimated at 14%.

Table 9 provides the parameters used for optimization and power balancing control, and

Table 10 provides the options assumed by the EV users, randomly generated in MATLAB, where five EVs are expected to come for charging. The grid peak hours are arbitrarily assumed to be 12:00–13:00 and 15:00–16:00. The energy tariffs are chosen arbitrarily in a way to prioritize the sources used for the EV charging as given by (3.43). The energy tariffs are only considered for their operational and no maintenance or levelized cost of energy are taken into consideration as the life cycle of the sources is not considered in this study.

$$c_S \leq c_G \leq c_{PVS} \leq c_{EV\_penalty}. \tag{3.43}$$

Table 9: Optimization and simulation parameter values.

SOC_{S_min}	20%	$P_{G\_I\_max}$	50 kW	c_S	0.01€/kWh
SOC_{S_max}	80%	$P_{G\_S\_max}$	50 kW	c_{PVS}	1.2€/kWh
SOC_{EV_min}	20%	P_{S_max}	34.5 kW	V_{ref}	400 V
SOC_{EV_max}	100%	N_{PV}	84 PV	E_{Bat}	90 kWh
SOC_{S_0}	50%	$p_{PV\ MPPT}$	28.98 kWp	E	50 kWh
$P_{EV\_fast\_max}$	50 kW	c_{G_NH}	0.1€/kWh		
$P_{EV\_aver\_max}$	22 kW	c_{G_PH}	0.7€/kWh		
$P_{EV\_slow\_max}$	7 kW	$c_{EV\_penalty}$	2.5€/kWh		

Table 10: Assumed options by the EV users.

EVs	SOC_{EV_arr}	SOC_{EV_des}	t_{arr}	t_{est_ch}	M
EV1	29%	74%	09:10	03:13	Slow
EV2	23%	78%	09:40	01:15	Average
EV3	22%	88%	12:20	04:43	Slow
EV4	32%	78%	14:20	03:18	Slow
EV5	29%	70%	14:30	00:25	Fast

At each event, like EV arrival, the optimization is executed. Then, the corresponding k_D is calculated as in (3.33) from the optimized power flow for the corresponding EV arrival event. The obtained k_D is then inserted into the Simulink model, which runs in real-time conditions. At each EV arrival, the desired parameters, soc_S and soc_{EV_v} currently in charge, are actualized and inserted; then, the supervisory control of the IIREVs executes the optimization, and the EV starts charging.

The following subsections present different case studies to prove the feasibility of the optimization problem formulated as MILP under different meteorological conditions.

III.4.1. Case 1—high irradiation profile without fluctuations

The case of 29 June 2019, in Compiegne, France, is considered. Figure 52 shows $p_{PV\ MPPT\ pred}$ and $p_{PV\ MPPT}$.

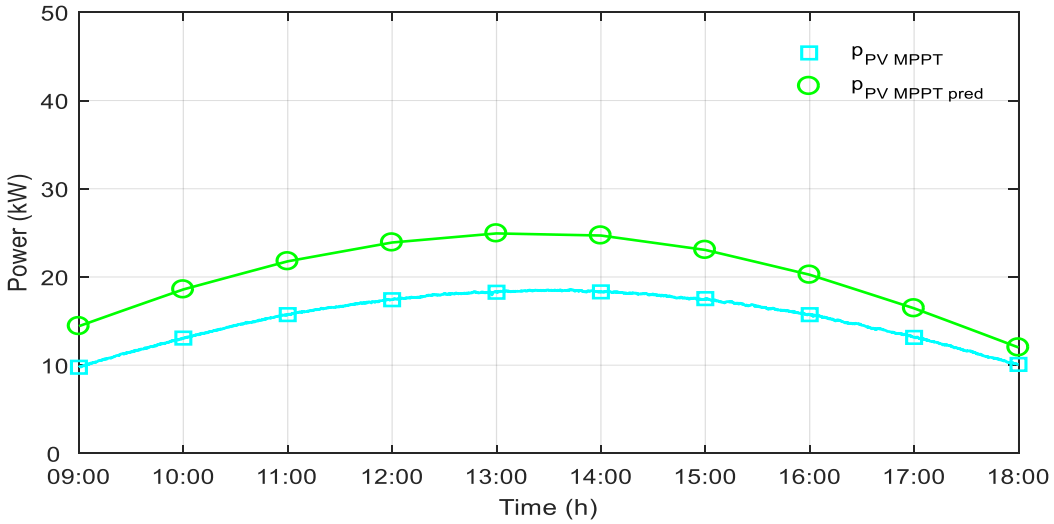

Figure 52: PV MPPT real and predicted powers—case 1.

In this case, the PV power production is considered significant since the weather is sunny and clear, so the irradiation is high, and there are no fluctuations. The IIREVs demand power is based on the data given in Table 10. Figure 53 shows the power flow and storage state of charge for "Sim w/o opt" and simulation with optimization "Sim with opt" for case 1, which is based on introducing the k_D, which is calculated in the optimization layer, into the real-time operation algorithm in Simulink.

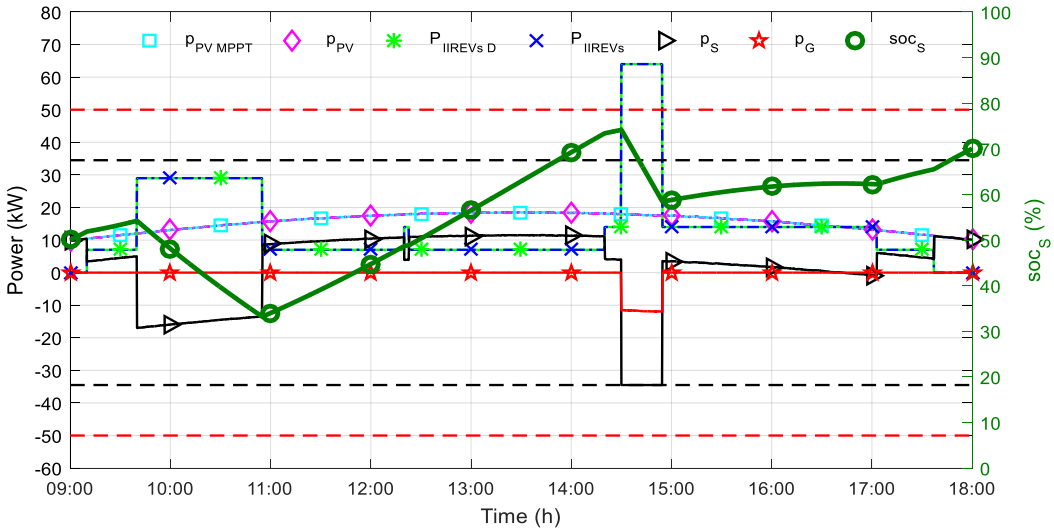

(a)

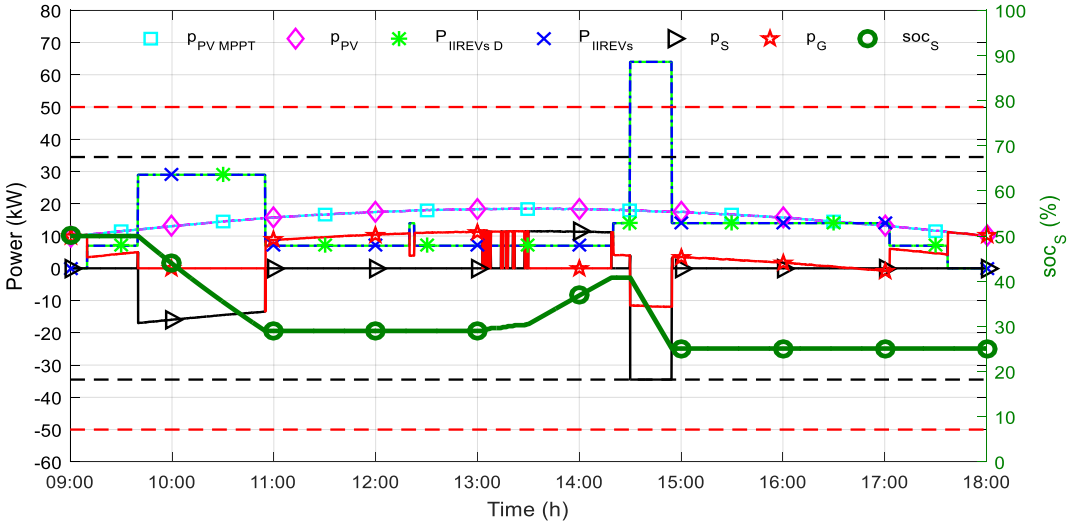

(b)

Figure 53: Power flow and storage state of charge in (a) "Sim w/o opt" and (b) "Sim with opt"—case 1.

In Figure 53a, the storage has priority over the grid either to be discharged or to be charged. However, when EV5 arrives, the IIREVs demand power greater than the PV and storage powers that they can supply, where the black dotted lines represent the maximum storage power and the red dotted lines represent the maximum grid power that can be reached. Therefore, the grid supplies power to charge the EVs. On the other hand, in Figure 53b, the power flow of the storage and the grid is based on the coefficient k_D. Since between 12:00 and 13:00 is considered a peak period, by selling energy to the grid operator, it is possible to make profits and, thus, reduce the total cost of energy. However, after 13:00, the storage can be recharged to be able to charge the future EVs with sufficient storage energy. Therefore, when EV5 arrives, the PV, storage and grid can together supply the EVs.

Figure 54 shows the EV energy distribution for "Sim w/o opt" and "Sim with opt". The calculation of EV energy distribution is detailed in [77].

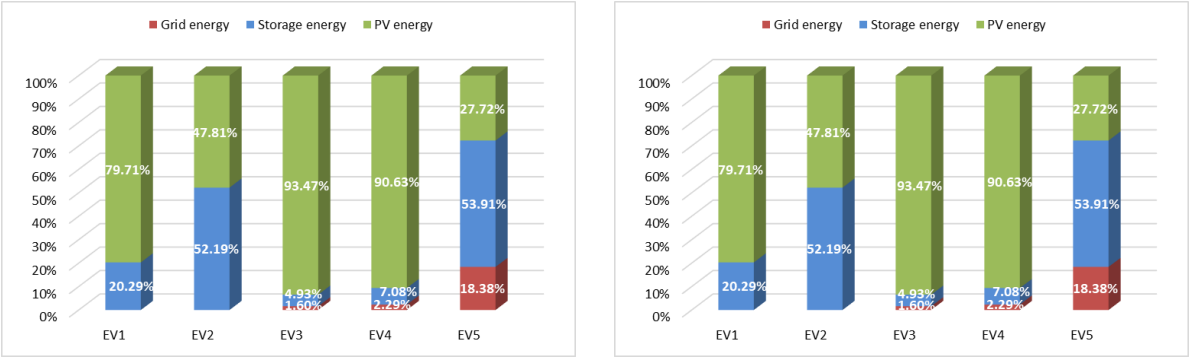

(a) **(b)**

Figure 54: EV energy distribution in (a) "Sim w/o opt" and (b) "Sim with opt"—case 1.

EV1, EV3, and EV4 depend mainly on PV energy since they charge in slow mode. EV2 depends on PV and storage with a slightly equal percentage. EV5 depends on the PV, storage and grid energy. The percentage of grid energy is significantly greater than the other EVs, since it is charging in fast mode.

Figure 55a shows the energy system distribution for "Sim w/o opt", "Sim with opt" and "Opt for real conditions". There is no grid injection in the "Sim w/o opt", while for the "Sim with opt" and "Opt for real conditions", there is grid injection, which indicates that selling energy to the grid and the charging energy of the storage was sufficient to get the best energy distribution for the EVs.

The percentage of accuracy is the ratio of the total cost over the total cost of the "Opt for real conditions". The closer the percentage to 100%, the more accurate it is. If the percentage is greater than 100%, the total cost is greater than "Opt for real conditions", while if the percentage is below 0%, the total cost is the opposite case of "Opt for real conditions". Figure 55b shows the energy system cost, where the energy costs in "Sim with opt" are closer to the ideal case "Opt for real conditions", resulting in profits with 99.95% accuracy. Conversely, it is the opposite situation in "Sim w/o opt" with −11.96% accuracy. Thus, this proves the superiority of the optimization algorithm over the storage priority algorithm. The negative sign implies that the IIREV operators make a profit in particular by selling energy to the grid.

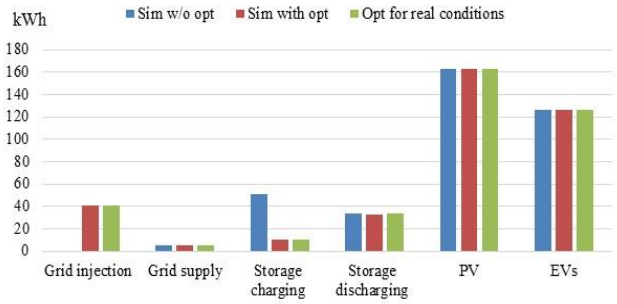

Case Operation	Grid Cost (c€)	Storage Cost (c€)	Total Cost (c€)	% of Accuracy
Sim w/o opt	48.22	84.47	132.69	−11.96%
Sim with opt	−1152.69	43.69	−1109.01	99.95%
Opt for real conditions	−1152.97	43.44	−1109.53	-

(a) **(b)**

Figure 55: (a) Energy system distribution and (b) energy system cost—case 1.

III.4.2. Case 2—low irradiation profile without fluctuations

The case of 5 October 2018, in Compiegne, France, is considered. Figure 56 shows $p_{PV\ MPPT\ pred}$, $p_{PV\ MPPT}$.

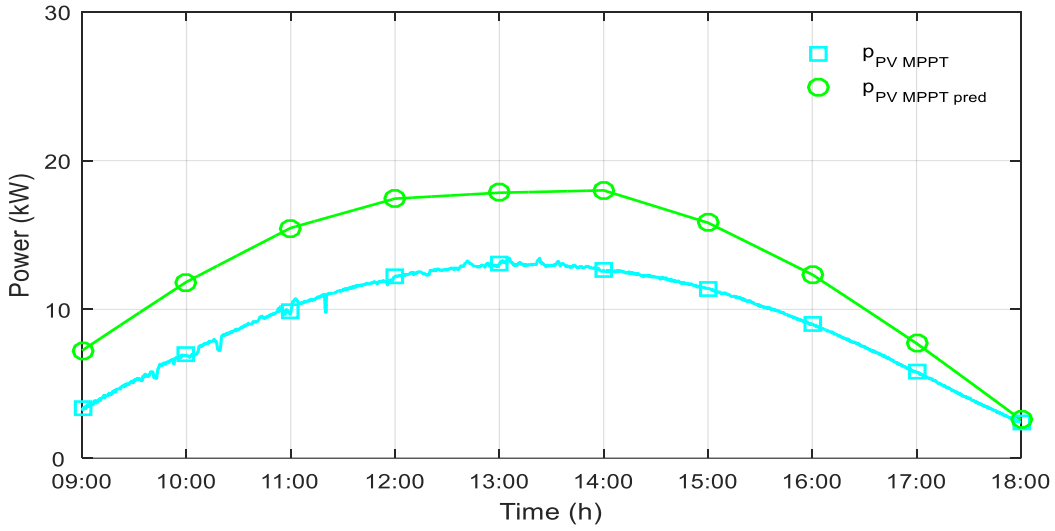

Figure 56: PV MPPT real and predicted powers—case 2.

In this case, the weather is clear, so there are no fluctuations; however, the PV power production is not very high. The IIREV demand power is based on the data in Table 10. Figure 57 shows the power flow and storage state of charge for "Sim w/o opt" and simulation with optimization "Sim with opt" for case 2.

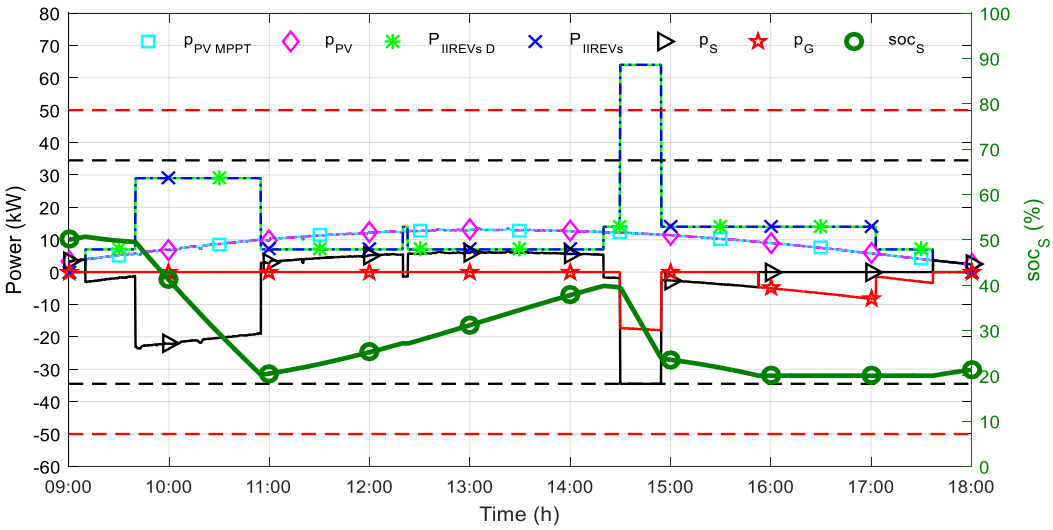

(a)

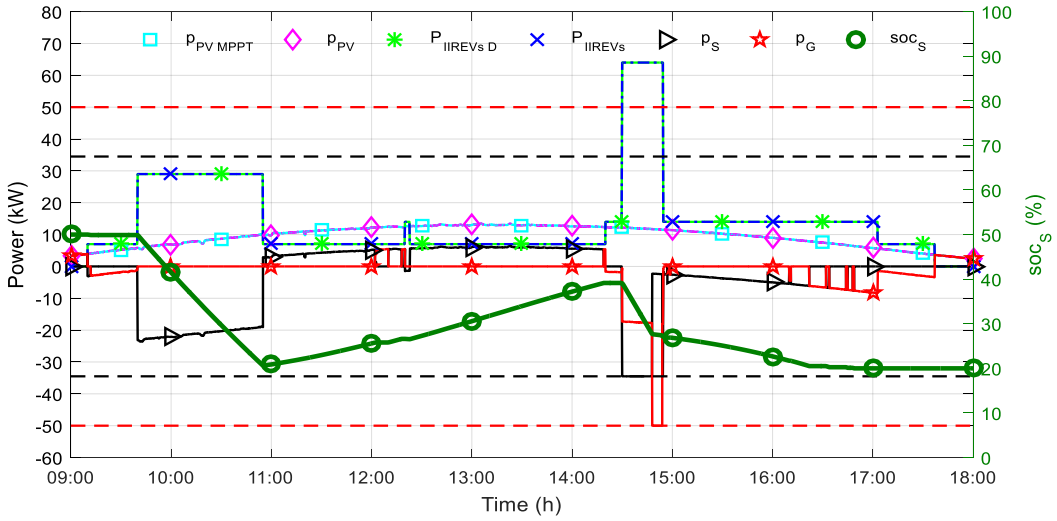

(b)

Figure 57: Power flow and storage state of charge in (a) "Sim w/o opt" and (b) "Sim with opt"—case 2.

In Figure 57a, the storage always has priority over the grid. However, when EV5 arrives, the grid supplies power with the PV and the storage to charge the EVs, where the black dotted lines represent the maximum storage power and the red dotted lines represent the maximum grid power that can be reached. On the other hand, in Figure 57b, the power flow of the storage and the grid is based on the coefficient k_D. Since the PV production is not high, the storage reached its lower limit at the departure of EV2. Therefore, the storage is required to be recharged to be able to charge the future EVs with sufficient storage energy. Therefore, when EV5 arrives, the PV, storage and grid can together supply the EVs. However, between 12:00 and 13:00 is considered a peak period, so by selling a little energy to the grid operator, it is possible to make small profits. Additionally, between 15:00 and 16:00 is a peak period, so in "Sim with opt", the power flow is better distributed since the storage is kept to supply power instead of grid power, while in "Sim w/o opt", the storage reached its lower limit before 16:00, and the grid continued to supply power to the EVs.

Figure 58 shows the EV energy distribution for "Sim w/o opt" and "Sim with opt".

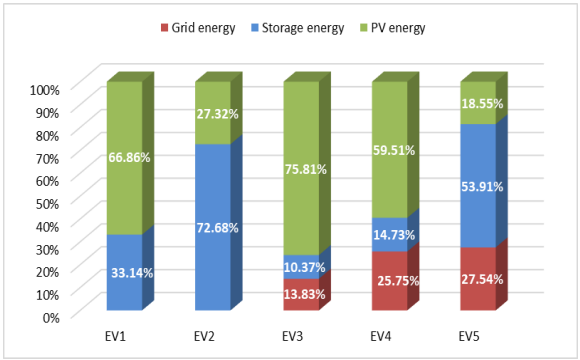

(a)

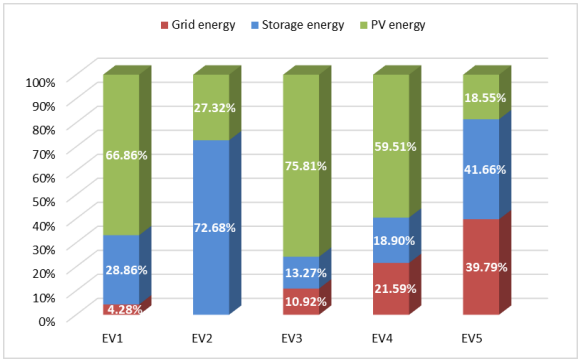

(b)

Figure 58: EV energy distribution in (a) "Sim w/o opt" and (b) "Sim with opt"—case 2.

EV1, EV3, and EV4 depend mainly on PV energy since they charge in slow mode. EV2 depends on PV and storage. Figure 58 shows that EV5, which is in fast mode, is charged from the grid with a high percentage. This will increase the charging price for the EV user. In Figure 58b, EV5 is charged from the grid with a higher percentage than in "Sim w/o opt", while EV3 and EV4 have been charged from the storage with a higher percentage than in "Sim w/o opt", based on k_D giving a better energy cost as shown.

Figure 59a shows the energy system distribution for "Sim w/o opt" and "Sim with opt". There is no grid injection in the "Sim w/o opt", while for the "Sim with opt", there is a little bit of grid injection, which refers to selling energy to the grid and having approximately the same storage charging energy. Figure 59b shows the energy system cost, where the energy costs in "Sim with opt" are closer to the ideal case "Opt for real conditions" with 99.37% accuracy and lower cost than in "Sim w/o opt" with 164.04% accuracy (overpriced). In this case, the PV production is not high; however, selling a little bit of energy to the grid during the peak time could reduce the total cost of the system. Thus, it proves the superiority of the optimization algorithm over the storage priority algorithm.

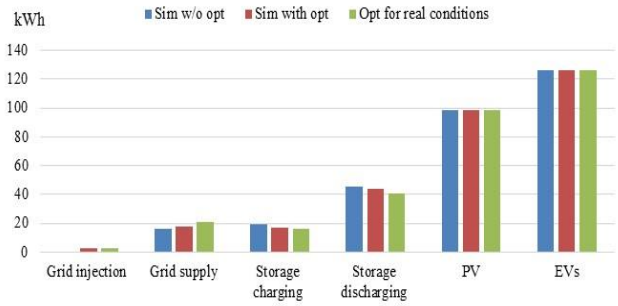

(**a**)

Case operation	Grid cost (c€)	Storage cost (c€)	Total cost (c€)	% of accuracy
Sim w/o opt	196.59	64.75	261.34	164.04%
Sim with opt	97.82	60.49	158.31	99.37%
Opt for real conditions	102.36	56.94	159.31	-

(**b**)

Figure 59: (a) Energy system distribution and (b) energy system cost—case 2.

III.4.3. Case 3—high irradiation profile with high fluctuations

The case of 12 May 2019, in Compiegne, France, is considered. Figure 60 shows $p_{PV\ MPPT\ pred}$, and $p_{PV\ MPPT}$.

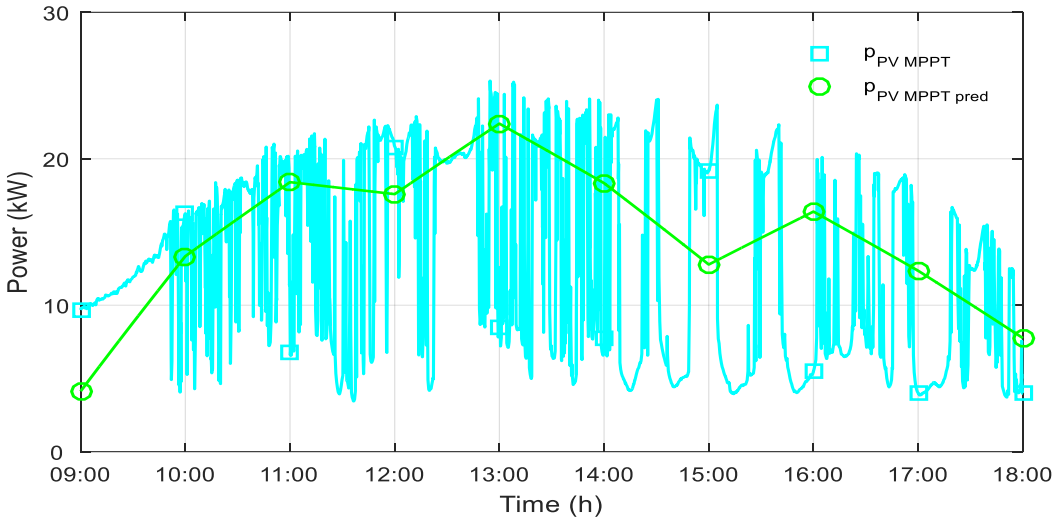

Figure 60: PV MPPT real and predicted powers and IIREV demand power—case 3.

In this case, the irradiations are high, and the weather is cloudy, so there are high fluctuations. The IIREVs demand power is based on the data in Table 10. Figure 61 shows the power flow and storage state of charge for "Sim w/o opt" and simulation with optimization "Sim with opt" for case 3.

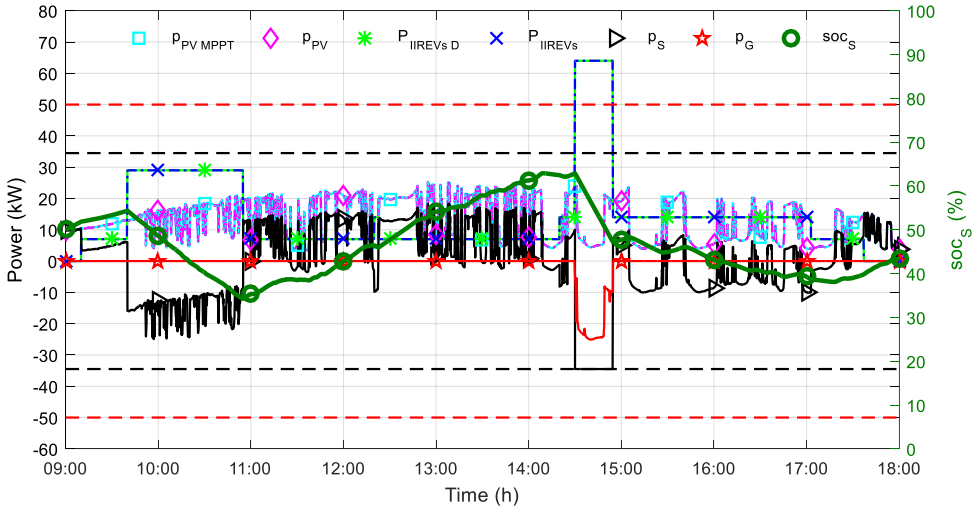

(**a**)

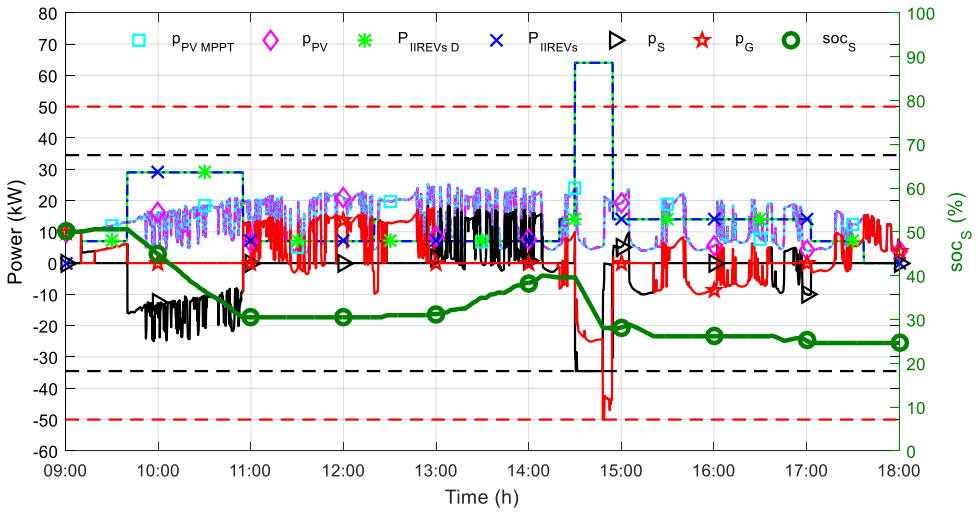

(b)

Figure 61: Power flow and storage state of charge in (a) "Sim w/o opt" and (b) "Sim with opt"—case 3.

In Figure 61a, the storage always has priority over the grid, either to be discharged or to be charged. However, when EV5 arrives, the IIREV demand power is greater than the PV and storage power that can be supplied, where the black dotted lines represent the maximum storage power and the red dotted lines represent the maximum grid power that can be reached. Therefore, the grid supplies power to charge the EVs. On the other hand, in Figure 61b, the power flow of the storage and the grid is based on the coefficient k_D. Since between 12:00 and 13:00 is considered a peak period, by selling energy to the grid operator, it is possible to make profits. However, after 13:00, the storage can be recharged to be able to charge the future EVs with sufficient storage energy. Therefore, when EV5 arrives, the PV, storage and grid can together supply the EVs.

Figure 62 shows the EV energy distribution for "Sim w/o opt" and "Sim with opt".

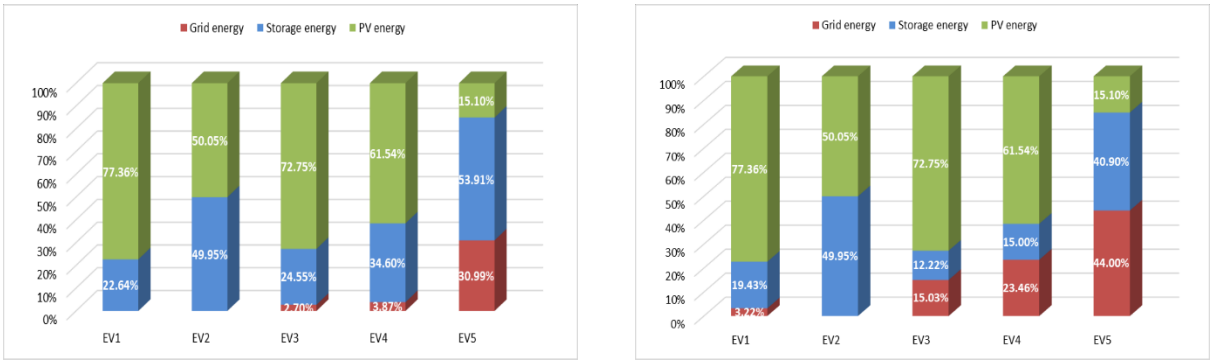

(a) **(b)**

Figure 62: EV energy distribution in (a) "Sim w/o opt" and (b) "Sim with opt"—case 3.

EV1, EV3, and EV4 depend mainly on PV energy since they charge in slow mode. EV2 depends on PV and storage with a slightly equal percentage. Figure 62 shows that EV5, which is in fast mode, is charged from the grid with a high percentage. This will increase the charging price for the EV user. In Figure 62b, EV3, EV4, andEV5 are charged from the grid with a higher percentage than in "Sim w/o opt"; due to the high fluctuations, the power distribution was not as suitable. However, the energy cost obtained from optimization stays better than in "Sim w/o opt" and returns profits due to selling energy to the grid.

Figure 63a shows the energy system distribution for "Sim w/o opt" and "Sim with opt". There is no grid injection in the "Sim w/o opt", while for the "Sim with opt", there is grid injection, which is referred to selling energy to the grid and maintaining a little storage charging energy. Figure 63b shows the energy system cost; due to the high fluctuations in the real PV profile, the prediction profile was not so accurate. However, the energy costs in "Sim with opt" are closer to the ideal case "Opt for real conditions" with 75.45% accuracy and return profits, while it is the opposite situation in "Sim w/o opt" with −26.46% accuracy. Thus, it proves the superiority of the optimization algorithm over the storage priority algorithm.

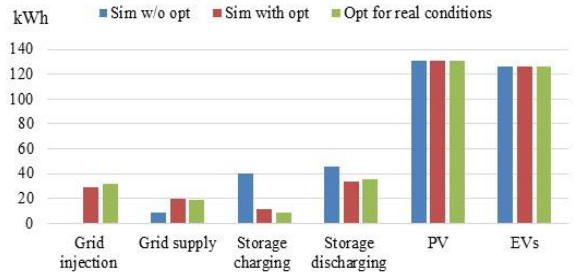

(**a**)

Case operation	Grid cost (c€)	Storage cost (c€)	Total cost (c€)	% of accuracy
Sim w/o opt	81.32	85.96	167.29	−26.46%
Sim with opt	−522.01	45.1	−476.92	75.45%
Opt for real conditions	−676.51	44.4	−632.12	-

(**b**)

Figure 63: (a) Energy system distribution and (b) energy system cost—case 3.

III.4.4. Case 4—low irradiation profile with low fluctuations

The case of 29 September 2018, in Compiegne, France, is considered. Figure 64 shows $p_{PV\ MPPT\ pred}$, and $p_{PV\ MPPT}$.

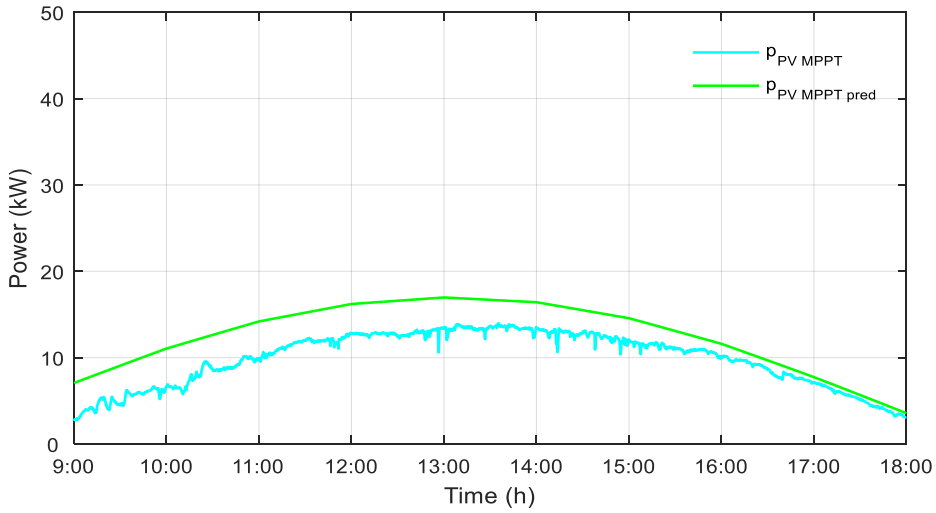

Figure 64: PV MPPT real and predicted powers—case 4.

In this case, the irradiations are not high and the weather is a bit cloudy, so there is low fluctuations. The IIREVs demand power is based on the data in Table 10. Figure 64 shows the power flow and storage state of charge for "Sim w/o opt" and simulation with optimization "Sim with opt" for case 4.

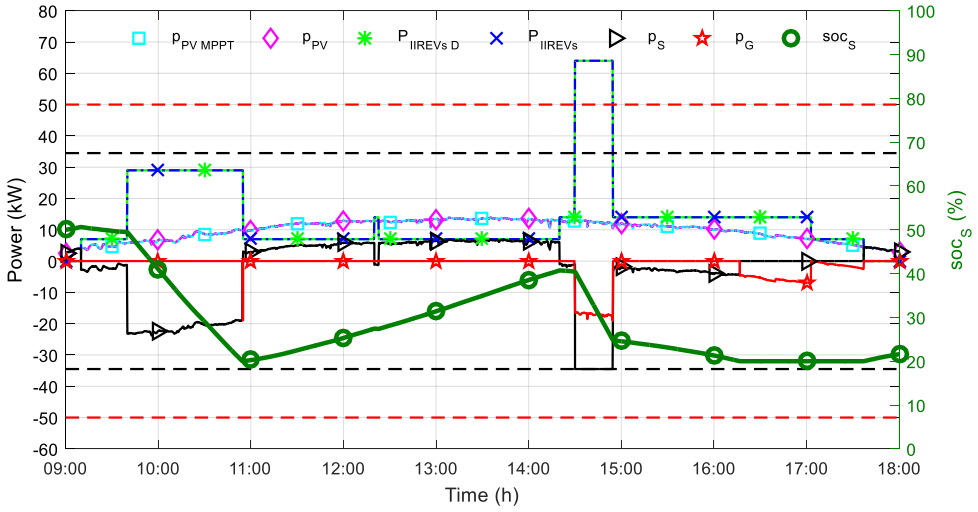

(a)

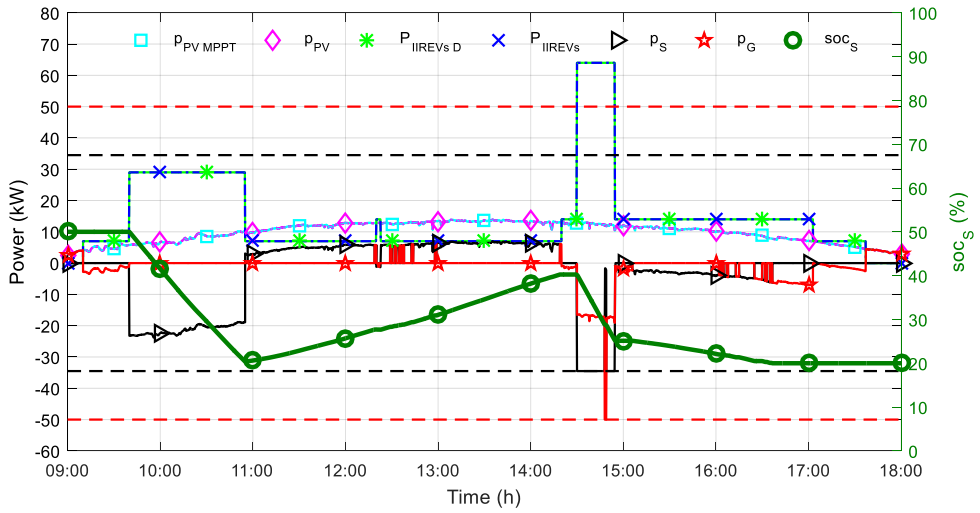

(b)

Figure 65: Power flow and storage state of charge in (a) "Sim w/o opt" and (b) "Sim with opt"—case 4.

In Figure 64a, the storage is always prioritized. However, when EV5 arrives, the grid supplies power with the PV and the storage to charge the EVs, where the black dotted lines represent the maximum storage power and the red dotted lines represent the maximum grid power that can be reached. On the other hand, in Figure 64b, the power flow of the storage and the grid is based on the coefficient k_D. Since, the PV production is not high, the storage reached its lower limit at the departure of EV2. Therefore, the storage is required to be recharged to be able to charge the future EVs with sufficient storage energy Therefore, when EV5 arrives, PV, storage and grid can together supply the EVs. However, between 12:00 and13:00 it is considered a peak period, so by selling a little energy to the grid operator, it is possible to make small profits. Also, between 15:00 and 16:00 it is a peak period, so in "Sim with opt" the storage is saved to this period to supply power instead of grid power.

Figure 66 shows the EVs energy distribution for "Sim w/o opt" and "Sim with opt".

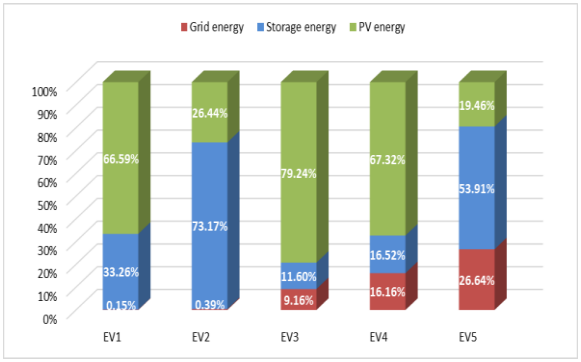

(a)

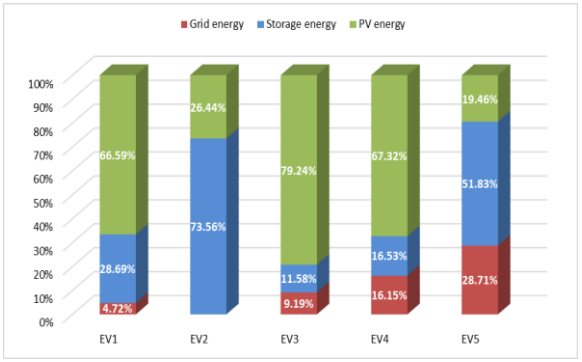

(b)

Figure 66: EVs energy distribution in (a) "Sim w/o opt" and (b) "Sim with opt"—case 4.

In Figure 66, the EVs energy distribution are approximately identical. EV1, EV3, and EV4 depend mainly on PV energy since they charge in slow mode. EV2 depends on PV and storage. EV5, which is in fast mode, is charged from the grid with high percentage. This will increase the charging price on the EV user.

Figure 67a shows the energy system distribution for "Sim w/o opt" and "Sim with opt". There is no grid injection in the "Sim w/o opt" while for the "Sim with opt" there is a little bit of grid injection, which is referred to selling energy to the grid and storage charging energy. Figure 67b shows the energy system cost, where the energy costs in "Sim with opt" are closer to the ideal case "Opt for real conditions" with 166%.61 accuracy and lower cost than in "Sim w/o opt" with 217.31% accuracy. In this case, the PV production is not high, however, selling a little bit of energy to the grid in the peak time could reduce the total cost of the system. Thus, it proves the superiority of the optimization algorithm over the storage priority algorithm.

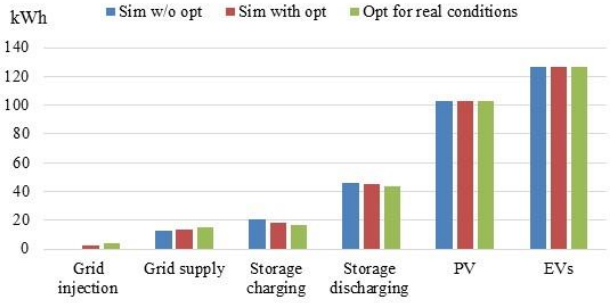

(a)

Case operation	Grid cost (c€)	Storage cost (c€)	Total cost (c€)	% of accuracy
Sim w/o opt	123	67.01	190.45	217.31%
Sim with opt	83.15	62.86	146.02	166.61%
Opt for real conditions	27.32	60.31	87.64	-

(b)

Figure 67: (a) Energy system distribution and (b) Energy system cost—case 4.

III.4.5. Discussion

In case 1, the PV production is high without fluctuations. In "Sim with opt", selling energy to the grid is preferred to make profits. Moreover, charging the storage a little bit could be interesting to get the same EVs energy distribution in "Sim with opt" as in "Sim w/o opt".

In case 2, the PV production is low without fluctuations. The energy distribution especially for EV5 is better in “Sim w/o opt” since it is charged with a lower percentage of grid energy than in “Sim with opt”. This could be explained by the fact that in “Sim w/o opt”, the storage is always used until it reaches its limits, while in “Sim with opt”, the power flow is based on the coefficient k_D to minimize the total cost. Therefore, the total cost in “Sim with opt” is lower than “Sim w/o opt”. Moreover, charging the storage is necessary after the departure of EV2, since the storage has reached its limit.

In case 3, the PV production is high with high fluctuations. In “Sim with opt”, selling energy to the grid is preferred to make profits. Moreover, charging the storage a little bit could be interesting to get a closer EV energy distribution in “Sim with opt” as in “Sim w/o opt”. Since there are high fluctuations, the power distribution is not that accurate; however, the total cost for “Sim w/o opt” brings profits to the IIREVs operator, and it is better than “Sim w/o opt”.

In case 4, the PV production is low with low fluctuations. In “Sim with opt”, charging the storage is necessary after the departure of EV2 since the storage has reached its limit. Therefore, the EVs energy distribution is approximately the same in “Sim with opt” as in “Sim w/o opt”. Moreover, the total cost in “Sim with opt” is lower than Sim w/o opt” due to selling energy to the grid in “Sim with opt”.

To summarize the four cases studied, “Sim with opt” performs better than “Sim w/o opt” in minimizing the total cost of the IIREVs with high accuracy in case 1 and case 2, where they are without fluctuations. For the EV energy distribution, in “Sim with opt”, the results are satisfying in case 1 and case 4 as they are approximately identical, while in case 2, the coefficient k_D gives better energy distribution for the system to have a lower cost than “Sim w/o opt” instead of giving a better energy distribution for EVs. Therefore, the EV user charging in fast mode should be willing to pay a high price. In case 3, due to high fluctuations, the optimization is not very accurate, as the PV prediction is hourly coming from Météo France. However, the total cost in “Sim with opt” is still better than “Sim with opt” due to selling energy to the grid and making profits, yet the EV energy distribution is not as well distributed in “Sim with opt” as in “Sim with opt”.

In optimization, it is always preferred to sell energy to the grid to make profits. However, the goal, besides minimizing the total cost, is to have better EV energy distribution by reducing the grid energy consumed by the EVs. Therefore, it is important to recharge the storage. For the four cases taken in this study, after the departure of EV2, SOC_S decreases, even more in case 2 and case 4, it has reached the lower limit. It is expected for three more EVs to come for recharging at the IIREVs, and it is supposed that at least one EV could charge in fast mode. The average energy demand for each EV is 25 kWh, and so it is 75 kWh for the three EVs to come. Based on the data from Table 2, the capacity of the storage that can be used is 27 kWh (30% of 90 kWh). After the departure of EV2, if SOC_S is 20%, then it is empty, and if it is 30%, then only 9 kWh with PV and grid energy could be used to charge 75 kWh. This will result in increasing the energy supplied by the grid to charge the coming EVs. Thus, after the departure of EV2, if PV power is higher than

the IIREV demand power, the storage should be recharged. Hence, the interest is to minimize the total cost of the IIREVs and to have the best EV energy distribution.

III.5. Conclusions

The simulation results prove the superiority of the optimization problem formulated as MILP and solved by CPLEX over the storage priority algorithm. The results also show the feasibility of the proposed supervisory control of the IIREVs, which contains the HMI and the energy management with power balancing and interacts with the smart grid. The proposed supervisory control executes efficiently with respect to the constraints and fulfilling the EV user demands. Furthermore, the EVs that charge in slow mode depend mainly on PV energy, while for average or fast charging, they depend on the PV, storage and grid power sources. The EV energy distribution is considered good compared to the storage priority; only in the case with high fluctuations was the EV energy distribution better in storage priority. In addition, selling energy to the grid returns profits to the IIREV operator and makes optimization better than the storage priority algorithm.

Chapitre IV. *Real-time power management including optimization problem for PV-powered electric vehicle charging stations*

This chapter presents real-time experimental tests including an optimization problem, formulated as MILP, for a MG-based IIREVs. The DC MG includes PV sources, stationary storage, a power grid connection, and EV batteries as load. The objective of the optimization problem is to minimize the total energy cost. Experimental results under different meteorological conditions prove the feasibility of the proposed control and its superiority over the storage priority strategy. This chapter, presented in [114] is constructed as follows: Section IV.1 gives a description of the experimental platform, Section IV.2 presents the experimental tests including the optimization problem, and Section IV.3 concludes the chapter.

IV.1. Description of the experimental platform

The real-time experimental tests were done in the testbed presented in Figure 68a that emulates the IIREVs, having a step time of 1/14 kHz. The chargers are emulated with two DC emulators having each 6 kW, designated by charging terminals equipped with multi-electrical outlets as shown in Figure 68b. It is considered that the DC emulator 1 is a charging terminal with two electrical outlets to emulate EV1 and EV2 and the DC emulator 2 is a charging terminal with three electrical outlets to emulate EV3, EV4, and EV5.

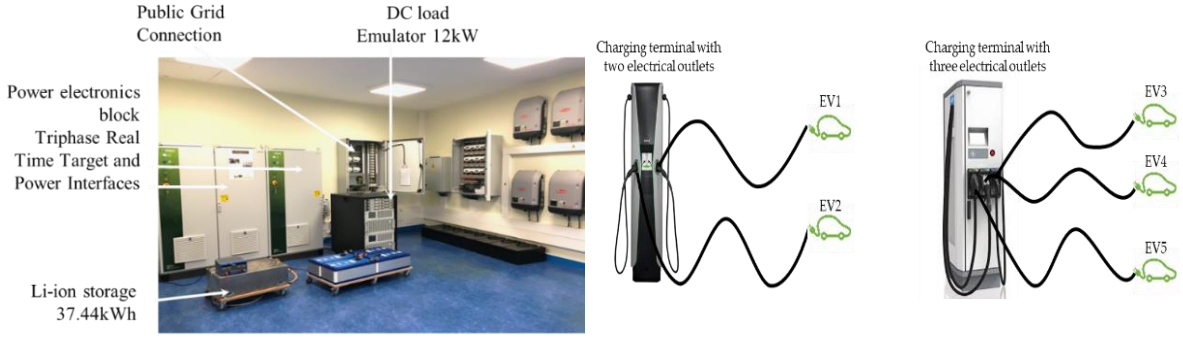

(**a**) (**b**)

Figure 68: Testbed for the IIREV experimental platform (a) and representative image of the multi-outlet charging terminals (b).

The existing testbed allows the PV power profile to be emulated, which permits it to repeat the experimental test and compare it in two scenarios, with and without optimization. One notes that M_v, $SOC_{EV\_arr_v}$, $SOC_{EV\_des_v}$, and t_{arr_v} are randomly generated.

In the real-time experiment, at each EV arrival, the optimization was executed when the EV user came to the charging station and inputs their preferences, which were communicated with the dSPACE. Then, Python read the data from dSPACE and created the files required to run the optimization in C++, solved by CPLEX. Then, Python calculated k_D and sent it in dSPACE to be read in a real-time experimental model. Figure 69 shows the flowchart of the optimization solving for the "real-time exp". The corresponding k_D was calculated as in (33) from the optimized power flow for the corresponding EV arrival event. The obtained k_D was then updated into the Simulink model.

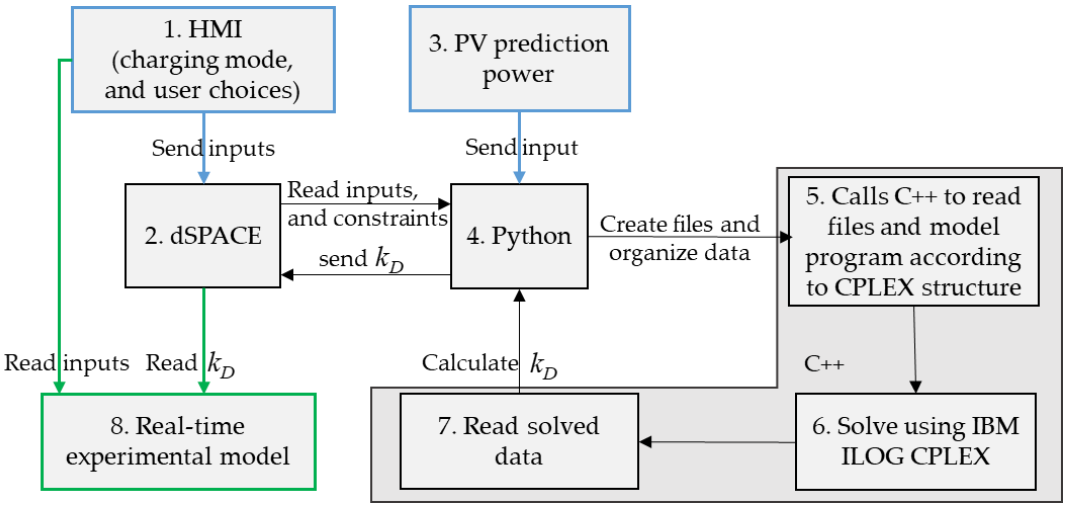

Figure 69: Flowchart of optimization solving.

To be specific, at the start of the real-time experimental test, when there were no EVs, the optimization algorithm was executed for the first time, using only the prediction of PV power. Then, when the first EV arrived at the station, the EV data were acknowledged, and the EV user chose his desired SOC and charging mode. These data were communicated instantly by the real-time experimental model and were sent through a real-time target via a fiber optic cable that ensured communication with analog input/output ports. After that, dSPACE received the EV data as an analog input; next, Python read these data and created the files required, including the parameters and the profiles of PV predicted power and EV power profiles acquired from the HMI. Later on, Python called C++ to resolve the optimization problem using the CPLEX solver, which the optimum solution is found within a fraction of a second (0.1-0.15 second). Once the problem was resolved, Python calculated k_D and sent it as analog output to the dSPACE; in turn, it sent it to the real-time experimental model. When another EV came to the station, the same procedure was performed with the actualized data of the DC microgrid (thus, the SOC of the stationary storage and SOC of the current EVs charging were actualized). The whole process takes around 60-90 seconds, the charging of EV starts directly when the start button is activated and when the optimization result is found, the power sources are used based on k_D as calculated.

The following subsections present two case studies to prove the feasibility of the optimization problem in real-time experimental tests formulated as MILP under different meteorological conditions.

IV.2. Real-time experimental tests

The following subsections presents real-time experimental test in different meteorological conditions and different EV charging profiles.

IV.2.1. Experimental test 1

Table 11 provides the parameters used for real-time experimental test ("real-time exp") and power balancing control for experimental tests 1, 2, 3, and 4.

Table 11: Real-time experiment parameter values for experimental tests 1, 2, and 3.

SOC_{S_min}	35%	$P_{G\_I\_max}$	5 kW	c_S	0.01€/kWh
SOC_{S_max}	60%	$P_{G\_S\_max}$	5 kW	c_{PVS}	1.2€/kWh
SOC_{EV_min}	20%	P_{S_max}	3.45 kW	V_{ref}	400 V
SOC_{EV_max}	100%	N_{PV}	12 PV	E_{Bat}	37.44 kWh
SOC_{S_0}	50%	$p_{PV\ MPPT}$	4.14 kWp	E	5 kWh
$P_{EV\_fast\_max}$	5 kW	c_{G_NH}	0.1€/kWh		
$P_{EV\_aver\_max}$	2.2 kW	c_{G_PH}	0.7€/kWh		
$P_{EV\_slow\_max}$	0.7 kW	$c_{EV\_penalty}$	2.5€/kWh		

The parameter values used in Table 11 were chosen with a scale divided by ten, compared to the simulation, due to the physical limitations of the available sources and equipment. The existing stationary storage had an energy capacity of 37.44 kWh, which is considered high; therefore, the SOC limits were chosen to be between 60% and 35% instead of 80% and 20%, to be able to present some periods where the storage is full or empty.

The case of 27 October 2021, in Compiegne, France, is considered. Figure 70 shows $p_{PV\ MPPT\ pred}$, and $p_{PV\ MPPT}$, where the irradiations are intermediate and the weather is a bit cloudy, so there are low fluctuations. The IIREV demand power is based on the data in Table 12.

Table 12: Assumed options by the EV users for experimental test 1.

EVs	SOC_{EV_arr}	SOC_{EV_des}	t_{arr}	t_{est_ch}	M
EV1	29%	74%	09:10	03:13	Slow
EV2	23%	78%	09:40	01:15	Average
EV3	22%	88%	12:20	04:43	Slow
EV4	32%	78%	14:20	03:18	Slow
EV5	29%	70%	14:30	00:25	Fast

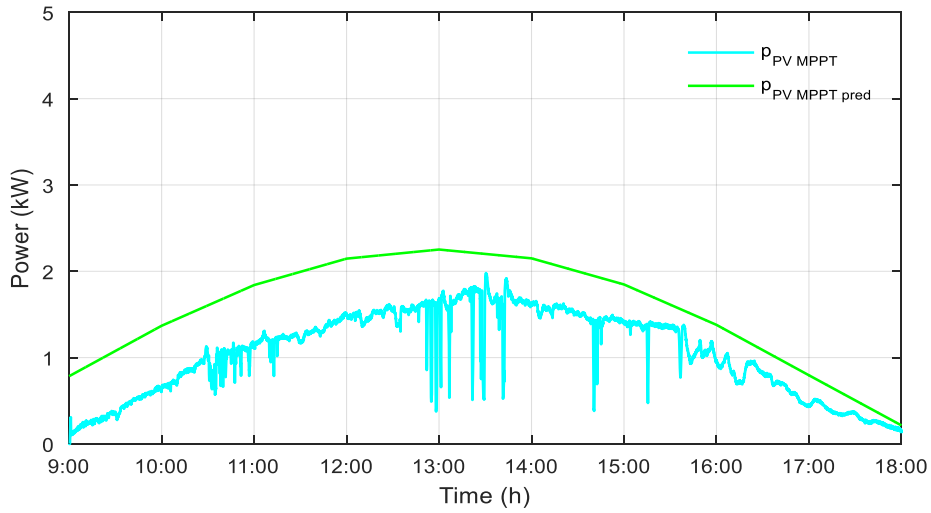

Figure 70: PV MPPT real and predicted powers—experimental test 1.

Figure 71 shows the power flow and storage state of charge for "real-time exp" without optimization and the DC bus voltage—experimental test 1a.

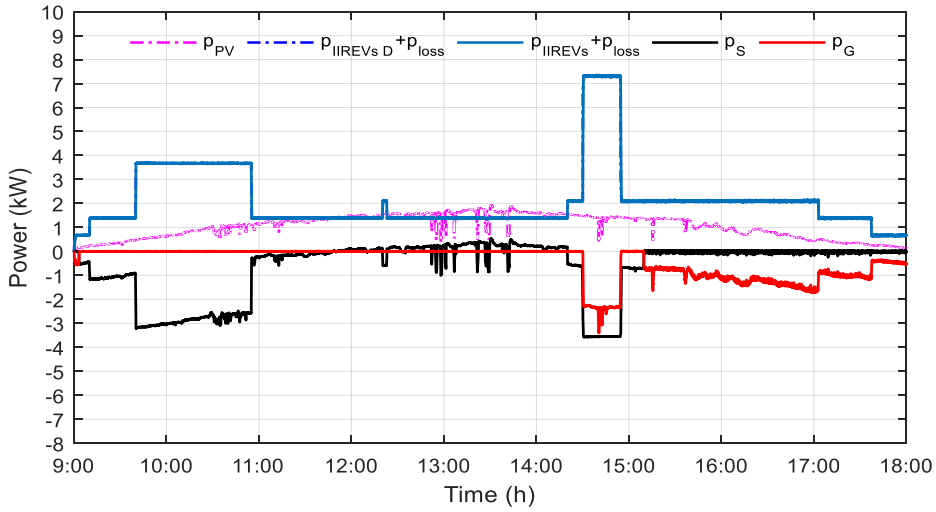

(a)

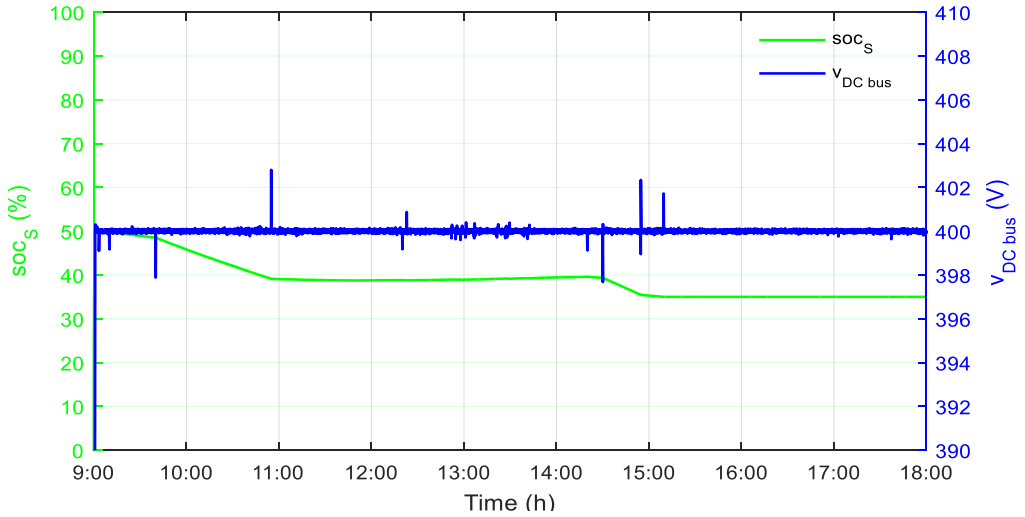

(b)

Figure 71: Power flow and storage state of charge for "real-time exp" without optimization (a) and (b) storage state of charge and DC bus voltage—experimental test 1a.

In Figure 71a, the storage is always prioritized to be either charged or discharged. When EV5 arrives, the IIREV demand power is greater than the PV and storage power that they can supply. Therefore, the grid supplies power to charge the EVs. The grid continues supplying power to the IIREVs as the storage is empty around 15:10. Figure 71b shows the evolution of the storage SOC, where it is always discharging almost all the time until it is empty around 15:10, and the stability of the DC bus voltage is present even with small fluctuations. Spikes of a few voltages (0.5%) happen when each EV starts charging and when it finishes charging.

Figure 72 shows the power flow and storage state of charge for "real-time exp" with optimization and the DC bus voltage—experimental test 1b.

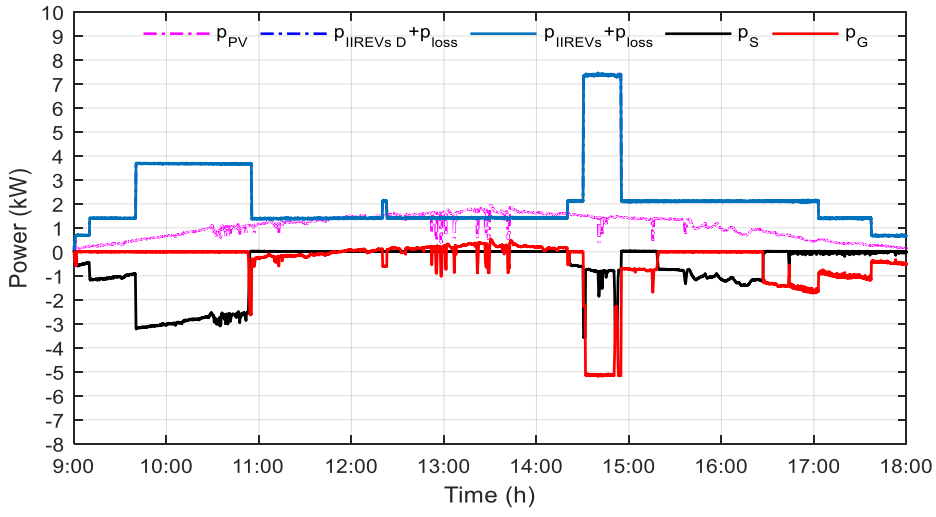

(a)

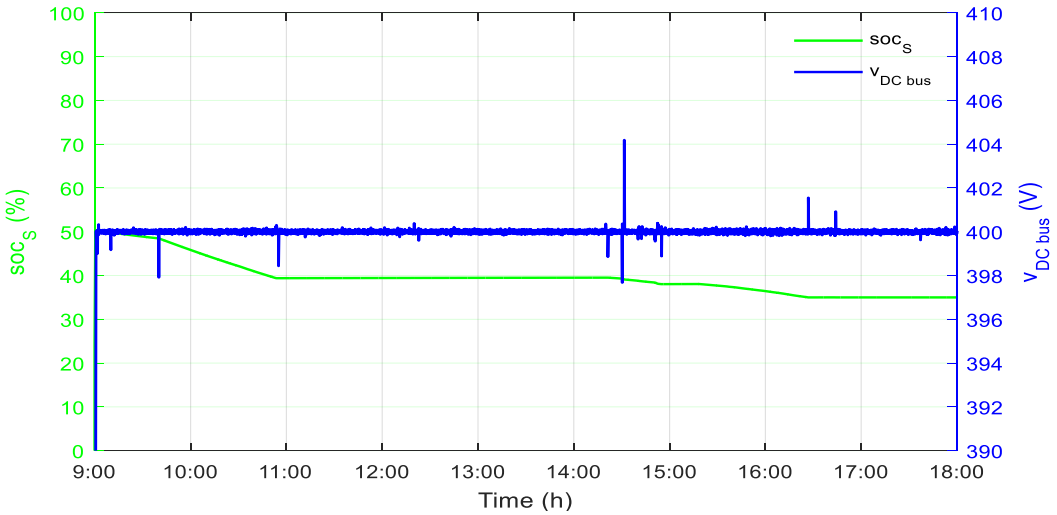

(b)

Figure 72: Power flow and storage state of charge for "real-time exp" with optimization (a) and (b) the storage state of charge and DC bus voltage—experimental test 1b.

In Figure 72a, the power flow of the storage and the grid is based on the coefficient k_D. From 12:00 until 14:20, the PV injects little energy to the grid during the peak hour, yet some fluctuations still happen where the grid supplies power. However, when EV5 arrives, the IIREV demand power is greater than the PV and storage power that they can supply. Therefore, the grid supplies power to charge the EVs with maximum power, and the storage is preserved. From 15:15 to 16:15, the storage discharges energy until it is empty to avoid the high cost of grid supply power, as it is considered a peak period. After 16:15, the grid supplies power, regardless of the k_D value. Figure 72b shows the evolution of the storage SOC, where the storage discharges energy from 09:10 to 10:50, 14:25 to 14:50 and around 15:15 to 16:15. Figure 72b also shows the stability of the DC bus voltage even with small fluctuations, which are due to the switching of DC converters, and the spikes of a few voltages (1 %) happen when each EV starts charging and when it finishes charging.

Table 13 shows the energy system cost for "real-time exp" without optimization, where the energy costs are higher than in optimization due to the cost of EV shedding. The real-time experiment with optimization is closer to the optimization for real conditions, as it avoids EV shedding and gives better energy costs of 56.69 c€. In "Opt for real conditions", where the optimization is performed without uncertainties, it gives the optimal energy cost without error, which is 39.50 c€. It avoids EV shedding and grid supply energy, and when EV5 arrives, the storage is discharged to the maximum power, then becomes empty around 14:45, provoking EV shedding. However, in "Opt for real conditions", the grid supplies its maximum power when EV5 arrives, and the storage is preserved to discharge at peak hours from 15:00 to 16:00. This explains the difference in the grid cost and the total cost for both cases.

Table 13. Energy system cost—experimental test 1.

Case operation	Grid cost (c€)	Storage cost (c€)	Total cost (c€)
Real-time exp w/o opt	83.86	6.75	90.98
Real-time exp with opt	50.69	6.00	56.69
Opt for real conditions	33.88	5.61	39.50

Figure 73 shows the energy system distribution for "real-time exp" with and without optimization.

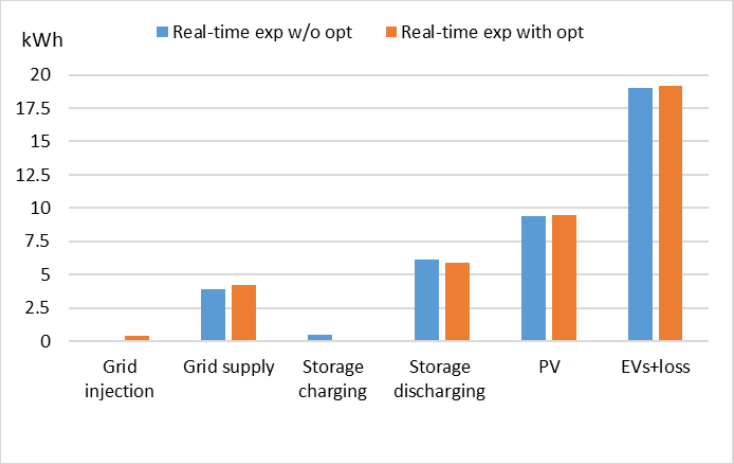

Figure 73: Energy system distribution—experimental test 1.

Figure 73 shows the energy system distribution for "Real-time w/o opt" and "Real-time with opt". There is no grid injection but a little of storage charging in the "Real-time w/o opt", while for the "Real-time with opt", there is a little bit of grid injection, which refers to selling energy to the grid and having approximately the same storage discharging energy.

Figure 74 shows the EV energy distribution for "real-time exp" with and without optimization.

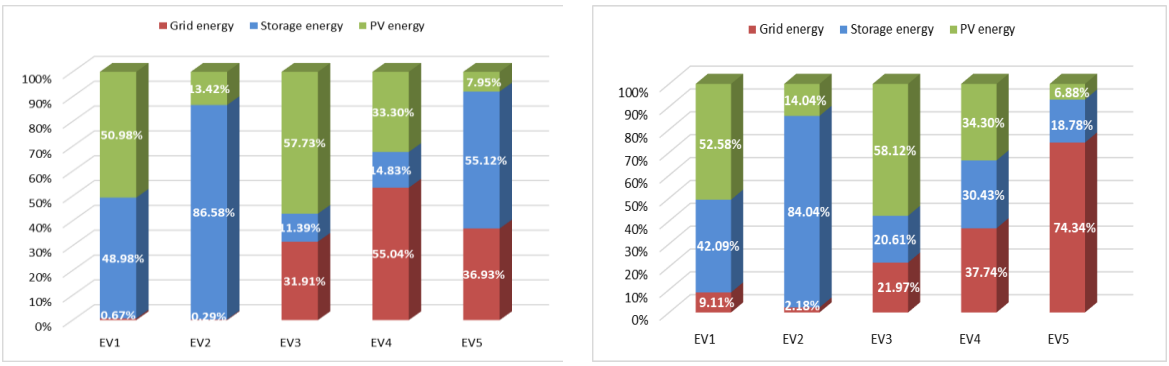

(a) **(b)**

Figure 74: EV energy distribution for "real-time exp" (a) without optimization and (b) with optimization—experimental test 1.

In Figure 74, the share of PV energy is not significant even for EVs charging in slow mode. Thus, the share of storage energy is high for EV1 and EV2, while the share of grid energy is high for EV3, EV4, and EV5 as the storage is empty early, around 15:15 in Figure 74a. Figure 74b shows a better EV energy distribution than in Figure 74a, where EV3 and EV4 were charged by the storage instead of the grid, whereas for EV5,

the storage was preserved to discharge at the peak hour from 15:00 to 16:00, and therefore EV5, charging in fast mode, was charged mainly by the grid.

IV.2.2. Experimental test 2

The case of 22 Mars 2022, in Compiegne, France, is considered. Figure 75 shows $p_{PV\ MPPT\ pred}$, and $p_{PV\ MPPT}$, where the irradiations are high and the weather is a globally sunny. The IIREV demand power is based on the data in Table 14.

Table 14: Assumed options by the EV users for experimental test 2 and 3.

EVs	SOC_{EV_arr}	SOC_{EV_des}	t_{arr}	t_{est_ch}	M
EV1	33%	82%	09:20	03:30	Slow
EV2	35%	75%	10:00	00:24	Fast
EV3	30%	80%	12:05	03:34	Slow
EV4	25%	78%	13:45	01:12	Average
EV5	29%	72%	14:25	03:04	Fast

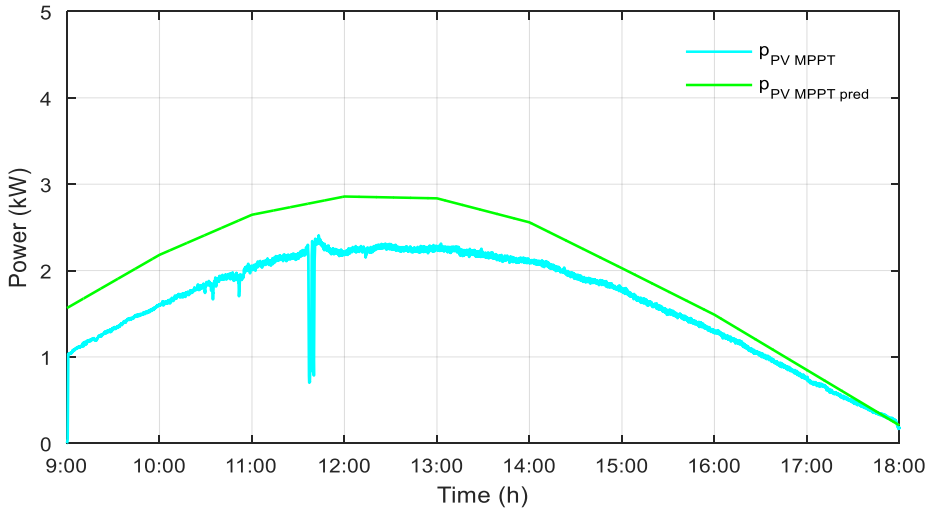

Figure 75: PV MPPT real and predicted powers—experimental test 2.

Figure 76 shows the power flow and storage state of charge for "real-time exp" without optimization and the DC bus voltage—experimental test 2a.

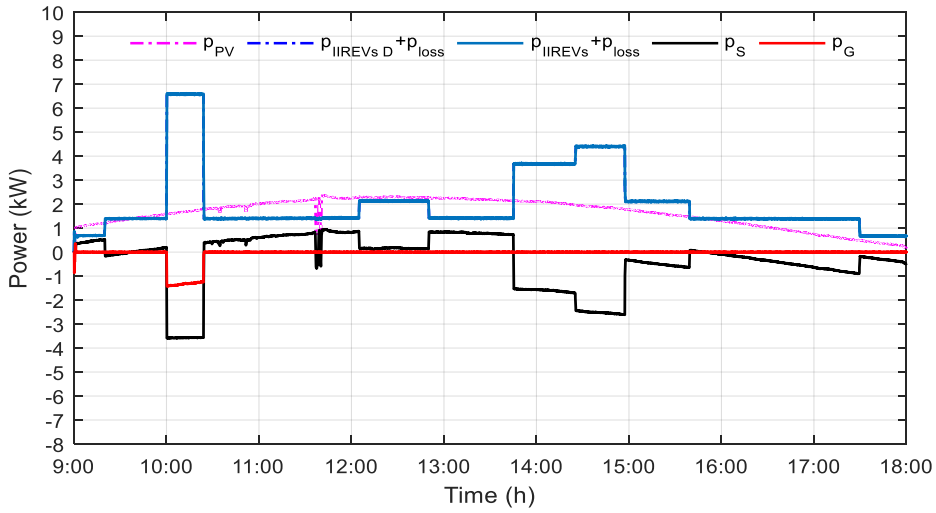

(a)

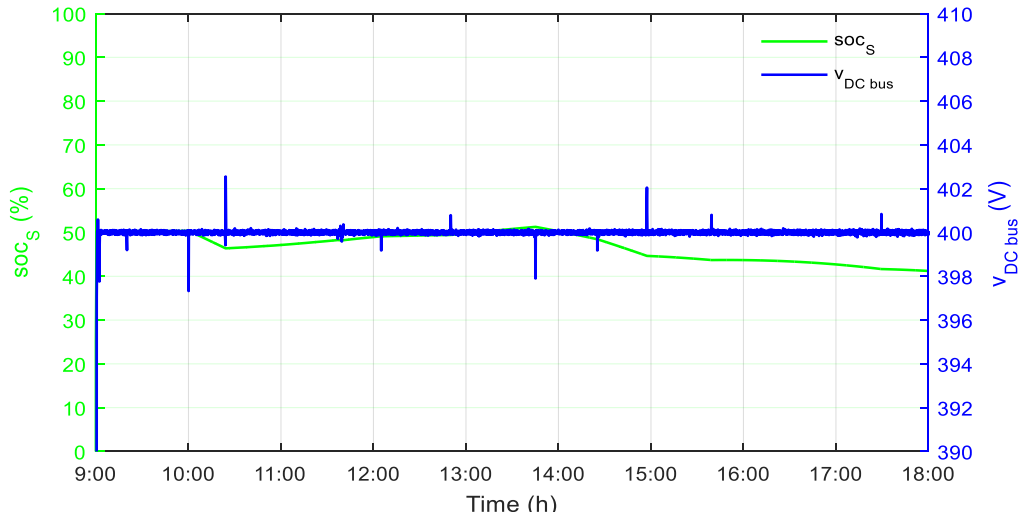

(b)

Figure 76: Power flow and storage state of charge for "real-time exp" without optimization (a) and (b) storage state of charge and DC bus voltage—experimental test 2a.

In Figure 76a, the storage is always prioritized to be either charged or discharged. when EV2 arrives, the IIREV demand power is greater than the PV and storage power that they can supply. Therefore, the grid supplies power to charge the EVs. Figure 76b shows the evolution of the storage SOC, where it starts recharging right after the departure of EV2 until the arrival of EV4 and discharges again until the end, and the stability of the DC bus voltage is present even with small fluctuations. Spikes of a few voltages (0.5%) happen when each EV starts charging and when it finishes charging.

Figure 77 shows the power flow and storage state of charge for "real-time exp" with optimization and the DC bus voltage—experimental test 2b.

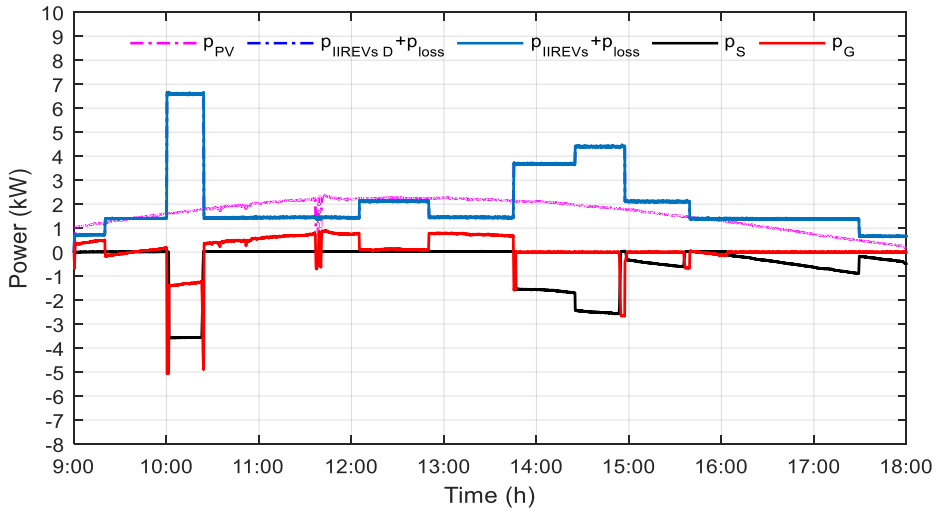

(a)

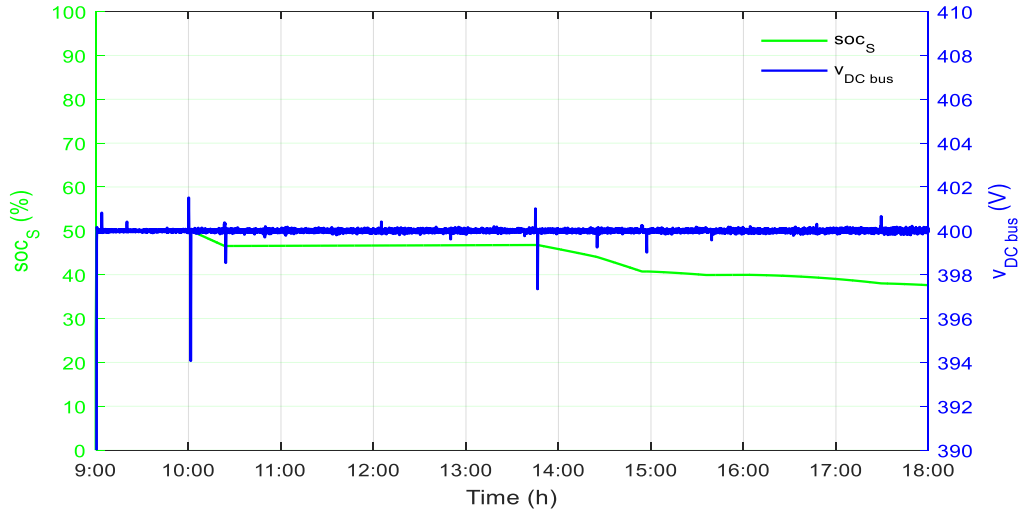

(b)

Figure 77: Power flow and storage state of charge for "real-time exp" with optimization (a) and (b) the storage state of charge and DC bus voltage—experimental test 2b.

In Figure 77a, the power flow of the storage and the grid is based on the coefficient k_D. Right after the departure of EV2 until the arrival of EV4, the PV injects energy to the grid, especially during the peak hour, yet some fluctuations still happen where the grid supplies power. However, when EV2 arrives, the IIREV demand power is greater than the PV and storage power that they can supply. Therefore, the grid supplies power to charge the EVs. From 15:00 to 15:45, peak hour, and then again from 16:00 until the end, the storage discharges energy to avoid the high cost of grid supply power. Figure 77b shows the evolution of the storage SOC, where the storage discharges energy from 10:00 to 10:25, 13:45 to 14:50, 15:00 to 15:45 and 16:00 until the end. Figure 77b also shows the stability of the DC bus voltage even with small fluctuations, which are due to the switching of DC converters, and the spikes of a few voltages (1.5%) happen when each EV starts charging and when it finishes charging.

Table 15 shows the energy system cost for “real-time exp” with optimization is closer to the optimization for real conditions, as it injects energy to the grid and gives better energy costs of -18.10 c€. In “Opt for real conditions”, where the optimization is performed without uncertainties, it gives the optimal energy cost without error, which is -67.35 c€. It avoids EV shedding and grid supply energy, and when EV2 arrives, the storage is discharged to the maximum power. However, in “Opt for real conditions”, the storage discharge from 15:45 to 16:00. This explains the difference in the grid cost and the total cost for both cases.

Table 15. Energy system cost—experimental test 2.

Case operation	Grid cost (c€)	Storage cost (c€)	Total cost (c€)
Real-time exp w/o opt	5.29	7.24	12.55
Real-time exp with opt	-22.96	4.84	-18.10
Opt for real conditions	-71.37	4.02	-67.35

Figure 78 shows the energy system distribution for “real-time exp” with and without optimization.

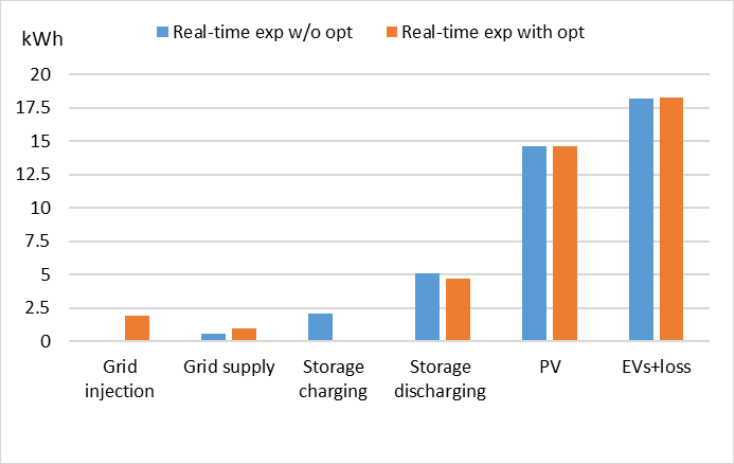

Figure 78: Energy system distribution—experimental test 2.

Figure 78 shows the energy system distribution for “Real-time w/o opt” and “Real-time with opt”. There is no grid injection in the “Real-time w/o opt”, while for the “Real-time with opt”, there is a little bit of grid injection, which refers to selling energy to the grid and having approximately the same storage charging energy.

Figure 79 shows the EV energy distribution for “real-time exp” with and without optimization.

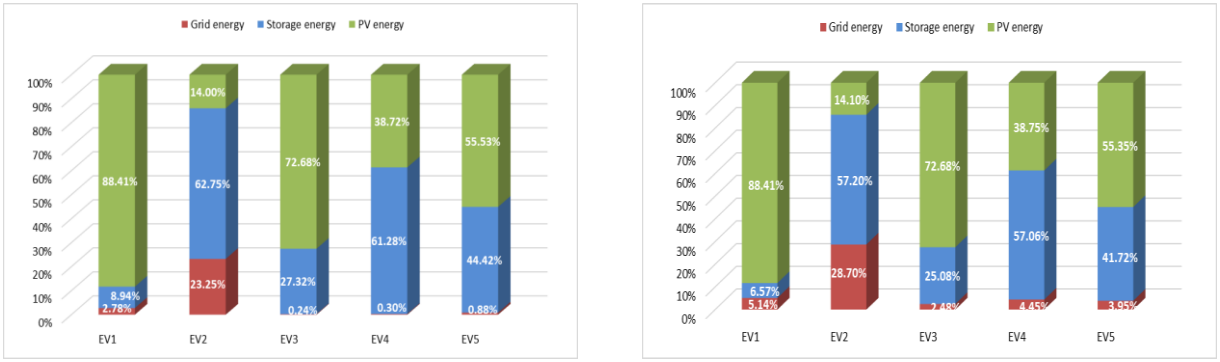

(**a**) (**b**)

Figure 79: EV energy distribution for "real-time exp" (a) without optimization and (b) with optimization—experimental test 2.

In Figure 79, EV1 and EV3 depend mainly on PV energy since they charge in slow mode. EV2 depends on PV, storage and grid energy. The percentage of grid energy is significantly greater than the other EVs since it is charging in fast mode. EV4 depends on storage more than PV. The energy distribution in both cases is very similar and is considered good as only EV2, charging in fast mode, has been charged with 23% and 28% in Figure 79a and Figure 79b respectively.

IV.2.3. Experimental test 3

The case of 8 November 2021, in Compiegne, France, is considered. Figure 80 shows $p_{PV\ MPPT\ pred}$, and $p_{PV\ MPPT}$, where the irradiations are low with fluctuations and the sundown is between 16:00 and 17:00.

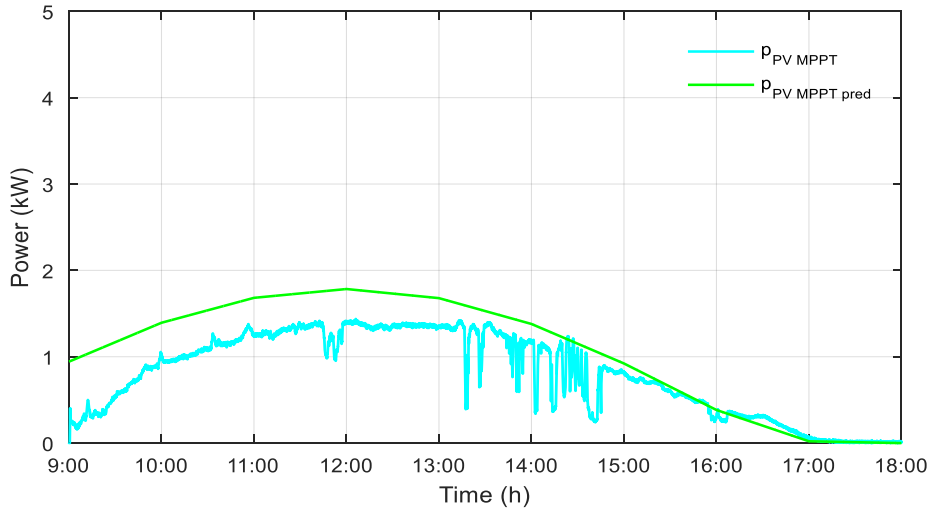

Figure 80: PV MPPT real and predicted powers—experimental test 3.

In this case, the IIREV demand power is based on the data in Table 14. Figure 81 shows the power flow and storage state of charge for "real-time exp" without optimization and the DC bus voltage—experimental test 3a.

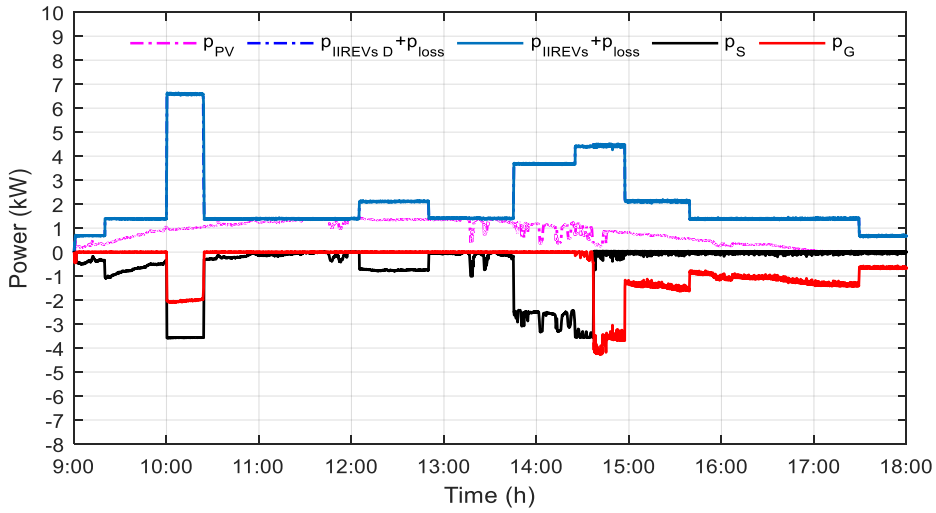

(a)

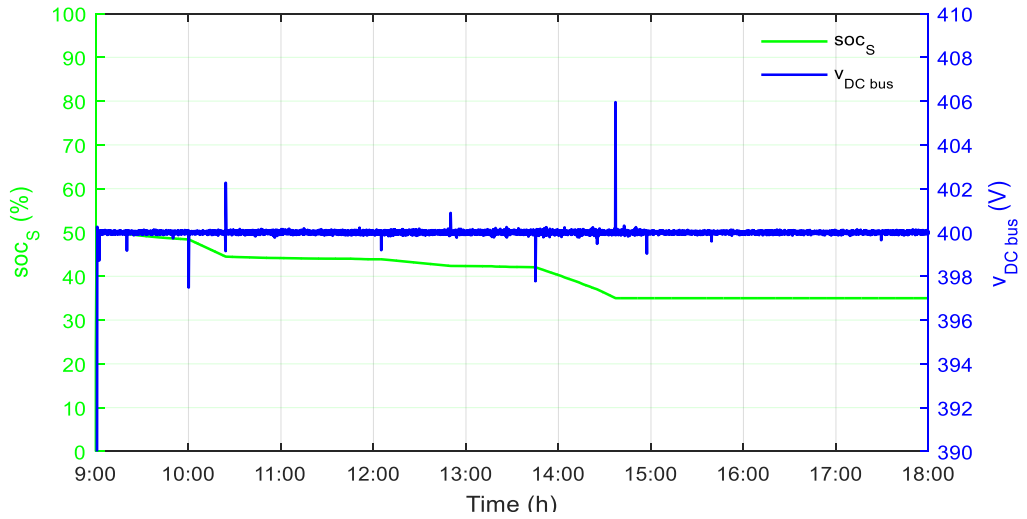

(b)

Figure 81: Power flow and storage state of charge for "real-time exp" without optimization (a) and (b) storage state of charge and DC bus voltage—experimental test 3a.

In Figure 81a, the storage is always prioritized to be either charged or discharged. when EV2 arrives, the IIREV demand power is greater than the PV and storage power that they can supply. Therefore, the grid supplies power to charge the EVs. The grid continues supplying power to the IIREVs as the storage is empty around 14:40. Figure 81b shows the evolution of the storage SOC, where it always discharges until its empty around 14:40, and the stability of the DC bus voltage is present even with small fluctuations. Spikes of a few voltages (1.5%) happen when each EV starts charging and when it finishes charging.

Figure 82 shows the power flow and storage state of charge for "real-time exp" with optimization and the DC bus voltage—experimental test 3b.

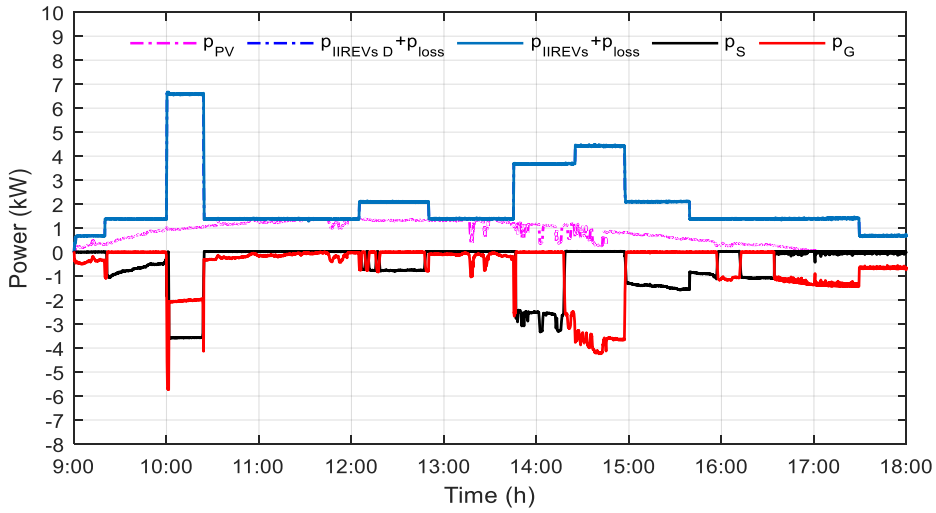

(a)

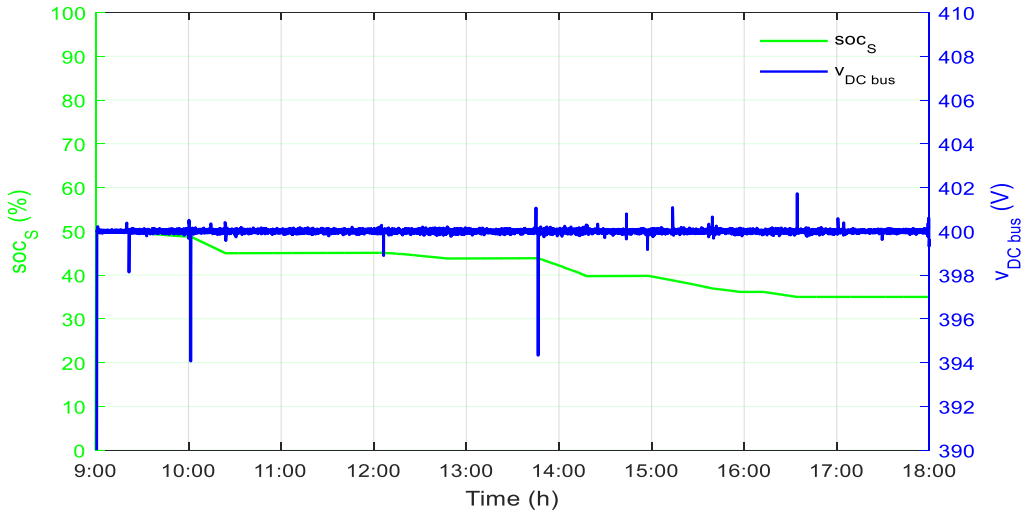

(b)

Figure 82: Power flow and storage state of charge for "real-time exp" with opt (a) and (b) storage state of charge and DC bus voltage—experimental test 3b.

In Figure 82a, the power flow of the storage and the grid is based on the coefficient k_D. Right after the departure of EV2 the grid supplies power, falsely as calculated by k_D. However, when EV2 arrives, the IIREV demand power is greater than the PV and storage power that they can supply. Therefore, the grid supplies power to charge the EVs. When EV4 arrives, the storage discharges until around 14:20, to preserve the storage until peak period at 15:00 until 16:00 to avoid the high cost of grid supply power. Figure 82b shows the evolution of the storage SOC, where the storage discharges energy from 09:20 to 10:25, 12:05 to 12:50, 13:45 to 14:20, 15:00 to 16:00 and 16:15 to 16:40 where its empty. Figure 82b also shows the stability of the DC bus voltage even with small fluctuations, which are due to the switching of DC converters, and the spikes of a few voltages (1.25%) happen when each EV starts charging and when it finishes charging.

Table 16 shows the energy system cost for “real-time exp” with optimization is closer to the optimization for real conditions, as it avoids grid supply in peak hours and gives better energy costs of 73.26 c€. For “real-time exp” without optimization, the energy cost is higher than in optimization as the storage emptied before 15:00 to 16:00 and so the grid supplied power in this period. As shown in Figure 80, the PV power prediction is overestimated and much higher than the real PV power. However, in “Opt for real conditions”, the grid supplies its maximum power when EV2 arrives, and the storage is preserved to discharge at peak hours from 12:00 to 13:00 and15:00 to 16:00, giving an energy cost of 32.35 c€. This explains the difference in the grid cost and the total cost for both cases.

Table 16: Energy system cost—experimental test 3.

Case operation	Grid cost (c€)	Storage cost (c€)	Total cost (c€)
Real-time exp w/o opt	132.15	5.60	137.75
Real-time exp with opt	67.77	5.49	73.26
Opt for real conditions	26.74	5.61	32.35

Figure 83 shows the energy system distribution for “real-time exp” with and without optimization.

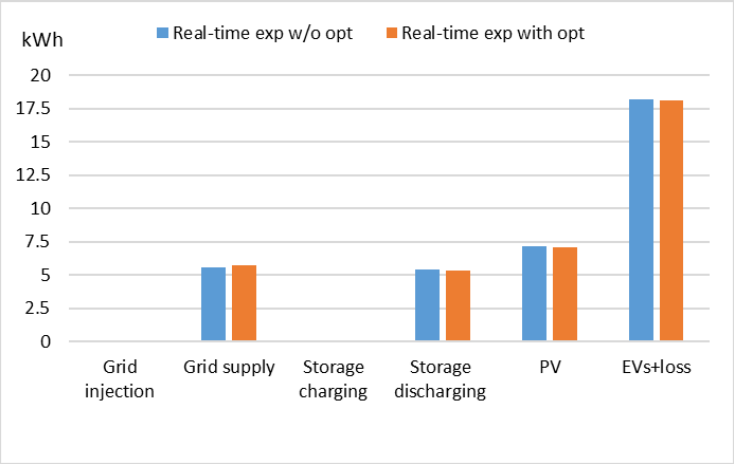

Figure 83: Energy system distribution—experimental test 3.

Figure 83 shows the energy system distribution for “Real-time w/o opt” and “Real-time with opt”. There is neither grid injection nor storage charging in the “Real-time w/o opt”, and “Real-time with opt”, whereas the storage discharging energy and grid supply energy are approximately the same, but the time of user of these sources is different.

Figure 84 shows the EV energy distribution for “real-time exp” with and without opt.

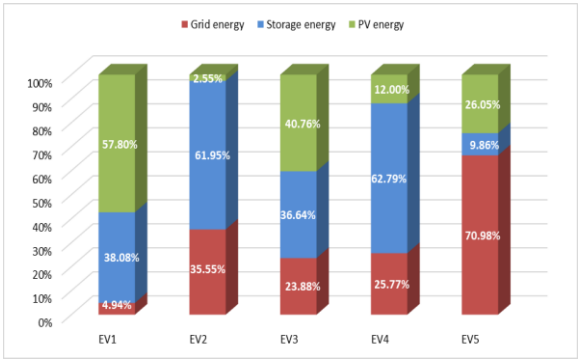

(a)

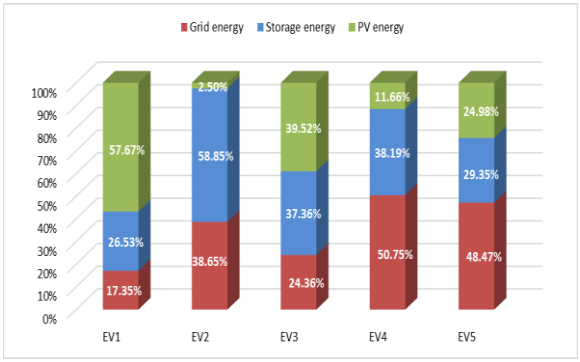

(b)

Figure 84: EV energy distribution for "real-time exp" (a) without opt and (b) with opt—experimental test 3.

In Figure 84, the share of PV energy is not significant even for EVs charging in slow mode. Thus, the share of storage energy is high for EV1 and EV3, while the share of grid energy is high for EV2, EV4, and EV5. Figure 84b shows a better EV energy distribution than in Figure 84a, where EV3 and EV5 were charged by the storage instead of the grid, whereas for EV4, the storage was preserved to discharge at the peak hour from 15:00 to 16:00, and therefore EV4, charging in average mode, was charged mainly by the grid.

IV.2.4. Experimental test 4

Table 17 provides the parameters used for "real-time exp" and power balancing control for experimental tests 4, 5, 6, and 7.

Table 17: Real-time experiment parameter values for experimental tests 4, 5, 6 and 7.

SOC_{S_min}	35%	$P_{G\_I\_max}$	10 kW	c_S	0.01€/kWh
SOC_{S_max}	60%	$P_{G\_S\_max}$	10 kW	c_{PVS}	1.2€/kWh
SOC_{EV_min}	20%	P_{S_max}	3.5 kW	V_{ref}	400 V
SOC_{EV_max}	100%	N_{PV}	12 PV	E_{Bat}	37.44 kWh
SOC_{S_0}	50%	$p_{PV\ MPPT}$	4.14 kWp	E	5 kWh
$P_{EV\_fast\_max}$	5 kW	c_{G_NH}	0.1€/kWh		
$P_{EV\_aver\_max}$	2.2 kW	c_{G_PH}	0.7€/kWh		
$P_{EV\_slow\_max}$	0.7 kW	$c_{EV\_penalty}$	2.5€/kWh		

The parameter values used in Table 17 were chosen to allow charging of more than one EV in fast or average mode, therefore, the grid limits are increased.

The case of 10 April 2022, in Compiegne, France, is considered. Figure 85 shows $p_{PV\ MPPT\ pred}$, and $p_{PV\ MPPT}$, where the irradiations are high and the weather is a partially sunny with low fluctuations. The IIREV demand power is based on the data in Table 18.

Table 18: Assumed options by the EV users for experimental test 4 and 5.

EVs	SOC_{EV_arr}	SOC_{EV_des}	t_{arr}	t_{est_ch}	M
EV1	25%	80%	09:15	03:55	Slow
EV2	23%	85%	09:50	00:37	Fast
EV3	35%	90%	10:05	01:15	Average
EV4	30%	75%	13:20	03:13	Slow
EV5	26%	82%	14:00	00:34	Fast

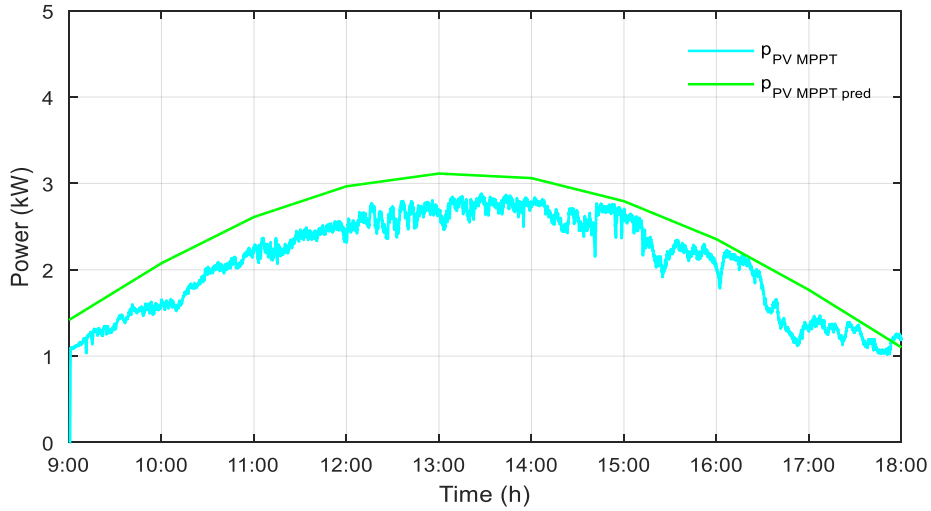

Figure 85: PV MPPT real and predicted powers—experimental test 4.

Figure 86 shows the power flow and storage state of charge for "real-time exp" without optimization and the DC bus voltage—experimental test 4a.

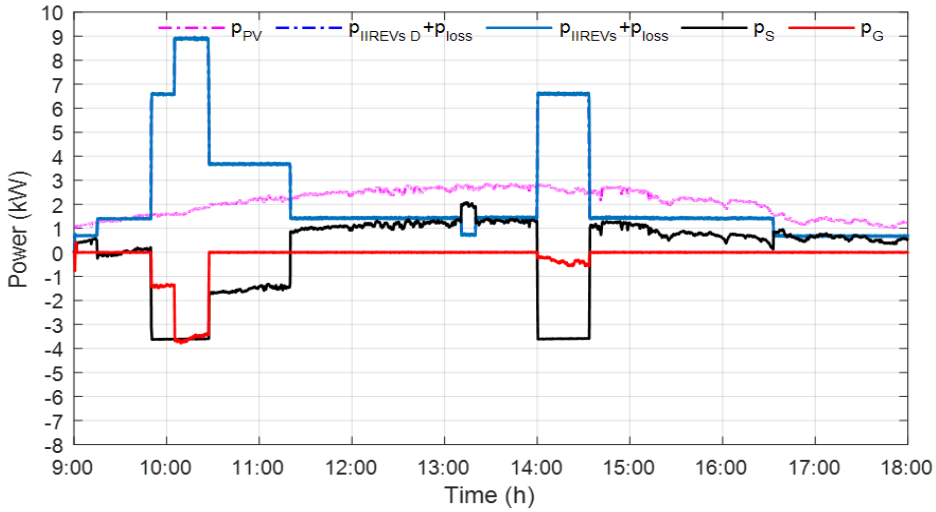

(a)

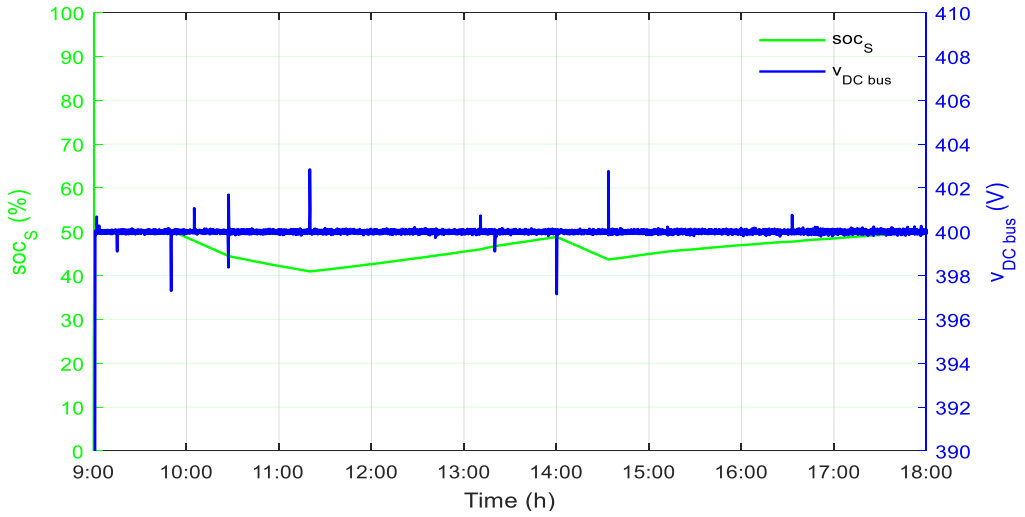

(b)

Figure 86: Power flow and storage state of charge for "real-time exp" without optimization (a) and (b) storage state of charge and DC bus voltage—experimental test 4a.

In Figure 86a, the storage is always prioritized to be either charged or discharged. when EV2 arrives, the IIREV demand power is greater than the PV and storage power that they can supply. Therefore, the grid supplies power to charge the EVs. Figure 86b shows the evolution of the storage SOC, where it starts recharging right after the departure of EV3 until the arrival of EV5 and recharges again after the departure of EV5, and the stability of the DC bus voltage is present even with small fluctuations. Spikes of a few voltages (0.5%) happen when each EV starts charging and when it finishes charging.

Figure 87 shows the power flow and storage state of charge for "real-time exp" with optimization and the DC bus voltage—experimental test 4b.

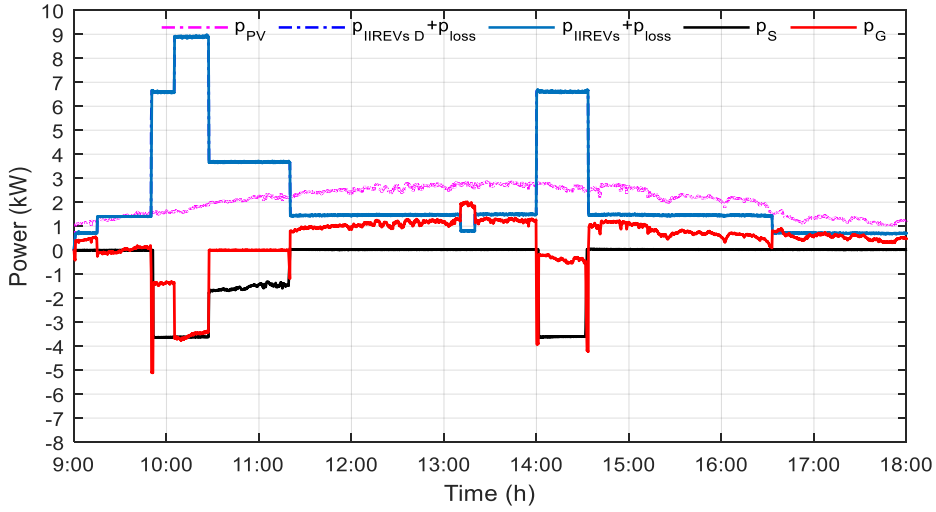

(a)

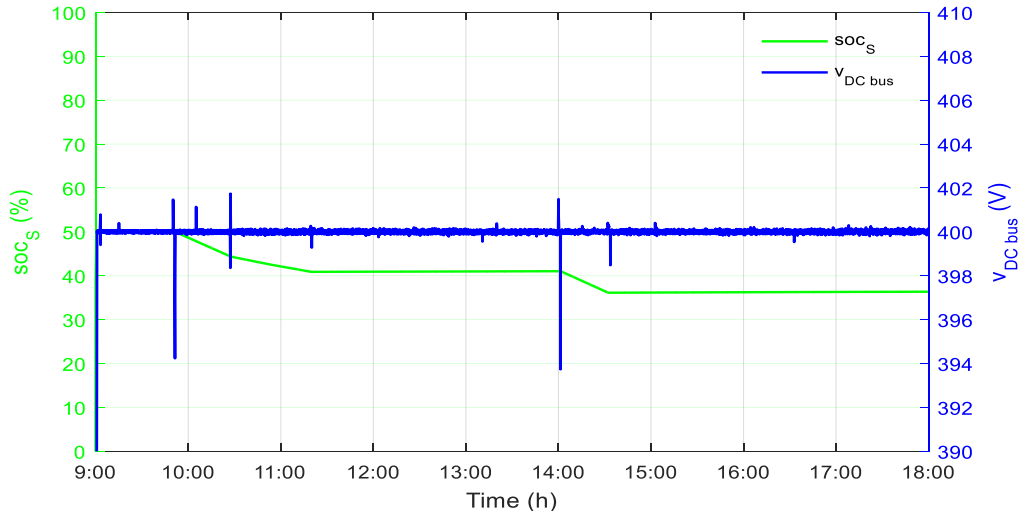

(b)

Figure 87: Power flow and storage state of charge for "real-time exp" with optimization (a) and (b) the storage state of charge and DC bus voltage—experimental test 4b.

In Figure 87a, the power flow of the storage and the grid is based on the coefficient k_D. However, when EV2 and EV3 comes to charge in fast and average mode respectively, the IIREV demand power is greater than the PV and storage power that they can supply, and therefore, storage and grid supply power. Right after the departure of EV3 until the arrival of EV5, the PV injects energy to the grid, especially during the peak hour. Despite the high demand power of IIREV in this case, yet the PV production is high, allowing grid injection most of the time. Figure 87b shows the evolution of the storage SOC, where the storage discharges energy from 09:50 to 11:20, and 14:00 to 14:34 when EV5 lefts the PVCS. Figure 87b also shows the stability of the DC bus voltage even with small fluctuations, which are due to the switching of DC converters, and the spikes of a few voltages (1.5%) happen when each EV starts charging and when it finishes charging.

Table 19 shows the energy system cost for "real-time exp" with optimization is closer to the optimization for real conditions, as it injects energy to the grid and gives better energy costs of -142.73 c€. In "Opt for real conditions", where the optimization is performed without uncertainties, it gives the optimal energy cost without error, which is -148.67 c€. It avoids grid supply energy when the storage can discharge energy instead, which explains the big difference in the grid cost and the total cost for both cases.

Table 19. Energy system cost—experimental test 4.

Case operation	Grid cost (c€)	Storage cost (c€)	Total cost (c€)
Real-time exp w/o opt	18.73	11.55	30.28
Real-time exp with opt	-148.27	5.54	-142.73
Opt for real conditions	-154.19	5.52	-148.67

Figure 88 shows the energy system distribution for "real-time exp" with and without optimization.

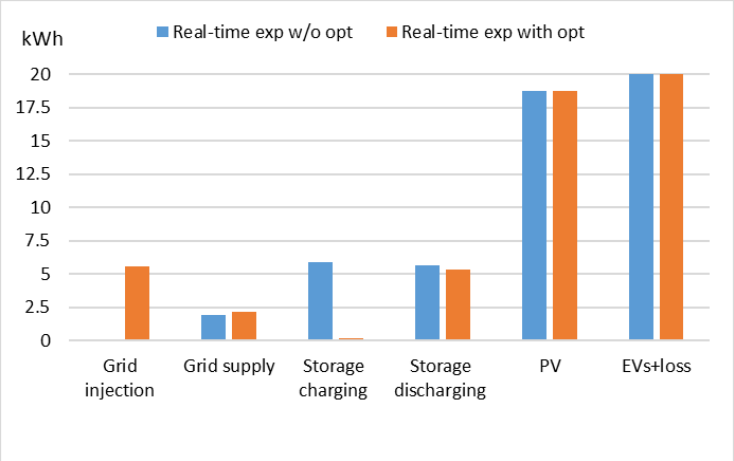

Figure 88: Energy system distribution—experimental test 4.

Figure 88 shows the energy system distribution for "Real-time w/o opt" and "Real-time with opt". There is no grid injection in the "Real-time w/o opt" but more than 5.5 kWh of storage charging, while for the "Real-time with opt", there is around 5 kWh of grid injection, which refers to selling energy to the grid and having approximately the same storage discharging energy.

Figure 89 shows the EV energy distribution for "real-time exp" with and without optimization.

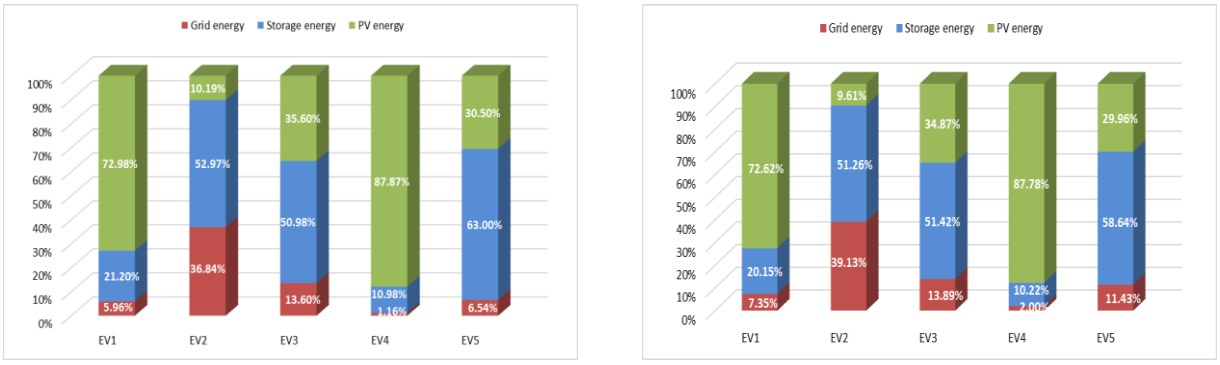

(**a**) (**b**)

Figure 89: EV energy distribution for "real-time exp" (a) without optimization and (b) with optimization—experimental test 4.

In Figure 89, EV1 and EV4 depend mainly on PV energy since they charge in slow mode. EV2 and EV5 depend on PV, storage and grid energy. The percentage of grid energy is significantly greater than the other EVs since it is charging in fast mode. EV3 depends on storage more than PV. The energy distribution in both cases is very similar and is considered good.

IV.2.5. Experimental test 5

The case of 22 September 2021, in Compiegne, France, is considered. Figure 90 shows $p_{PV\ MPPT\ pred}$, and $p_{PV\ MPPT}$, where the irradiations are intermediate with fluctuations.

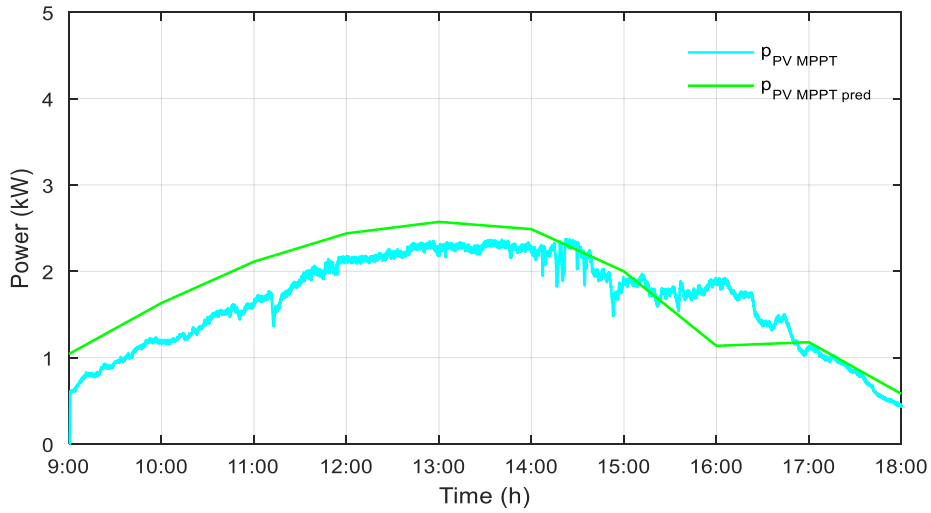

Figure 90: PV MPPT real and predicted powers—experimental test 5.

In this case, the IIREV demand power is based on the data in Table 18. Figure 91 shows the power flow and storage state of charge for "real-time exp" without optimization and the DC bus voltage—experimental test 5a.

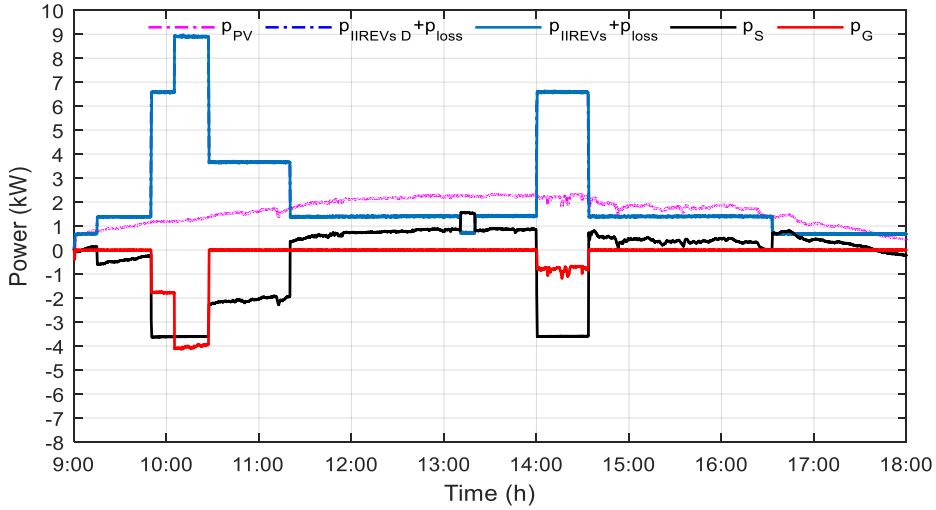

(a)

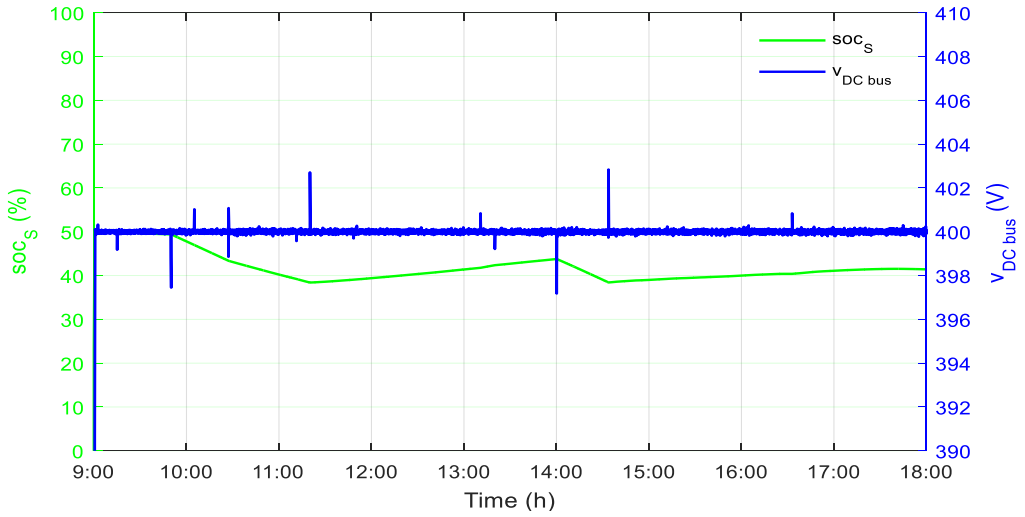

(b)

Figure 91: Power flow and storage state of charge for "real-time exp" without optimization (a) and (b) storage state of charge and DC bus voltage—experimental test 5a.

In Figure 91a, the storage is always prioritized to be either charged or discharged. when EV2 arrives, the IIREV demand power is greater than the PV and storage power that they can supply. Therefore, the grid supplies power to charge the EVs. Figure 91b shows the evolution of the storage SOC, where it starts recharging right after the departure of EV3 until the arrival of EV5 and recharges again after the departure of EV5, and the stability of the DC bus voltage is present even with small fluctuations. Spikes of a few voltages (0.5%) happen when each EV starts charging and when it finishes charging.

Figure 92 shows the power flow and storage state of charge for "real-time exp" with optimization and the DC bus voltage—experimental test 5b.

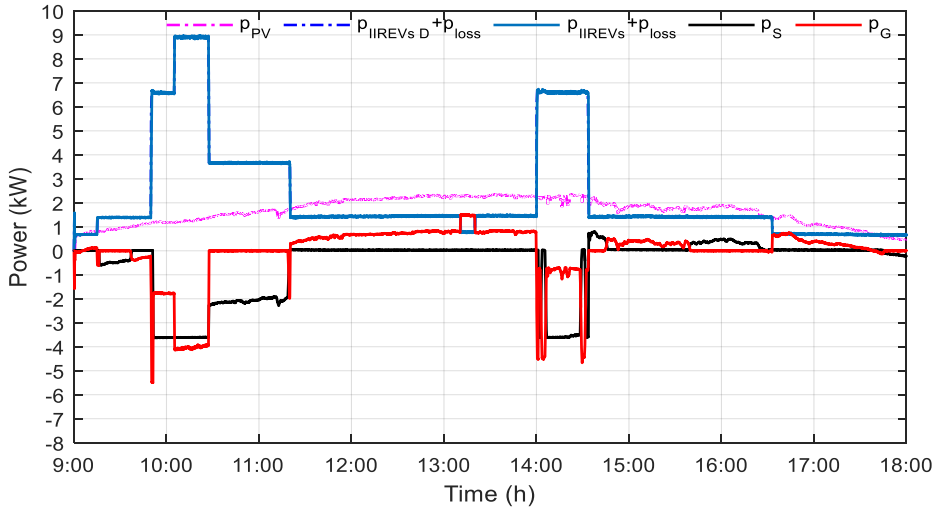

(a)

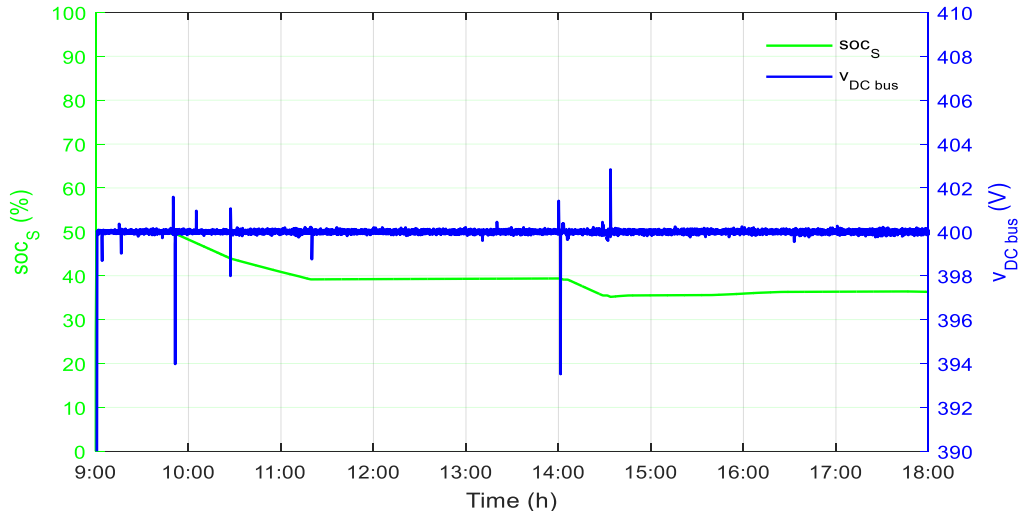

(b)

Figure 92: Power flow and storage state of charge for "real-time exp" with opt (a) and (b) storage state of charge and DC bus voltage—experimental test 5b.

In Figure 92a, the power flow of the storage and the grid is based on the coefficient k_D. However, when EV2 and EV3 comes to charge in fast and average mode respectively, the IIREV demand power is greater than the PV and storage power that they can supply, and therefore, storage and grid supply power. Right after the departure of EV3 until the arrival of EV5, the PV injects energy to the grid, especially during the peak hour. Despite the high demand power of IIREV in this case, yet the PV production is high, allowing grid injection most of the time. Figure 92b shows the evolution of the storage SOC, where the storage discharges energy from 09h15 to 09:40 and from 09:50 to 11:20, and 14:00 to 14:34 when EV5 lefts the PVCS, whereas, it has been charging from around 15:40 to around 16:30. Figure 92b also shows the stability of the DC bus voltage even with small fluctuations, which are due to the switching of DC converters, and the spikes of a few voltages (1.5%) happen when each EV starts charging and when it finishes charging.

Table 20 shows the energy system cost for "real-time exp" with optimization is closer to the optimization for real conditions, as it injects energy to the grid and gives better energy costs of -47.57 c€. In "Opt for real conditions", where the optimization is performed without uncertainties, it gives the optimal energy cost without error, which is -63.60 c€. It avoids grid supply energy when the storage can discharge energy instead and injects PV energy into the grid instead of charging the storage, which explains the difference in the grid cost and the total cost for both cases.

Table 20: Energy system cost—experimental test 5.

Case operation	Grid cost (c€)	Storage cost (c€)	Total cost (c€)
Real-time exp w/o opt	23.73	9.74	33.47
Real-time exp with opt	-53.89	6.32	-47.57
Opt for real conditions	-69.22	5.61	-63.60

Figure 93 shows the energy system distribution for "real-time exp" with and without optimization.

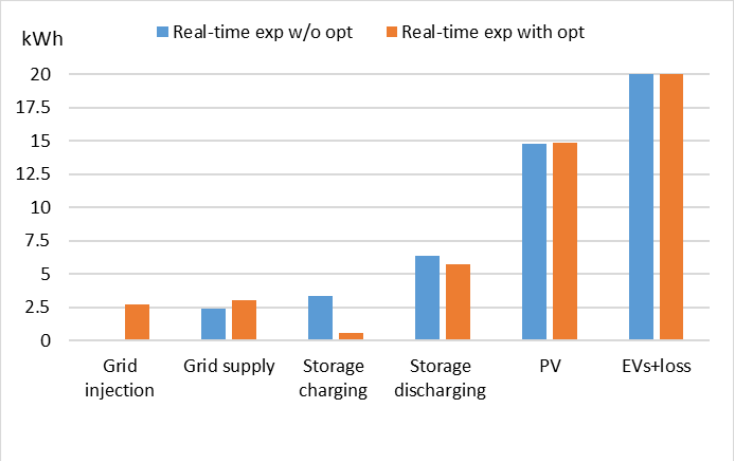

Figure 93: Energy system distribution—experimental test 5.

Figure 93 shows the energy system distribution for "Real-time w/o opt" and "Real-time with opt". There is no grid injection in the "Real-time w/o opt" but around 3.5 kWh of storage charging instead, while for the "Real-time with opt", there is around 2.5 kWh of grid injection, which refers to selling energy to the grid and having nearly the same storage discharging energy.

Figure 94 shows the EV energy distribution for "real-time exp" with and without opt.

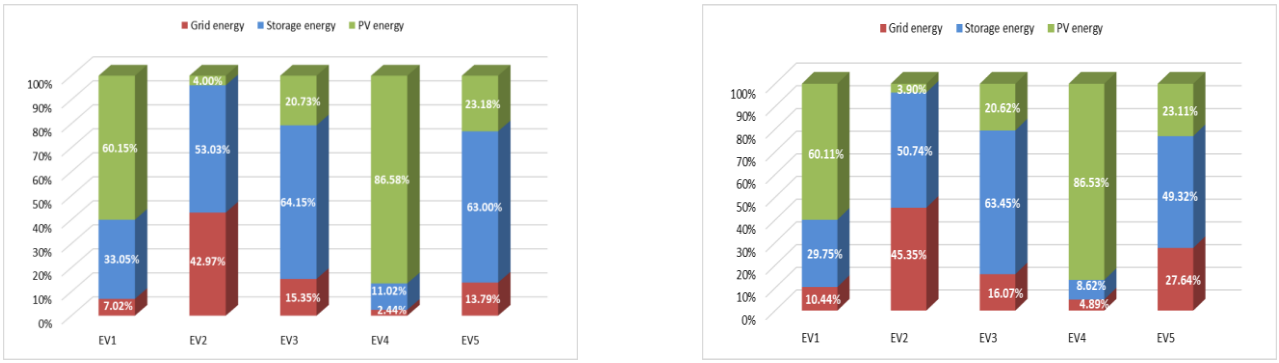

(a) **(b)**

Figure 94: EV energy distribution for "real-time exp" (a) without opt and (b) with opt—experimental test 5.

In Figure 94, EV1 and EV4 depend mainly on PV energy since they charge in slow mode. EV2 and EV5 depend on PV, storage and grid energy. The percentage of grid energy is significantly greater than the other EVs since it is charging in fast mode. EV3 depends on storage more than PV. The energy distribution in both cases is very similar and is considered good.

IV.2.6. Experimental test 6

The case of 14 May 2022, in Compiegne, France, is considered. Figure 95 shows $p_{PV\ MPPT\ pred}$, $p_{PV\ MPPT}$, where the irradiations are high and the weather is a partially sunny with low fluctuations. The IIREV demand power is based on the data in Table 21.

Table 21: Assumed options by the EV users for experimental test 6 and 7.

EVs	SOC_{EV_arr}	SOC_{EV_des}	t_{arr}	t_{est_ch}	M
EV1	22%	79%	09:15	04:04	Slow
EV2	35%	88%	09:35	03:47	Slow
EV3	24%	82%	09:55	04:08	Slow
EV4	33%	77%	10:20	03:09	Slow
EV5	36%	90%	11:00	03:51	Slow

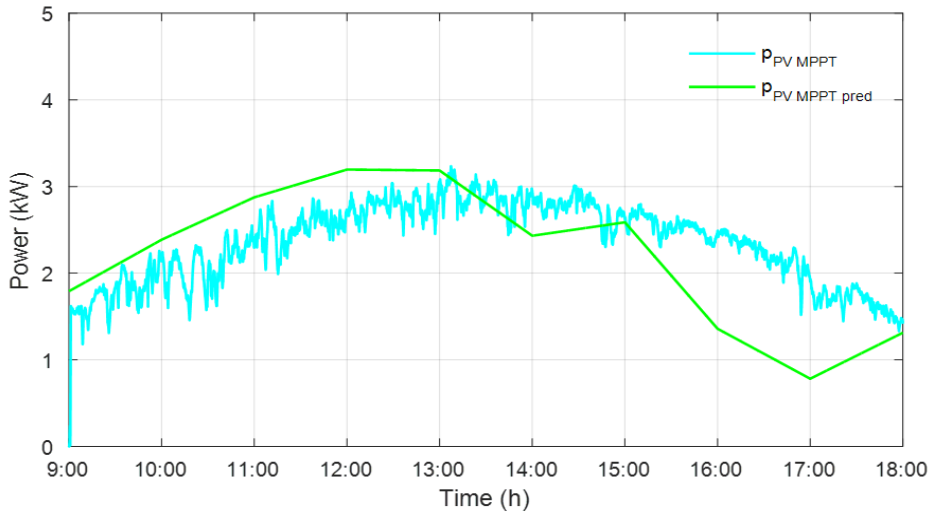

Figure 95: PV MPPT real and predicted powers—experimental test 6.

Figure 96 shows the power flow and storage state of charge for "real-time exp" without optimization and the DC bus voltage—experimental test 6a.

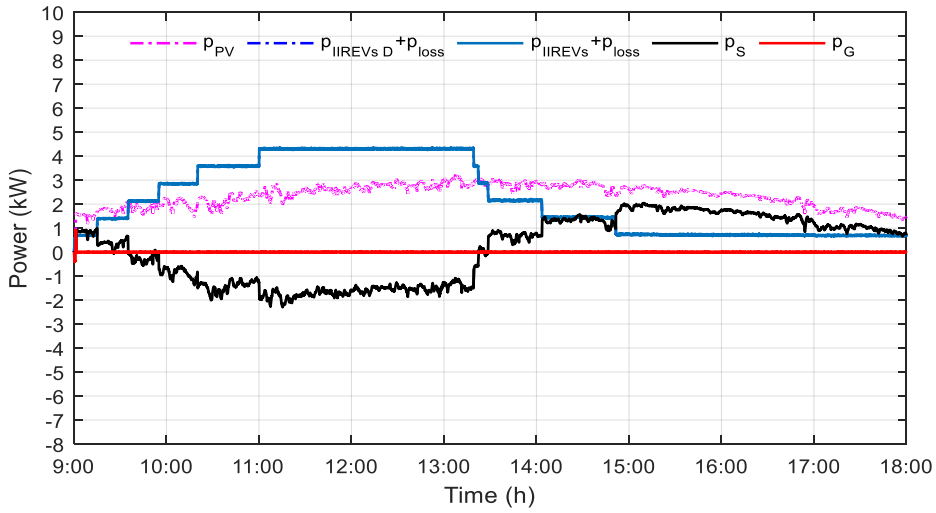

(a)

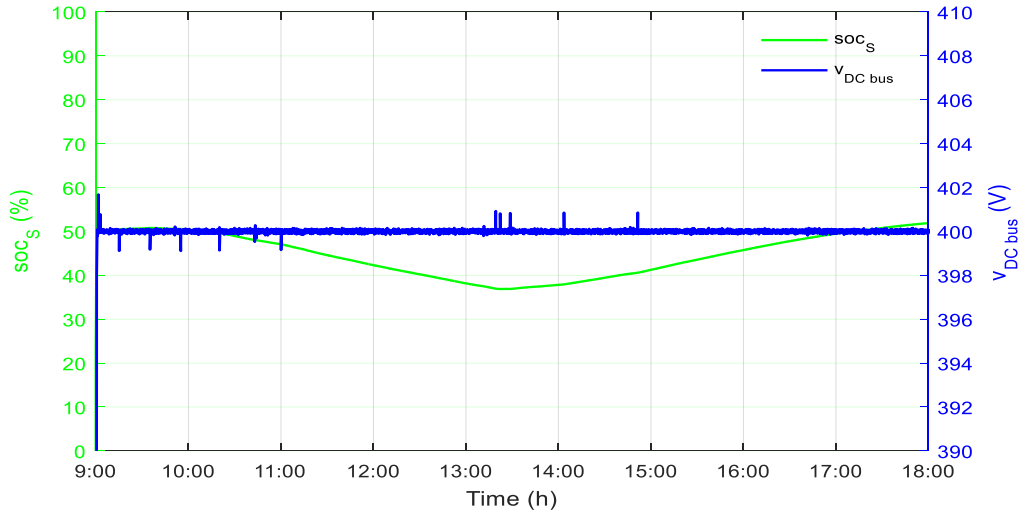

(b)

Figure 96: Power flow and storage state of charge for "real-time exp" without optimization (a) and (b) storage state of charge and DC bus voltage—experimental test 6a.

In Figure 96a, the storage is always prioritized to be either charged or discharged. All EVs are charging in slow mode, therefore, only the storage discharged power into the EVs. Figure 96b shows the evolution of the storage SOC, where it starts recharging right after the departure of EV3 until 18:00, and the stability of the DC bus voltage is present even with small fluctuations (0.25%).

Figure 97 shows the power flow and storage state of charge for "real-time exp" with optimization and the DC bus voltage—experimental test 6b.

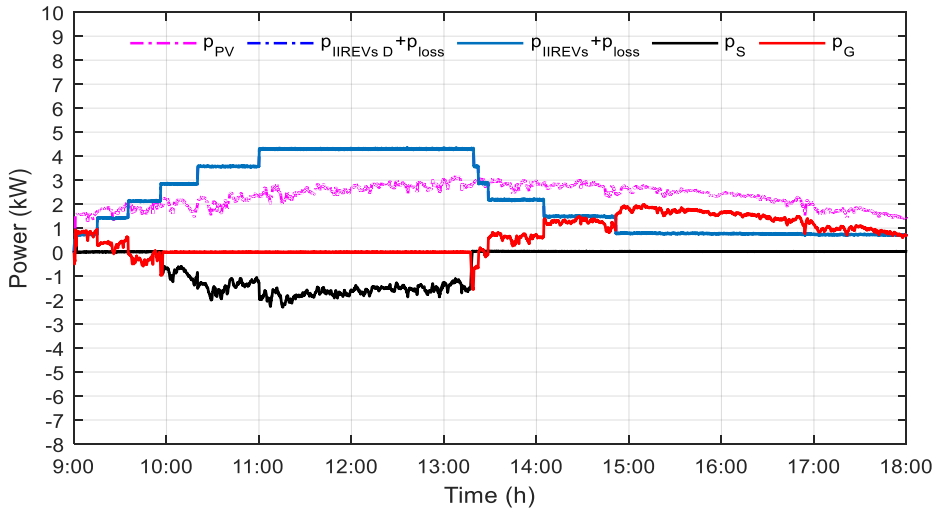

(a)

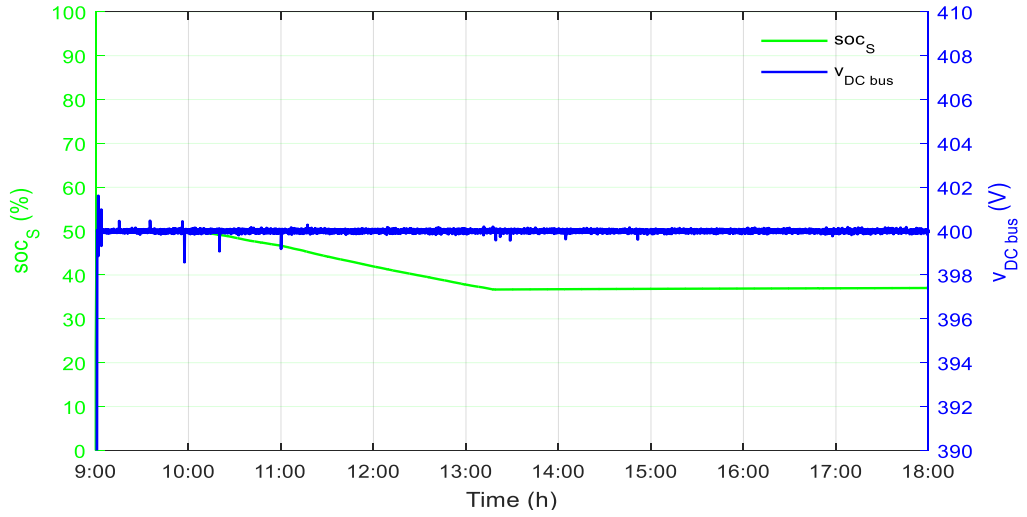

(b)

Figure 97: Power flow and storage state of charge for "real-time exp" with optimization (a) and (b) the storage state of charge and DC bus voltage—experimental test 6b.

In Figure 97a, the power flow of the storage and the grid is based on the coefficient k_D. All EVs are charging in slow mode, therefore, only the storage discharged power into the EVs. Right after the departure of EV3 until the arrival of EV5, the PV injects energy to the grid, especially during the peak hour. Despite the high demand power of IIREV in this case, yet the PV production is high, allowing grid injection most of the time. In Figure 97a b shows the evolution of the storage SOC, where it starts recharging right after the departure of EV3 until 18:00, and the stability of the DC bus voltage is present even with small fluctuations (0.25%).

Table 22 shows the energy system cost for "real-time exp" with optimization is closer to the optimization for real conditions, as it injects energy to the grid and gives better energy costs of -156.63 c€. In "Opt for

real conditions", where the optimization is performed without uncertainties, it gives the optimal energy cost without error, which is -167.46 c€. It avoids grid supply energy when the storage can discharge energy instead, which explains the difference in the grid cost and the total cost for both cases.

Table 22. Energy system cost—experimental test 6.

Case operation	Grid cost (c€)	Storage cost (c€)	Total cost (c€)
Real-time exp w/o opt	0	1.54	11.54
Real-time exp with opt	-161.80	5.17	-156.63
Opt for real conditions	-172.65	5.19	-167.46

Figure 98 shows the energy system distribution for "real-time exp" with and without optimization.

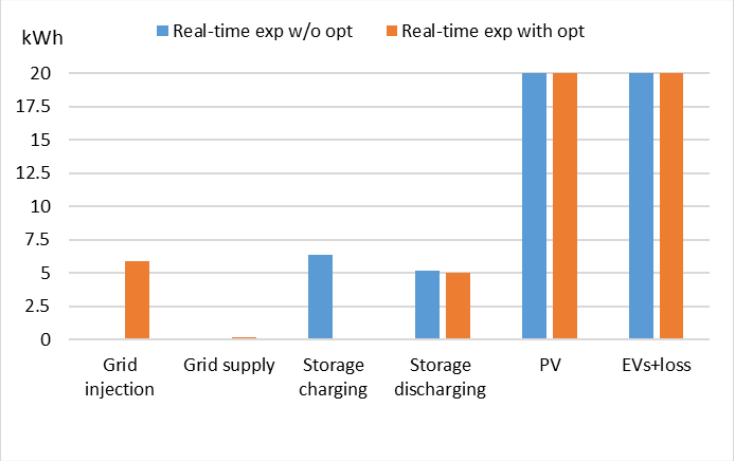

Figure 98: Energy system distribution—experimental test 6.

Figure 98 shows the energy system distribution for "Real-time w/o opt" and "Real-time with opt". There is no grid injection in the "Real-time w/o opt" but around 6.5 kWh of storage charging instead, while for the "Real-time with opt", there is around 5.5 kWh of grid injection, which refers to selling energy to the grid and having nearly the same storage discharging energy.

Figure 99 shows the EV energy distribution for "real-time exp" with and without optimization.

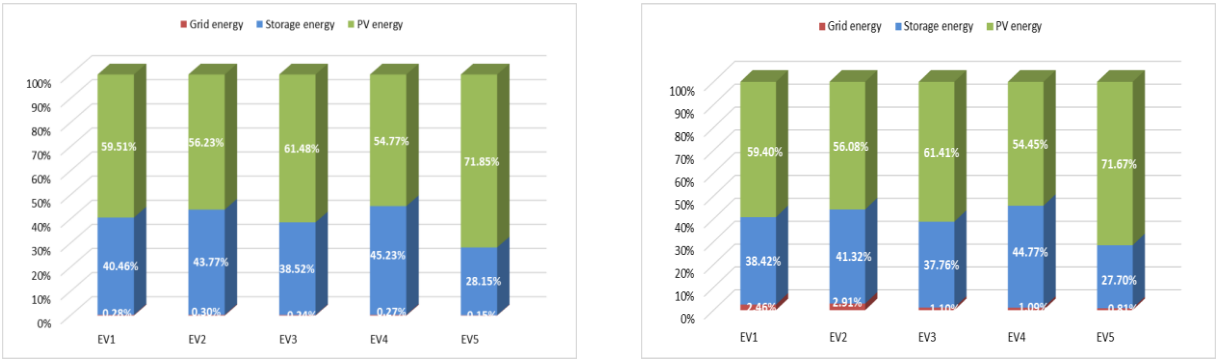

(**a**) (**b**)

Figure 99: EV energy distribution for "real-time exp" (a) without optimization and (b) with optimization—experimental test 6.

In Figure 99, all EVs charged in slow mode, therefore, they are charged mainly by PV and the storage as second source. The energy distribution in both cases is very similar and is considered good.

IV.2.7. Experimental test 7

The case of 27 October 2022, in Compiegne, France, is considered. Figure 70 shows $p_{PV\ MPPT\ pred}$, and $p_{PV\ MPPT}$, where the irradiations are intermediate and the weather is a bit cloudy, so there are low fluctuations. The IIREV demand power is based on the data in Table 21.

Figure 71Figure 100 shows the power flow and storage state of charge for "real-time exp" without optimization and the DC bus voltage—experimental test 7a.

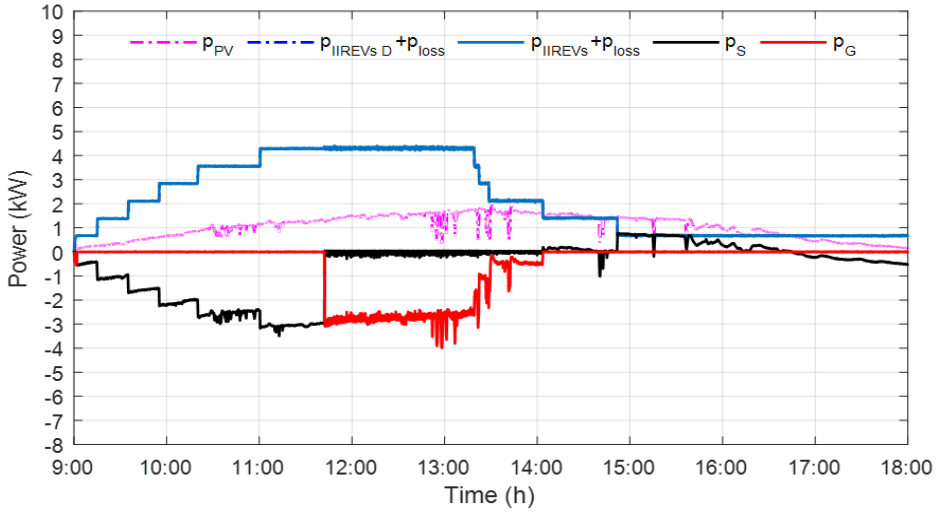

(**a**)

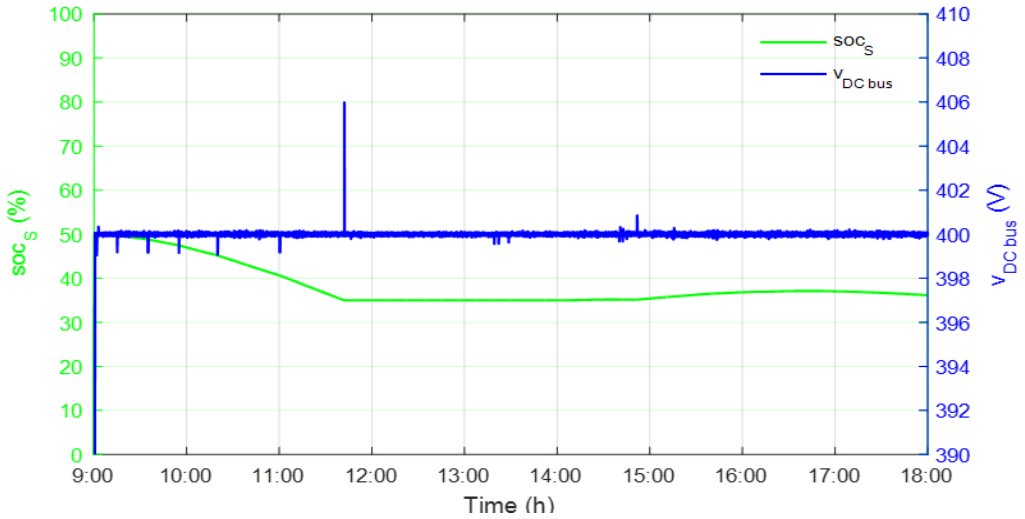

(**b**)

Figure 100: Power flow and storage state of charge for "real-time exp" without optimization (a) and (b) storage state of charge and DC bus voltage—experimental test 7a.

In Figure 100a, the storage is always prioritized to be either charged or discharged. All EVs are charging in slow mode, however, the storage is empty around 11:45 where the grid continues charging the EVs. After the departure of all EVs except for EV5, the storage regain charging a bit and then discharges afterwards until the end. Figure 100b shows the evolution of the storage SOC, where it starts recharging right after the departure of EV3 until 18:00, and the stability of the DC bus voltage is present even with small fluctuations (1.5%).

Figure 101 shows the power flow and storage state of charge for "real-time exp" with optimization and the DC bus voltage—experimental test 7b.

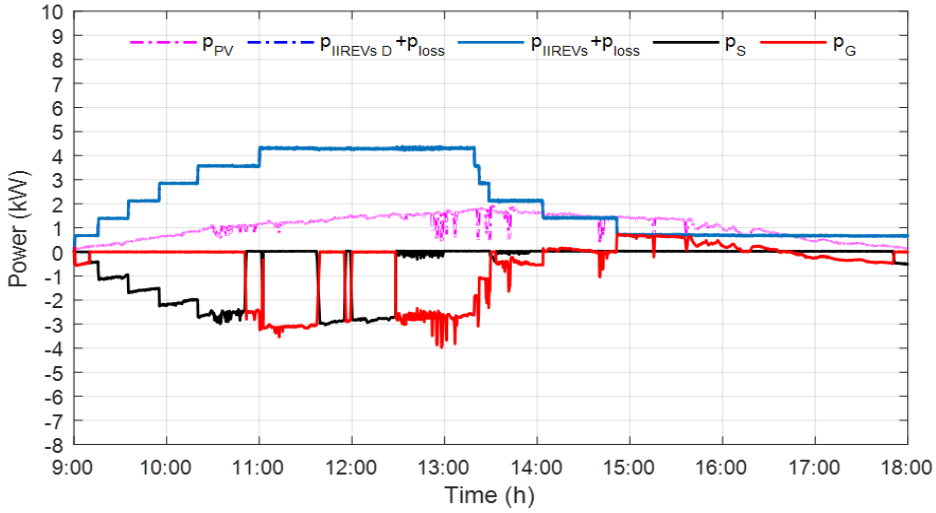

(**a**)

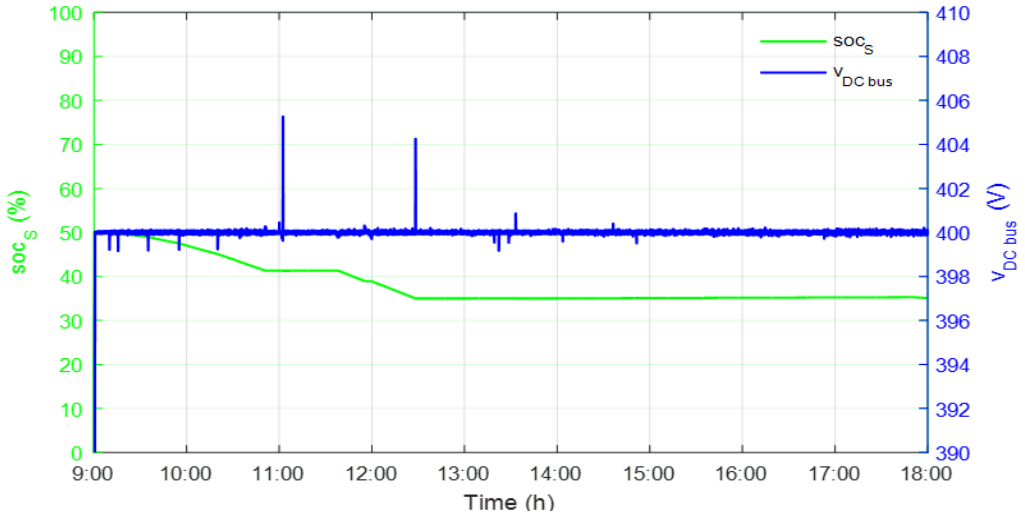

(b)

Figure 101: Power flow and storage state of charge for "real-time exp" with optimization (a) and (b) the storage state of charge and DC bus voltage—experimental test 7b.

In Figure 101a, the power flow of the storage and the grid is based on the coefficient k_D. All EVs are charging in slow mode, however, the grid supplied power when all EVs are charging to preserve the storage for the peak hour (12:00 until 13:00) but the storage becomes empty around 12:30. After the departure of all EVs except for EV5, the PV injects energy to the grid, especially during the peak hour (15:00 until 16:00). In Figure 101b shows the evolution of the storage SOC, and the stability of the DC bus voltage is present even with small fluctuations (1.5%).

Table 23 shows the energy system cost for "real-time exp" with optimization is closer to the optimization for real conditions, as it injects energy to the grid and gives better energy costs of 115.05 c€. In "Opt for real conditions", where the optimization is performed without uncertainties, it gives the optimal energy cost without error, which is 24.13 c€. It avoids grid supply energy when the storage can discharge energy instead, which explains the difference in the grid cost and the total cost for both cases.

Table 23. Energy system cost—experimental test 7.

Case operation	Grid cost (c€)	Storage cost (c€)	Total cost (c€)
Real-time exp w/o opt	219.86	7.18	227.04
Real-time exp with opt	109.4	5.64	115.05
Opt for real conditions	18.51	5.61	24.13

Figure 102 shows the energy system distribution for "real-time exp" with and without optimization.

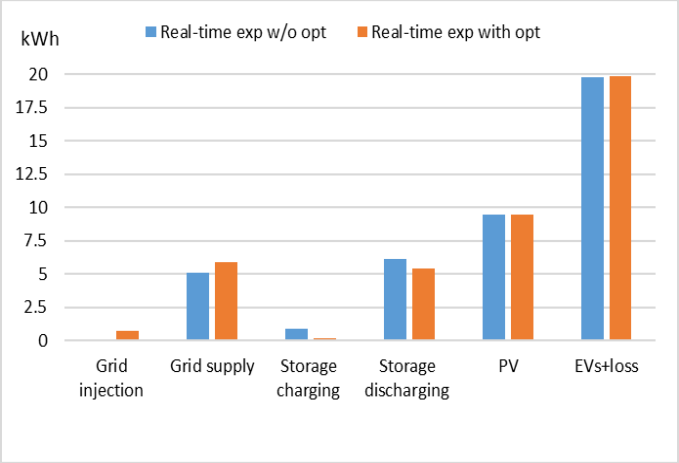

Figure 102: Energy system distribution—experimental test 7.

Figure 102 shows the energy system distribution for "Real-time w/o opt" and "Real-time with opt". There is no grid injection in the "Real-time w/o opt" but around 1 kWh of storage charging instead, while for the "Real-time with opt", there is around 0.5 kWh of grid injection, which refers to selling energy to the grid and having nearly the same storage discharging energy and grid supply energy.

Figure 103 shows the EV energy distribution for "real-time exp" with and without optimization.

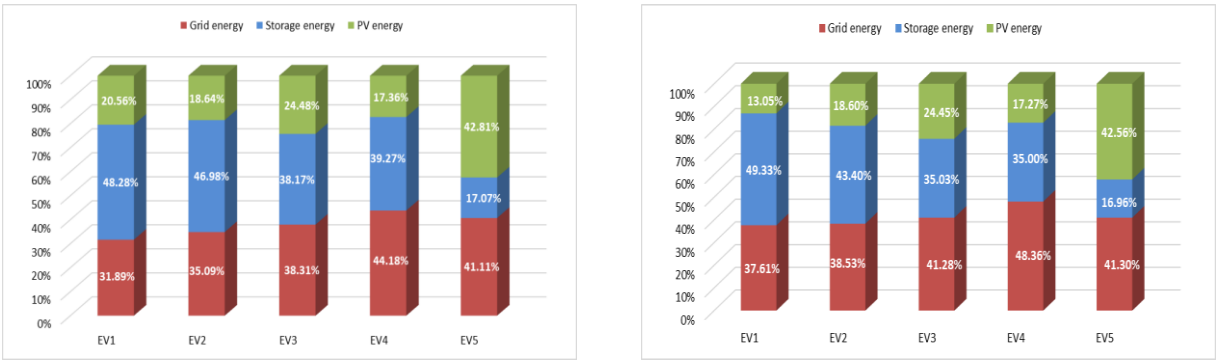

(a) **(b)**

Figure 103: EV energy distribution for "real-time exp" (a) without optimization and (b) with optimization—experimental test 7.

In Figure 103, all EVs charged in slow mode, however, as PV production is not that high, they are charged with the three sources. The energy distribution in both cases is very similar.

IV.2.8. Discussion

For "real-time exp" with optimization, selling energy to the grid is preferred to make profits based on the coefficient k_D to minimize the total cost. Thus, the test with optimization gives better energy cost than without optimization. Furthermore, the EV energy distribution can be considered for "real-time exp" with optimization to be better than without optimization.

To sum up, “with opt” performs better than “w/o opt” in minimizing the total cost of the IIREVs, and for the EV energy distribution, the results are satisfying with optimization, which is not the case without optimization, as the share of storage and grid energies are higher than the share of PV energy. For the experimental test, where all EVs are charged in slow mode and the PV production is high, the PV benefits are highlighted in this case, where EVs are mainly charged with PV energy and storage as secondary source, this reinforce the results found in chapter II.

IV.3. Conclusions

The real-time experimental results prove the superiority of the optimization problem formulated as MILP and solved by CPLEX over the storage priority algorithm. The results also show the feasibility of the proposed supervisory control of the IIREVs, which contains the HMI and the energy management with power balancing and interacts with the smart grid. The proposed supervisory control executes efficiently with respect to the constraints and fulfilling the EV user demands. Furthermore, the EVs that charge in slow mode depend mainly on PV energy, while for average or fast charging, they depend on the PV, storage and grid power sources. The EV energy distribution is considered good compared to the storage priority; only in the case with high fluctuations was the EV energy distribution better in storage priority. In addition, selling energy to the grid returns profits to the IIREV operator and makes optimization better than the storage priority algorithm.

Chapitre V. *PV-powered charging station: energy management with V2G operation and energy cost analyses*

As the adoption of EVs is increasing, the charging of EVs in large scale will increase the load demand on the public grid. However, EVs are mostly all the time in idle positions, so by the implementation of V2G service, they could be a promising solution to overcome grid challenges due to their various advantages. In this chapter, a PVCS equipped with five chargers that could support slow, average and fast charging. The PVCS integrates PV sources, storage system, connection to the public grid and EVs as a controllable load as they could operate in V2G mode. The HMI lets the EV users, who come arbitrarily at the PVCS, interacts with the PVCS which allows them to choose their preferences; desired SOC at departure, charging mode, participation in V2G service. This chapter, presented in [155], is constructed as follows: Section V.1 gives an introduction. Section V.2 presents the literature review. Section V.3 represents the PVCS design and its power management. Section v.4 represents some case studies with the implementation of V2G service. Section V.5 shows the energy cost results and analyses. Section V.6 concludes the chapter.

V.1. Introduction

The integration of RES into the grid needs storage system. Storage system is a vital element to overcome the intermittency of RES and ensure grid stability. The charging of EVs in a large scale will impose challenges on the grid. Since, they are most of the time idles, therefore, when plugged-in they can be used as energy storage system and reduce the burden on the grid. They can charge in off-peak periods and discharge in peak periods to support the public grid or the MG. Thus, EVs are considered as controllable loads and act as a distributed energy resources (DER). Hence, V2G is a promising feature in smart grid technologies [156]–[158]. The users of these EVs can be rewarded when participating in V2G service [159].

V2G service can offer voltage support, increase electricity reliability, shift the load demand, increase renewable energy integration, and improve power quality [160], [161]. It can, also, provide grid services, as voltage and frequency regulation, peak load shaving and valley filling, and spinning reserve [162]. The increased number of charging/discharging cycles may affect the battery of an EV and lead to its degradation. However, new studies are being realized proving that EV can operate in V2G service without battery degradation [163]. While in [164], the benefits are classed as follows; for the EV users, participating in V2G service can decrease the total ownership cost of EVs, V2G is seen as an alternative energy source to use for local utilization for home. For the grid operator, V2G is seen as a power source, mitigate fluctuations due to the intermittence of RES, and provides ancillary services. For the government, V2G improves the reliability and security of the power grid, increases the penetration of RES and greener environment. For

the EV operator, V2G service provides grid balancing services. For the office and business entities, V2G service can provide peak shaving and valley filling, balance load demand, which leads to reduce the total energy cost. The benefits of V2G service are summarized in [165] as:

- an alternative energy source at peak periods;
- improving reliability of the system;
- decreasing the total cost of the system;
- reducing voltage drops and line losses in the distribution grid;
- reducing power quality problems;
- reducing frequency fluctuations;
- reducing voltage stability problems;
- providing ancillary services;
- providing benefits for users who participate in V2G service.

Moreover, Some advantages of V2G services are [166]:

- providing power to home appliances in peak periods or when there is loss of electricity and later on EV can be recharged during the night when the electricity prices are low;
- providing flexibility which allows EVs to be recharged from renewable energy making it more environmentally friendly;
- handling fluctuations in load demand more efficiently;

  offering incentive cost for participants of EV users that can help them reduce their energy bill.

V.2. Literature review

In [167], the authors have developed a charging and discharging strategy for EVs in different cities in China, proving the effectiveness of their V2G operation in different cities with different trip patterns. Their objective is to minimize the cost of the distribution grid. The impacts of providing V2G service have been identified on the total cost of ownership of EVs in the Flanders region of Belgium [168]. The V2G service was balancing the peaks and valleys of electricity demands and ensuring grid stability. A grid-connected battery swapping station has been proposed in [169] with the implementation of V2G service to improve the reliability of supply in the future distribution grids. In [170], the authors have predicted, using automated machine learning, the potential location for EV charging and their participation to V2G service. The authors in [171] have demonstrated that the participation of EVs in the V2G service when they are idles in the EV charging station can alleviate the increase demand of EV charging. An improved harmony particle swarm

optimization algorithm has been proposed in [172] to solve a bi-level model to find the optimal allocation of distributed generation and EV charging station with the V2G service. The optimized model can satisfy the charging demand of EV users, improve the voltage quality, mitigate load fluctuations, encourage the use of renewable energy and improve the global performance of the planning scheme. An optimization framework has been developed in [173] to reduce GHG-intensive electricity imports in the Switzerland power system with a controlled charging/discharging of EVs. In [174], the authors have proposed a PV based off grid charging station with two bidirectional converters for charging and discharging the EVs and the storage system. An optimization model has been proposed in [175] to jointly install EV charging station and DER, where V2G service is considered with minimized annual social costs in a distribution system in China. An optimization problem has been modeled in [176] as a nonlinear stochastic programming with uncertainty of PV energy and it is solved by GAMS software. The EVs can operate in V2G mode, where they can charge during off-peak periods and discharge during peak periods to minimize the cost of energy. The proposed problem can optimize the operation of EVs in charging and discharging and minimize their batteries' cycles to avoid battery degradation. A novel control system has been presented in [177] to underpin V2G service by deploying a fleet of EVs, which allows the V2G aggregator to support voltage and frequency services to the grid, reduces the charging cost, maximizes the benefits of V2G service and minimizes the battery level degradation. A case study of an EV charging station MG based in a university campus in Jordan has been presented in [178], which investigates the feasibility of the V2G service of the EVs to minimize the global consumption of energy drawn from the public grid. A computational model of an EV with battery degradation has been studied in [179] to supply power to the grid, gaining profit for the EV owner, alleviates the load on the grid. The results show that the potential benefits from V2G is greater than the cost of battery degradation.

Some research studies have focused on charging EVs in a PVCS with the implementation of V2G service. In [78], the authors have presented a PVCS for EVs with V2G operation. They have proposed a dynamic searching peak and valley algorithm where the optimal charging and discharging start time of EVs is determined, in consideration to their charging mode, arrival time, initial SOC, departure time, and peak periods of electricity. Their objective is to lessen the burden on the public grid and reduce its energy cost. The authors in [180] have proposed a grid-connected inverter for a PVCS to improve the voltage and frequency stability of the DC MG with the integration of V2G operation. The proposed inverter can detect unusual malfunctions of the MG and operates in islanding mode. The modeling of a PVCS to provide ancillary services has been described in [181] where EV owners can be rewarded by providing frequency response services to the grid. An energy management strategy has been proposed in [182] for real-time control of a multi-source EV charging station considering DER to minimize the operating cost considering battery degradation of stationary storage and EVs for storing energy at off-peak periods and reinjecting it at peak periods. A PVCS is modeled with the implementation of V2G service in [183] to reduce the stress on the public grid and improve its stability during peak hours. Moreover, the authors have discussed the potential financial incentives needed to encourage EV users to participate in the demand response operation.

An energy management and control system of an EV charging station has been presented in [184], where V2G operation is implemented. The EV charging station is a hybrid power system, which integrates a wind turbine, PV system, a controlled solid oxide fuel cell and a connection to the public grid.

Some research studies have focused on the impact of V2G on the power system and ancillary services. A case study in Japan was conducted in [185] to study the marginal value of V2G ancillary services to balance the Japanese power system. The authors in [186] have presented a novel primary frequency control with V2G operation in coordination of the charging station operator, EV operator, and EV aggregator. In [187], the authors have studied the impact of the PHEVs on the primary frequency regulation with the participation of EVs in the V2G operation in an isolated grid of Cyprus island. Using the local flexibility resources, as stationary storage, smart charging of EV, local generation, and V2G service, the authors in [188] have discussed the optimal mix of flexibility resources to reduce grid challenged in a charging station in Norway.

Some research studies have focused on optimization problems with V2G service. In [189], the authors has investigated the optimal EV coordination with V2G service for the cost-benefit analysis, where the battery degradation of EV is considered and the firefly algorithm has been applied to optimize the system cost. The authors in [190] have proposed an effective strategy using adjustable robust optimization to enhance the security and economy of the MG. EVs can operate in V2G mode to discharge in peak periods and valley filling to lower the cost of operation under various constraints. A comprehensive multi-objective optimization model has been proposed in [191] for the energy management with the operation of V2G for EVs. Their objectives are to maximize the profit of the system operator and to minimize the CO2 emissions. The optimization problem is formulated as LP model and solved by CPLEX, considering office buildings in Italy. An MILP model has been proposed in [192] for a parking lot of EVs powered with PV/wind/hydrogen energy and storage system to minimize the total sustainability cost. The EVs can operate in V2G mode, to participate in demand response and encourage EV users to charge in off-peak periods instead of peak periods. An optimal day-ahead operation planning has been proposed in [193] for a MG integrating EVs with V2G service to minimize the daily operation costs. A heuristic optimization problem has been studied in [194] to find the optimal sizing of a hybrid PV-battery-diesel generator for an EV parking lot with V2G service, where EVs are considered as a controllable load. A multi-objective optimization model has been proposed in [195] for a MG integrating EVs with V2G service to minimize grid load fluctuation, maximize the use of renewable energy, and maximize the benefits for EV users. A two-stage smart charging algorithm has been proposed in [196] for buildings integrating EVs, PV sources, storage system and heat pump. The optimization problem is formulated as a non-linear programming model to optimize the charging of EVs. The results show the benefits of V2G service as primary frequency regulation reserve, the reduction of the energy cost, however, the degradation of Li-ion battery is non-negligible.

The development of V2G technology puts forward higher needs for chargers. In [197], the authors have designed an optimization problem to reduce the bidirectional DC-DC LLC resonant converter cost and to enhance the control frequency feasibility zone. A new on-board charging – driving integrated topology has

been designed in [198], which can improve the power, the performance of the system and reduce significantly the charging/discharging times of the EV battery. An off-board multi-functional EV charging station is presented in [199], which has a single AC interface and two DC interfaces to be able to perform DC charging and discharging of the EVs in a smart home and in a smart grid. In [200], the authors have studied the optimal charging/discharging scheduling strategies of EVs and storage system for EV charging station, considering the conversion efficiency of bidirectional chargers to maximize the profits of each EV and storage system based on electricity tariffs and demand response. A sustainable bidirectional EV charging station in the distribution network has been designed in [201] to enhance the quality of the charging station using an adaptive neuro-fuzzy controller and to reduce the grid current harmonics using a distribution static compensator.

Some research studies have focused on the V2G service for homes. In [202], the authors have proposed a charging and discharging scheme in a home energy management system that integrates PV, storage system, and EV, to reduce the energy cost, extend the battery life, maximize the load demand and the user's needs. An efficient home energy management approach has been proposed in [203] for a PVCS to support the distribution grid, by using the battery of the EV as a storage system. The proposed system with the application of V2G service can reduce the peak load demand in the residence, improve grid stability in peak periods and help supply the critical loads in the residence during a loss of power from the public grid.

[204] is a chronological literature review from 1973 to 2019 that presents the interaction between EVs and power grids, such topics are power quality, demand response, power system stability, demand management, electricity markets, study of scenarios, V2G service, and optimal location battery swap and charging stations. [205] is a review paper that gives an overview of MG technology in recent years, considering distributed energy resources, storage system, loads, and EVs with V2G service.

V.3. PV-powered charging station with V2G energy management

The PVCS considered in this chapter as illustrated in Figure 104 integrates PV sources, stationary storage and public grid connection, modeled using MATLAB/Simulink R2015b.

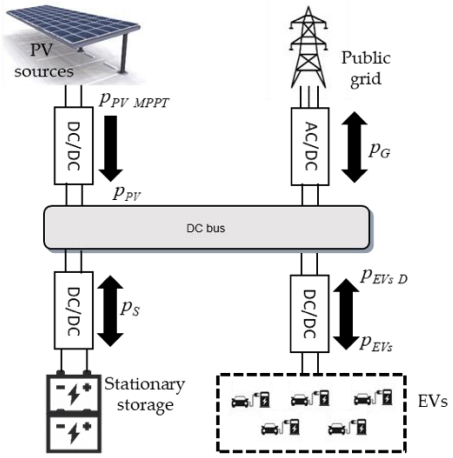

Figure 104: PV-powered charging station scheme with V2G service.

In Figure 104, $p_{PV\ MPPT}$ is the PV power in MPPT mode, p_{PV} is the PV power, p_G is the public grid power, p_S is the stationary storage power, $p_{EVs\ D}$ the EVs total demand power, and p_{EVs} is the total EVs power. The public grid can feed or absorb power. The components of the PVCS are coupled to the DC bus, represented by the capacitor C, through their dedicated converters. PV sources are connected to the DC bus through the DC/DC converter to extract the MPPT power. The stationary storage is required to set up the DC MG and it is connected through a bidirectional DC/DC converter. The DC load, represented by the EVs' batteries, is a controllable load as the EVs can be charged or discharged. Therefore, it is connected through a bidirectional DC/DC converter. The public grid connection should provide power at all times and reduce the power difference between the power production and the load demand; it is connected through a three-phase bidirectional AC/DC converter. The stationary storage is charged only by PV sources and can discharge power to the DC bus.

Figure 105 shows the energy management strategy, where EVs as load are firstly charged by PV sources, by stationary storage as second source, and by the public grid as the last energy source. PV sources charge the stationary storage with the excess energy and then inject power to the public grid when the stationary storage is full or has reached its power limit. If EV user accepts to participate in V2G service, EV can discharge during the peak periods for a short duration, 30 minutes or until it is fully discharged, then regain charging after V2G operation to its desired SOC at departure, with the possible charging power regardless of the charging mode chosen at the start.

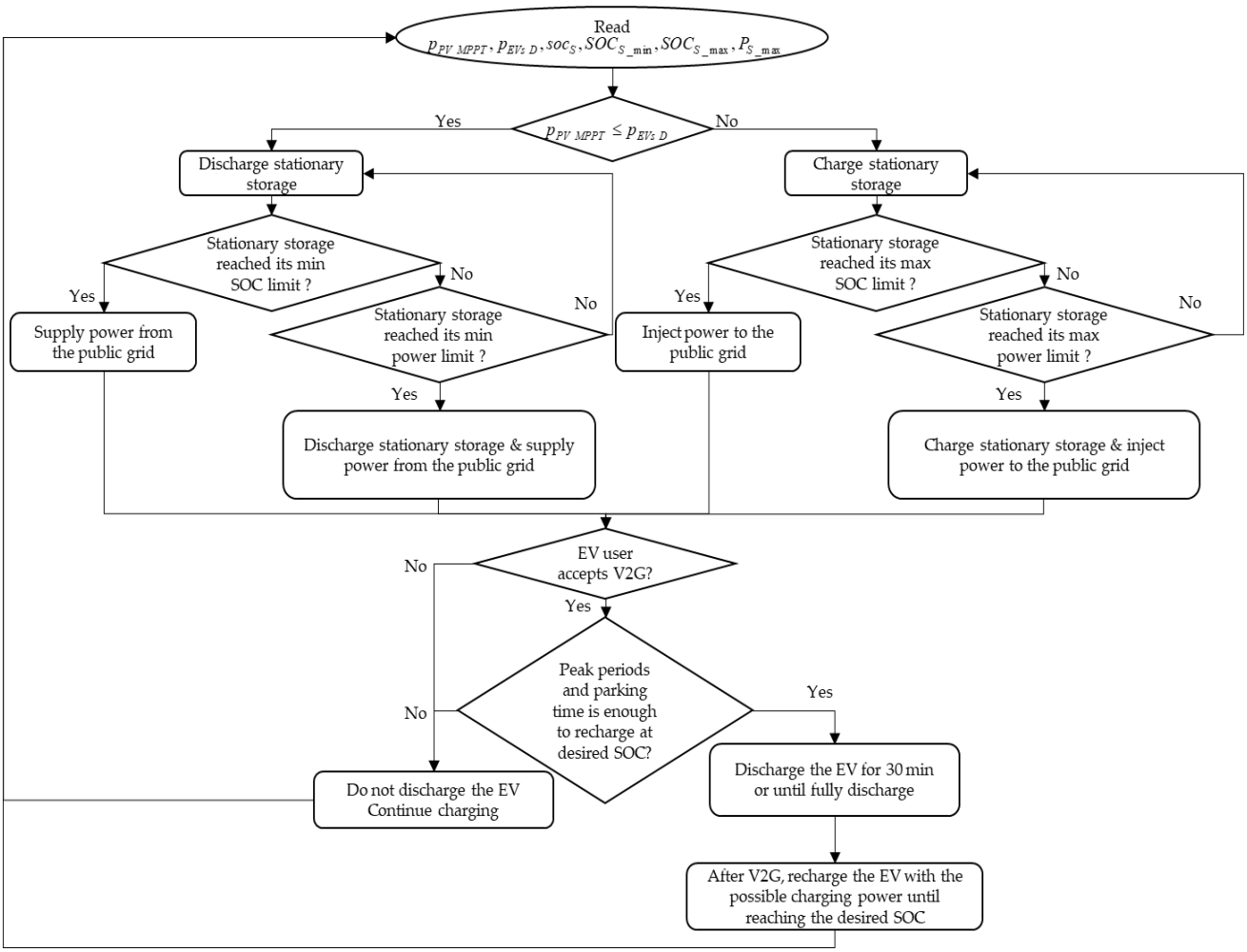

Figure 105: Energy management strategy of the PV-powered charging station with V2G service.

The design of the PV-powered charging station is a DC MG based, as shown in Figure 104. Therefore, the power balance is achieved by (2.1). The PV power is calculated in MPPT mode, $p_{PV\ MPPT}$, by (2.2) and (2.3). A simplified state of charge of the stationary storage, soc_S, is given by (2.4) for its simplicity, where temperature and self-discharge are not considered, and the over-charging/discharging protections are expressed by (2.5) and (2.6). Regarding the EV battery, the dynamic state of charge, soc_{EV_v}, is used as in (2.7), where p_{EV_v} is the EV charging power of v vehicle as. When the EV is charging p_{EV_v} is positive, while, when the EV operates in V2G mode p_{EV_v} is negative.

V.4. PV-powered charging station with V2G simulation cases

This section presents four case studies for the PVCS equipped with five chargers for nine parking places at the university campus. The four cases were simulated under different solar irradiation profiles. Regarding the EVs, lithium-ion batteries were considered and it was assumed they have the same battery capacity of 50 kWh.

For all scenarios, the following assumptions were considered:

- PVCS is located in Compiegne, France, where the yearly average solar irradiation is not significantly high;
- Sunpower SPR X21-345 is used as PV panels with 21% efficiency under STC;
- mounting position is fixed and optimized with a slope angle 38° and azimuth angle −2°;
- system loss was estimated at 14%,
- for the stationary storage, lithium-ion batteries were considered and its limits were considered as 20% and 80% for SOC_{S_min} and SOC_{S_max} respectively.

Figure 106 shows the installation of the PVCS, which consists of 84 PV panels in the Innovation Center of the Université de Technologie de Compiègne, i.e., 29.8 kWp. The stationary storage system has an energy capacity of 37.44 kWh. However, no power injection limit for the public grid was set in the V2G operation. Table 24 shows the parameters used in the following scenarios for the PVCS with V2G service.

Figure 106: PV-powered charging station installation for nine spots.

Table 24: Simulation parameter values for the V2G service.

$P_{G\_I\_max}$	-	SOC_{S_min}	20%	c_{G_NH}	0.1 €/kWh
$P_{G\_S\_max}$	50 kW	SOC_{S_max}	80%	c_{G_PH}	0.7 €/kWh
P_{S_max}	7 kW	SOC_{EV_min}	20%	c_S	0.01 €/kWh
$P_{EV\_fast\_max}$	50 kW	SOC_{EV_max}	100%	c_{PVS}	1.2 €/kWh
$P_{EV\_aver\_max}$	22 kW	SOC_{S_0}	50%	$c_{EV\_penalty}$	2.5 €/kWh
$P_{EV\_slow\_max}$	7 kW	E_{Bat}	37.44 kWh	$p_{PV\ MPPT}$	28.98 kWp
E	50 kWh	N_{PV}	84 PV		

With the objective of proving the benefits of the V2G service can bring to a PVCS, the following subsections present and analyze several scenarios as well as simulation results.

V.4.1. Case 1—PVCS with V2G service in a sunny day

Figure 107 shows the solar irradiation g and $p_{PV\ MPPT}$ for 29 June 2019 in Compiegne, which is a perfectly sunny day with high irradiations. Table 25 shows the data and preferences of EV users.

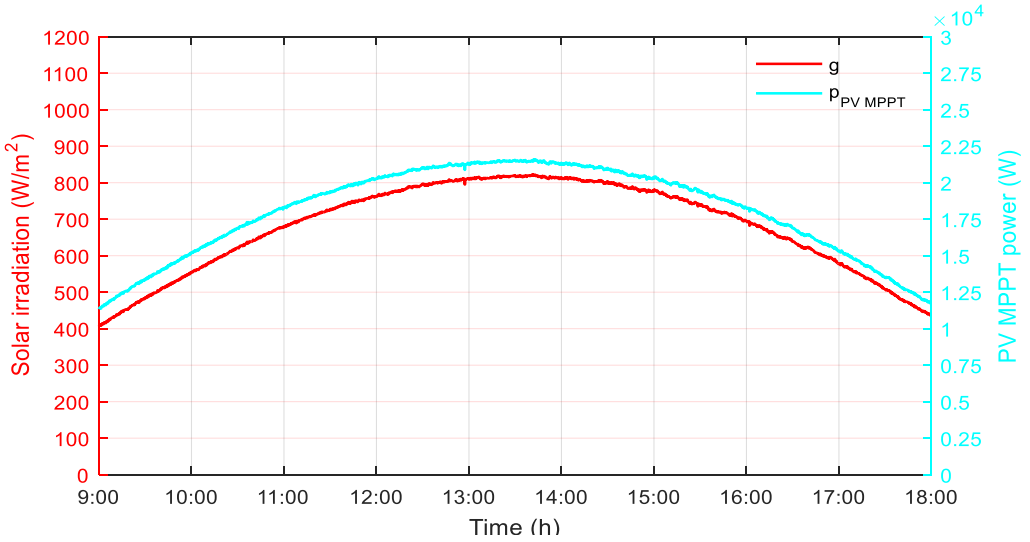

Figure 107: Solar irradiation and PV MPPT power—case 1.

Table 25: Data and preferences of EV users in V2G service – case 1, 2, and 3.

EVs	SOC_{EV_arr}	SOC_{EV_des}	t_{arr}	t_{est_ch}	M	V2G
EV1	31%	85%	09:20	03:52	Slow	Yes
EV2	35%	75%	10:00	00:24	Fast	No
EV3	50%	80%	12:05	02:08	Slow	Yes
EV4	25%	78%	13:45	01:13	Average	No
EV5	29%	72%	14:25	03:05	Slow	No

Only two EV users accept participating in V2G service:

- EV1 arrives at the PVCS at 09:20 and choses slow mode with 7 kW charging power, it stays at the charging station approximately 4 hours. At 12:00, it will start discharging into the grid for 30 minutes or until it is fully discharged,
- EV3 arrives at the PVCS at 12:05 and choses slow mode with 7 kW charging power, it stays at the charging station 02:08. Directly, it will start discharging into the grid for 30 minutes or until it is fully discharged.

In case 1, two scenarios are considered:

– Scenario 1: the EVs start discharging at peak periods with a constant power then recharge again after V2G with the same constant charging power as chosen by the EV user until the time of departure,

– Scenario 2: the EVs start discharging at peak periods with a maximum power at 50 kW then recharge again after V2G with a variable charging power regardless of the charging mode chosen by the EV to reach its desired SOC at departure.

V.4.1.1. Scenario 1a – PV and EVs inject to the grid

In this scenario, only PV and EVs can inject power into the grid at peak periods. Figure 108 shows the power flow of the PVCS with V2G service in constant power, the stationary storage SOC and the DC bus voltage for scenario 1a.

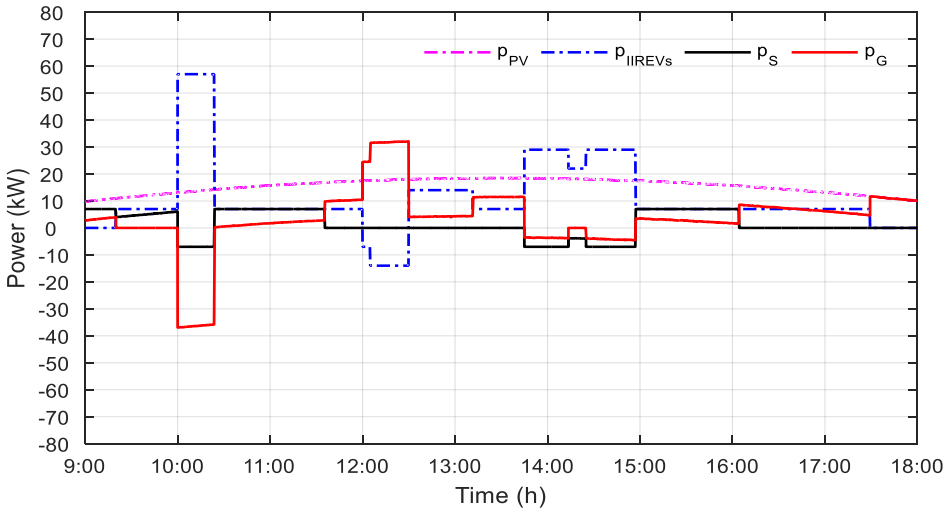

(a)

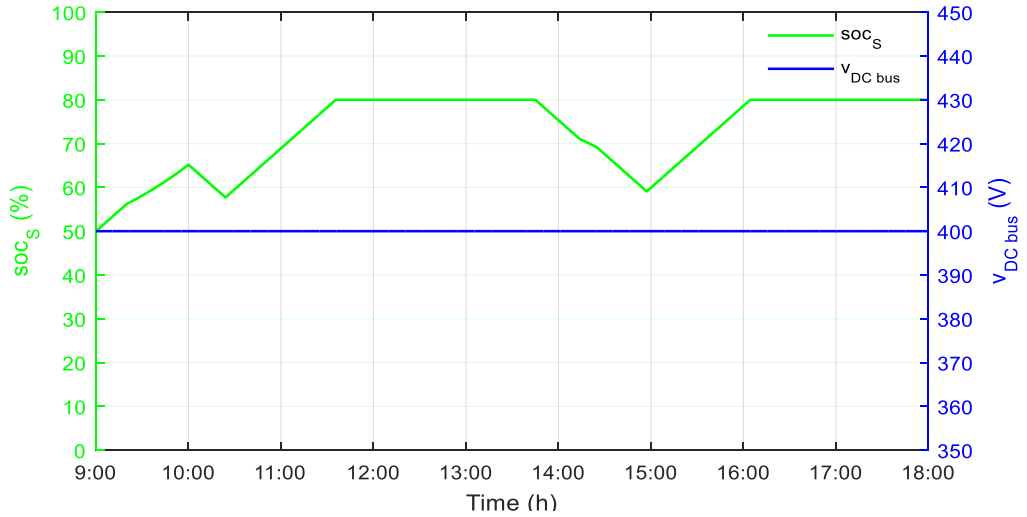

(b)

Figure 108: (a) Power flow with V2G service and (b) the stationary storage SOC and the DC bus voltage — scenario 1a.

Figure 108a, EV1 starts to discharge at 12:00 for 30 minutes and EV3 starts to discharge directly as it comes at the station at12:05 during the peak period and continue to discharge for 30 minutes. Both EVs chose slow charging mode, therefore, when operating in V2G mode, they will discharge with the same power and then recharge after V2G with the slow charging mode. In Figure 108b, the stationary storage is full around 11:30 and then again around 16:00, where charging the storage has stopped and the excess of PV power is injected into the grid as shown in Figure 108a. During V2G operation, the storage remains idle. The DC bus is stable at 400 V, as shown in Figure 108b. The losses and the switching of the dedicated converters are neglected.

V.4.1.2. Scenario 1b – PV, storage and EVs inject to the grid

In this scenario, PV, storage and EVs can inject power into the grid at peak periods. Figure 109 shows the power flow of the PVCS with V2G service in constant power, the stationary storage SOC and the DC bus voltage for scenario 1b.

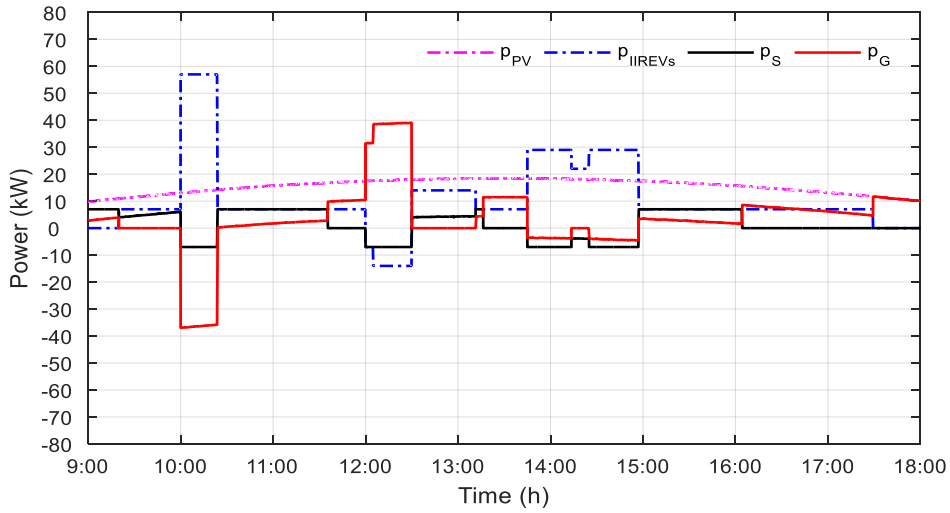

(a)

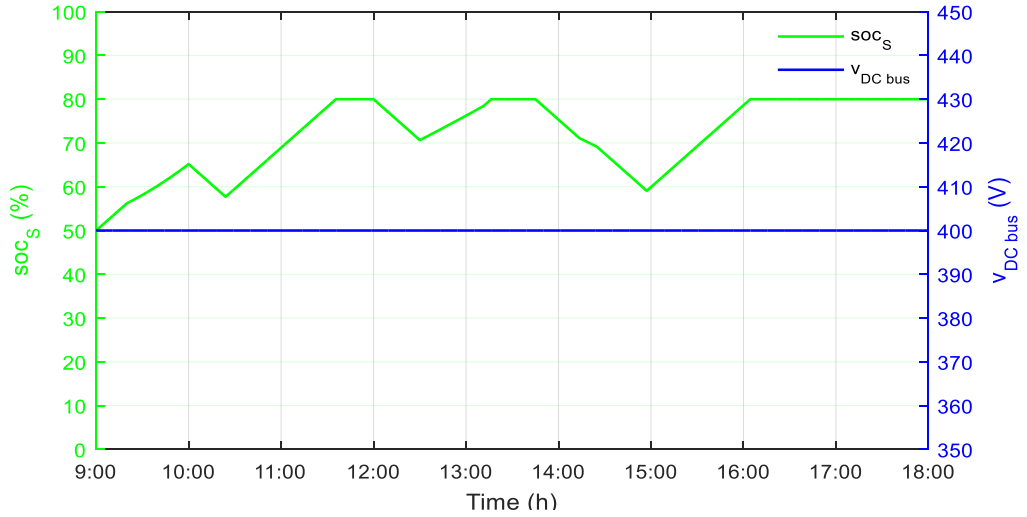

(b)

Figure 109: (a) Power flow with V2G service and (b) the stationary storage SOC and the DC bus voltage — scenario 1b.

In Figure 109a, similarly to the scenario 1a but the stationary storage discharges at peak periods for 30 minutes. In Figure 109b, during V2G operation, the storage discharges from 12:00 until 12:30. The DC bus is stable at 400 V, as shown in Figure 109b.

Figure 110 shows the charging/discharging power of each EV and their SOC for case 1 scenario 1a and scenario 1b.

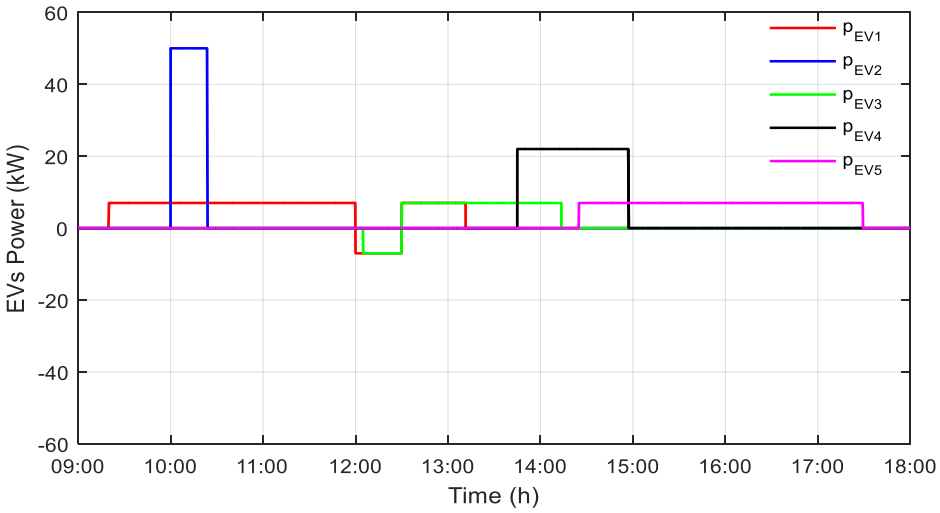

(a)

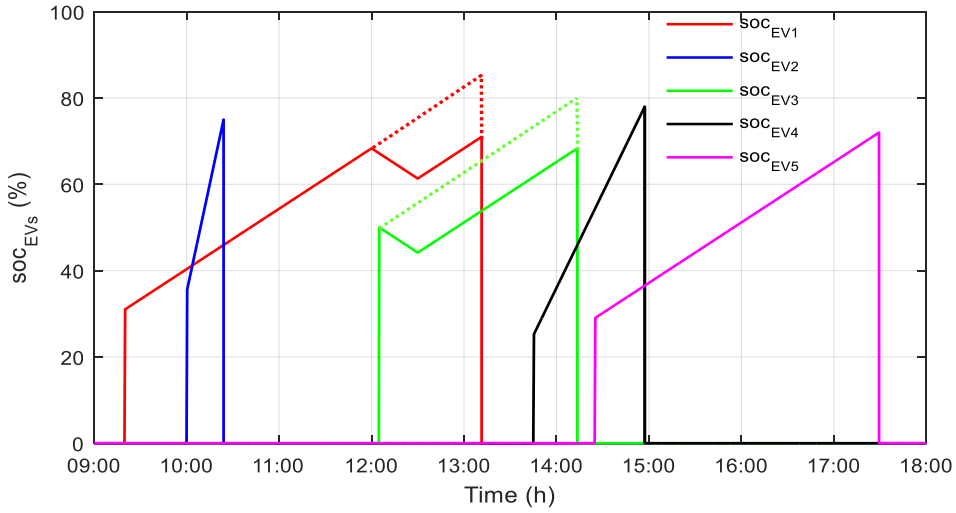

(b)

Figure 110: (a) Charging/discharging power of EVs and (b) the SOC of EVs – scenario 1.

In Figure 110a, EV1 and EV3 start discharging at peak periods until 12:30 and then regain charging after V2G directly until their departure time. Since the users of these two EVs chose slow mode, their charging and discharging power will remain constant at 7 kW. Therefore, EV1 and EV3 did not reach their desired SOC at departure, as shown in Figure 110b, where EV1 reaches 71% instead of 85% and EV2 reaches 68.33% instead of 80% at departure.

V.4.1.3. Scenario 2a – PV and EVs inject to the grid

In this scenario, only PV and EVs can inject power into the grid at peak periods. Figure 111 shows the power flow of the PVCS with V2G service in variable power, the stationary storage SOC and the DC bus voltage for scenario 2a.

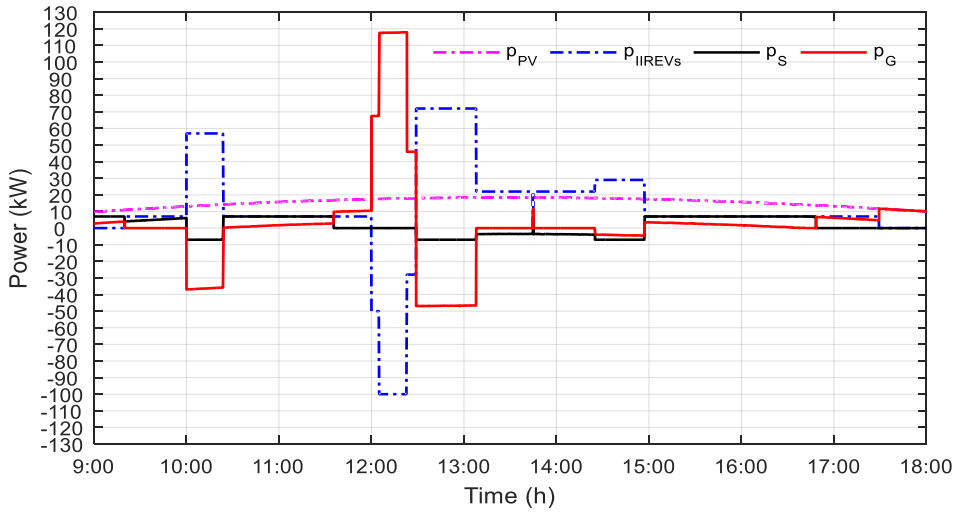

(a)

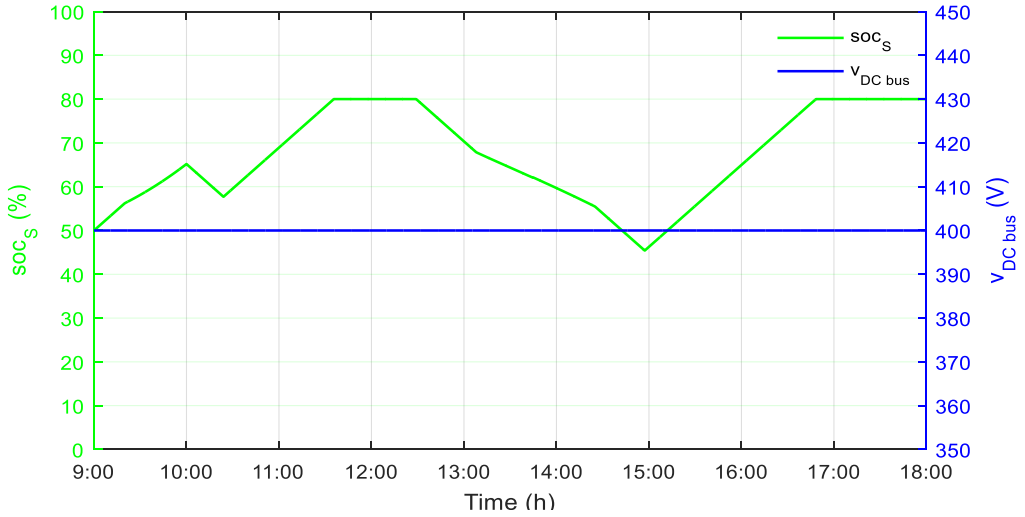

(b)

Figure 111: (a) Power flow with V2G service and (b) the stationary storage SOC and the DC bus voltage — scenario 2a.

In Figure 111a, EV1 starts to discharge at 12:00 for 30 minutes and EV3 starts to discharge directly as it comes at the station at12:05 during the peak period and continues to fully discharge. Both EVs chose slow charging mode, However, when operating in V2G mode, they will discharge with the maximum power 50 kW and then recharge after V2G with the suitable charging power to satisfy the EV user, in consideration of the remaining parking time. In Figure 111b, the stationary storage is full around 11:30 and then again around 16:50, where charging the storage has stopped and the excess of PV power is injected into the grid as shown in Figure 111a. During V2G operation, the storage remains idle. The DC bus is stable at 400 V, as shown in Figure 111b.

V.4.1.4. Scenario 2b – PV, storage and EVs inject to the grid

In this scenario, PV, storage and EVs can inject power into the grid at peak periods. Figure 112 shows the power flow of the PVCS with V2G service in variable power, the stationary storage SOC and the DC bus voltage for scenario 2b.

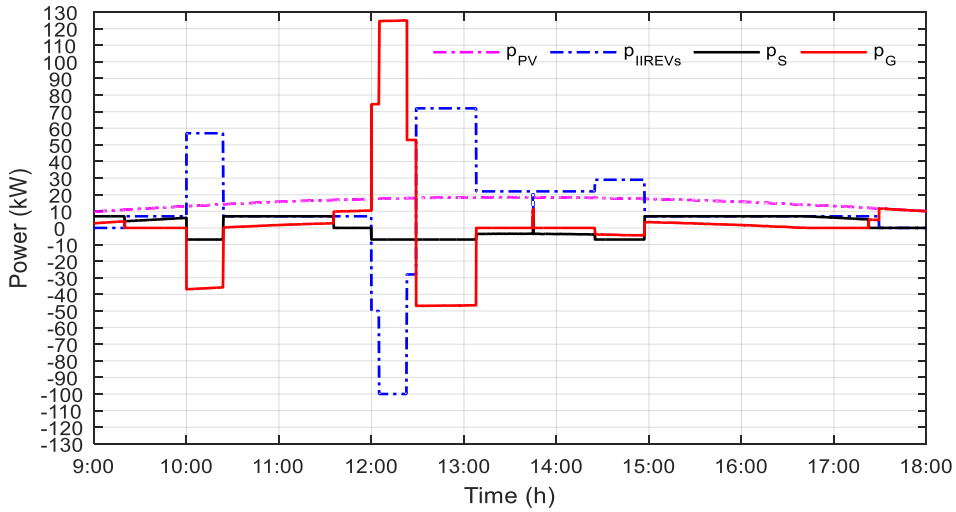

(a)

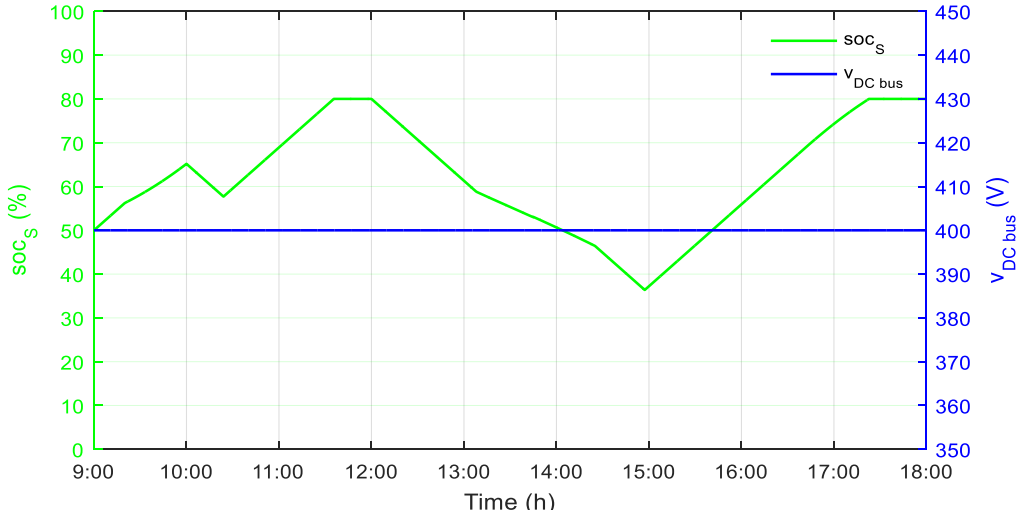

(b)

Figure 112: (a) Power flow with V2G service and (b) the stationary storage SOC and the DC bus voltage — scenario 2b.

In Figure 112a, similarly to the scenario 2a but the stationary storage discharges at peak periods for 30 minutes into the grid. Then, it continues discharging but into the EVs to recharge them as they require high charging power after V2G. In Figure 112b, during V2G operation, the storage discharges from 12:00 until 12:30. The DC bus is stable at 400 V, as shown in Figure 112b.

Figure 113 shows the charging/discharging power of each EV and their SOC for case 1 scenario 2a and scenario 2b.

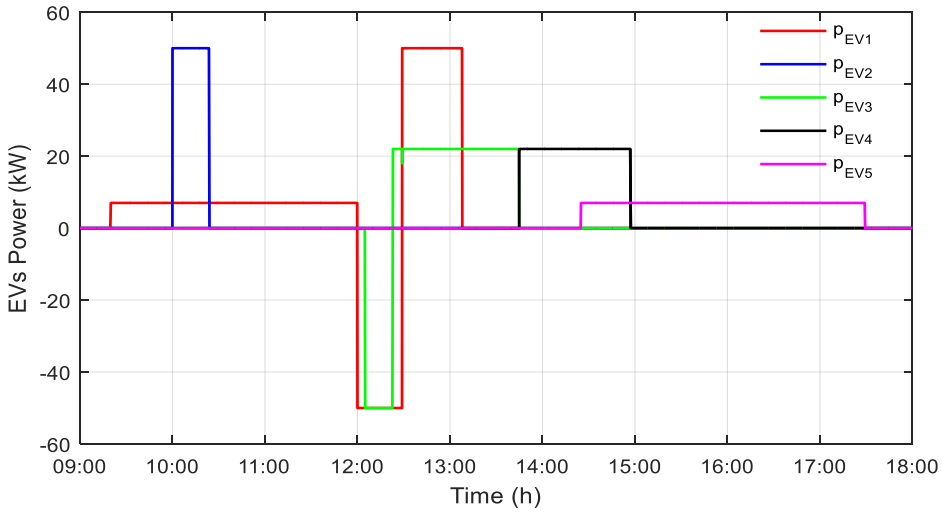

(a)

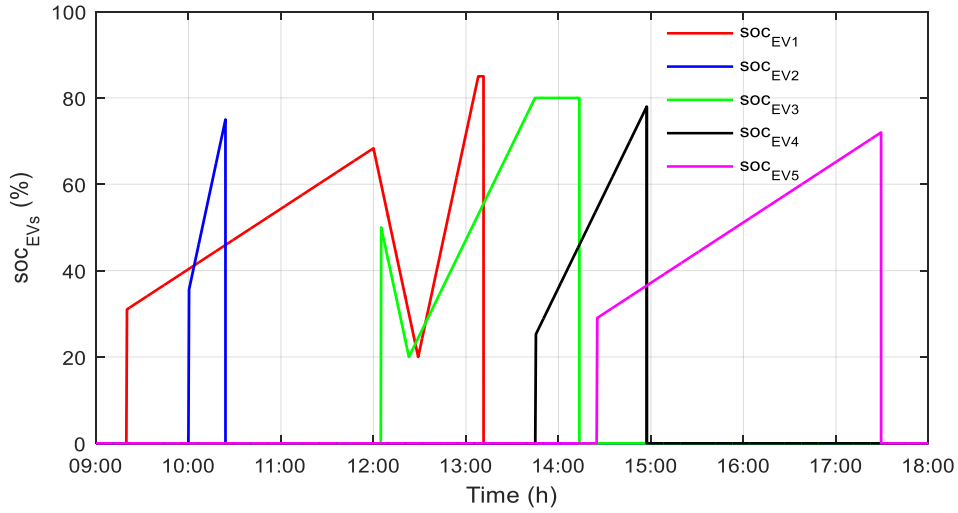

(b)

Figure 113: (a) Charging/discharging power of EVs and (b) the SOC of EVs – scenario 2.

In Figure 113a, EV1 starts discharging with 50 kW from 12:00 until 12:30 and then regain charging with 50 kW after V2G directly until its departure time. In addition, EV3 starts discharging directly until it is fully discharged (less than 30 minutes). After V2G, EV1 charges with 50 kW to compensate the discharging time, which allows the EV to reach its desired SOC at departure. While the remaining charging of EV3 after V2G allows the charging with 22 kW. Figure 113b shows that all EVs have reached their desired SOC at departure.

Scenario 1 with the constant charging/discharging power prove its unfeasibility, as EVs will never reach their desired SOC at departure. For the rest of the case studies, only scenario 2 is applied where EVs recharge after V2G operation with a variable power regardless of their chosen charging mode initially to satisfy the EV user after participating in V2G service.

V.4.2. Case 2—PVCS with V2G service in a partial sunny day with low irradiations

Figure 114 shows the solar irradiation g and $p_{PV\ MPPT}$ for 29 September 2018 in Compiegne, which is a partially sunny day with low irradiations. The data and preferences of EV users are the same as in Table 25.

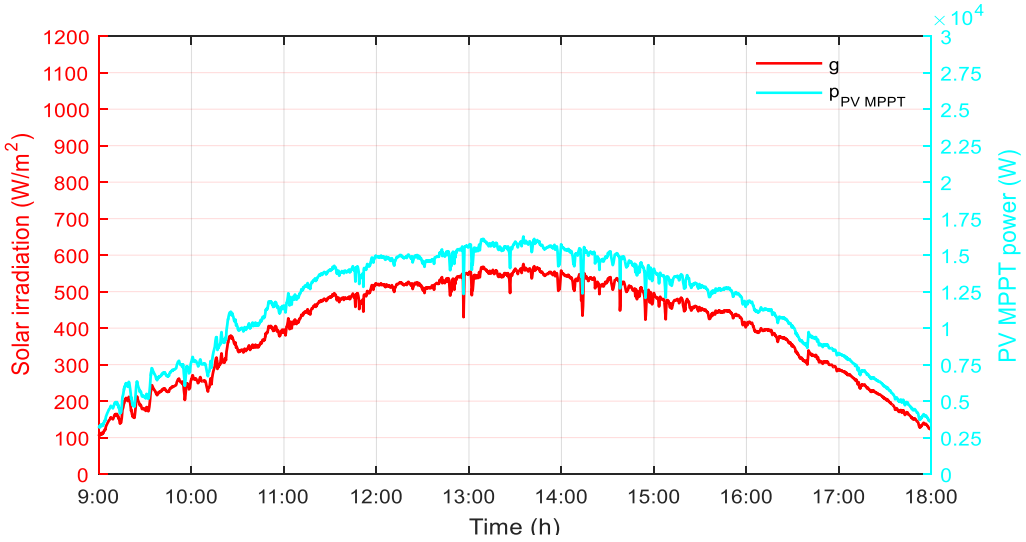

Figure 114: Solar irradiation and PV MPPT power—case 2.

V.4.2.1. Case 2a – PV and EVs inject to the grid

In this scenario, only PV and EVs can inject power into the grid at peak periods. Figure 115 shows the power flow of the PVCS with V2G service in variable power, the stationary storage SOC and the DC bus voltage for case 2a.

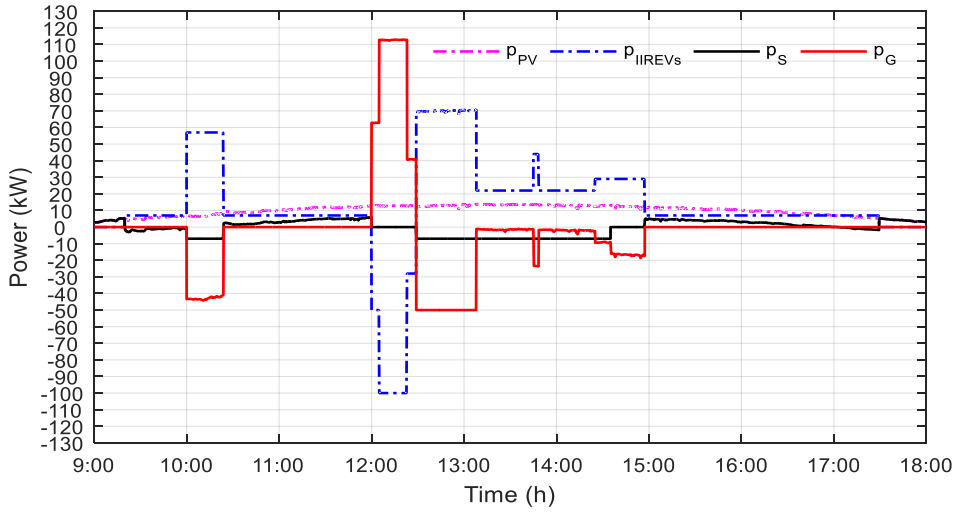

(a)

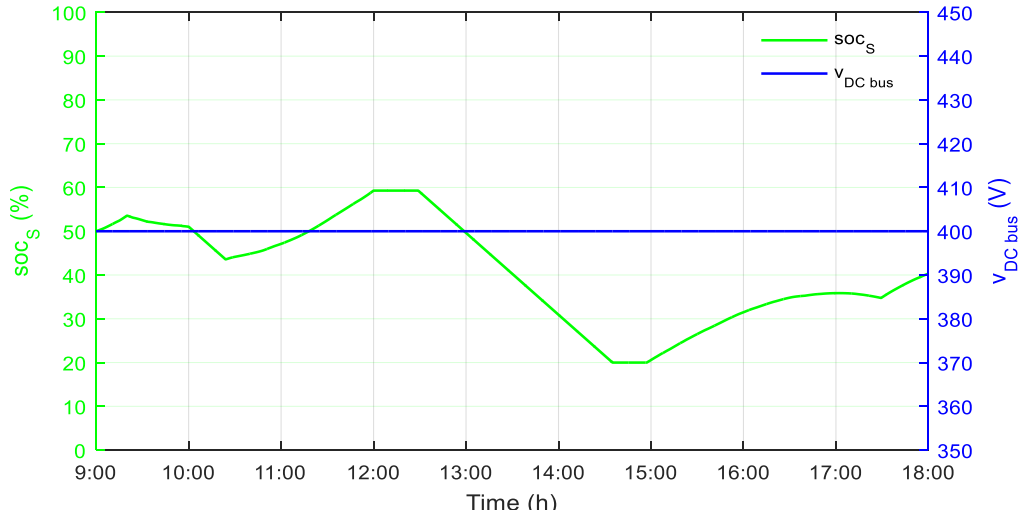

(b)

Figure 115: (a) Power flow with V2G service and (b) the stationary storage SOC and the DC bus voltage — case 2a.

In Figure 115a, EV1 starts to discharge at 12:00 for 30 minutes and EV3 starts to discharge directly as it comes at the station at12:05 during the peak period and continues to fully discharge. Both EVs chose slow charging mode, However, when operating in V2G mode, they will discharge with the maximum power 50 kW and then recharge after V2G with the suitable charging power to satisfy the EV users. In Figure 115b, the stationary storage is full around 12:00. After 12:30, it discharges into the EVs as the charging power is high. It is empty around 14:30 until 15:00, where the public grid supply power to the EVs. During V2G operation, the storage remains idle. The DC bus is stable at 400 V, as shown in Figure 115b.

V.4.2.2. Case 2b – PV, storage and EVs inject to the grid

In this scenario, PV, storage and EVs can inject power into the grid at peak periods. Figure 116 shows the power flow of the PVCS with V2G service in variable power, the stationary storage SOC and the DC bus voltage for case 2b.

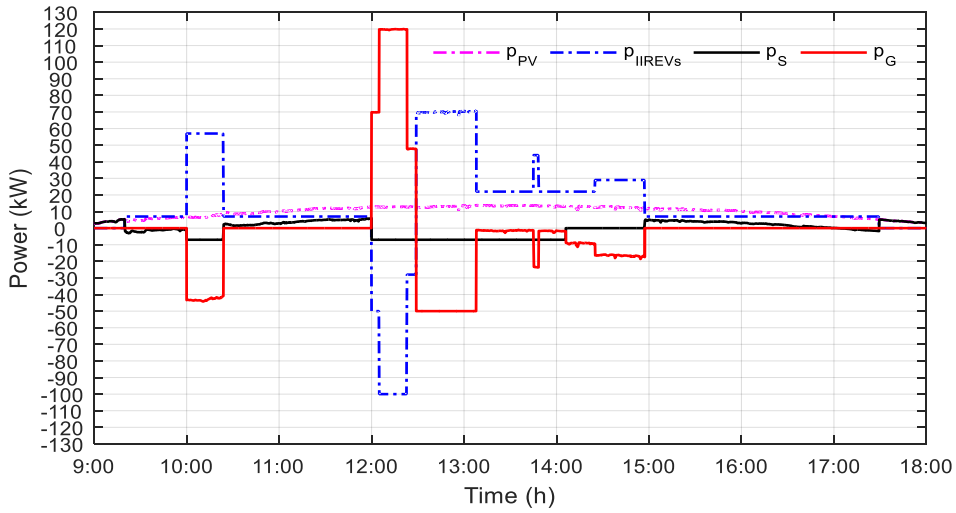

(a)

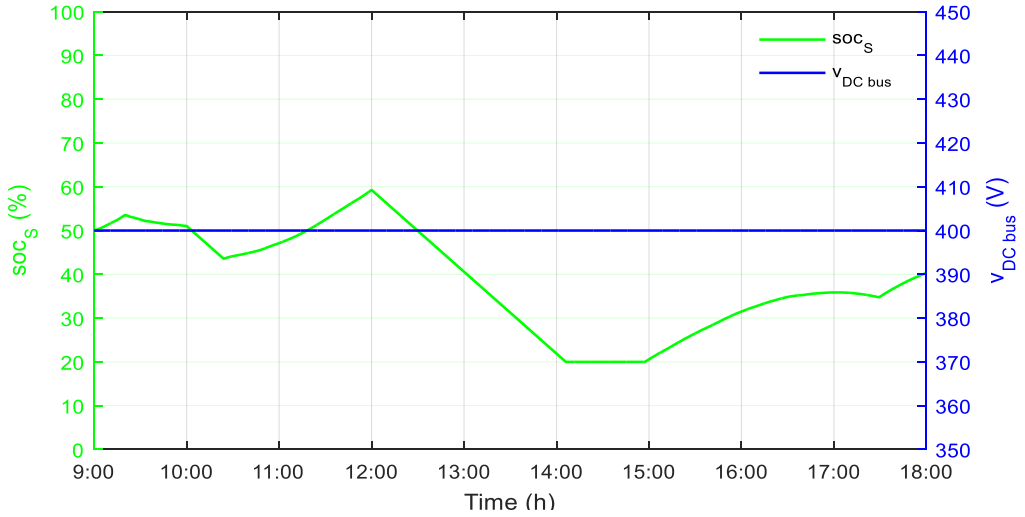

(b)

Figure 116: (a) Power flow with V2G service and (b) the stationary storage SOC and the DC bus voltage — case 2b.

In Figure 116a, similarly to the case 2a but the stationary storage discharges at peak periods for 30 minutes into the grid. Then, it continues discharging but into the EVs to recharge them as they require high charging power after V2G. In Figure 116b, during V2G operation, the storage discharges from 12:00 until 12:30. It is empty around 14:00 until 15:00, where the public grid supply power to the EVs. The DC bus is stable at 400 V, as shown in Figure 116b.

Figure 117 shows the charging/discharging power of each EV and their SOC for case 2.

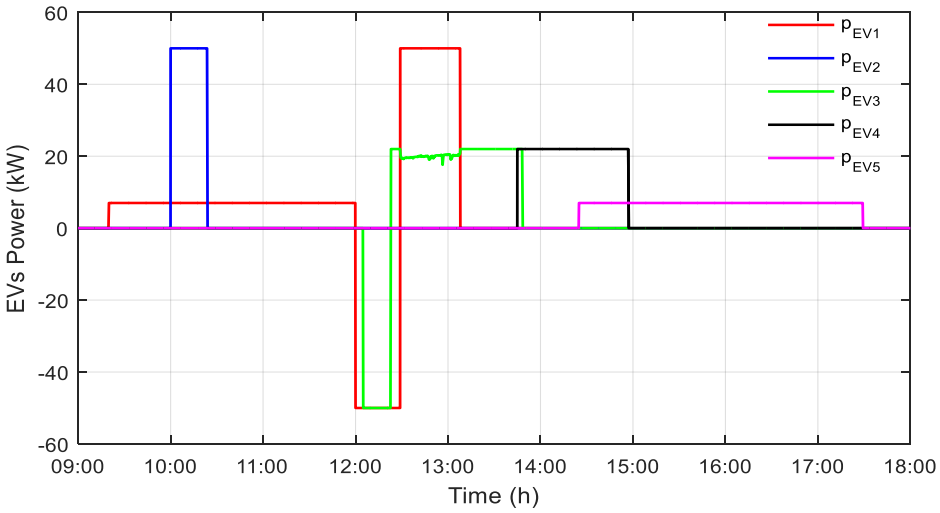

(a)

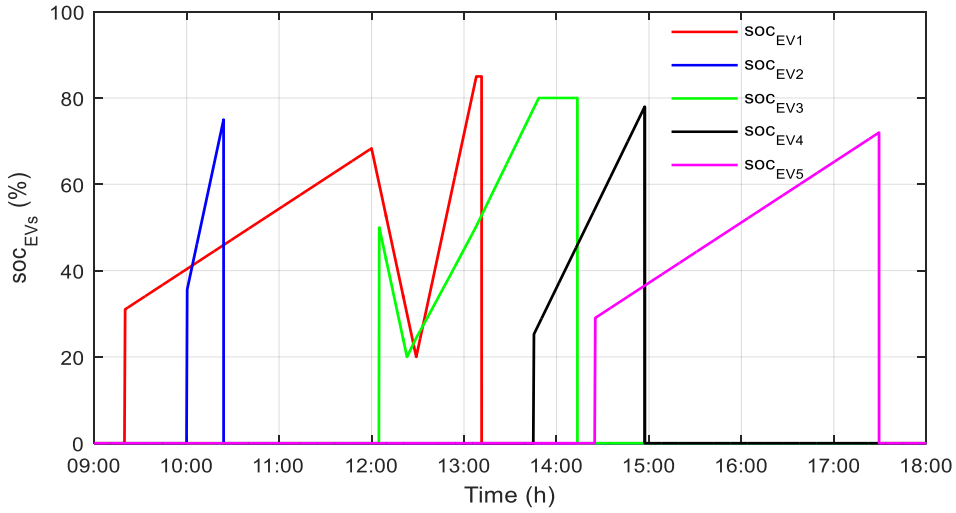

(b)

Figure 117: (a) Charging/discharging power of EVs and (b) the SOC of EVs – case 2.

In Figure 117a, EV1 starts discharging with 50 kW from 12:00 until 12:30 and then regain charging with 50 kW after V2G directly until its departure time. In addition, EV3 starts discharging directly until it is fully discharged (less than 30 minutes). After V2G, EV1 charges with 50 kW to compensate the discharging time, which allows the EV to reach to its desired SOC at departure. While the remaining charging time of EV3 after V2G allows it to recharge with 22 kW. Figure 117b shows that all EVs have reached their desired SOC at departure.

V.4.3. Case 3—PVCS with V2G service in a cloudy day with high fluctuations

Figure 118 shows the solar irradiation g and $p_{PV\ MPPT}$ for 10 October 2019 in Compiegne, which is a cloudy day with high fluctuations. The data and preferences of EV users are the same as in Table 25.

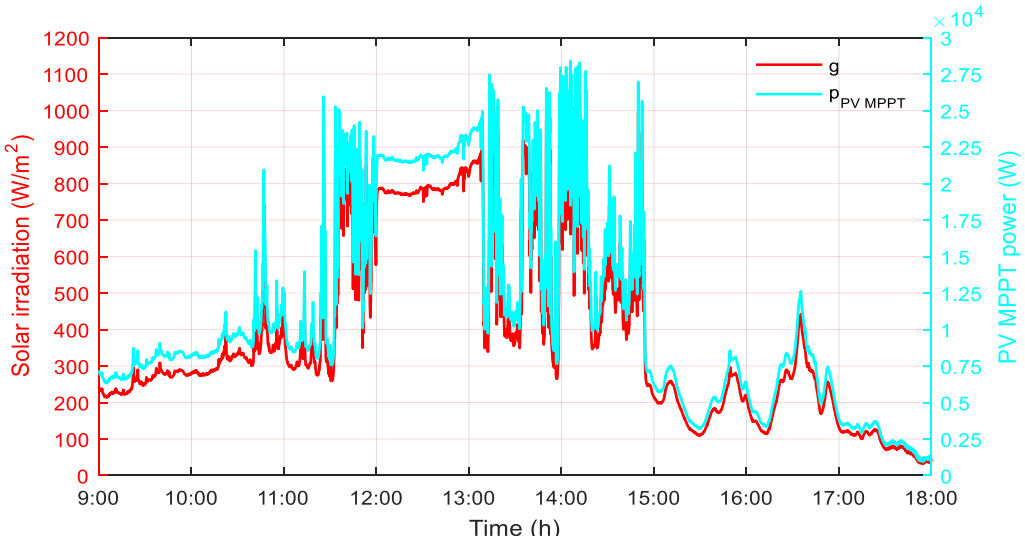

Figure 118: Solar irradiation and PV MPPT power—case 3.

V.4.3.1. Case 3a – PV and EVs inject to the grid

In this scenario, only PV and EVs can inject power into the grid at peak periods. Figure 119 shows the power flow of the PVCS with V2G service in variable power, the stationary storage SOC and the DC bus voltage for case 3a.

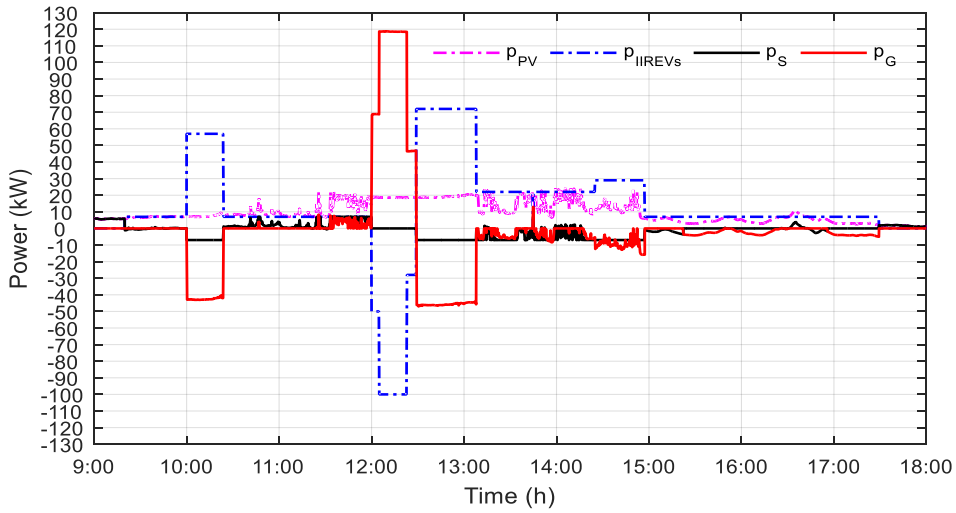

(a)

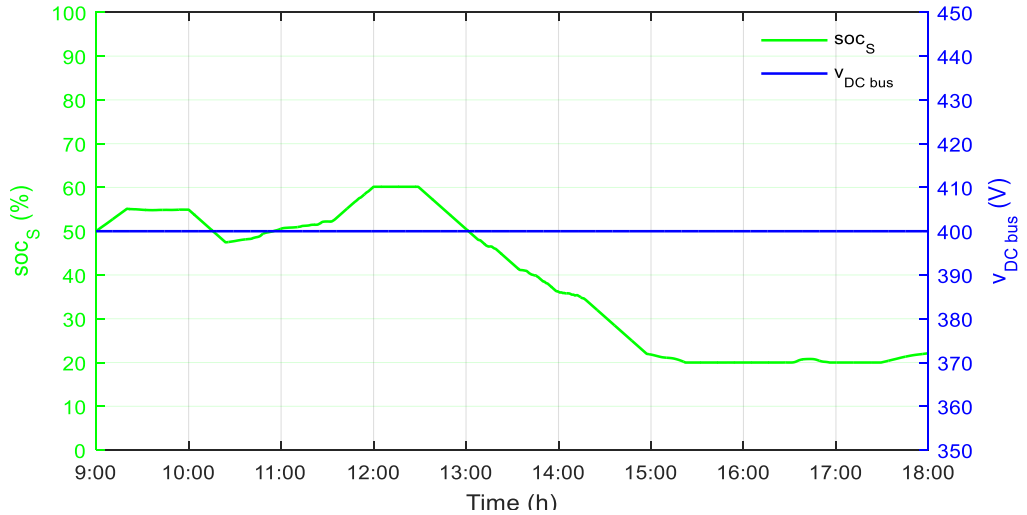

(b)

Figure 119: (a) Power flow with V2G service and (b) the stationary storage SOC and the DC bus voltage — case 3a.

In Figure 119a, EV1 starts to discharge at 12:00 for 30 minutes and EV3 starts to discharge directly as it comes at the station at12:05 during the peak period and continue to fully discharge. Both EVs chose slow charging mode, However, when operating in V2G mode, they will discharge with the maximum power 50 kW and then recharge after V2G with the suitable charging power to satisfy the EV users. In Figure 119b, the stationary storage, at 12:30, starts to discharge into the EVs as the charging power is high. It is empty around 15:20, where the public grid supply power to the EVs. During V2G operation, the storage remains idle. The DC bus is stable at 400 V, as shown in Figure 119b.

V.4.3.2. Case 3b – PV, storage and EVs inject to the grid

In this scenario, PV, storage and EVs can inject power into the grid at peak periods. Figure 120 shows the power flow of the PVCS with V2G service in variable power, the stationary storage SOC and the DC bus voltage for case 3b.

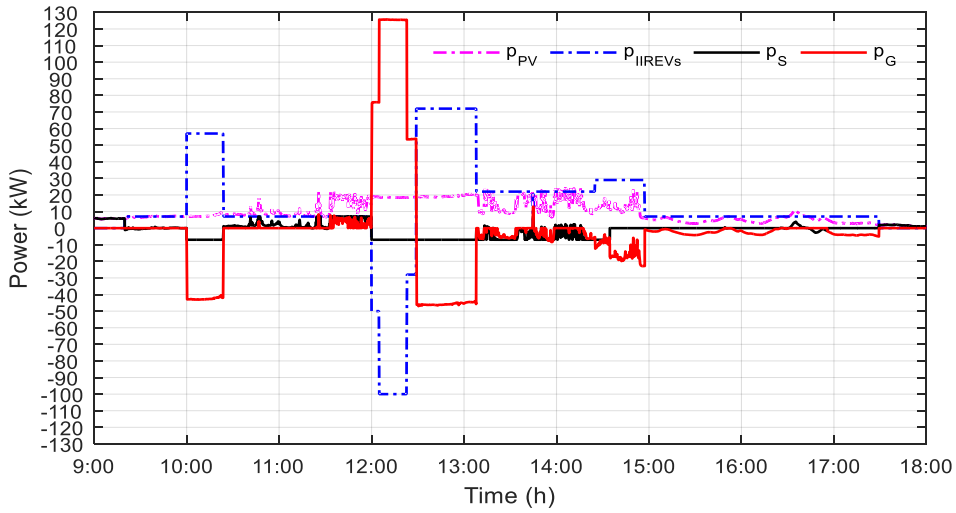

(a)

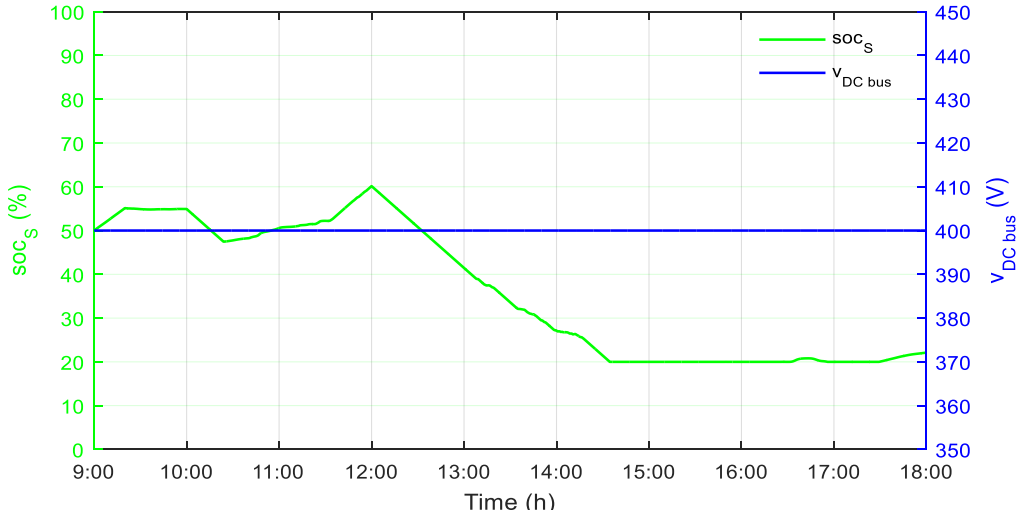

(b)

Figure 120: (a) Power flow with V2G service and (b) the stationary storage SOC and the DC bus voltage — case 3b.

In Figure 120a, similarly to the case 3a but the stationary storage discharges at peak periods for 30 minutes into the grid. Then, it continues discharging but into the EVs to recharge them as they require high charging power after V2G. In Figure 120b, during V2G operation, the storage discharges from 12:00 until 12:30. It is empty around 14:30, where the public grid supply power to the EVs. The DC bus is stable at 400 V, as shown in Figure 120b.

Figure 121 shows the charging/discharging power of each EV and their SOC for case 3.

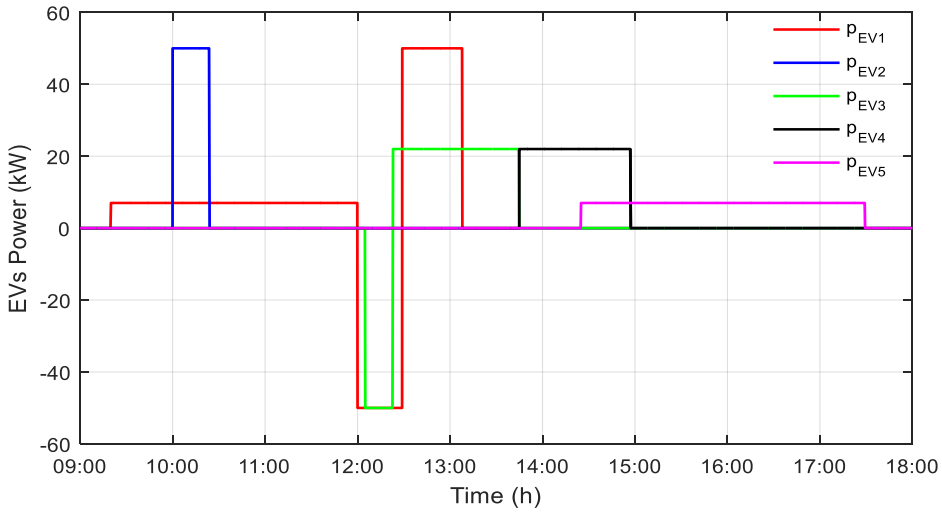

(a)

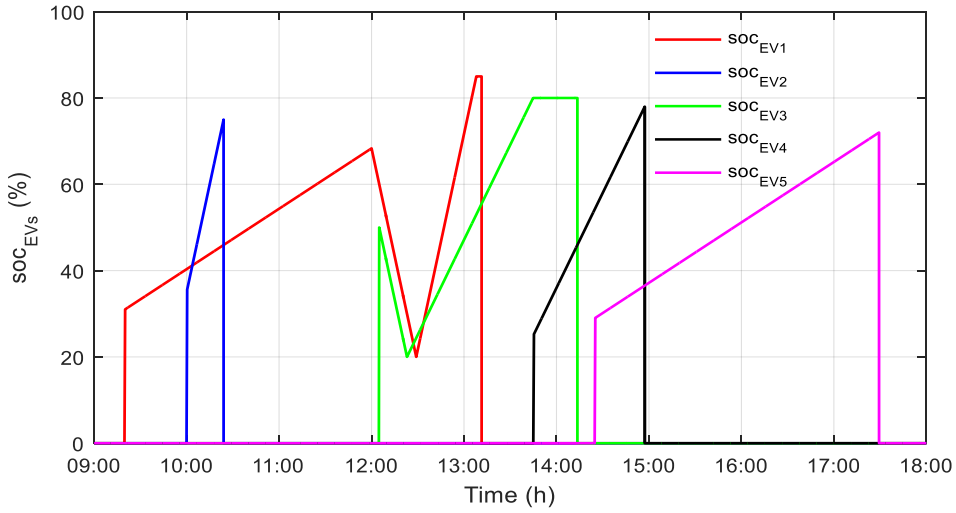

(b)

Figure 121: (a) Charging/discharging power of EVs and (b) the SOC of EVs – case 3.

In Figure 121a, EV1 starts discharging with 50 kW from 12:00 until 12:30 and then regain charging with 50 kW after V2G directly until its departure time. In addition, EV3 starts discharging directly until it is fully discharged (less than 30 minutes). After V2G, EV1 charges with 50 kW to compensate the discharging time, which allows the EV to reach to its desired SOC at departure. While the remaining charging time of EV3 after V2G allows it to recharge with 22 kW. Figure 121b shows that all EVs have reached their desired SOC at departure.

V.4.4. Case 4—PVCS with V2G service in a cloudy day with multiple EVs

The solar irradiation profile and the PV MPPT power are the same as in case 3. The data and preferences of EV users are shown in Table 26.

Table 26: Data and preferences of EV users in V2G service – case 4.

EVs	SOC_{EV_arr}	SOC_{EV_des}	t_{arr}	t_{est_ch}	M	V2G
EV1	31%	85%	10:30	03:52	Slow	Yes
EV2	35%	75%	11:50	00:24	Fast	Yes
EV3	40%	90%	12:05	01:09	Average	Yes
EV4	25%	78%	13:45	01:13	Average	No
EV5	31%	85%	10:30	03:52	Slow	Yes

Three EV users accept participating in V2G service:

- EV1 arrives at the PVCS at 10:30 and choses slow mode with 7 kW charging power, it stays at the charging station approximately 4 hours. At 12:00, it will start discharging into the grid for 30 minutes or until it is fully discharged,
- EV2 arrives at the PVCS at 11:50 and choses fast mode with 50 kW charging power, it stays at the charging station 24 minutes. At 12:00, it may discharge into the grid,
- EV3 arrives at the PVCS at 12:05 and choses average mode with 22 kW charging power, it stays in the charging station 01:09. Directly, it will start discharging into the grid for 30 minutes or until it is fully discharged.

V.4.4.1. Case 4a – PV and EVs inject to the grid

In this scenario, only PV and EVs can inject power into the grid at peak periods. Figure 122 shows the power flow of the PVCS with V2G service in variable power, the stationary storage SOC and the DC bus voltage for case 4a.

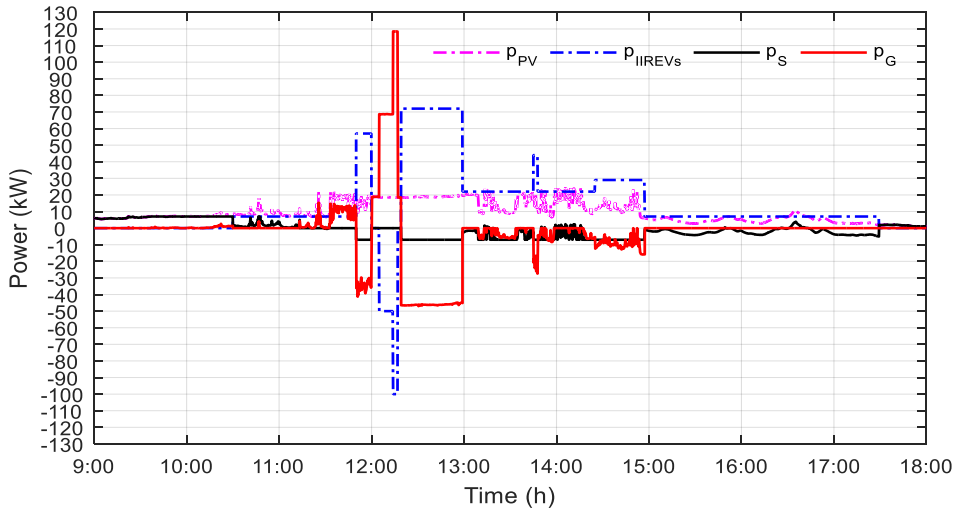

(a)

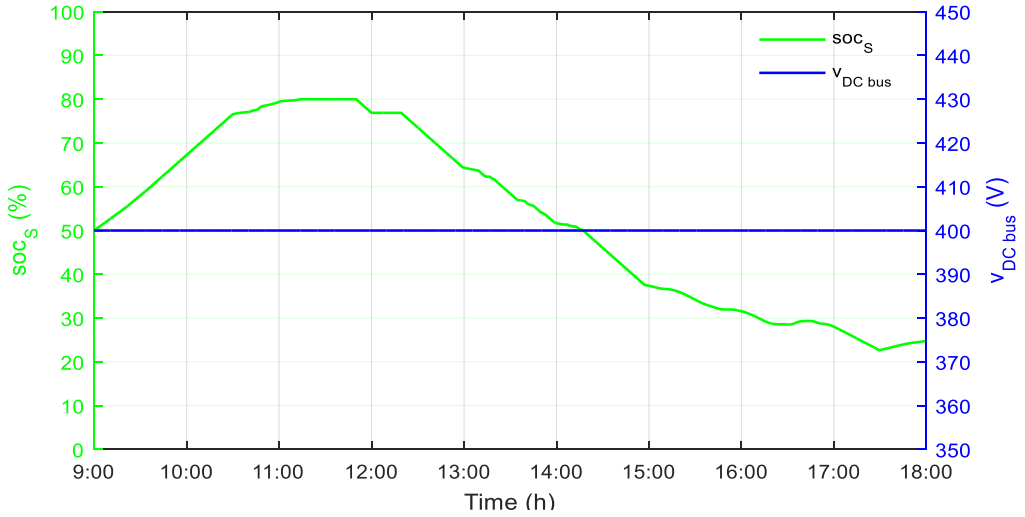

(b)

Figure 122: (a) Power flow with V2G service and (b) the stationary storage SOC and the DC bus voltage — case 4a.

In Figure 122a, EV1 starts to discharge at 12:00 for 30 minutes and EV3 starts to discharge directly as it comes at the station at12:05 during the peak period and continues to fully discharge. However, EV2 could not participate in V2G as the parking time will not allow to discharge and recharge again with 50 kW and satisfy the EV user. EV1 and EV3, when operating in V2G mode, they will discharge with the maximum power 50 kW and then recharge after V2G with the suitable charging power to satisfy their EV users. In Figure 122b, the stationary storage is full around 11:15. After 12:30, it discharges into the EVs as the charging power is high. When the stationary storage discharges at it maximum power, the public grid supply power to the EVs. During V2G operation, the storage remains idle. The DC bus is stable at 400 V, as shown in Figure 122b.

V.4.4.2. Case 4b – PV, storage and EVs inject to the grid

In this scenario, PV, storage and EVs can inject power into the grid at peak periods. Figure 123 shows the power flow of the PVCS with V2G service in variable power, the stationary storage SOC and the DC bus voltage for case 4b.

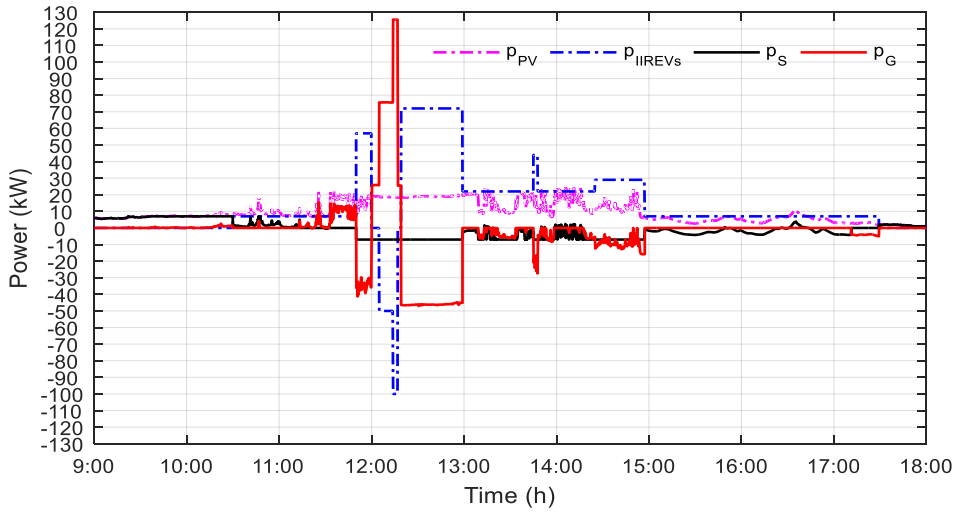

(a)

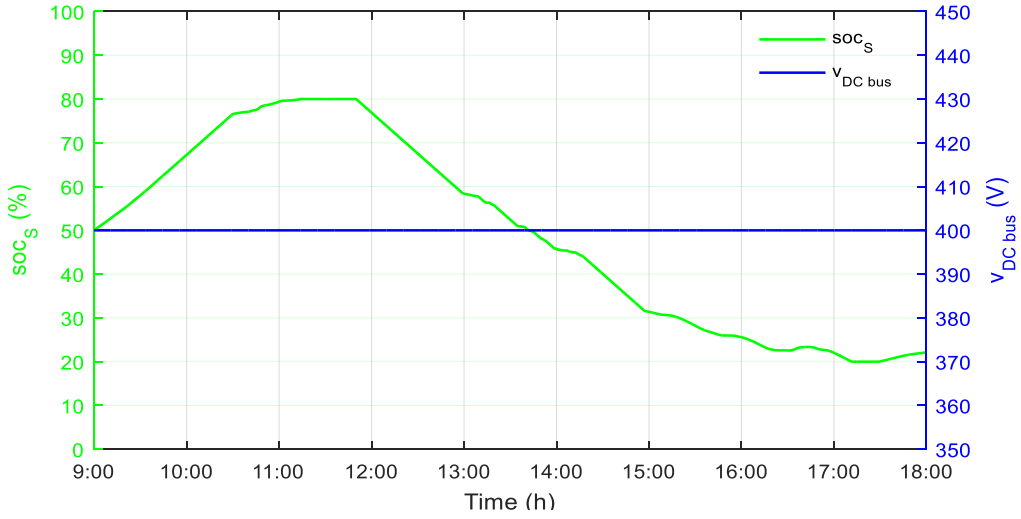

(b)

Figure 123: (a) Power flow with V2G service and (b) the stationary storage SOC and the DC bus voltage — case 4b.

In Figure 123a, similarly to the case 4a but the stationary storage discharges at peak periods for 30 minutes into the grid. Then, it continues discharging but into the EVs to recharge them as they require high charging power after V2G. In Figure 123b, during V2G operation, the storage discharges from 12:00 until 12:30. It is empty around 17:15, where the public grid supply power to the EVs. The DC bus is stable at 400 V, as shown in Figure 123b.

Figure 124 shows the charging/discharging power of each EV and their SOC for case 4.

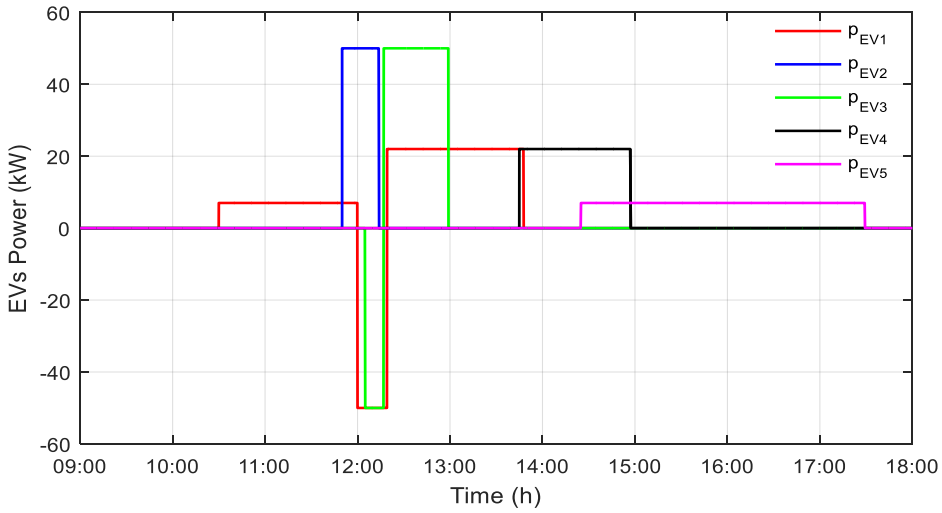

(a)

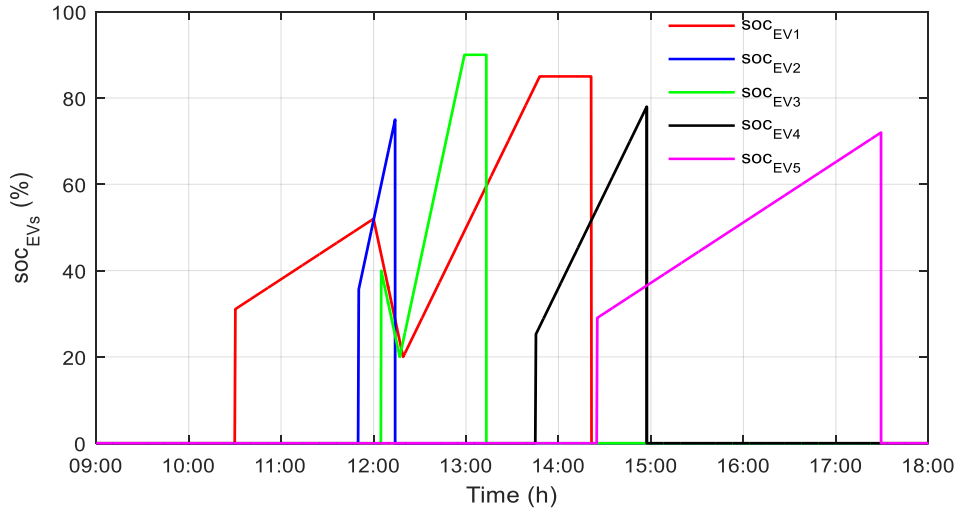

(b)

Figure 124: (a) Charging/discharging power of EVs and (b) the SOC of EVs – case 4.

In Figure 124a, EV1 starts discharging with 50 kW from 12:00 until 12:30 and then regain charging with 50 kW after V2G directly until its departure time. In addition, EV3 starts discharging directly until it is fully discharged (less than 30 minutes). After V2G, EV1 charges with 50 kW to compensate the discharging time, which allows the EV to reach to its desired SOC at departure. While the remaining charging time of EV3 after V2G allows it to recharge with 22 kW. Even though, EV2 accepts participating into V2G service but the limited parking time did not allow the EV to discharge. Figure 124b shows that all EVs have reached their desired SOC at departure.

V.5. PV-powered charging station with V2G energy cost analyses

Table 27 presents the energy injected into the grid for case 1.

Table 27: Energy injected into the grid – case 1.

Operation case		PV (kWh)	EVs (kWh)	Sto (kWh)	Total energy during V2G (kWh)	% EVs/V2G (kWh)	% PV/V2G (kWh)	Total energy during the day (kWh)
Constant (scenario 1)	EVs only		6.41		6.41			
	PV+EVs	8.88	6.41	0	15.29	41.92%	58.08%	49.87
	PV+Sto+EVs	8.88	6.41	3.5	18.79	34.11%	47.26%	49.87
Variable (scenario 2)	EVs only		36.97		36.97			
	PV+ EVs	8.57	36.97	0	45.54	81.18%	19.82%	65.7
	PV+Sto+EVs	8.57	36.97	3.38	48.92	75.57%	17.52%	65.7

The two scenarios in case 1 are presented, where the energy injected into the grid from EVs in scenario 2 is greater than scenario 1. In scenario 1, the percentage of energy injected from the EVs into the grid is less than the percentage of energy injected from PV into the grid. In scenario 2, the percentage of energy injected from EVs into the grid, which is greater than 75%, is higher than then percentage of energy injected from PV into the grid.

Table 28 presents the energy cost for case 1.

Table 28: Energy cost – case 1.

Operation case		Grid (c€)	Storage (c€)	EV penalty (c€)	Total (c€)
Constant (scenario 1)	PV+EVs	-1514.44	32.50	3208.82	1726.88
	PV+Sto+EVs	-1598.89	39.50	3208.82	1649.42
Variable (scenario 2)	PV+EVs	-1624.13	42.77	0	-1581.36
	PV+Sto+EVs	-1827.13	49.53	0	-1777.59

The two scenarios in case 1 are presented, where the energy cost in scenario 1 is much higher than in scenario 2 due to the EV penalties as they did not reach their desired SOC at departure. In scenario 2, the total energy cost is negative referring to selling energy to the grid. The energy cost is more profitable when the storage also discharges into the grid during peak periods.

Table 27 and Table 28 prove the unfeasibility of scenario 1, as in scenario 1, the energy injected into the grid from EVs are not very significant as they discharge in constant power. Moreover, the total energy cost is high due to the penalties, as the EVs did not recharge to their desired SOC.

Table 29 presents the energy injected into the grid for case 2.

Table 29: Energy injected into the grid – case 2.

Operation case		PV (kWh)	EVs (kWh)	Sto (kWh)	Total energy during V2G (kWh)	% EVs/V2G (kWh)	% PV/V2G (kWh)	Total energy during the day (kWh)
Variable	EVs only		36.97		36.97			
	PV+ EVs	6.16	36.97	0	43.13	85.72%	14.28%	43.13
	PV+Sto+EVs	6.16	36.97	3.38	46.51	79.48%	13.24%	46.51

The percentage of energy injected from EVs into the grid, which is greater than 79%, is higher than then percentage of energy injected from PV into the grid.

Table 30 presents the energy cost for case 2.

Table 30: Energy cost – case 2.

Operation case		Grid (c€)	Storage (c€)	EV penalty (c€)	Total (c€)
Variable	PV+EVs	-860.07	34.10	0	-825.97
	PV+Sto+EVs	-1063.07	34.10	0	-1018.97

The total energy cost is higher, when stationary storage discharges into the grid during V2G period, referring to selling more energy to the grid. The energy cost is more profitable when the storage also discharges into the grid during peak periods.

Table 31 presents the energy injected into the grid for case 3.

Table 31: Energy injected into the grid – case 3.

Operation case		PV (kWh)	EVs (kWh)	Sto (kWh)	Total energy during V2G (kWh)	% EVs/V2G (kWh)	% PV/V2G (kWh)	Total energy during the day (kWh)
Variable	EVs only		36.97		36.97			
	PV+ EVs	8.99	36.97	0	45.96	80.44%	19.56%	47.47
	PV+Sto+EVs	8.99	36.97	3.38	49.34	74.93%	18.22%	50.85

The percentage of energy injected from EVs into the grid, which is greater than 74%, is higher than then percentage of energy injected from PV into the grid.

Table 32 presents the energy cost for case 3.

Table 32: Energy cost – case 3.

Operation case		Grid (c€)	Storage (c€)	EV penalty (c€)	Total (c€)
Variable	PV+EVs	-1118.29	26.41	0	-1091.87
	PV+Sto+EVs	-1280.45	26.41	0	-1254.03

The total energy cost is higher, when stationary storage discharge into the grid during V2G period, referring to selling more energy to the grid. The energy cost is more profitable when the storage also discharges into the grid during peak periods.

Table 33 presents the energy injected into the grid for case 4.

Table 33: Energy injected into the grid – case 4.

Operation case		PV (kWh)	EVs (kWh)	Sto (kWh)	Total energy during V2G (kWh)	% EVs/V2G (kWh)	% PV/V2G (kWh)	Total energy during the day (kWh)
Variable	EVs only		12.5		12.5			
	PV+ EVs	5.96	12.5	0	18.46	67.71%	32.29%	22.31
	PV+Sto+EVs	5.96	12.5	2.24	20.7	60.38%	28.79%	24.55

The percentage of energy injected from EVs into the grid, which is greater than 60%, is higher than then percentage of energy injected from PV into the grid.

Table 34 presents the energy cost for case 4.

Table 34: Energy cost – case 4.

Operation case		Grid (c€)	Storage (c€)	EV penalty (c€)	Total (c€)
Variable	PV+EVs	961.36	34.38	0	995.74
	PV+Sto+EVs	817.09	35.37	0	852.46

The total energy cost is less, when stationary storage discharge into the grid during V2G period, reducing the energy cost. The energy cost is more profitable when the storage also discharges into the grid during peak periods.

In case 4, multiple EVs with different charging mode, accept to participate in V2G service. Despite EV2 accepts to participate in V2G, which it charges with fast mode, it could not participate in V2G operation as the charging time is insufficient to discharge and recharge again after V2G. Therefore, EV2 continues charging while EV1 and EV3 participate in V2G service. In this case, not all the energy discharged from the EVs were injected into the grid but a part of this energy was injected into EV2, as some sort of vehicle-to-vehicle. This explains the difference of energy injected from EVs into the grid between case 4 and the previous cases. The total energy cost is positive, paying for energy consumption, is due to the high energy consumption from EVs in a cloudy day with high fluctuations.

V.6. Conclusions

This chapter presents a PVCS and its energy management with the application of V2G service. Various case studies with different meteorological conditions and EV profiles have been conducted to highlight the advantages of the V2G service. Simulation results show the significance of energy injected from EVs into the grid, where this will reduce the burden on the public grid operator as the EVs are considered as DER and in the meantime will reduce the energy cost or may even bring profits on the PVCS operator.

For the EVs to be able to participate in the V2G operation, despite their charging mode, the charging terminals should allow bidirectional flow of energy with variable charging power. This will allow EVs to charge with their chosen charging mode, discharge in V2G with a maximum 50 kW, recharge again with a

suitable power to satisfy the EV users, in consideration of the remaining parking time, and to reach their desired SOC at departure.

Chapitre VI. *PV-powered charging station: Carbon impact methodology*

EVs are expanding vastly since they are carbon free during a part of their life cycle, therefore, they are considered as a promising solution to combat climate change and environmental pollution as in [1]. Among the most well-known GHG are CO_2 and methane. The accumulation of CO_2 and other air pollutants in the atmosphere, which absorb sunlight and solar radiation that have bounced off the earth's surface, is at the origin of the current global warming. This chapter investigates the carbon impact of a PVCS, based on a life cycle assessment (LCA) mixed with carbon impact methodology, the goal is to assess the carbon impact of the PVCS and then to compare with a grid-powered charging station (PGCS). The obtained results show that the carbon impact of the PVCS is reduced, but this strongly depends on the electricity mix of the public grid. This chapter, presented in [206], [207] is constructed as follows: Section VI.1 gives an introduction. Section VI.2 presents the literature review. Section VI.3 describes the methodology for carbon impact calculation for the PVCS. Section VI.4 presents the comparison of the carbon impact between the PVCS and PGCS. Section VI.5 concludes the chapter.

VI.1. Introduction

The CO_2 is a major GHG and requires an accounting methodology to estimate its impact. However, the main issues related to GHG accounting are available databases, availability of recent data, data quality and data uncertainty, and available methodologies. To increase consistency and transparency in CO_2 accounting and reporting several organizations provide methodologies for the GHG balance accounting: GHG Protocol [208], Bilan Carbone® France and its base carbon database [209], EcoInvent - Switzerland [210], European Life Cycle Database [211], and standards ISO 14064, ISO 14067 [212]. These methodologies are often recommended to GHG accounting related to organizations, territories, and products. However, estimating the CO_2 emissions of a complex technological system, based on unit processes as well as on benchmarks for each category of technology, is a very complicated GHG accounting. Hence, even some recent research work emphases on the environmental footprint for the EV charging infrastructure, its carbon impact estimation is not consistently reported by the literature today.

VI.2. Literature review

In [213], the authors have focused to maximize the usage of PV energy in EVs charging and to minimize the GHG emissions in a university campus in Bangladesh. A LCA has been used in [214] to compare the carbon footprint of an EV and a hydrogen fuel cell car. LCA has been used also to study the impact of an

EV public charging infrastructure on the GHG emissions in comparison with internal combustion engine vehicles (ICEVs) across China in [215] and California in [216]. The authors in [217] have used the LCA to study the environmental impact of chargers in an EV charging infrastructure in China. In [218], a comparative study using the LCA has been considered in California and Detroit to measure the carbon impact of different regional energy mixes for EVs and ICEVS. The authors in [219] have compared the GHG emission costs in universal EV charging infrastructure with only residential charging in Australia. In [220], the authors have studied the life cycle carbon emissions for a PHEV and battery EV in the USA under marginal versus average grid emission factors. Other authors have compared in [221] the carbon emissions in different EV charging strategies in the UK in perspective to 2030 and 2040 targets. In [222] various passenger vehicle technologies have been studied and the GHG emissions have been compared using the LCA across 50 states in the USA.

A LCA for a PV-powered vehicles, or called vehicle integrated PV, has been presented in [223], taking into consideration shadowing factor. This study has been done in Cologne, Germany, where the energy mix is highly dependent on coal. The environmental impact is compared for charging the vehicle from PV and from the grid, the results show how the location, the annual irradiation and carbon emissions from the grid may affect the outcomes. An analysis of directed emissions of CO_2 generated by ICEVS and indirect emissions CO_2 from EVs has been proposed in [224] in Poland, where the energy mix is highly dependent on solid fossil fuels. The results showed that the indirect emissions of CO_2 from EVs are higher than the direct emission of CO_2 from ICEVS for a daily usage. However, increasing the share of RES in energy production will have a positive effect on the carbon impact of EVs in Poland. An analysis of CO_2 emissions in different scenarios for the electrification of the vehicle fleet in Finland has been presented in [225]. The results showed that in the high adoption of EVs will reduce CO_2 emissions but not to their ambitions, set by the European Union and the Finnish government. A comparative analysis of CO_2 emissions based on LCA has been presented in [226] for EVs and ICEVS in China, considering energy mix composition. The results showed that under the existing energy mix of the Chinese grid, which is highly dependent on fossil fuels, the CO_2 emissions of the EVs are higher than the ICEVS. However, with the increase of RES in the energy mix composition in the Chinese grid, the impact of the EVs on the CO_2 emissions will be highlighted. A cradle-to-grave LCA has been studied in [227], considering energy mix for the USA states and more integration of RES from 2020 to 2050, on CO_2 emissions in EVs and gasoline vehicles. The results showed that EVs can bring benefits in comparison with gasoline vehicles nearly in all the states. A comparative environmental cradle-to-grave LCA has been presented in [228] between EVs and ICEVS in Lithuania, where various scenarios of energy mix is studied until 2050. The results showed that EVs are advantageous over ICEVS for their eco-environmental impacts with the increase penetration of RES in the energy mix of the national grid.

In [229], a LCA on CO_2 emissions of EVs, PHEVs, and ICEVS for the USA, japan, China, European Union, and Canada has been studied, under various grid energy mix and under a large-scale of adoption. The results showed that EVs have a positive impact on the CO_2 emissions reduction. In addition, the grid energy mix

has an impact on the CO_2 emissions, as in China the CO_2 emissions are still intense as they highly depend on coal. A LCA has been used in [230] for energy consumption and CO_2 emissions in China for EVs and ICEVS under various driving cycles from manufacturing, to usage and to the recycling phases. The results showed that EVs have lower CO_2 emissions than ICEVS, but with higher cost due to the high retail cost without incentives. The recycling reduce the CO_2 emissions but will increase the cost, which is related to the high cost of battery recycling. An adaptive LCA has been studied in [231] for CO_2 emissions for EVs, hybrid EVs, PHEVs, fuel cell EVs, and ICEVS. This study was conducted in different provinces in Canada, where grid energy mix is different, and considering battery chemistry, battery capacity, and mileage. A LCA for CO_2 emissions has been studied in [232] for EV charging based on marginal emissions in Great Britain in comparison with European countries. The CO_2 emissions is correlated with the percentage of fossil fuel energy in the grid energy mix. A LCA of electric bus charging station in [233] has been studied in Australia, particularly in Sydney city and Inner West regions, for CO_2 emissions through manufacturing, transportation, operation, decommissioning phases. The results showed that the CO_2 emissions has increased as the Australian grid energy mix is predominated by fossil fuels. A LCA on CO_2 emissions for EVs through production, transportation, and use phases has been studied in [234] in 10 countries, with the highest EV sales, for current and future of grid energy mix. The results showed that China present the worse CO_2 emissions for EVs, while France, Sweden, Norway presents actually lower CO_2 emissions for EVs and Sweden and Norway presents in 2030 the best scenario with the increase of cleaner energy.

The best approach to our work is presented in [235], where a PVCS has been studied in a technical, financial, and environmental perspective in two US cities in comparison with two Chinese cities with different scenarios of PV shares. The results proved that PVCS has lower CO_2 emissions than a charging station only grid-connected, which depends on the energy mix in each city. Whereas, the installation of a PVCS has lower net present cost than a charging station only grid-connected due to the high initial cost of the storage system, which remains a key element in a PVCS. However, The CO_2 emissions were not well detailed and their project lifetime is considered 10 years.

The previously cited references have not discussed the carbon impact of a PVCS as a French case study. In this chapter, the carbon impact of a PVCS is detailed; the PVCS is a car parking shade equipped with PV sources, stationary storage, and grid connection. Then, a comparison with a PGCS is presented and analysed.

VI.3. Carbon impact methodology for PVCS

The transition to electro-mobility is a promising solution towards a carbon free for transport sector. However, the environmental impact of the EVs depends on the manufacturing of EVs' components and their charging energy sources. Therefore, EVs could be charged with RES as the PVCS that integrates PV sources, Li-Ion batteries as stationary storage, public grid connection, inverter, and charging terminals

(CTs). Although the PVCS is based on renewable energies, its life cycle emits indirectly GHG through its manufacturing, maintenance, and recycling. Therefore, it is important to evaluate the carbon impact of the PVCS to analyze its value in comparison with charging stations only connected to the public grid.

This study is carried out using the LCA method, based on ISO 14067 [236], and, thus, considering the manufacturing and recycling of PV, of CTs, and of stationary storage based on Li-Ion, as well as the materials for construction of the PVCS and the traveling for maintenance of the PV and CTs. As mentioned above, the PVCS involves also a public grid connection; therefore, the carbon impact for the electricity grid is considered. Figure 125 shows the global overview of the methodology for this study.

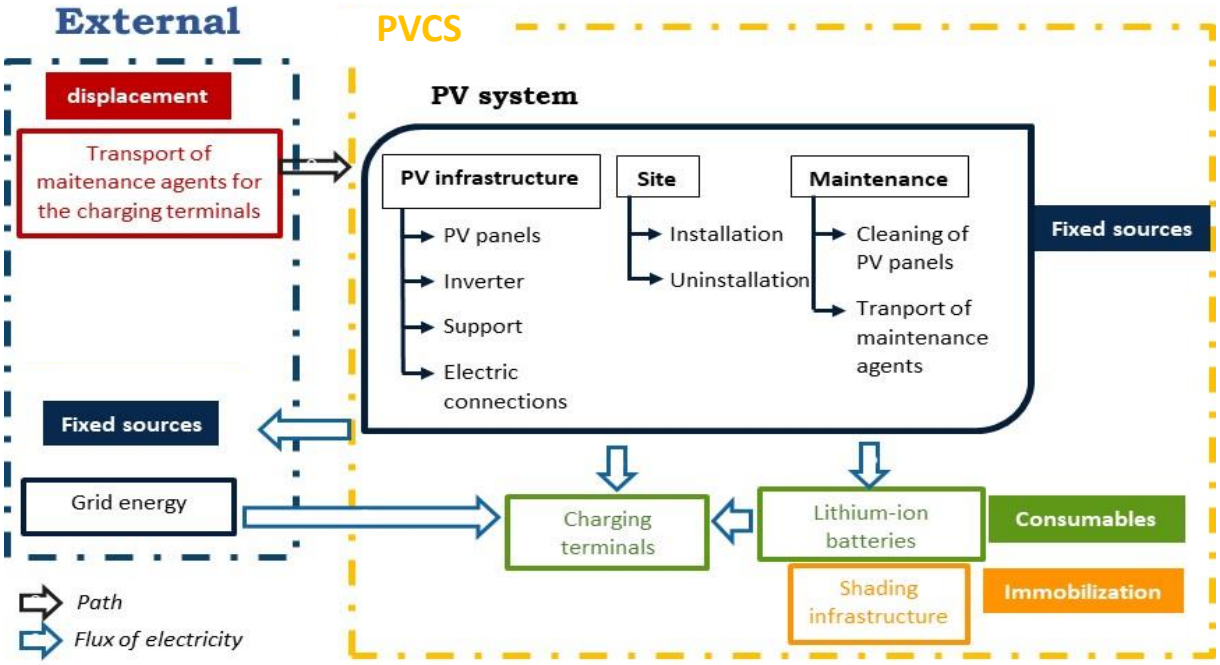

Figure 125: Global overview of the study methodology.

This study is based on carbon emissions coefficient issued by the Base Carbon ® of the French Agency for ecological transition, ADEME, [209] and EcoInvent database [210]. Each component of the PVCS has a specific coefficient. The carbon impact is calculated based on PV's life cycle, which is the largest one among all components. In this study, the PV's life cycle is considered 30 years, whereas, the life cycle of the Li-Ion battery, the inverter, and the CT are 10, 15 [237], and 10 years respectively. The following subsections presents the carbon impact of each component of the PVCS, whose estimations are based on [238], which is the benchmark database for LCA.

The carbon impact for any component, Imp_n, is given by the general equation (6.1):

$$Imp_n = CO_{2,n} \cdot Q_n, \tag{6.1}$$

where $CO_{2,n}$ and Q_n are the carbon emission coefficient ($kgCO_{2,eq}$/unit) and quantity of *n* component.

VI.3.1. Carbon Impact of PV System

The carbon emissions coefficient for the PV differs from one country of manufacturing to another. It also depends on the installation and uninstallation, the use, the maintenance and the recycling of the PV system. Figure 126 shows the different factors of the PV system that influence the carbon impact calculation.

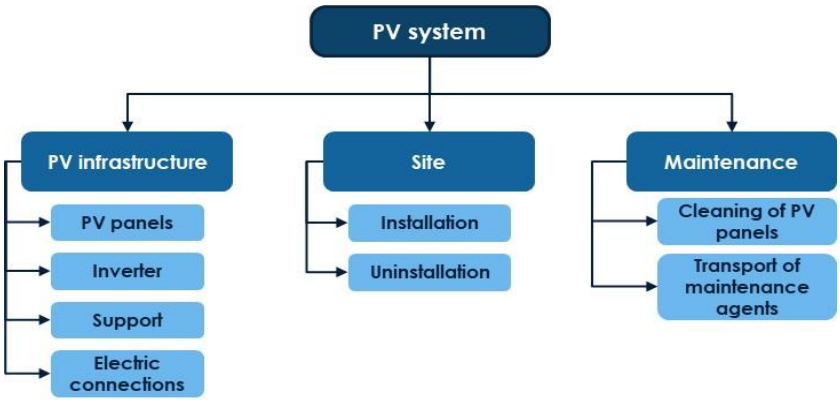

Figure 126: PV system's factors influencing the carbon impact calculation.

The considered PV system is based on monocrystalline silicon PV panels. Its carbon impact depends on the energy produced by the PV system. The carbon emissions coefficient of PV system, $CO_{2,PV}$ ($kgCO_{2,eq}/kWh$) is given by (6.2):

$$CO_{2,PV} = Imp_{PV} / E_{PV} , \tag{6.2}$$

where Imp_{PV} is the carbon impact of PV ($kgCO_{2,eq}$) and E_{PV} is the energy produced by PV (kWh) during analysis period. The Imp_{PV} is calculated as in (6.3):

$$Imp_{PV} = Imp_{Infra,\,PV} + Imp_{site} + Imp_{mtn} , \tag{6.3}$$

where $Imp_{Infra,\,PV}$, Imp_{site}, and Imp_{mtn} are the carbon impacts of the PV infrastructure, construction site, and maintenance of PV infrastructure respectively ($kgCO_{2,eq}$). Each of these three impacts is calculated as the sum of the impacts of the corresponding subgroups shown in Figure 126.

The $Imp_{Infra,\,PV}$ is given by (6.4):

$$Imp_{Infra,\,PV} = Imp_{PV\ panels} + Imp_{inv} + Imp_{supp} + Imp_{wiring} \tag{6.4}$$

$$Imp_{Infra,\,PV} = CO_{2,PV\ panels} \cdot P_p + (CO_{2,inv,a} \cdot P_{inv} + CO_{2,inv,b}) + CO_{2,supp} \cdot S_{PV} + CO_{2,wiring} \cdot P_p \tag{6.4}$$

where $Imp_{PV\ panels}$, Imp_{inv}, Imp_{supp}, and Imp_{wiring} are the carbon impact of PV panels, inverters, PV panels support and wiring connections respectively ($kgCO_{2,eq}$), $CO_{2,PV\ panels}$, $CO_{2,inv,a}$, $CO_{2,inv,b}$, $CO_{2,supp}$, and $CO_{2,wiring}$ are the carbon emissions coefficient of PV panels ($kgCO_{2,eq}/kWp$), inverter a

($kgCO_{2,eq}$/kVA), inverter b ($kgCO_{2,eq}$), PV panels support ($kgCO_{2,eq}/m^2$), and wiring connections respectively ($kgCO_{2,eq}$/kWp), P_p, P_{inv}, and S_{PV} are the PV pic power (kWp), inverter power (kVA) and PV surface area (m^2) respectively.

The Imp_{site} is given by (6.5):

$$Imp_{site} = Imp_{instal} + Imp_{uninstal}, \tag{6.5}$$

$$Imp_{site} = CO_{2,instal} \cdot P_p + CO_{2,uninstal} \cdot P_p, \tag{6.5}$$

where Imp_{instal}, and $Imp_{uninstal}$, are the carbon impact of PV system installation and uninstallation respectively, ($kgCO_{2,eq}$), $CO_{2,instal}$, and $CO_{2,uninstal}$ are the carbon emissions coefficient of PV system installation and uninstallation respectively ($kgCO_{2,eq}$/kWp).

The Imp_{mtn} is given by (6.6):

$$Imp_{mtn} = Imp_{clean} + Imp_{servicing}, \tag{6.6}$$

$$Imp_{mtn} = CO_{2,clean} \cdot S_{PV} + CO_{2,servicing} \cdot d \cdot q, \tag{6.6}$$

where Imp_{clean}, and $Imp_{servicing}$, are the carbon impact of PV system cleaning and servicing of transport agents for PV system maintenance respectively, ($kgCO_{2,eq}$), $CO_{2,clean}$, $CO_{2,servicing}$, d, and q are the carbon emissions coefficient of PV system cleaning ($kgCO_{2,eq}/m^2$), servicing of transport agents for PV system maintenance ($kgCO_{2,eq}$/km), annual distance travelled by the maintenance agents (km/year), and the lifetime of PV panels (years) respectively.

VI.3.2. Carbon Impact of Li-Ion Batteries

The carbon emissions coefficient of Li-Ion battery includes its manufacturing and recycling. Equation (6.7) shows the carbon emissions coefficient of Li-Ion, $CO_{2,Li-Ion}$ ($kgCO_{2,eq}$/kWh):

$$CO_{2,Li-Ion} = CO_{2,Li-Ion,man} + CO_{2,Li-Ion,recy}, \tag{6.7}$$

where $CO_{2,Li-Ion,man}$ and $CO_{2,Li-Ion,recy}$ are the carbon emissions coefficients of the Li-Ion manufacturing and recycling respectively ($kgCO_{2,eq}$/kWh) [239]. The $CO_{2,Li-Ion,man}$ depends on the type of Li-Ion [240]. Two recycling methods exist in France [240], pyrometallurgy and hydrometallurgy. The carbon impact of Li-Ion batteries Imp_{Li-Ion} ($kgCO_{2,eq}$) is given by (6.8):

$$Imp_{Li-Ion} = CO_{2,Li-Ion} \cdot C_{Li-Ion} \cdot (r_{Li-Ion} + 1), \tag{6.8}$$

where C_{Li-Ion} is the Li-Ion batteries' capacity (kWh) and r_{Li-Ion} is the number of Li-Ion replacement in the study period.

VI.3.3. Carbon Impact of the Charging Terminals

The carbon emissions coefficient of the CTs depends on their type implementation, suspended on the infrastructure's beam or grounded.

VI.3.3.1. Suspended Charging Terminals

The carbon emissions coefficient for the suspended type is based on EVLink Wallbox Plus [17]. This device is considered as similar to an electrical wallbox. The carbon impact of the suspended CT, $Imp_{CT,sus}$, is given by (6.9):

$$Imp_{CT,sus} = CO_{2,CT,sus} \cdot N_{CT,sus} \cdot (r_{CT} + 1) + Imp_{CT,mtn}, \quad (6.9)$$

where $CO_{2,CT,sus}$ is the carbon emissions coefficient for one suspended CT, $N_{CT,sus}$ is the number of suspended CT, r_{CT} is the number of CT replacement in this study period and $Imp_{CT,mtn}$ ($kgCO_{2,eq}$) is the maintenance impact.

VI.3.3.2. Grounded Charging Terminals

The carbon emissions coefficient for the grounded type is based as EVLink City [4]. The maintenance impact for the grounded CT is the same as suspended CT. the carbon emissions coefficient for the grounded $CO_{2,CT,gnd}$ ($kgCO_{2,eq}$/CT) is given by (6.10):

$$CO_{2,CT,gnd} = CO_{2,CT,sus} \cdot m_{CT,gnd} / m_{CT,sus}, \quad (6.10)$$

where $m_{CT,gnd}$, $m_{CT,sus}$ are the weight of the CT grounded and suspended respectively (kg).

The carbon impact of the civil engineering work for the installation of CTs Imp_{CE} ($kgCO_{2,eq}$) is given by (6.11):

$$Imp_{CE} = V_c \cdot CO_{2,cc} \cdot \rho_c \cdot N_{CT}, \quad (6.11)$$

where V_c, $CO_{2,cc}$, ρ_c, N_{CT} are the concrete volume (m^3), carbon emissions coefficient of concrete cement ($kgCO_{2,eq}$/ton), density of concrete (kg/m^3), and number of CTs respectively.

Therefore, and the carbon impact of the grounded CT $Imp_{CT,gnd}$ ($kgCO_{2,eq}$) is given by (6.12):

$$Imp_{CT,gnd} = CO_{2,CT,gnd} \cdot N_{CT} \cdot (r_{CT} + 1) + Imp_{mtn} + Imp_{CE}, \quad (6.12)$$

VI.3.4. Carbon Impact of the Infrastructure

The carbon impact of the infrastructure, Imp_{infra}, is represented by the carbon impact of the car parking shades. The car parking shades is dedicated to several parking places. The dimensions of the infrastructure are known, therefore, the volume of reinforced concrete (RC) needed for the foundation of one shade, V_{RC} (m^3), is given by (6.13):

$$V_{RC} = L_{found} \cdot W_{found} \cdot H_{found} \cdot N_{poles}, \quad (6.13)$$

where L_{found}, W_{found}, H_{found}, N_{poles} are the length, width, height of the reinforced concrete for the foundation in (m) and number of poles respectively. Thereafter, the carbon impact of RC for the foundations of *m* car parking shades, $Imp_{RC,found}$, ($kgCO_{2,eq}$) is given by (6.14):

$$Imp_{RC,found} = CO_{2,RC} \cdot \rho_c \cdot V_{RC} \cdot m, \quad (6.14)$$

where $CO_{2,RC}$ is the carbon emissions coefficient of RC ($kgCO_{2,eq}/m^3$).

The carbon impact of the steel used in the metallic structure Imp_{Steel} ($kgCO_{2,eq}$) is given by (6.15):

$$Imp_{Steel} = m_{Steel} \cdot CO_{2,Steel}, \quad (6.15)$$

where m_{Steel} is the weight of the steel used (kg) and $CO_{2,Steel}$ is the carbon emissions coefficient of the steel given by ADEME (2211 $kgCO_{2,eq}$/ton). Thus, the carbon impact for *m* car parking shades, Imp_{m_shades}, ($kgCO_{2,eq}$) is given by (6.16):

$$Imp_{m\_shades} = Imp_{RC,found} + Imp_{Steel} \quad (6.16)$$

Hence, the carbon emissions coefficient for one parking place $CO_{2,shade}$ and Imp_{infra} are given by (6.17) and (6.18):

$$CO_{2,shade} = Imp_{m\_shades} / m, \quad (6.17)$$

$$Imp_{infra} = CO_{2,shade} \cdot N_{places}, \quad (6.18)$$

where N_{places} is the number of parking places.

VI.3.5. Carbon Impact of the Public Grid

The carbon emissions coefficient of a public grid $CO_{2,PG}$ depends on the production modes of electricity. The primary energy sources mostly used are as in [243]: nuclear, hydro, coal, and gas. Each primary energy source has a different carbon emissions coefficient. The carbon impact of a public grid, Imp_{PG}, ($kgCO_{2,eq}$) is given by (6.19):

$$Imp_{PG} = E_{PG} \cdot CO_{2,PG}, \tag{6.19}$$

where E_{PG} is the energy supplied by the public grid (kWh) for the considered time duration. However, the $CO_{2,PG}$ depends on the electricity mix of each country; its value varies for a country to another. As stated in [220], marginal grid emission can help to assess robustness, while considering the exchange of energy from another regions or countries. The reference [244] is a data source for marginal emissions. However, in the present study, average grid emissions are considered, as in France, where $CO_{2,PG}$ is 0.0599 $kgCO_{2,eq}$/kWh. This coefficient is very low as the majority of electricity in France is generated by nuclear energy, having a very low carbon emissions coefficient of 0.006 $kgCO_{2,eq}$/kWh.

VI.4. Analysis of the carbon impact for the PVCS

The following subsection present the carbon impact evaluation for the PVCS and is compared with the PGCS. Then, based on the results obtained, the action levers that should be taken.

VI.4.1. Carbon impact evaluation for the PVCS

The carbon emissions coefficients and the carbon impacts described earlier are used to calculate the carbon impact of the PVCS Imp_{PVCS} ($kgCO_{2,eq}$) for 30 years, as in (6.20):

$$Imp_{PVCS} = Imp_{PV} + Imp_{Li-Ion} + Imp_{CT,sus} + Imp_{infra} + Imp_{PG}. \tag{6.20}$$

As numerical application, an existing French PVCS is considered with the following characteristics: 10 car parking places, 5 suspended CTs, 22 kWh Li-Ion battery's capacity and recycled by pyrometallurgy method, 28 kWp of 70 PV panels for the PV power installed on an infrastructure surface space of 124 m^2. The inverter average efficiency is taken as 90% and therefore $P_{inv} = 25.2\ kVA$. For an average annual irradiation of 1309.11 kWh/m^2 in the north of France and an optimal angle of PV panels, an estimation of the electricity produced and used by the PVCS for 30 years is 1.257 GWh, including 307.476 MWh from the public grid which maximum power is considered 200 kW. This estimation is based on the study presented in [21] following the realistic scenario considering an eco-drive profile as well as a normal drive

profile and EV battery capacity being the same at 50 kWh for all EVs. The occupancy rate of CTs is arbitrarily fixed and distributed by time slot of two hours, reflecting the arrivals and departures of 10 EVs throughout the day as given here below:

- between 08:00 and 10:00: two EVs at 2.3 kW;
- between 10:00 and 12:00: one EV at 22 kW, four EVs at 2.3 kW;
- between 12:00 and 14:00: two EVs at 2.3 kW;
- between 14:00 and 16:00: one EV at 22 kW, four EVs at 2.3 kW;
- between 16:00 and 18:00: one EV at 22 kW, three EVs at 2.3 kW.

The carbon emission coefficient of the PV panels is 40 $gCO_{2,eq}$/kWh and it is taken from the national renewable energy laboratory [245] based on the LCA harmonization project.

Table 35 show the results of the carbon impact of the PVCS.

Table 35: Carbon impact of the PVCS.

PVCS			Imp ($kgCO_{2,eq}$)
PV sys	PV infra	PV panels	37,996
		Inverter	1,501
		Support	7,087
		Wiring	1,962
	Site	Installation	1
		Uninstallation	1
	Maint	Cleaning	23
		Servicing	424
CT sus	Maint		1,023
	Fabrication		1,095
Li-Ion			5,869
Infra			15,439
Public grid			13,540
Total			85,961

Thus, the global carbon emission of the PVCS could be find based on the power supplied of all the components in the PVCS and it is equivalent to 0.068 $kgCO_{2,eq}$/kWh. Hence, it is interesting to compare these values with a PGCS.

VI.4.2. Comparison of Carbon Impact with the French Public Grid

The carbon impact of the PVCS is compared with PGCS for which, the carbon impacts considered are Imp_{PG} and $Imp_{CT,sus}$ for 30 years since there is no need to consider the infrastructure of PV installation neither the Li-Ion batteries.

Therefore, for 1.257 GWh the carbon impact of the PGCS, Imp_{PGCS}, is 77,436 $kgCO_{2,eq}$. In comparison with the PVCS, the rate variation is given by (6.21):

$$Rate\ variation = \frac{Imp_{PVCS} - Imp_{PGCS}}{Imp_{PGCS}} \cdot 100\% \cdot \quad (6.21)$$

Thus, the rate variation for the PVCS is 11% higher than that of PGCS. One notes that when comparing these two cases, the carbon impact of CTs could be neglected since it is a common element.

VI.4.3. Discussion

The difference of carbon impact could be surprising since the PVCS is considered as a promising levitate to reduce carbon emissions. This could be referred for high nuclear energy use, as in France, the PGCS has a lower carbon impact than the PVCS. The Imp_{PG} is different from one country to another; it depends mainly on the distribution of the nuclear energy, thermal power plants, and renewable energies capacities. For example, in Greece where $CO_{2,PG}$ is 718 $gCO_{2,eq}$/kWh [246], a PVCS becomes much less polluting in CO_2 than that of PGCS. However, although the calculation principle is known, each country displays its coefficient without giving details concerning the life cycle of each category of power plant. It can be noticed also that the PV system is the most impacting element, yet the data are not very recent. However, PV technology is growing fast and its carbon impact is decreasing. Therefore, as given in following, the carbon impact of the PVCS is reduced with recent data.

VI.4.4. Levers of action to improve the carbon impact of PVCS

The carbon impact of PV panels has reduced from 409 $gCO_{2,eq}$/kWh in 1986 to 25 $gCO_{2,eq}$/kWh in 2016, i.e. 93% less carbon emissions [247], while the previous value used in this study based on [245] database is 40 $gCO_{2,eq}$/kWh. Moreover, the infrastructure is the second most impacting element in the PVCS. Therefore, their carbon impact could be reduced by using recycled materials.

Two scenarios are presented below:

- scenario 1: $CO_{2,PV\ panels}$ is considered 25 $gCO_{2,eq}$/kWh,
- scenario 2: $CO_{2,PV\ panels}$ is considered 25 $gCO_{2,eq}$/kWh and the infrastructure of PVCS is based on recycled materials.

Scenario 1: by reducing the carbon emissions coefficient to 25 $gCO_{2,eq}$/kWh, the carbon impact of the PV panels has reduced from 37,996 $kgCO_{2,eq}$ to 23,748 $kgCO_{2,eq}$ and the new carbon impact of the PVCS has reduced from approximately 85,961 $kgCO_{2,eq}$ to 71,713 $kgCO_{2,eq}$; 17.2% reduction. In comparison with the PGCS, the rate variation becomes -7.4%, which means that the carbon impact of the PVCS is lower than of the PGCS.

Scenario 2: by reducing the carbon emissions coefficient to 25 $gCO_{2,eq}$/kWh, and using recycled materials for the infrastructure of PVCS, the carbon impact of the infrastructure has reduced from 15,439 $kgCO_{2,eq}$

to 8,616 $kgCO_{2,eq}$ and the new carbon impact of the PVCS has reduced from approximately 85,961 $kgCO_{2,eq}$ to 64,890 $kgCO_{2,eq}$; 24.5% reduction. In comparison with the PGCS, the rate variation becomes -16.2%, which means that the carbon impact of the PVCS is lower than of the PGCS.

Figure 127 compares the carbon impact of different scenarios of the PVCS. Both scenarios 1 and 2 have lower carbon impact than of the PGCS, but the scenario 2 is the lowest.

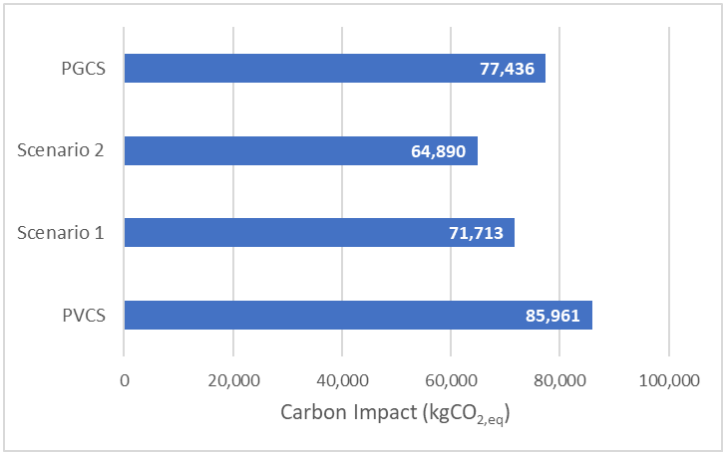

Figure 127: Carbon impact of the PVCS in different scenarios.

This study proves that, despite the highly French decarbonized energy mix, the PVCS could reduce the emission of GHG. With the fast growth and development of PV technology, the carbon emissions of PV panels are reduced significantly.

Based on ADEME database [246], Figure 128 shows the carbon impact of the PVCS, in comparison with the energy mix of different countries and Europe (EU), including France that is highly decarbonized. The carbon impact of the PVCS, even calculated with 2014 data, is 0.0516 $kgCO_{2,eq}$/kWh and is lower than the energy mixes of different countries even including France.

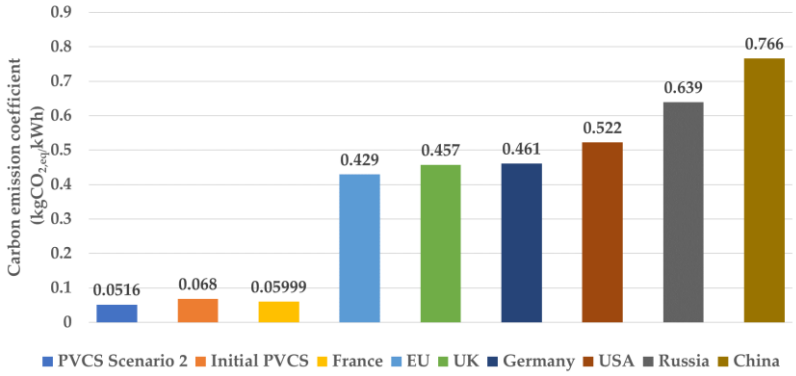

Figure 128: Carbon impact of PVCS in comparison with the energy mix of different countries.

VI.5. Conclusions

The LCA is used in this chapter to study the carbon impact of a PVCS. The carbon impact of the PVCS is then compared with a PGCS. The results show that PGCS has a higher carbon impact than the PVCS in several countries whose electricity mix depend less on nuclear energy and use more of thermal power plants. Although, for high nuclear energy use, as in France, the PGCS has a low carbon impact while the PVCS's carbon impact approaches the latter with recent improvements in PV technologies. However, the radioactive waste issued from nuclear energy production is not considered in the whole environmental impact of a public grid. Also, the PV system has the largest part of the carbon impact in the PVCS and with the recent technologies and using more recent data, therefore, the carbon impact will be even more reduced.

General conclusion and perspectives

As climate change is a major problem that will affect lives on the planet and do major changes, thus, the transformation towards RES can help reducing the dependency of the fossil fuel energy. RES are a key factor in the future power system as they are considered environmentally friendly and more efficient than traditional sources. Moreover, the transport sector is one of the major sources of CO_2 emissions, therefore, the transition towards electromobility is considered as an alternative solution to combat climate change and reduce CO_2 emissions. It is important to highlight that EVs when rolling on the roads emit zero or low carbon emissions, yet their global carbon emission pass from their production phase through charging process and to their end-of-life phase. Hence, the transition towards electromobility combined with the transition towards RES as being the main source of energy for charging is a promising solution towards carbon neutrality. This manuscript presented a PVCS based on a DC MG, which includes PV sources, stationary storage, public grid connection, and EVs as load.

The first chapter began with a global overview on the electromobility and the recent data in different regions and countries showing the trend of evolution in the stock market as well their charging infrastructure. Then, charging process, chargers' type, charging levels were described. Further, a MG-based charging station was presented along with its three architecture and hierarchical control. Thereafter, PVCS is introduced and presenting some existing charging station and the positioning of the thesis with the current state of the art.

The second chapter started by giving the driver characteristics and charging profiles and then the PVCS is modeled and simulation scenarios were studied in the lowest month of PV production. The main objective of chapter two was to identify the preliminary requirements and feasibility conditions of the PVCS in an urban area. The simulation results show that the EV charging is not constrained; slow and fast charging are possible with no restriction on the EV charging capacity. PV benefits increased when the average daily trip is considered 20-40 km, and the EV consumption is considered 10-15 kWh/km, resulting in daily charge of 2-6 kWh. The preliminary requirements and feasibility conditions can be summed as follows: slow charging is done by PV sources and stationary storage, which is charged only by the stationary storage, and it is up to 7 kW and EV battery can be filled up to 6 kWh. Proper sizing of the stationary storage is required and its power should be limited. EV user should be willing to stay long time and accept slow charging to increase PV benefits. Fast charging depends highly on public grid and is from 7 kW up to 22 kW. Also, the stationary storage should be well sized and its power should be limited. However, EV user should be willing to pay high charging cost.

The third chapter described the intelligent infrastructure for recharging EVs, which is the same PVCS presented in the previous chapter but it optimizes the energy flow to get the minimum energy cost with respect to constraints. The supervisory control system is outlined as it consists of four layers: Prediction layer, human-machine interface, energy cost optimization, and operation layer. Simulation results were conducted under different meteorological conditions and proved the feasibility of the optimization

algorithm and its superiority over the storage priority algorithm. Simulation results showed that for cases when there is no fluctuations, the optimization performs efficiently, whereas, with high fluctuations, the optimization is not very accurate which is impacted by the time-horizon of the previsions. The supervisory control system performs efficiently with the interaction of EV users and their demands. In optimization, selling energy to the grid in peak hours is preferable allowing making profits to the IIREVs operator.

The fourth chapter presented the experimental platform STELLA, where real-time experimental test were conducted under different meteorological conditions and different EV profiles. Similarly to the simulation, experimental results proved the efficiency of the supervisory control and the optimization algorithm with respect to constraints and meeting the EV demands as requested.

The fifth chapter studied the implementation of V2G service in the PVCS and its energy management system. Different simulation cases were considered under different meteorological conditions and EV profiles to highlight the benefits of V2G service. Simulation results showed the benefits of discharging the energy in EVs into the grid, where it reduced the impact on the public grid in peak hours, and could offer profits to participants in V2G service.

The six chapter presented the carbon impact methodology of a PVCS based on a LCA and compared it to PGCS. Results showed that the carbon impact of a PGCS is highly depending on the electricity energy mix of each country. Moreover, PV system is the major contributor on the carbon impact of a PVCS, thus after applying recent data and recycled materials for the PV, the carbon impact of a PVCS is lower than PGCS.

The work done in this thesis opens up new perspectives, which are also essentials that need to be improved:

For the requirement and feasibility conditions, two charging modes are possible; slow mode up to 7 kW based mainly on PV energy and storage and EV filling capacity up to 6 kWh, fast mode from 7 kW and up to 22 kW based mainly on public grid energy. Proper sizing of the stationary storage system is required and social acceptance relative to longer charging duration for slow mode and higher charging price for fast mode, so a business model is important. The two main concerns, highlighted in the case studies, are the control-command of the system, i.e., PV-powered EV charging station based on stationary storage and public grid, and the business model that is able to influence consumer behavior through price charging. Furthermore, defining the barriers, solutions for PV-powered EV charging stations, and a survey on social acceptance must be conducted, and proposing new services vehicle-to-x associated with PV-powered EV charging stations.

For the real-time optimization, the optimum energy cost highly depends highly on the accuracy of the previsions. As, human-machine interface provides EV data in real-time, thus, the prevision is only considered for the PV power profile. Météo France provides hourly solar irradiation, long-term, where in between passing clouds, represented by fluctuations, could not be well predicted. Therefore, solar irradiation previsions should be more accurate. Clear sky algorithm could be used to predict solar irradiations in short-term could but this may not predict clouds passage. Another technique is applying some machine learning technique based on the sensor capturing the solar irradiations on STELLA platform.

Moreover, the complexity of the problem should be taken care of and the time of calculation to give the optimization results in real-time.

For the EVs to be able to participate in the V2G operation, despite their charging mode, the charging terminals should allow bidirectional flow of energy with variable charging power. This will allow EVs to charge with their chosen charging mode, discharge in V2G with a maximum 50 kW, recharge again with a suitable power to satisfy the EV users, in consideration of the remaining parking time, and to reach their desired SOC at departure. For future research, an optimization problem could be studied on the PVCS with V2G service. Different case studies should be carried out to validate the optimization problem and prove its feasibility.

For the carbon impact, it would be possible to deepen the calculation of the carbon emissions of each subsystem of the PVCS based on any more recent data, to consider second-life batteries, and by completing the methodology of the global cost by providing updated prices and by rectifying the evolution of technologies related to PVCS.

Finally, the intelligent infrastructure for recharging EVs is dedicated to offer services as V2G, V2H, and I2H. Therefore, it would be interesting to study these services along with the optimization algorithm as well for a complete day scenario.

Appendix A

The case of 26 October 2021, in Compiegne, France, is considered. Figure A.1 shows $p_{PV\ MPPT\ pred}$, and $p_{PV\ MPPT}$, where it is a cloudy and rainy day thus the irradiations are very low with fluctuations.

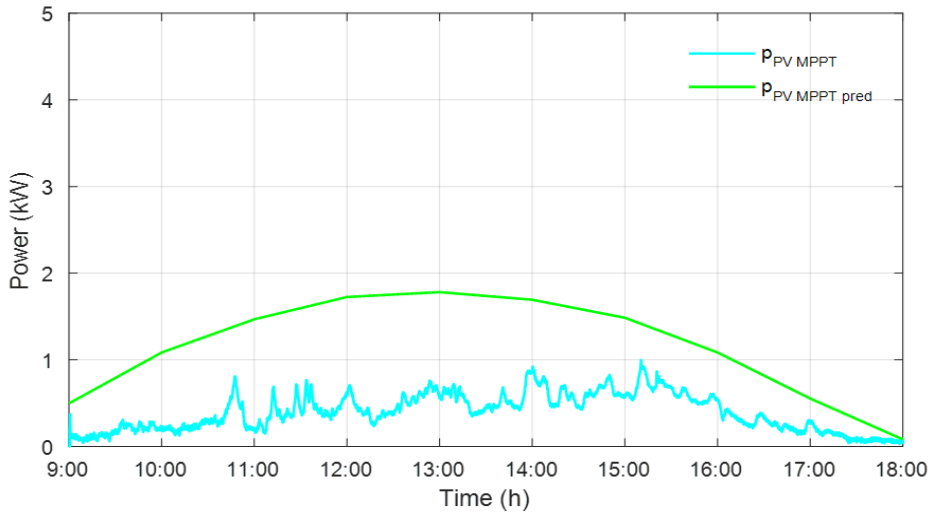

Figure A.1: PV MPPT real and predicted powers—experimental test App A.

In this case, the IIREV demand power is based on the data in Table 14. Figure A.2 shows the power flow and storage state of charge for "real-time exp" without optimization and the DC bus voltage—experimental test App Aa.

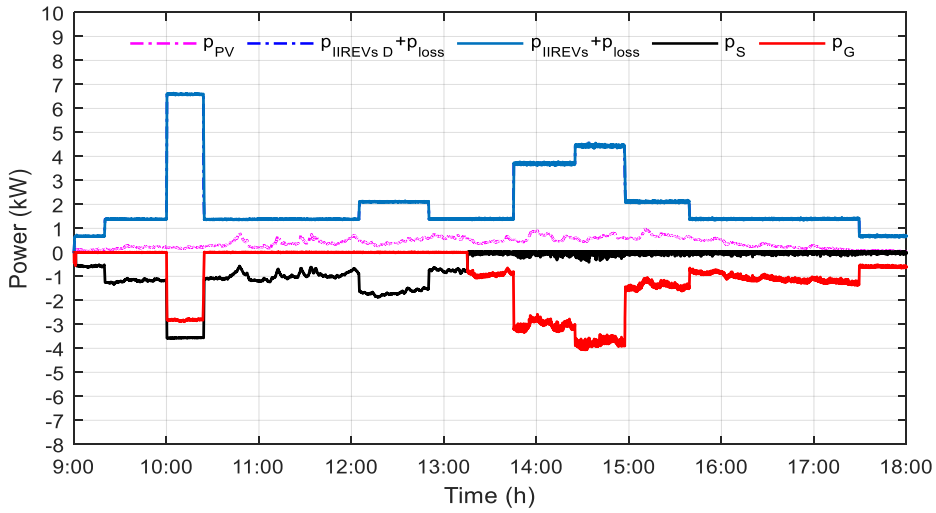

(a)

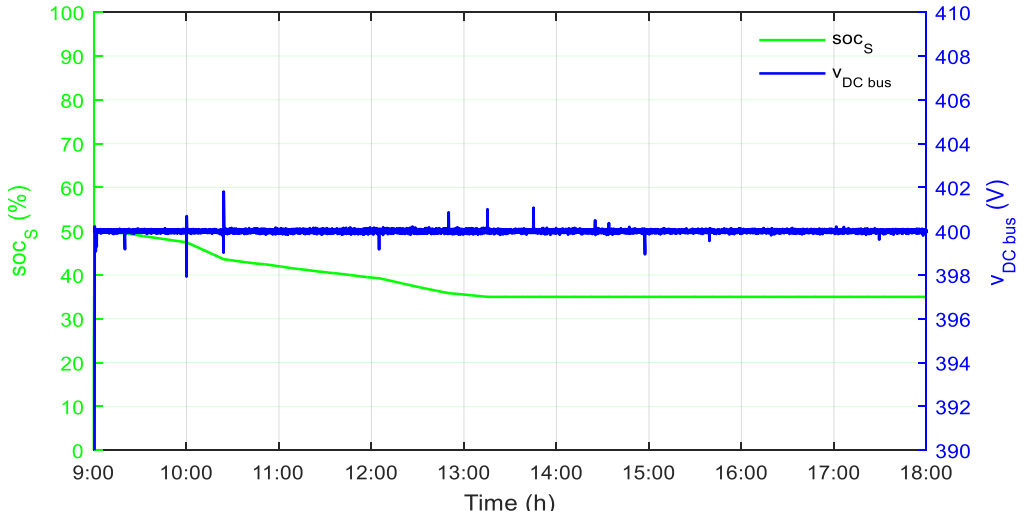

(b)

Figure A.2: Power flow and storage state of charge for "real-time exp" without optimization (a) and (b) storage state of charge and DC bus voltage—experimental test App Aa.

Figure A.3 Figure 82shows the power flow and storage state of charge for "real-time exp" with optimization and the DC bus voltage—experimental test App Ab.

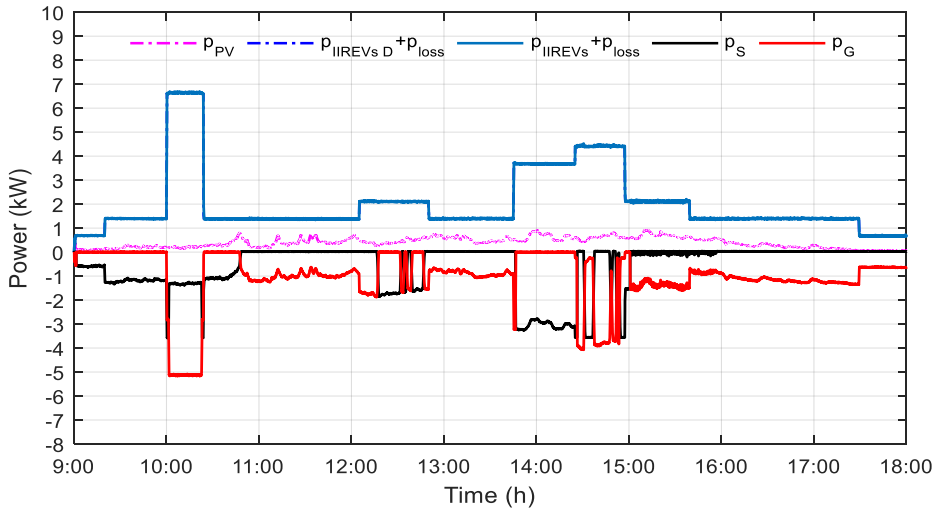

(a)

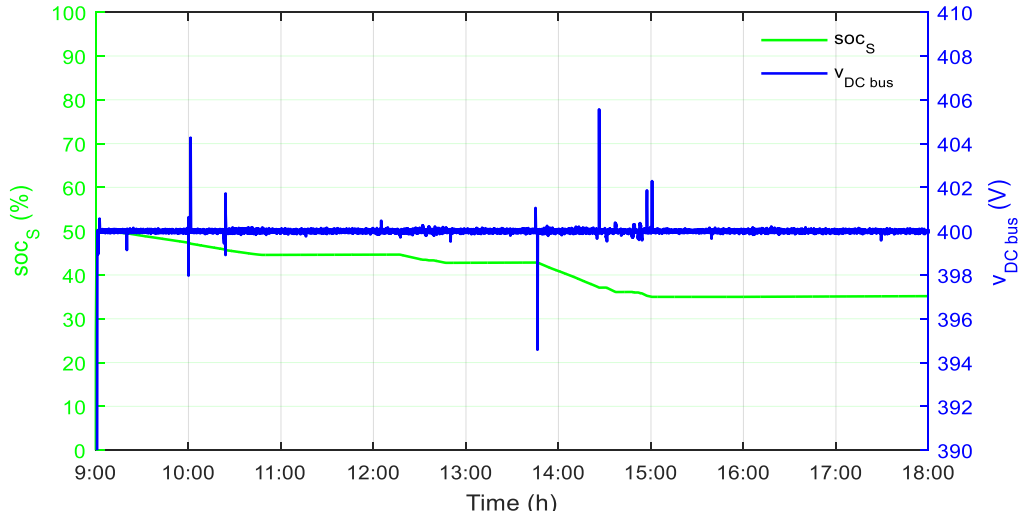

(b)

Figure A.3: Power flow and storage state of charge for "real-time exp" with opt (a) and (b) storage state of charge and DC bus voltage—experimental test App Ab.

Table A shows the energy system cost for App A.

Table A: Energy system cost—experimental test App A.

Case Operation	Grid cost (c€)	Storage cost (c€)	Total cost (c€)
Real-time exp w/o opt	163.46	5.90	169.36
Real-time exp with opt	210.66	5.66	216.33
Opt for real conditions	90.26	5.61	95.88

Figure A.4 shows the energy system distribution for "real-time exp" with and without optimization.

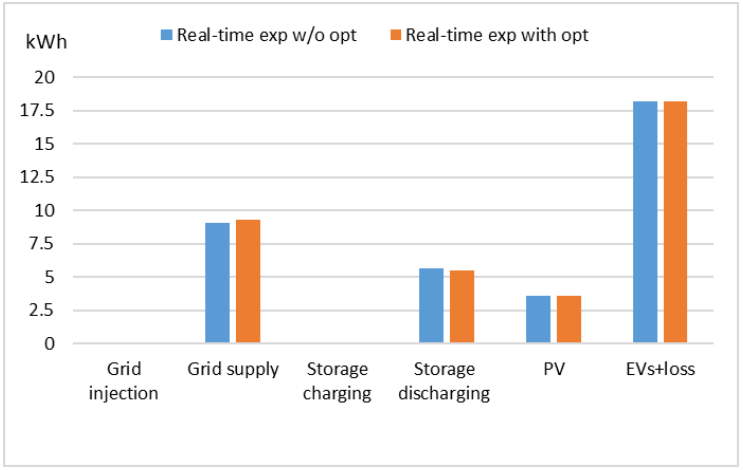

Figure A.4: Energy system distribution—experimental test App A.

Figure A.5 shows the EV energy distribution for "real-time exp" with and without opt.

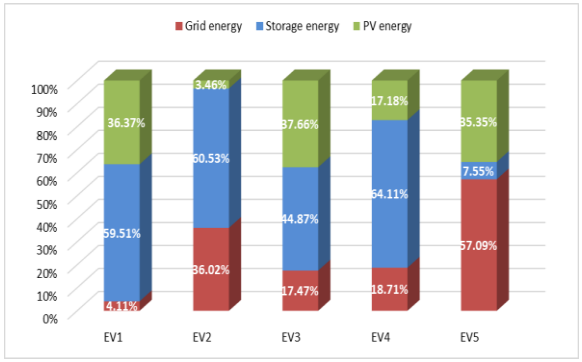

(a)

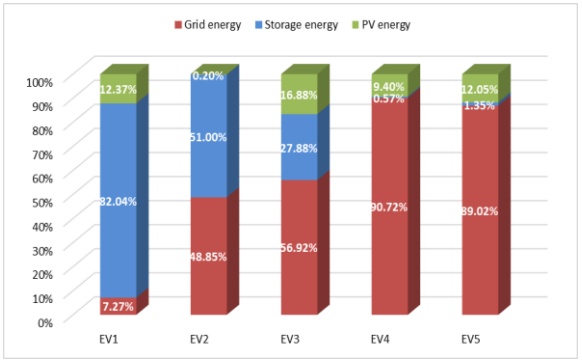

(b)

Figure A.5: EV energy distribution for "real-time exp" (a) without opt and (b) with opt—experimental test App A.

Appendix B

The case of 27 October 2021, in Compiegne, France, is considered. Figure B.1 shows $p_{PV\ MPPT\ pred}$, and $p_{PV\ MPPT}$, where the irradiations are intermediate and the weather is a bit cloudy, so there are low fluctuations.

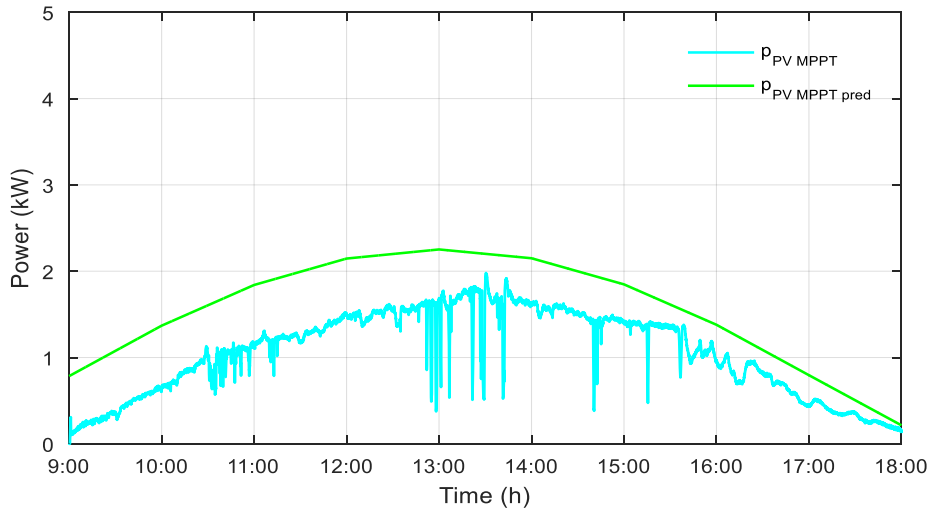

Figure B.1: PV MPPT real and predicted powers—experimental test App B.

In this case, the IIREV demand power is based on the data in Table 18. Figure B.2 shows the power flow and storage state of charge for "real-time exp" without optimization and the DC bus voltage—experimental test App Ba.

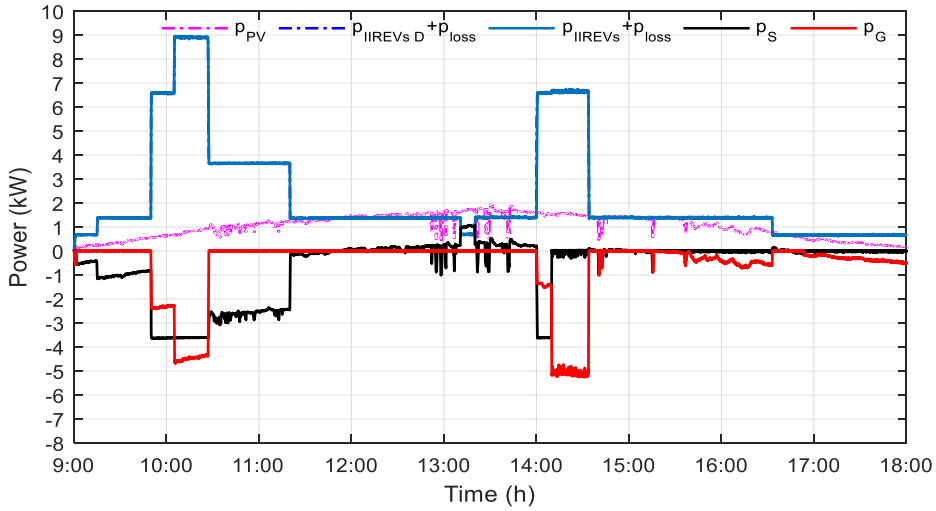

(a)

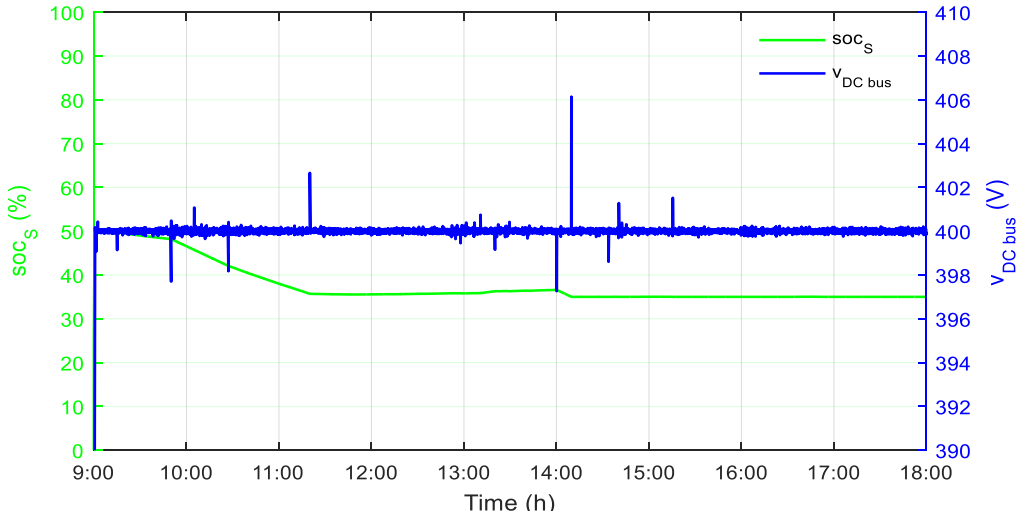

(b)

Figure B.2: Power flow and storage state of charge for "real-time exp" without optimization (a) and (b) storage state of charge and DC bus voltage—experimental test App Ba.

Figure B.3 Figure 82shows the power flow and storage state of charge for "real-time exp" with optimization and the DC bus voltage—experimental test App Bb.

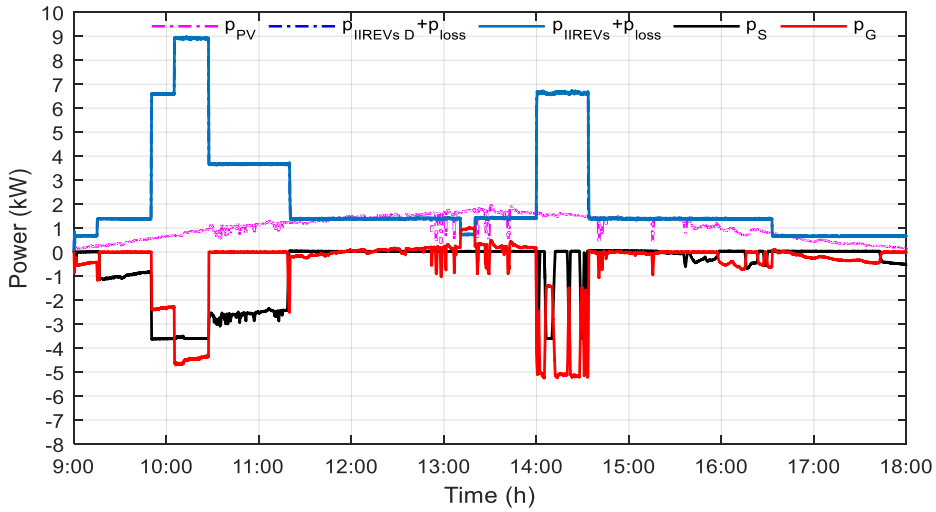

(a)

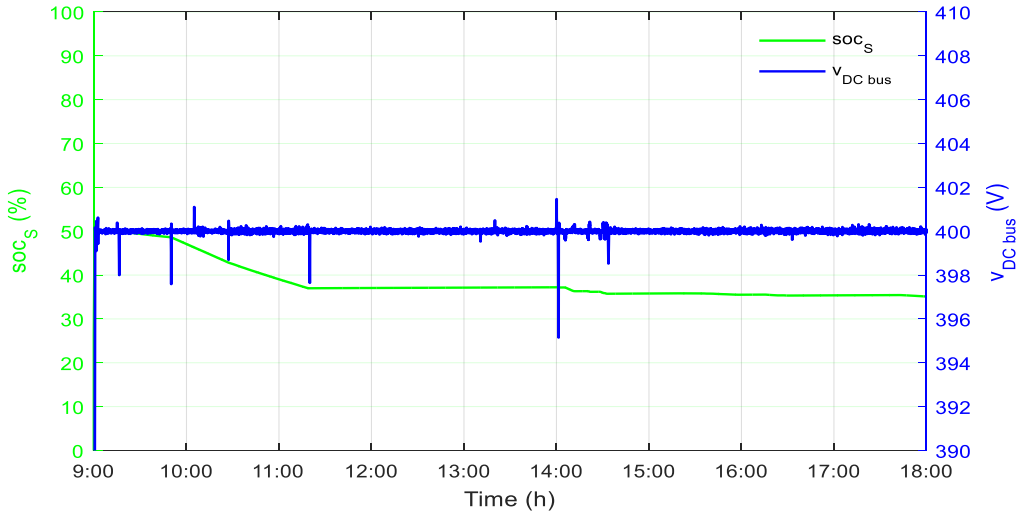

(b)

Figure B.3: Power flow and storage state of charge for "real-time exp" with opt (a) and (b) storage state of charge and DC bus voltage—experimental test App Bb.

Table B shows the energy system cost for App B.

Table B: Energy system cost—experimental test App B.

Case operation	Grid cost (c€)	Storage cost (c€)	Total cost (c€)
Real-time exp w/o opt	48.87	6.12	54.90
Real-time exp with opt	61.91	6.57	68.48
Opt for real conditions	47.55	5.61	53.17

Figure B.4 shows the energy system distribution for "real-time exp" with and without optimization.

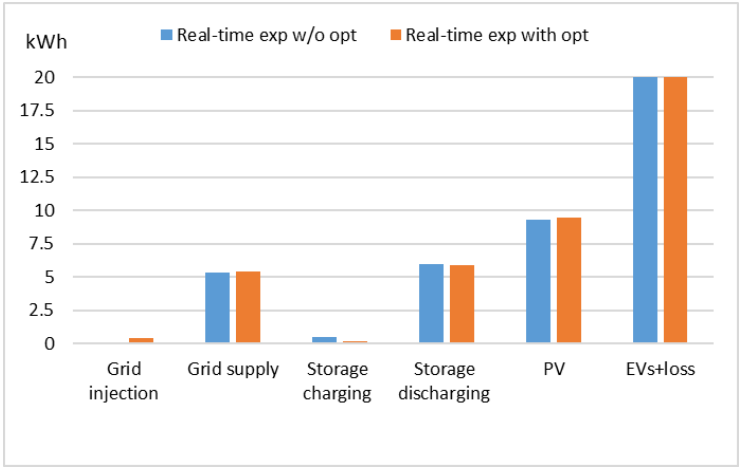

Figure B.4: Energy system distribution—experimental test App B.

Figure B.5 shows the EV energy distribution for "real-time exp" with and without opt.

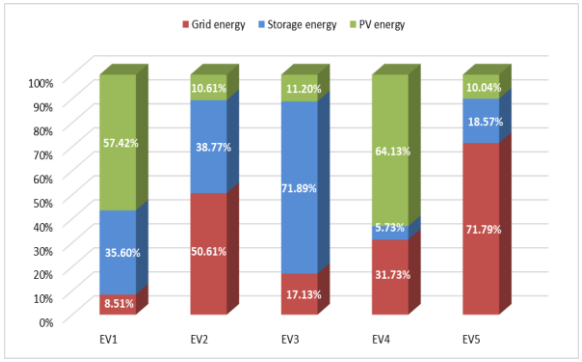

(a)

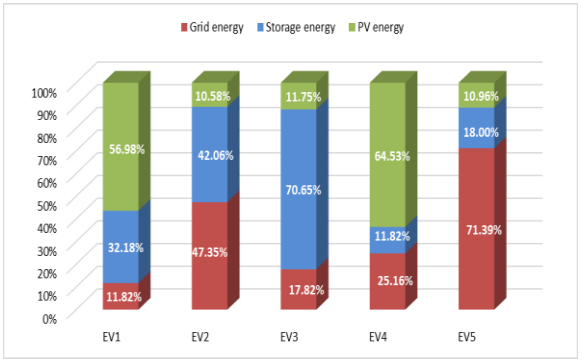

(b)

Figure B.5: EV energy distribution for "real-time exp" (a) without opt and (b) with opt—experimental test App B.

Appendix C

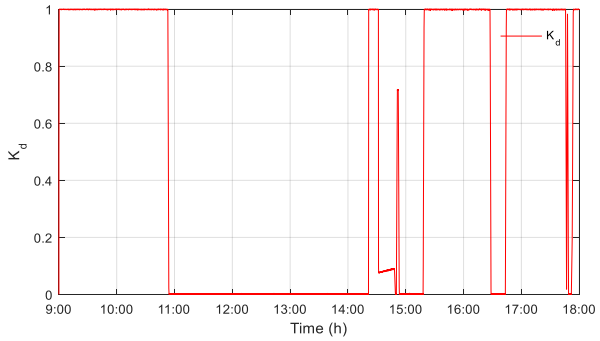

(a)

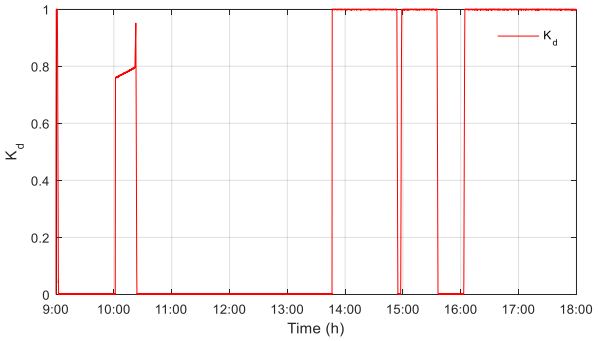

(b)

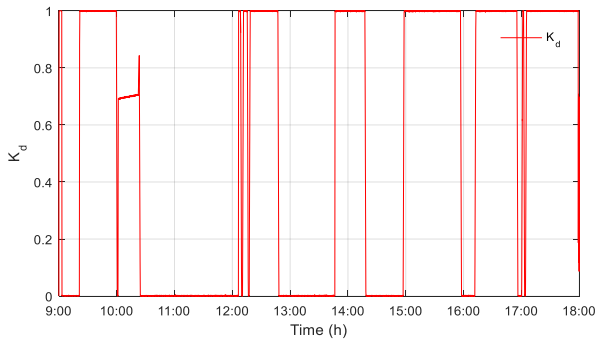

(c)

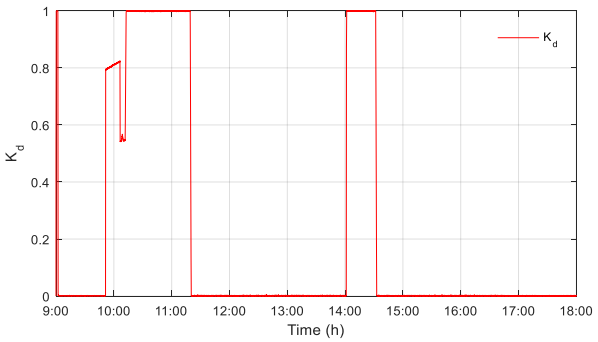

(d)

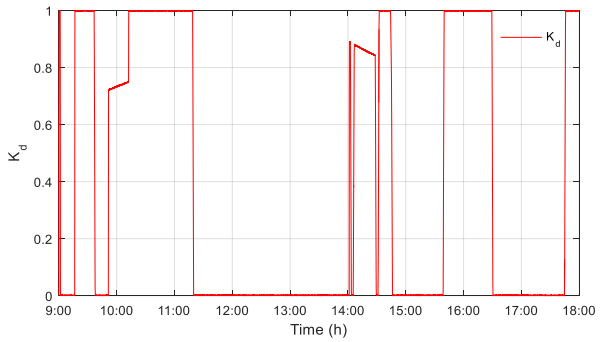

(e)

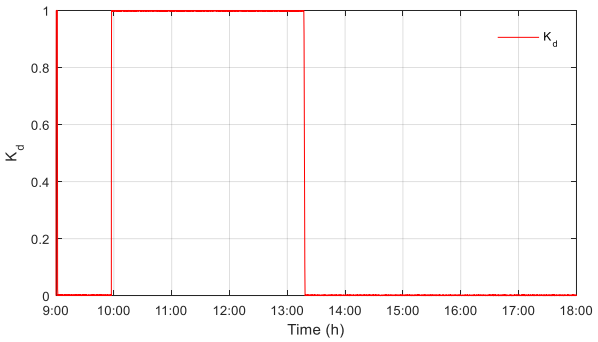

(f)

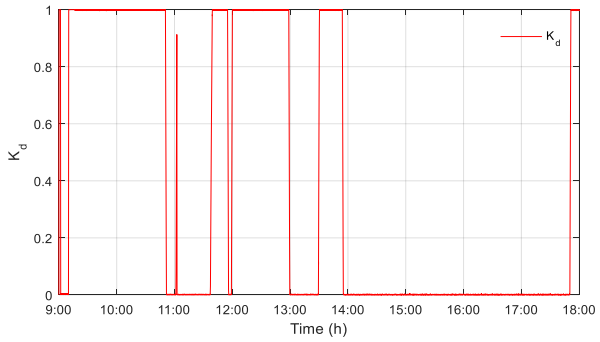

(g)

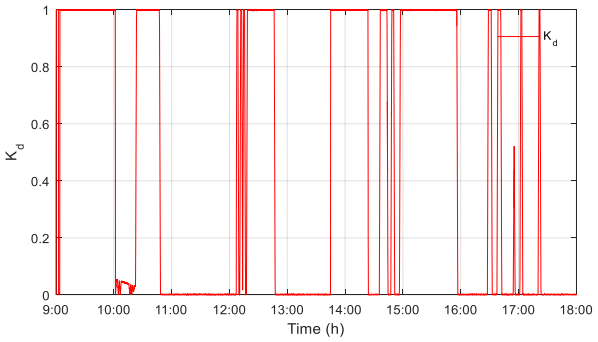

(h)

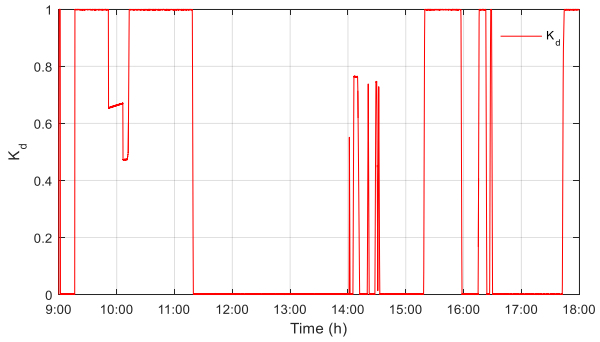

(i)

Figure C: Power coefficient distribution k_D —experimental test with opt (a) test 1, (b) test 2, (c) test 3, (d) test 4, (e) test 5, (f) test 6, (g) test 7, (h) App A, and (i) App B.

References

[1] X. Yang, J. Pang, F. Teng, R. Gong, and C. Springer, “The environmental co-benefit and economic impact of China’s low-carbon pathways: Evidence from linking bottom-up and top-down models,” *Renewable and Sustainable Energy Reviews*, vol. 136, p. 110438, Feb. 2021, doi: 10.1016/j.rser.2020.110438.

[2] J. Curtin, C. McInerney, B. Ó Gallachóir, C. Hickey, P. Deane, and P. Deeney, “Quantifying stranding risk for fossil fuel assets and implications for renewable energy investment: A review of the literature,” *Renewable and Sustainable Energy Reviews*, vol. 116, p. 109402, Dec. 2019, doi: 10.1016/j.rser.2019.109402.

[3] A. G. Olabi *et al.*, “Assessment of the pre-combustion carbon capture contribution into sustainable development goals SDGs using novel indicators,” *Renewable and Sustainable Energy Reviews*, vol. 153, p. 111710, Jan. 2022, doi: 10.1016/j.rser.2021.111710.

[4] L. Gustavsson, T. Nguyen, R. Sathre, and U. Y. A. Tettey, “Climate effects of forestry and substitution of concrete buildings and fossil energy,” *Renewable and Sustainable Energy Reviews*, vol. 136, p. 110435, Feb. 2021, doi: 10.1016/j.rser.2020.110435.

[5] X. He *et al.*, “Well-to-wheels emissions, costs, and feedstock potentials for light-duty hydrogen fuel cell vehicles in China in 2017 and 2030,” *Renewable and Sustainable Energy Reviews*, vol. 137, p. 110477, Mar. 2021, doi: 10.1016/j.rser.2020.110477.

[6] M. de l’Europe et des A. étrangères, “COP21: The key points of the Paris Agreement,” *France Diplomacy - Ministry for Europe and Foreign Affairs*. https://www.diplomatie.gouv.fr/en/french-foreign-policy/climate-and-environment/the-fight-against-climate-change/2015-paris-climate-conference-cop21/cop21-the-paris-agreement-in-four-key-points/ (accessed Feb. 08, 2022).

[7] S. J. Bhore, “Paris Agreement on Climate Change: A Booster to Enable Sustainable Global Development and Beyond,” *International Journal of Environmental Research and Public Health*, vol. 13, no. 11, Art. no. 11, Nov. 2016, doi: 10.3390/ijerph13111134.

[8] A. G. Olabi, K. Elsaid, M. K. H. Rabaia, A. A. Askalany, and M. A. Abdelkareem, “Waste heat-driven desalination systems: Perspective,” *Energy*, vol. 209, p. 118373, Oct. 2020, doi: 10.1016/j.energy.2020.118373.

[9] R. Pili, L. García Martínez, C. Wieland, and H. Spliethoff, “Techno-economic potential of waste heat recovery from German energy-intensive industry with Organic Rankine Cycle

technology," *Renewable and Sustainable Energy Reviews*, vol. 134, p. 110324, Dec. 2020, doi: 10.1016/j.rser.2020.110324.

[10] A. G. Olabi, M. A. Abdelkareem, T. Wilberforce, and E. T. Sayed, "Application of graphene in energy storage device – A review," *Renewable and Sustainable Energy Reviews*, vol. 135, p. 110026, Jan. 2021, doi: 10.1016/j.rser.2020.110026.

[11] E. T. Sayed *et al.*, "Synthesis and performance evaluation of various metal chalcogenides as active anodes for direct urea fuel cells," *Renewable and Sustainable Energy Reviews*, vol. 150, p. 111470, Oct. 2021, doi: 10.1016/j.rser.2021.111470.

[12] A. Hussain, S. M. Arif, and M. Aslam, "Emerging renewable and sustainable energy technologies: State of the art," *Renewable and Sustainable Energy Reviews*, vol. 71, pp. 12–28, May 2017, doi: 10.1016/j.rser.2016.12.033.

[13] E. Madi, K. Pope, W. Huang, and T. Iqbal, "A review of integrating ice detection and mitigation for wind turbine blades," *Renewable and Sustainable Energy Reviews*, vol. 103, pp. 269–281, Apr. 2019, doi: 10.1016/j.rser.2018.12.019.

[14] N. L. Panwar, S. C. Kaushik, and S. Kothari, "Role of renewable energy sources in environmental protection: A review," *Renewable and Sustainable Energy Reviews*, vol. 15, no. 3, pp. 1513–1524, Apr. 2011, doi: 10.1016/j.rser.2010.11.037.

[15] A. G. Olabi and M. A. Abdelkareem, "Renewable energy and climate change," *Renewable and Sustainable Energy Reviews*, vol. 158, p. 112111, Apr. 2022, doi: 10.1016/j.rser.2022.112111.

[16] A. G. Olabi and M. A. Abdelkareem, "Energy storage systems towards 2050," *Energy*, vol. 219, p. 119634, Mar. 2021, doi: 10.1016/j.energy.2020.119634.

[17] N. Duarte Souza Alvarenga Santos, V. Rückert Roso, A. C. Teixeira Malaquias, and J. G. Coelho Baêta, "Internal combustion engines and biofuels: Examining why this robust combination should not be ignored for future sustainable transportation," *Renewable and Sustainable Energy Reviews*, vol. 148, p. 111292, Sep. 2021, doi: 10.1016/j.rser.2021.111292.

[18] J.-M. Cariolet, M. Colombert, M. Vuillet, and Y. Diab, "Assessing the resilience of urban areas to traffic-related air pollution: Application in Greater Paris," *Science of The Total Environment*, vol. 615, pp. 588–596, Feb. 2018, doi: 10.1016/j.scitotenv.2017.09.334.

[19] A. R. Bhatti, Z. Salam, M. J. B. A. Aziz, and K. P. Yee, “A critical review of electric vehicle charging using solar photovoltaic,” *International Journal of Energy Research*, vol. 40, no. 4, pp. 439–461, 2016, doi: 10.1002/er.3472.

[20] “Futurs énergétiques 2050 : les scénarios de mix de production à l’étude permettant d’atteindre la neutralité carbone à l’horizon 2050.” https://www.rte-france.com/analyses-tendances-et-prospectives/bilan-previsionnel-2050-futurs-energetiques (accessed May 20, 2022).

[21] “Rapport sur le pilotage de la recharge des véhicules électriques et le réseau de distribution | Enedis.” https://www.enedis.fr/presse/rapport-sur-le-pilotage-de-la-recharge-des-vehicules-electriques-et-le-reseau (accessed May 20, 2022).

[22] M. Sechilariu, N. Molines, G. Richard, H. MAR^{TEL}L FLORES, F. Locment, and J. Baert, “Electromobility Framework Study: Infrastructure and Urban Planning for EV Charging Station Empowered by PV-based Microgrid,” *IET Electrical Systems in Transportation*, 2019, doi: 10.1049/iet-est.2019.0032.

[23] “Global EV Outlook 2021 – Analysis,” *IEA*. https://www.iea.org/reports/global-ev-outlook-2021 (accessed Feb. 07, 2022).

[24] D. Savio Abraham *et al.*, “Electric Vehicles Charging Stations’ Architectures, Criteria, Power Converters, and Control Strategies in Microgrids,” *Electronics*, vol. 10, no. 16, Art. no. 16, Jan. 2021, doi: 10.3390/electronics10161895.

[25] “Swappable batteries on the horizon: Giants team up to make swap-in, swap-out battery packs a reality.” https://www.motorcyclenews.com/news/electric-motorbike-swappable-batteries/ (accessed Jun. 01, 2022).

[26] “U.K. to test roads that charge electric cars as they drive - National | Globalnews.ca,” *Global News*. https://globalnews.ca/news/2171804/uk-to-test-roads-that-charge-electric-cars-as-they-drive/ (accessed Jun. 01, 2022).

[27] “PV Powered Electric Vehicle Charging Stations - Preliminary Requirements and Feasibility Conditions,” *IEA-PVPS*. https://iea-pvps.org/key-topics/pv-powered-electric-vehicle-charging-stations/ (accessed Feb. 11, 2022).

[28] “Sustainable EV Charging, Lowest TCO and Fastest to Deploy,” *Beam*. https://beamforall.com/product/ev-arc-2020/ (accessed Feb. 11, 2022).

[29] “Fastned,” *Fastned*. http://fastnedcharging.com/en/ (accessed Feb. 11, 2022).

[30] S. SunStation, “Lead the Charge. Drive Solar!,” p. 2.

[31] “SECAR Technologies E-Port.” http://www.secar.at/index.php/en/ (accessed Feb. 14, 2022).

[32] “Solar Carports | MDT-tex.” https://www.mdt-tex.com/en/products/solar-canopies/solar-carports (accessed Feb. 14, 2022).

[33] “Introducing V3 Supercharging,” Mar. 06, 2019. https://www.tesla.com/blog/introducing-v3-supercharging (accessed Feb. 14, 2022).

[34] “Powerpack - Commercial & Utility Energy Storage Solutions | Tesla.” https://www.tesla.com/powerpack (accessed Feb. 14, 2022).

[35] “Irisolaris associé au projet d’ombrières de parking de la métropole Aix-Marseille Provence,” Jun. 2020, Accessed: Feb. 14, 2022. [Online]. Available: https://www.usinenouvelle.com/article/irisolaris-associe-au-projet-d-ombieres-de-parking-de-la-metropole-aix-marseille-provence.N978556

[36] B. Schmidt, “Transdev to trial ‘100% solar-powered’ electric bus in Queensland,” *The Driven*, Sep. 17, 2020. https://thedriven.io/2020/09/17/transdev-to-trial-100-solar-powered-electric-bus-in-queensland/ (accessed Feb. 14, 2022).

[37] A. Sierra Rodriguez, T. de Santana, I. MacGill, N. j. Ekins-Daukes, and A. Reinders, “A feasibility study of solar PV-powered electric cars using an interdisciplinary modeling approach for the electricity balance, CO2 emissions, and economic aspects: The cases of The Netherlands, Norway, Brazil, and Australia,” *Progress in Photovoltaics: Research and Applications*, vol. 28, no. 6, pp. 517–532, 2020, doi: 10.1002/pip.3202.

[38] B. Robisson, S. Guillemin, L. Marchadier, G. Vignal, and A. Mignonac, “Solar Charging of Electric Vehicles: Experimental Results,” *Applied Sciences*, vol. 12, no. 9, Art. no. 9, Jan. 2022, doi: 10.3390/app12094523.

[39] R. Razi, K. Hajar, A. Hably, and S. Bacha, “A user-friendly smart charging algorithm based on energy-awareness for different PEV parking scenarios,” in *2021 29th Mediterranean Conference on Control and Automation (MED)*, Jun. 2021, pp. 392–397. doi: 10.1109/MED51440.2021.9480287.

[40] R. Razi, K. Hajar, M. Mehrasa, A. Labbone, A. Hably, and S. Bacha, “Limiting discharge cycles numbers for plug-in electric vehicles in bidirectional smart charging algorithm,” in

IECON 2021 – 47th Annual Conference of the IEEE Industrial Electronics Society, Oct. 2021, pp. 1–6. doi: 10.1109/IECON48115.2021.9589844.

[41] K. Hajar, B. Guo, A. Hably, and S. Bacha, "Smart charging impact on electric vehicles in presence of photovoltaics," in *2021 22nd IEEE International Conference on Industrial Technology (ICIT)*, Mar. 2021, vol. 1, pp. 643–648. doi: 10.1109/ICIT46573.2021.9453600.

[42] L. Yao, Z. Damiran, and W. H. Lim, "Optimal Charging and Discharging Scheduling for Electric Vehicles in a Parking Station with Photovoltaic System and Energy Storage System," *Energies*, vol. 10, no. 4, Art. no. 4, Apr. 2017, doi: 10.3390/en10040550.

[43] D. van der Meer, G. R. Chandra Mouli, G. Morales-España Mouli, L. R. Elizondo, and P. Bauer, "Energy Management System With PV Power Forecast to Optimally Charge EVs at the Workplace," *IEEE Transactions on Industrial Informatics*, vol. 14, no. 1, pp. 311–320, Jan. 2018, doi: 10.1109/TII.2016.2634624.

[44] N. Odkhuu, K.-B. Lee, M. A. Ahmed, and Y.-C. Kim, "Optimal Energy Management of V2B with RES and ESS for Peak Load Minimization," *Applied Sciences*, vol. 8, no. 11, Art. no. 11, Nov. 2018, doi: 10.3390/app8112125.

[45] J. Rivera, C. Goebel, and H.-A. Jacobsen, "Distributed Convex Optimization for Electric Vehicle Aggregators," *IEEE Transactions on Smart Grid*, vol. 8, no. 4, pp. 1852–1863, Jul. 2017, doi: 10.1109/TSG.2015.2509030.

[46] L. Yao, W. H. Lim, and T. S. Tsai, "A Real-Time Charging Scheme for Demand Response in Electric Vehicle Parking Station," *IEEE Transactions on Smart Grid*, vol. 8, no. 1, pp. 52–62, Jan. 2017, doi: 10.1109/TSG.2016.2582749.

[47] W. Tushar, C. Yuen, S. Huang, D. B. Smith, and H. V. Poor, "Cost Minimization of Charging Stations With Photovoltaics: An Approach With EV Classification," *IEEE Transactions on Intelligent Transportation Systems*, vol. 17, no. 1, pp. 156–169, Jan. 2016, doi: 10.1109/TITS.2015.2462824.

[48] D. Yan and C. Ma, "Optimal Sizing of A PV Based Electric Vehicle Charging Station Under Uncertainties," in *IECON 2019 - 45th Annual Conference of the IEEE Industrial Electronics Society*, Oct. 2019, vol. 1, pp. 4310–4315. doi: 10.1109/IECON.2019.8926749.

[49] L. Yao, Z. Damiran, and W. H. Lim, "A fuzzy logic based charging scheme for electric vechicle parking station," in *2016 IEEE 16th International Conference on Environment*

and Electrical Engineering (EEEIC), Jun. 2016, pp. 1–6. doi: 10.1109/EEEIC.2016.7555799.

[50] C. Jin, J. Tang, and P. Ghosh, "Optimizing Electric Vehicle Charging: A Customer's Perspective," *IEEE Transactions on Vehicular Technology*, vol. 62, no. 7, pp. 2919–2927, Sep. 2013, doi: 10.1109/TVT.2013.2251023.

[51] D. M. Anand, R. T. de Salis, Y. Cheng, J. Moyne, and D. M. Tilbury, "A Hierarchical Incentive Arbitration Scheme for Coordinated PEV Charging Stations," *IEEE Transactions on Smart Grid*, vol. 6, no. 4, pp. 1775–1784, Jul. 2015, doi: 10.1109/TSG.2015.2408213.

[52] B. Škugor and J. Deur, "Dynamic programming-based optimisation of charging an electric vehicle fleet system represented by an aggregate battery model," *Energy*, vol. 92, pp. 456–465, Dec. 2015, doi: 10.1016/j.energy.2015.03.057.

[53] Y. Wu, A. Ravey, D. Chrenko, and A. Miraoui, "Demand side energy management of EV charging stations by approximate dynamic programming," *Energy Conversion and Management*, vol. 196, pp. 878–890, Sep. 2019, doi: 10.1016/j.enconman.2019.06.058.

[54] K. L. López and C. Gagné, "Optimal Scheduling for Smart Charging of Electric Vehicles Using Dynamic Programming," in *Advances in Artificial Intelligence*, Cham, 2018, pp. 279–284. doi: 10.1007/978-3-319-89656-4_27.

[55] C. Tang, M. Liu, Q. Liu, and P. Dong, "A per-node granularity decentralized optimal power flow for radial distribution networks with PV and EV integration," *International Journal of Electrical Power & Energy Systems*, vol. 116, p. 105513, Mar. 2020, doi: 10.1016/j.ijepes.2019.105513.

[56] M. M. Rahman, E. A. Al-Ammar, H. S. Das, and W. Ko, "Technical Assessment of Plug-In Hybrid Electric Vehicle Charging Scheduling for Peak Reduction," in *2019 10th International Renewable Energy Congress (IREC)*, Mar. 2019, pp. 1–5. doi: 10.1109/IREC.2019.8754588.

[57] A. Houbbadi, R. Trigui, S. Pelissier, E. Redondo-Iglesias, and T. Bouton, "A quadratic programming based optimisation to manage electric bus fleet charging," *International Journal of Electric and Hybrid Vehicles*, vol. 11, no. 4, pp. 289–307, Jan. 2019, doi: 10.1504/IJEHV.2019.102862.

[58] E. Yao, V. W. S. Wong, and R. Schober, "Robust Frequency Regulation Capacity Scheduling Algorithm for Electric Vehicles," *IEEE Transactions on Smart Grid*, vol. 8, no. 2, pp. 984–997, Mar. 2017, doi: 10.1109/TSG.2016.2530660.

[59] M. Shafie-khah *et al.*, "Optimal Behavior of Electric Vehicle Parking Lots as Demand Response Aggregation Agents," *IEEE Transactions on Smart Grid*, vol. 7, no. 6, pp. 2654–2665, Nov. 2016, doi: 10.1109/TSG.2015.2496796.

[60] L. Zhang and Y. Li, "A Game-Theoretic Approach to Optimal Scheduling of Parking-Lot Electric Vehicle Charging," *IEEE Transactions on Vehicular Technology*, vol. 65, no. 6, pp. 4068–4078, Jun. 2016, doi: 10.1109/TVT.2015.2487515.

[61] N. Tutkun and A. N. Afandi, "Design of a PV Powered Charging Station for PHEVs," in *2018 6th International Renewable and Sustainable Energy Conference (IRSEC)*, Dec. 2018, pp. 1–5. doi: 10.1109/IRSEC.2018.8702940.

[62] G. Liu, Y. Xue, M. S. Chinthavali, and K. Tomsovic, "Optimal Sizing of PV and Energy Storage in an Electric Vehicle Extreme Fast Charging Station," in *2020 IEEE Power Energy Society Innovative Smart Grid Technologies Conference (ISGT)*, Feb. 2020, pp. 1–5. doi: 10.1109/ISGT45199.2020.9087792.

[63] A. Houbbadi, R. Trigui, S. Pelissier, E. Redondo-Iglesias, and T. Bouton, "Optimal Scheduling to Manage an Electric Bus Fleet Overnight Charging," *Energies*, vol. 12, no. 14, Art. no. 14, Jan. 2019, doi: 10.3390/en12142727.

[64] T. Fujita, T. Yasuda, and H. Akagi, "A Dynamic Wireless Power Transfer System Applicable to a Stationary System," *IEEE Transactions on Industry Applications*, vol. 53, no. 4, pp. 3748–3757, Jul. 2017, doi: 10.1109/TIA.2017.2680400.

[65] S. Sheng, C.-T. Hsu, P. Li, and B. Lehman, "Energy management for solar battery charging station," in *2013 IEEE 14th Workshop on Control and Modeling for Power Electronics (COMPEL)*, Jun. 2013, pp. 1–8. doi: 10.1109/COMPEL.2013.6626426.

[66] Y. Wu, "System operation and energy management of EV charging stations in smart grid integration applications," These de doctorat, Bourgogne Franche-Comté, 2019. Accessed: Mar. 26, 2022. [Online]. Available: https://www.theses.fr/2019UBFCA030

[67] B. Haidar, "A Techno-Economic Analysis of the Electric Vehicle Transition : Policy, Infrastructure, Usage, and Design," These de doctorat, université Paris-Saclay, 2021. Accessed: Mar. 28, 2022. [Online]. Available: https://www.theses.fr/2021UPAST122

[68] F. Eltoumi, “Charging station for electric vehicle using hybrid sources,” These de doctorat, Bourgogne Franche-Comté, 2020. Accessed: Mar. 28, 2022. [Online]. Available: https://www.theses.fr/2020UBFCA009

[69] I. Houssamo, “Contribution à l’étude théorique, à la modélisation et à la mise en oeuvre d’un système multisource appartenant à un micro-réseau électrique : considération sur la qualité de l’énergie,” These de doctorat, Compiègne, 2012. Accessed: Mar. 02, 2022. [Online]. Available: https://www.theses.fr/2012COMP2020

[70] B. Wang, “Intelligent control and power flow optimization of microgrid : energy management strategies,” These de doctorat, Compiègne, 2013. Accessed: Mar. 02, 2022. [Online]. Available: https://www.theses.fr/2013COMP2122

[71] L. Trigueiro dos Santos, “Contribution on the day-ahead and operational optimization for DC microgrid building-integrated,” These de doctorat, Compiègne, 2017. Accessed: Mar. 04, 2022. [Online]. Available: https://www.theses.fr/2017COMP2352

[72] C. Yin, “Impact of diesel generator operating modes on standalone DC microgrid and control strategies implying supercapacitor,” These de doctorat, Compiègne, 2018. Accessed: Jun. 22, 2022. [Online]. Available: https://www.theses.fr/2018COMP2411

[73] H. Wu, “Étude et analyse globale de l’efficacité énergétique d’un micro-réseau urbain à courant continu,” These de doctorat, Compiègne, 2017. Accessed: Mar. 11, 2022. [Online]. Available: https://www.theses.fr/2017COMP2386

[74] W. Bai, “DC Microgrid optimized energy management and real-time control of power systems for grid-connected and off-grid operating modes,” These de doctorat, Compiègne, 2021. Accessed: Mar. 14, 2022. [Online]. Available: https://www.theses.fr/2021COMP2586

[75] D. Wang, “Microgrid based on photovoltaic energy for charging electric vehicle stations : charging and discharging management strategies in communication with the smart grid,” These de doctorat, Compiègne, 2021. Accessed: Mar. 14, 2022. [Online]. Available: https://www.theses.fr/2021COMP2584

[76] Y. Krim, M. Sechilariu, and F. Locment, “PV Benefits Assessment for PV-Powered Charging Stations for Electric Vehicles,” *Applied Sciences*, vol. 11, no. 9, Art. no. 9, Jan. 2021, doi: 10.3390/app11094127.

[77] S. Cheikh-Mohamad, M. Sechilariu, F. Locment, and Y. Krim, “PV-Powered Electric Vehicle Charging Stations: Preliminary Requirements and Feasibility Conditions,” *Applied Sciences*, vol. 11, no. 4, Art. no. 4, Jan. 2021, doi: 10.3390/app11041770.

[78] D. Wang, M. Sechilariu, and F. Locment, “PV-Powered Charging Station for Electric Vehicles: Power Management with Integrated V2G,” *Applied Sciences*, vol. 10, no. 18, Art. no. 18, Jan. 2020, doi: 10.3390/app10186500.

[79] M. Sechilariu, F. Locment, and N. Darene, “Social Acceptance of Microgrids Dedicated to Electric Vehicle Charging Stations,” 2018, pp. 1374–1379. doi: 10.1109/ICRERA.2018.8566787.

[80] N. Liu *et al.*, “A Heuristic Operation Strategy for Commercial Building Microgrids Containing EVs and PV System,” *IEEE Transactions on Industrial Electronics*, vol. 62, no. 4, pp. 2560–2570, Apr. 2015, doi: 10.1109/TIE.2014.2364553.

[81] C. Liu, K. T. Chau, D. Wu, and S. Gao, “Opportunities and Challenges of Vehicle-to-Home, Vehicle-to-Vehicle, and Vehicle-to-Grid Technologies,” *Proceedings of the IEEE*, vol. 101, no. 11, pp. 2409–2427, Nov. 2013, doi: 10.1109/JPROC.2013.2271951.

[82] M. Nour, J. P. Chaves-Ávila, G. Magdy, and Á. Sánchez-Miralles, “Review of Positive and Negative Impacts of Electric Vehicles Charging on Electric Power Systems,” *Energies*, vol. 13, no. 18, Art. no. 18, Jan. 2020, doi: 10.3390/en13184675.

[83] C. Chen and S. Duan, “Microgrid economic operation considering plug-in hybrid electric vehicles integration,” *Journal of Modern Power Systems and Clean Energy*, vol. 3, no. 2, pp. 221–231, Jun. 2015, doi: 10.1007/s40565-015-0116-0.

[84] L. Zhang, T. Brown, and G. S. Samuelsen, “Fuel reduction and electricity consumption impact of different charging scenarios for plug-in hybrid electric vehicles,” *Journal of Power Sources*, vol. 196, no. 15, pp. 6559–6566, 2011, doi: https://doi.org/10.1016/j.jpowsour.2011.03.003.

[85] H. Li, X. Gong, W. Chen, and X. Zeng, “Optimal Scheduling of Electric Vehicles and Isolated Microgrid based on Differential Search Algorithm,” in *2018 13th World Congress on Intelligent Control and Automation (WCICA)*, Jul. 2018, pp. 1115–1119. doi: 10.1109/WCICA.2018.8630690.

[86] J.-M. Clairand, J. Rodríguez-García, and C. Álvarez-Bel, “Smart Charging for Electric Vehicle Aggregators Considering Users’ Preferences,” *IEEE Access*, vol. 6, pp. 54624–54635, 2018, doi: 10.1109/ACCESS.2018.2872725.

[87] T. Rawat and K. R. Niazi, “Comparison of EV smart charging strategies from multiple stakeholders’ perception,” *The Journal of Engineering*, vol. 2017, no. 13, pp. 1356–1361, 2017, doi: 10.1049/joe.2017.0553.

[88] K. N. Kumar, B. Sivaneasan, and P. L. So, “Impact of Priority Criteria on Electric Vehicle Charge Scheduling,” *IEEE Transactions on Transportation Electrification*, vol. 1, no. 3, pp. 200–210, Oct. 2015, doi: 10.1109/TTE.2015.2465293.

[89] U. Akram, M. Khalid, and S. Shafiq, “An Improved Optimal Sizing Methodology for Future Autonomous Residential Smart Power Systems,” *IEEE Access*, vol. 6, pp. 5986–6000, 2018, doi: 10.1109/ACCESS.2018.2792451.

[90] Tong Huang and Jie Wang, “Research on charging and discharging control strategy of electric vehicles and its economic benefit in microgrid,” in *2016 IEEE International Conference on Power and Renewable Energy (ICPRE)*, Oct. 2016, pp. 518–522. doi: 10.1109/ICPRE.2016.7871130.

[91] G. N. Prodromidis, D. E. Mytakis, and F. A. Coutelieris, “Natural Gas as a New Prospect in Everyday Use of Electric Vehicles,” *Applied Sciences*, vol. 10, no. 18, Art. no. 18, Jan. 2020, doi: 10.3390/app10186590.

[92] G. Talluri, F. Grasso, and D. Chiaramonti, “Is Deployment of Charging Station the Barrier to Electric Vehicle Fleet Development in EU Urban Areas? An Analytical Assessment Model for Large-Scale Municipality-Level EV Charging Infrastructures,” *Applied Sciences*, vol. 9, no. 21, Art. no. 21, Jan. 2019, doi: 10.3390/app9214704.

[93] H.-J. Lee, H.-J. Cha, and D. Won, “Economic Routing of Electric Vehicles using Dynamic Pricing in Consideration of System Voltage,” *Applied Sciences*, vol. 9, no. 20, Art. no. 20, Jan. 2019, doi: 10.3390/app9204337.

[94] B. Aluisio, S. Bruno, L. De Bellis, M. Dicorato, G. Forte, and M. Trovato, “DC-Microgrid Operation Planning for an Electric Vehicle Supply Infrastructure,” *Applied Sciences*, vol. 9, no. 13, Art. no. 13, Jan. 2019, doi: 10.3390/app9132687.

[95] H. Zang *et al.*, “Bi-Level Planning Model of Charging Stations Considering the Coupling Relationship between Charging Stations and Travel Route,” *Applied Sciences*, vol. 8, no. 7, Art. no. 7, Jul. 2018, doi: 10.3390/app8071130.

[96] S. M. Shariff, M. S. Alam, F. Ahmad, Y. Rafat, M. S. J. Asghar, and S. Khan, “System Design and Realization of a Solar-Powered Electric Vehicle Charging Station,” *IEEE*

Systems Journal, vol. 14, no. 2, pp. 2748–2758, Jun. 2020, doi: 10.1109/JSYST.2019.2931880.

[97] Z. Moghaddam, I. Ahmad, D. Habibi, and Q. V. Phung, "Smart Charging Strategy for Electric Vehicle Charging Stations," *IEEE Transactions on Transportation Electrification*, vol. 4, no. 1, pp. 76–88, Mar. 2018, doi: 10.1109/TTE.2017.2753403.

[98] K. Chaudhari, N. K. Kandasamy, A. Krishnan, A. Ukil, and H. B. Gooi, "Agent-Based Aggregated Behavior Modeling for Electric Vehicle Charging Load," *IEEE Transactions on Industrial Informatics*, vol. 15, no. 2, pp. 856–868, Feb. 2019, doi: 10.1109/TII.2018.2823321.

[99] W. Lee, L. Xiang, R. Schober, and V. W. S. Wong, "Electric Vehicle Charging Stations With Renewable Power Generators: A Game Theoretical Analysis," *IEEE Transactions on Smart Grid*, vol. 6, no. 2, pp. 608–617, Mar. 2015, doi: 10.1109/TSG.2014.2374592.

[100] B. Singh, A. Verma, A. Chandra, and K. Al-Haddad, "Implementation of Solar PV-Battery and Diesel Generator Based Electric Vehicle Charging Station," *IEEE Transactions on Industry Applications*, vol. 56, no. 4, pp. 4007–4016, Jul. 2020, doi: 10.1109/TIA.2020.2989680.

[101] D. Wang, F. Locment, and M. Sechilariu, "Modelling, Simulation, and Management Strategy of an Electric Vehicle Charging Station Based on a DC Microgrid," *Applied Sciences*, vol. 10, no. 6, Art. no. 6, Jan. 2020, doi: 10.3390/app10062053.

[102] A. Hassoune, M. Khafallah, A. Mesbahi, and T. Bouragba, "Power Management Strategies of Electric Vehicle Charging Station Based Grid Tied PV-Battery System," *International Journal of Renewable Energy Research*, vol. 8, Jun. 2018.

[103] K. Mahmud, M. J. Hossain, and J. Ravishankar, "Peak-Load Management in Commercial Systems With Electric Vehicles," *IEEE Systems Journal*, vol. 13, no. 2, pp. 1872–1882, Jun. 2019, doi: 10.1109/JSYST.2018.2850887.

[104] G. R. C. Mouli, P. Bauer, and M. Zeman, "System design for a solar powered electric vehicle charging station for workplaces," *Applied Energy*, vol. 168, pp. 434–443, 2016, doi: https://doi.org/10.1016/j.apenergy.2016.01.110.

[105] G. Liu, L. Kang, Z. Luan, J. Qiu, and F. Zheng, "Charging Station and Power Network Planning for Integrated Electric Vehicles (EVs)," *Energies*, vol. 12, no. 13, Art. no. 13, Jan. 2019, doi: 10.3390/en12132595.

[106]A. Hove and D. Sandalow, “ELECTRIC VEHICLE CHARGING IN CHINA AND THE UNITED STATES,” p. 88.

[107]F. Beach, D. Tuttle, and R. Duncan, *Electric Vehicle Charging Infrastructure: Publicly Funded Necessity or Commercially Funded Convenience? PRP 204*. LBJ School of Public Affairs, 2019. doi: 10.26153/tsw/2961.

[108]“Recharge EU: How many charge points will EU countries need by 2030 | Transport & Environment.” https://www.transportenvironment.org/publications/recharge-eu-how-many-charge-points-will-eu-countries-need-2030 (accessed Oct. 29, 2020).

[109]J. Zhang, J. Yan, Y. Liu, H. Zhang, and G. Lv, “Daily electric vehicle charging load profiles considering demographics of vehicle users,” *Applied Energy*, vol. 274, p. 115063, 2020, doi: https://doi.org/10.1016/j.apenergy.2020.115063.

[110]M. Sechilariu and F. Locment, “Chapter 4 - Direct Current Microgrid Power Modeling and Control,” in *Urban DC Microgrid*, M. Sechilariu and F. Locment, Eds. Butterworth-Heinemann, 2016, pp. 133–170. doi: 10.1016/B978-0-12-803736-2.00004-9.

[111]M. Sechilariu and F. Locment, “Chapter 2 - Photovoltaic Source Modeling and Control,” in *Urban DC Microgrid*, M. Sechilariu and F. Locment, Eds. Butterworth-Heinemann, 2016, pp. 35–91. doi: 10.1016/B978-0-12-803736-2.00002-5.

[112]M. Sechilariu and F. Locment, “Backup Power Resources for Microgrid,” in *Urban DC Microgrid: Intelligent Control and Power Flow Optimization*, Elsevier, 2016, pp. 93–132. [Online]. Available: https://hal.archives-ouvertes.fr/hal-01955254

[113]“Industrial Parking Solar Panel Structure,” *indiamart.com*. https://www.indiamart.com/proddetail/industrial-parking-solar-panel-structure-19639127591.html (accessed Oct. 28, 2020).

[114]S. Cheikh-Mohamad, M. Sechilariu, and F. Locment, “Real-Time Power Management Including an Optimization Problem for PV-Powered Electric Vehicle Charging Stations,” *Applied Sciences*, vol. 12, no. 9, Art. no. 9, Jan. 2022, doi: 10.3390/app12094323.

[115]K. Chaudhari, A. Ukil, K. N. Kumar, U. Manandhar, and S. K. Kollimalla, “Hybrid Optimization for Economic Deployment of ESS in PV-Integrated EV Charging Stations,” *IEEE Transactions on Industrial Informatics*, vol. 14, no. 1, pp. 106–116, Jan. 2018, doi: 10.1109/TII.2017.2713481.

[116]H. Suyono, M. T. Rahman, H. Mokhlis, M. Othman, H. A. Illias, and H. Mohamad, "Optimal Scheduling of Plug-in Electric Vehicle Charging Including Time-of-Use Tariff to Minimize Cost and System Stress," *Energies*, vol. 12, no. 8, Art. no. 8, Jan. 2019, doi: 10.3390/en12081500.

[117]R. Deepak Mistry, F. T. Eluyemi, and T. M. Masaud, "Impact of aggregated EVs charging station on the optimal scheduling of battery storage system in islanded microgrid," in *2017 North American Power Symposium (NAPS)*, Sep. 2017, pp. 1–5. doi: 10.1109/NAPS.2017.8107335.

[118]N. Davis, B. Johnson, T. McJunkin, D. Scoffield, and S. White, "Dispatch control with PEV charging and renewables for multiplayer game application," in *2016 IEEE Conference on Technologies for Sustainability (SusTech)*, Oct. 2016, pp. 156–161. doi: 10.1109/SusTech.2016.7897159.

[119]N. Liu *et al.*, "A Heuristic Operation Strategy for Commercial Building Microgrids Containing EVs and PV System," *IEEE Transactions on Industrial Electronics*, vol. 62, no. 4, pp. 2560–2570, Apr. 2015, doi: 10.1109/TIE.2014.2364553.

[120]A. Petrusic and A. Janjic, "Renewable Energy Tracking and Optimization in a Hybrid Electric Vehicle Charging Station," *Applied Sciences*, vol. 11, no. 1, Art. no. 1, Jan. 2021, doi: 10.3390/app11010245.

[121]J. Faraji, A. Abazari, M. Babaei, S. M. Muyeen, and M. Benbouzid, "Day-Ahead Optimization of Prosumer Considering Battery Depreciation and Weather Prediction for Renewable Energy Sources," *Applied Sciences*, vol. 10, no. 8, Art. no. 8, Jan. 2020, doi: 10.3390/app10082774.

[122]P. Bucić, V. Lešić, and M. Vašak, "Distributed Optimal Batteries Charging Control for Heterogenous Electric Vehicles Fleet," in *2018 26th Mediterranean Conference on Control and Automation (MED)*, Jun. 2018, pp. 837–842. doi: 10.1109/MED.2018.8442784.

[123]T. Xu, H. Sun, B. Zhu, Y. Long, H. Wang, and Z. Li, "Economic Optimization Control of Microgrid with Electric Vehicles," in *2018 5th International Conference on Information Science and Control Engineering (ICISCE)*, Jul. 2018, pp. 733–736. doi: 10.1109/ICISCE.2018.00157.

[124]F. D. Moya, J. L. Torres-Moreno, and J. D. Álvarez, "Optimal Model for Energy Management Strategy in Smart Building with Energy Storage Systems and Electric Vehicles," *Energies*, vol. 13, no. 14, Art. no. 14, Jan. 2020, doi: 10.3390/en13143605.

[125]R. Shi, P. Zhang, J. Zhang, L. Niu, and X. Han, “Multidispatch for Microgrid including Renewable Energy and Electric Vehicles with Robust Optimization Algorithm,” *Energies*, vol. 13, no. 11, Art. no. 11, Jan. 2020, doi: 10.3390/en13112813.

[126]R. Ghotge, Y. Snow, S. Farahani, Z. Lukszo, and A. van Wijk, “Optimized Scheduling of EV Charging in Solar Parking Lots for Local Peak Reduction under EV Demand Uncertainty,” *Energies*, vol. 13, no. 5, Art. no. 5, Jan. 2020, doi: 10.3390/en13051275.

[127]H. E. Oliveira Farias *et al.*, “Combined Framework with Heuristic Programming and Rule-Based Strategies for Scheduling and Real Time Operation in Electric Vehicle Charging Stations,” *Energies*, vol. 14, no. 5, Art. no. 5, Jan. 2021, doi: 10.3390/en14051370.

[128]H. Nafisi, S. M. M. Agah, H. Askarian Abyaneh, and M. Abedi, “Two-Stage Optimization Method for Energy Loss Minimization in Microgrid Based on Smart Power Management Scheme of PHEVs,” *IEEE Transactions on Smart Grid*, vol. 7, no. 3, pp. 1268–1276, May 2016, doi: 10.1109/TSG.2015.2480999.

[129]D. Yan and C. Ma, “Stochastic planning of electric vehicle charging station integrated with photovoltaic and battery systems,” *Transmission Distribution IET Generation*, vol. 14, no. 19, pp. 4217–4224, 2020, doi: 10.1049/iet-gtd.2019.1737.

[130]H. Jiang, S. Ning, and Q. Ge, “Multi-Objective Optimal Dispatching of Microgrid With Large-Scale Electric Vehicles,” *IEEE Access*, vol. 7, pp. 145880–145888, 2019, doi: 10.1109/ACCESS.2019.2945597.

[131]Q. Dai, J. Liu, and Q. Wei, “Optimal Photovoltaic/Battery Energy Storage/Electric Vehicle Charging Station Design Based on Multi-Agent Particle Swarm Optimization Algorithm,” *Sustainability*, vol. 11, no. 7, Art. no. 7, Jan. 2019, doi: 10.3390/su11071973.

[132]T. Lan, K. Jermsittiparsert, S. T. Alrashood, M. Rezaei, L. Al-Ghussain, and M. A. Mohamed, “An Advanced Machine Learning Based Energy Management of Renewable Microgrids Considering Hybrid Electric Vehicles’ Charging Demand,” *Energies*, vol. 14, no. 3, Art. no. 3, Jan. 2021, doi: 10.3390/en14030569.

[133]P. V. Minh, S. Le Quang, and M.-H. Pham, “Technical Economic Analysis of Photovoltaic-Powered Electric Vehicle Charging Stations under Different Solar Irradiation Conditions in Vietnam,” *Sustainability*, vol. 13, no. 6, Art. no. 6, Jan. 2021, doi: 10.3390/su13063528.

[134]M. K. Rafique *et al.*, “An Intelligent Hybrid Energy Management System for a Smart House Considering Bidirectional Power Flow and Various EV Charging Techniques,” *Applied Sciences*, vol. 9, no. 8, Art. no. 8, Jan. 2019, doi: 10.3390/app9081658.

[135]B. Zeng, H. Dong, R. Sioshansi, F. Xu, and M. Zeng, “Bilevel Robust Optimization of Electric Vehicle Charging Stations With Distributed Energy Resources,” *IEEE Transactions on Industry Applications*, vol. 56, no. 5, pp. 5836–5847, Sep. 2020, doi: 10.1109/TIA.2020.2984741.

[136]H. Wu, G. K. H. Pang, K. L. Choy, and H. Y. Lam, “An Optimization Model for Electric Vehicle Battery Charging at a Battery Swapping Station,” *IEEE Transactions on Vehicular Technology*, vol. 67, no. 2, pp. 881–895, Feb. 2018, doi: 10.1109/TVT.2017.2758404.

[137]C.-H. Chung, S. Jangra, Q. Lai, and X. Lin, “Optimization of Electric Vehicle Charging for Battery Maintenance and Degradation Management,” *IEEE Transactions on Transportation Electrification*, vol. 6, no. 3, pp. 958–969, Sep. 2020, doi: 10.1109/TTE.2020.3000181.

[138]M. Hosseinzadeh and F. R. Salmasi, “Robust Optimal Power Management System for a Hybrid AC/DC Micro-Grid,” *IEEE Transactions on Sustainable Energy*, vol. 6, no. 3, pp. 675–687, Jul. 2015, doi: 10.1109/TSTE.2015.2405935.

[139]M. B. Sigalo, A. C. Pillai, S. Das, and M. Abusara, “An Energy Management System for the Control of Battery Storage in a Grid-Connected Microgrid Using Mixed Integer Linear Programming,” *Energies*, vol. 14, no. 19, Art. no. 19, Jan. 2021, doi: 10.3390/en14196212.

[140]A. Moser *et al.*, “A MILP-based modular energy management system for urban multi-energy systems: Performance and sensitivity analysis,” *Applied Energy*, vol. 261, p. 114342, Mar. 2020, doi: 10.1016/j.apenergy.2019.114342.

[141]A. A. Abou El-Ela, R. A. El-Sehiemy, S. M. Allam, A. M. Shaheen, N. A. Nagem, and A. M. Sharaf, “Renewable Energy Micro-Grid Interfacing: Economic and Environmental Issues,” *Electronics*, vol. 11, no. 5, Art. no. 5, Jan. 2022, doi: 10.3390/electronics11050815.

[142]A. A. A. El-Ela, R. A. El-Seheimy, A. M. Shaheen, W. A. Wahbi, and M. T. Mouwafi, “PV and battery energy storage integration in distribution networks using equilibrium algorithm,” *Journal of Energy Storage*, vol. 42, p. 103041, Oct. 2021, doi: 10.1016/j.est.2021.103041.

[143]A. M. Shaheen, M. A. Hamida, R. A. El-Sehiemy, and E. E. Elattar, “Optimal parameter identification of linear and non-linear models for Li-Ion Battery Cells,” *Energy Reports*, vol. 7, pp. 7170–7185, Nov. 2021, doi: 10.1016/j.egyr.2021.10.086.

[144]M. A. Hamida, R. A. El-Sehiemy, A. R. Ginidi, E. Elattar, and A. M. Shaheen, “Parameter identification and state of charge estimation of Li-Ion batteries used in electric vehicles using artificial hummingbird optimizer,” *Journal of Energy Storage*, vol. 51, p. 104535, Jul. 2022, doi: 10.1016/j.est.2022.104535.

[145]M. Sechilariu and F. Locment, “Photovoltaic Source Modeling and Control,” in *Urban DC Microgrid*, Elsevier, 2016, pp. 35–91. doi: 10.1016/B978-0-12-803736-2.00002-5.

[146]M. Sechilariu and F. Locment, “Backup Power Resources for Microgrid,” in *Urban DC Microgrid*, Elsevier, 2016, pp. 93–132. doi: 10.1016/B978-0-12-803736-2.00003-7.

[147]S. Cheikh-Mohamad, M. Sechilariu, and F. Locment, “PV-Powered Charging Station: Energy Management and Cost Optimization,” in *2021 IEEE 30th International Symposium on Industrial Electronics (ISIE)*, Jun. 2021, pp. 1–6. doi: 10.1109/ISIE45552.2021.9576324.

[148]M. Sechilariu, N. Molines, G. Richard, H. Martell-Flores, F. Locment, and J. Baert, “Electromobility framework study: infrastructure and urban planning for EV charging station empowered by PV-based microgrid,” *IET Electrical Systems in Transportation*, vol. 9, no. 4, pp. 176–185, 2019, doi: 10.1049/iet-est.2019.0032.

[149]M. Sechilariu and F. Locment, “Direct Current Microgrid Power Modeling and Control,” in *Urban DC Microgrid*, Elsevier, 2016, pp. 133–170. doi: 10.1016/B978-0-12-803736-2.00004-9.

[150]M. Sechilariu and F. Locment, “Experimental Evaluation of Urban Direct Current Microgrid,” in *Urban DC Microgrid*, Elsevier, 2016, pp. 209–250. doi: 10.1016/B978-0-12-803736-2.00006-2.

[151]C. E. Montaño-Salcedo, M. Sechilariu, and F. Locment, “Human-System Interfaces for PV-Powered Electric Vehicles Charging Station,” in *2021 IEEE 30th International Symposium on Industrial Electronics (ISIE)*, Jun. 2021, pp. 1–6. doi: 10.1109/ISIE45552.2021.9576251.

[152]F. Marra, G. Y. Yang, C. Træholt, E. Larsen, C. N. Rasmussen, and S. You, “Demand profile study of battery electric vehicle under different charging options,” in *2012 IEEE Power and Energy Society General Meeting*, Jul. 2012, pp. 1–7. doi: 10.1109/PESGM.2012.6345063.

[153]Y. Riffonneau, “GESTION DES FLUX ÉNERGÉTIQUE DANS UN SYSTÈME PHOTOVOLTAÏQUE AVEC STOCKAGE CONNECTER AU RÉSEAU – Application à

l'habitat," phdthesis, Université Joseph-Fourier - Grenoble I, 2009. Accessed: Jun. 24, 2022. [Online]. Available: https://tel.archives-ouvertes.fr/tel-00458260

[154]"ILOG CPLEX Optimization Studio - Overview," Oct. 07, 2021. https://www.ibm.com/products/ilog-cplex-optimization-studio (accessed Mar. 16, 2022).

[155]S. Cheikh-Mohamad, M. Sechilariu, and F. Locment, "PV-Powered Charging Station: Energy Management with V2G Operation and Energy Cost Analysis," p. 6.

[156]Y. Yoo, Y. Al-Shawesh, and A. Tchagang, "Coordinated Control Strategy and Validation of Vehicle-to-Grid for Frequency Control," *Energies*, vol. 14, no. 9, Art. no. 9, Jan. 2021, doi: 10.3390/en14092530.

[157]M. Latifi, R. Sabzehgar, P. Fajri, and M. Rasouli, "A Novel Control Strategy for the Frequency and Voltage Regulation of Distribution Grids Using Electric Vehicle Batteries," *Energies*, vol. 14, no. 5, Art. no. 5, Jan. 2021, doi: 10.3390/en14051435.

[158]Y. Ota, H. Taniguchi, T. Nakajima, K. M. Liyanage, J. Baba, and A. Yokoyama, "Autonomous Distributed V2G (Vehicle-to-Grid) Satisfying Scheduled Charging," *IEEE Transactions on Smart Grid*, vol. 3, no. 1, pp. 559–564, Mar. 2012, doi: 10.1109/TSG.2011.2167993.

[159]S. Han, S. Han, and K. Sezaki, "Development of an Optimal Vehicle-to-Grid Aggregator for Frequency Regulation," *IEEE Transactions on Smart Grid*, vol. 1, no. 1, pp. 65–72, Jun. 2010, doi: 10.1109/TSG.2010.2045163.

[160]L. Noel, G. Zarazua de Rubens, J. Kester, and B. K. Sovacool, *Vehicle-to-Grid: A Sociotechnical Transition Beyond Electric Mobility*. Cham: Springer International Publishing, 2019. doi: 10.1007/978-3-030-04864-8.

[161]G. Saldaña, J. I. San Martin, I. Zamora, F. J. Asensio, and O. Oñederra, "Electric Vehicle into the Grid: Charging Methodologies Aimed at Providing Ancillary Services Considering Battery Degradation," *Energies*, vol. 12, no. 12, Art. no. 12, Jan. 2019, doi: 10.3390/en12122443.

[162]S. Habib, M. Kamran, and U. Rashid, "Impact analysis of vehicle-to-grid technology and charging strategies of electric vehicles on distribution networks – A review," *Journal of Power Sources*, vol. 277, pp. 205–214, Mar. 2015, doi: 10.1016/j.jpowsour.2014.12.020.

[163]A. W. Thompson, “Economic implications of lithium ion battery degradation for Vehicle-to-Grid (V2X) services,” *Journal of Power Sources*, vol. 396, pp. 691–709, Aug. 2018, doi: 10.1016/j.jpowsour.2018.06.053.

[164]S. S. Ravi and M. Aziz, “Utilization of Electric Vehicles for Vehicle-to-Grid Services: Progress and Perspectives,” *Energies*, vol. 15, no. 2, Art. no. 2, Jan. 2022, doi: 10.3390/en15020589.

[165]S. Habib, M. M. Khan, F. Abbas, L. Sang, M. U. Shahid, and H. Tang, “A Comprehensive Study of Implemented International Standards, Technical Challenges, Impacts and Prospects for Electric Vehicles,” *IEEE Access*, vol. 6, pp. 13866–13890, 2018, doi: 10.1109/ACCESS.2018.2812303.

[166]“How does V2G, or vehicle-to-grid, work? - Renault Group.” https://www.renaultgroup.com/en/news-on-air/news/whats-the-deal-with-v2g-or-vehicle-to-grid/ (accessed Jan. 18, 2022).

[167]S. Qi *et al.*, “Research on Charging-Discharging Operation Strategy for Electric Vehicles Based on Different Trip Patterns for Various City Types in China,” *World Electric Vehicle Journal*, vol. 13, no. 1, Art. no. 1, Jan. 2022, doi: 10.3390/wevj13010007.

[168]D. Huber, Q. De Clerck, C. De Cauwer, N. Sapountzoglou, T. Coosemans, and M. Messagie, “Vehicle to Grid Impacts on the Total Cost of Ownership for Electric Vehicle Drivers,” *World Electric Vehicle Journal*, vol. 12, no. 4, Art. no. 4, Dec. 2021, doi: 10.3390/wevj12040236.

[169]B. Zeng, Y. Luo, C. Zhang, and Y. Liu, “Assessing the Impact of an EV Battery Swapping Station on the Reliability of Distribution Systems,” *Applied Sciences*, vol. 10, no. 22, Art. no. 22, Jan. 2020, doi: 10.3390/app10228023.

[170]R. Shipman, J. Waldron, S. Naylor, J. Pinchin, L. Rodrigues, and M. Gillott, “Where Will You Park? Predicting Vehicle Locations for Vehicle-to-Grid,” *Energies*, vol. 13, no. 8, Art. no. 8, Jan. 2020, doi: 10.3390/en13081933.

[171]H.-S. Han, E. Oh, and S.-Y. Son, “Study on EV Charging Peak Reduction with V2G Utilizing Idle Charging Stations: The Jeju Island Case,” *Energies*, vol. 11, no. 7, Art. no. 7, Jul. 2018, doi: 10.3390/en11071651.

[172]L. Liu, F. Xie, Z. Huang, and M. Wang, “Multi-Objective Coordinated Optimal Allocation of DG and EVCSs Based on the V2G Mode,” *Processes*, vol. 9, no. 1, Art. no. 1, Jan. 2021, doi: 10.3390/pr9010018.

[173]L. Di Natale *et al.*, "The Potential of Vehicle-to-Grid to Support the Energy Transition: A Case Study on Switzerland," *Energies*, vol. 14, no. 16, Art. no. 16, Jan. 2021, doi: 10.3390/en14164812.

[174]V. Kumar, V. R. Teja, M. Singh, and S. Mishra, "PV Based Off-Grid Charging Station for Electric Vehicle," *IFAC-PapersOnLine*, vol. 52, no. 4, pp. 276–281, Jan. 2019, doi: 10.1016/j.ifacol.2019.08.211.

[175]L. Luo, Z. Wu, W. Gu, H. Huang, S. Gao, and J. Han, "Coordinated allocation of distributed generation resources and electric vehicle charging stations in distribution systems with vehicle-to-grid interaction," *Energy*, vol. 192, p. 116631, Feb. 2020, doi: 10.1016/j.energy.2019.116631.

[176]H. Mehrjerdi and E. Rakhshani, "Vehicle-to-grid technology for cost reduction and uncertainty management integrated with solar power," *Journal of Cleaner Production*, vol. 229, pp. 463–469, Aug. 2019, doi: 10.1016/j.jclepro.2019.05.023.

[177]S.-A. Amamra and J. Marco, "Vehicle-to-Grid Aggregator to Support Power Grid and Reduce Electric Vehicle Charging Cost," *IEEE Access*, vol. 7, pp. 178528–178538, 2019, doi: 10.1109/ACCESS.2019.2958664.

[178]A. AbuElrub, F. Hamed, and O. Saadeh, "Microgrid integrated electric vehicle charging algorithm with photovoltaic generation," *Journal of Energy Storage*, vol. 32, p. 101858, Dec. 2020, doi: 10.1016/j.est.2020.101858.

[179]T. Steffen, A. Fly, and W. Mitchell, "Optimal Electric Vehicle Charging Considering the Effects of a Financial Incentive on Battery Ageing," *Energies*, vol. 13, no. 18, Art. no. 18, Jan. 2020, doi: 10.3390/en13184742.

[180]Y. Jang *et al.*, "Grid-Connected Inverter for a PV-Powered Electric Vehicle Charging Station to Enhance the Stability of a Microgrid," *Sustainability*, vol. 13, no. 24, Art. no. 24, Jan. 2021, doi: 10.3390/su132414022.

[181]Y. Wang and D. Gladwin, "Power Management Analysis of a Photovoltaic and Battery Energy Storage-Based Smart Electrical Car Park Providing Ancillary Grid Services," *Energies*, vol. 14, no. 24, Art. no. 24, Jan. 2021, doi: 10.3390/en14248433.

[182]U. Abronzini, C. Attaianese, M. D'Arpino, M. Di Monaco, and G. Tomasso, "Cost Minimization Energy Control Including Battery Aging for Multi-Source EV Charging Station," *Electronics*, vol. 8, no. 1, Art. no. 1, Jan. 2019, doi: 10.3390/electronics8010031.

[183] A. Ul-Haq, C. Cecati, and E. A. Al-Ammar, “Modeling of a Photovoltaic-Powered Electric Vehicle Charging Station with Vehicle-to-Grid Implementation,” *Energies*, vol. 10, no. 1, Art. no. 1, Jan. 2017, doi: 10.3390/en10010004.

[184] S. Mumtaz, S. Ali, S. Ahmad, L. Khan, S. Z. Hassan, and T. Kamal, “Energy Management and Control of Plug-In Hybrid Electric Vehicle Charging Stations in a Grid-Connected Hybrid Power System,” *Energies*, vol. 10, no. 11, Art. no. 11, Nov. 2017, doi: 10.3390/en10111923.

[185] R. Kataoka, K. Ogimoto, and Y. Iwafune, “Marginal Value of Vehicle-to-Grid Ancillary Service in a Power System with Variable Renewable Energy Penetration and Grid Side Flexibility,” *Energies*, vol. 14, no. 22, Art. no. 22, Jan. 2021, doi: 10.3390/en14227577.

[186] S. Iqbal *et al.*, “V2G Strategy for Primary Frequency Control of an Industrial Microgrid Considering the Charging Station Operator,” *Electronics*, vol. 9, no. 4, Art. no. 4, Apr. 2020, doi: 10.3390/electronics9040549.

[187] N. Neofytou, K. Blazakis, Y. Katsigiannis, and G. Stavrakakis, “Modeling Vehicles to Grid as a Source of Distributed Frequency Regulation in Isolated Grids with Significant RES Penetration,” *Energies*, vol. 12, no. 4, Art. no. 4, Jan. 2019, doi: 10.3390/en12040720.

[188] I. Ilieva and B. Bremdal, “Utilizing Local Flexibility Resources to Mitigate Grid Challenges at Electric Vehicle Charging Stations,” *Energies*, vol. 14, no. 12, Art. no. 12, Jan. 2021, doi: 10.3390/en14123506.

[189] M. Sufyan, N. A. Rahim, M. A. Muhammad, C. K. Tan, S. R. S. Raihan, and A. H. A. Bakar, “Charge coordination and battery lifecycle analysis of electric vehicles with V2G implementation,” *Electric Power Systems Research*, vol. 184, p. 106307, Jul. 2020, doi: 10.1016/j.epsr.2020.106307.

[190] R. Shi, S. Li, P. Zhang, and K. Y. Lee, “Integration of renewable energy sources and electric vehicles in V2G network with adjustable robust optimization,” *Renewable Energy*, vol. 153, pp. 1067–1080, Jun. 2020, doi: 10.1016/j.renene.2020.02.027.

[191] M. Di Somma, L. Ciabattoni, G. Comodi, and G. Graditi, “Managing plug-in electric vehicles in eco-environmental operation optimization of local multi-energy systems,” *Sustainable Energy, Grids and Networks*, vol. 23, p. 100376, Sep. 2020, doi: 10.1016/j.segan.2020.100376.

[192] V. C. Onishi, C. H. Antunes, and J. P. F. Trovão, “Optimal Energy and Reserve Market Management in Renewable Microgrid-PEVs Parking Lot Systems: V2G, Demand

Response and Sustainability Costs," *Energies*, vol. 13, no. 8, Art. no. 8, Jan. 2020, doi: 10.3390/en13081884.

[193]B. Aluisio, A. Conserva, M. Dicorato, G. Forte, and M. Trovato, "Optimal operation planning of V2G-equipped Microgrid in the presence of EV aggregator," *Electric Power Systems Research*, vol. 152, pp. 295–305, Nov. 2017, doi: 10.1016/j.epsr.2017.07.015.

[194]A. Modarresi Ghazvini and J. Olamaei, "Optimal sizing of autonomous hybrid PV system with considerations for V2G parking lot as controllable load based on a heuristic optimization algorithm," *Solar Energy*, vol. 184, pp. 30–39, May 2019, doi: 10.1016/j.solener.2019.03.087.

[195]T. Zhou and W. Sun, "Research on multi-objective optimisation coordination for large-scale V2G," *IET Renewable Power Generation*, vol. 14, no. 3, pp. 445–453, 2020, doi: 10.1049/iet-rpg.2019.0173.

[196]W. Vermeer, G. R. Chandra Mouli, and P. Bauer, "Real-Time Building Smart Charging System Based on PV Forecast and Li-Ion Battery Degradation," *Energies*, vol. 13, no. 13, Art. no. 13, Jan. 2020, doi: 10.3390/en13133415.

[197]H. Al Attar, M. A. Hamida, M. Ghanes, and M. Taleb, "LLC DC-DC Converter Performances Improvement for Bidirectional Electric Vehicle Charger Application," *World Electric Vehicle Journal*, vol. 13, no. 1, Art. no. 1, Jan. 2022, doi: 10.3390/wevj13010002.

[198]F. Zhang *et al.*, "A New On-board Charging-Driving Integrated Topology for V2G Technology," *World Electric Vehicle Journal*, vol. 12, no. 4, Art. no. 4, Dec. 2021, doi: 10.3390/wevj12040231.

[199]V. Monteiro, P. Lima, T. J. C. Sousa, J. S. Martins, and J. L. Afonso, "An Off-Board Multi-Functional Electric Vehicle Charging Station for Smart Homes: Analysis and Experimental Validation," *Energies*, vol. 13, no. 8, Art. no. 8, Jan. 2020, doi: 10.3390/en13081864.

[200]J.-T. Liao, H.-W. Huang, H.-T. Yang, and D. Li, "Decentralized V2G/G2V Scheduling of EV Charging Stations by Considering the Conversion Efficiency of Bidirectional Chargers," *Energies*, vol. 14, no. 4, Art. no. 4, Jan. 2021, doi: 10.3390/en14040962.

[201]C. Balasundar, C. K. Sundarabalan, J. Sharma, N. S. Srinath, and J. M. Guerrero, "Design of power quality enhanced sustainable bidirectional electric vehicle charging station in distribution grid," *Sustainable Cities and Society*, vol. 74, p. 103242, Nov. 2021, doi: 10.1016/j.scs.2021.103242.

[202] A. Mohammad *et al.*, “Integration of Electric Vehicles and Energy Storage System in Home Energy Management System with Home to Grid Capability,” *Energies*, vol. 14, no. 24, Art. no. 24, Jan. 2021, doi: 10.3390/en14248557.

[203] V. T. Tran, Md. R. Islam, K. M. Muttaqi, and D. Sutanto, “An Efficient Energy Management Approach for a Solar-Powered EV Battery Charging Facility to Support Distribution Grids,” *IEEE Transactions on Industry Applications*, vol. 55, no. 6, pp. 6517–6526, Nov. 2019, doi: 10.1109/TIA.2019.2940923.

[204] A. Arias-Londoño, O. D. Montoya, and L. F. Grisales-Noreña, “A Chronological Literature Review of Electric Vehicle Interactions with Power Distribution Systems,” *Energies*, vol. 13, no. 11, Art. no. 11, Jan. 2020, doi: 10.3390/en13113016.

[205] O. Ouramdane, E. Elbouchikhi, Y. Amirat, and E. Sedgh Gooya, “Optimal Sizing and Energy Management of Microgrids with Vehicle-to-Grid Technology: A Critical Review and Future Trends,” *Energies*, vol. 14, no. 14, Art. no. 14, Jan. 2021, doi: 10.3390/en14144166.

[206] S. Cheikh-Mohamad, M. Sechilariu, and F. Locment, “Carbon Impact Methodology for PV-powered Infrastructure for Recharging Electric Vehicles,” p. 6.

[207] Y. Krim, M. Sechilariu, F. Locment, and A. Alchami, “Global Cost and Carbon Impact Assessment Methodology for Electric Vehicles’ PV-Powered Charging Station,” *Applied Sciences*, vol. 12, no. 9, Art. no. 9, Jan. 2022, doi: 10.3390/app12094115.

[208] “Greenhouse Gas Protocol |.” https://ghgprotocol.org/ (accessed May 03, 2022).

[209] “ADEME - Site Bilans GES.” https://bilans-ges.ademe.fr/ (accessed May 03, 2022).

[210] “EcoInvent – Switzerland,” *ecoinvent*. https://ecoinvent.org/ (accessed May 03, 2022).

[211] “European Commission Service Site.” https://eplca.jrc.ec.europa.eu/ (accessed May 03, 2022).

[212] “ISO - Standards,” *ISO*. https://www.iso.org/standards.html (accessed May 03, 2022).

[213] N. Chowdhury, C. A. Hossain, M. Longo, and W. Yaïci, “Optimization of Solar Energy System for the Electric Vehicle at University Campus in Dhaka, Bangladesh,” *Energies*, vol. 11, no. 9, Art. no. 9, Sep. 2018, doi: 10.3390/en11092433.

[214] E. Y. C. Wong, D. C. K. Ho, S. So, C.-W. Tsang, and E. M. H. Chan, “Life Cycle Assessment of Electric Vehicles and Hydrogen Fuel Cell Vehicles Using the GREET

Model—A Comparative Study," *Sustainability*, vol. 13, no. 9, Art. no. 9, Jan. 2021, doi: 10.3390/su13094872.

[215]Z. Wu, C. Wang, P. Wolfram, Y. Zhang, X. Sun, and E. Hertwich, "Assessing electric vehicle policy with region-specific carbon footprints," *Applied Energy*, vol. 256, p. 113923, Dec. 2019, doi: 10.1016/j.apenergy.2019.113923.

[216]R. J. Javid, M. Salari, and R. Jahanbakhsh Javid, "Environmental and economic impacts of expanding electric vehicle public charging infrastructure in California′s counties," *Transportation Research Part D: Transport and Environment*, vol. 77, pp. 320–334, Dec. 2019, doi: 10.1016/j.trd.2019.10.017.

[217]Z. Zhang, X. Sun, N. Ding, and J. Yang, "Life cycle environmental assessment of charging infrastructure for electric vehicles in China," *Journal of Cleaner Production*, vol. 227, pp. 932–941, Aug. 2019, doi: 10.1016/j.jclepro.2019.04.167.

[218]T. Aljohani and G. Alzahrani, "Life Cycle Assessment to Study the Impact of the Regional Grid Mix and Temperature Differences on the GHG Emissions of Battery Electric and Conventional Vehicles," in *2019 SoutheastCon*, Apr. 2019, pp. 1–9. doi: 10.1109/SoutheastCon42311.2019.9020666.

[219]G. Mills and I. F. MacGill, "Assessing the generation capacity, energy, and GHG emission reduction value of public electric vehicle recharging infrastructure in the Australian National Electricity Market," in *2014 IEEE International Electric Vehicle Conference (IEVC)*, Dec. 2014, pp. 1–7. doi: 10.1109/IEVC.2014.7056093.

[220]M.-A. M. Tamayao, J. J. Michalek, C. Hendrickson, and I. M. L. Azevedo, "Regional Variability and Uncertainty of Electric Vehicle Life Cycle CO_2 Emissions across the United States," *Environ. Sci. Technol.*, vol. 49, no. 14, pp. 8844–8855, Jul. 2015, doi: 10.1021/acs.est.5b00815.

[221]I. T. Vadium, R. Das, Y. Wang, G. Putrus, and R. Kotter, "Electric vehicle Carbon footprint reduction via intelligent charging strategies," in *2019 8th International Conference on Modern Power Systems (MPS)*, May 2019, pp. 1–6. doi: 10.1109/MPS.2019.8759783.

[222]N. C. Onat, M. Kucukvar, and O. Tatari, "Conventional, hybrid, plug-in hybrid or electric vehicles? State-based comparative carbon and energy footprint analysis in the United States," *Applied Energy*, vol. 150, pp. 36–49, 2015, doi: https://doi.org/10.1016/j.apenergy.2015.04.001.

[223]O. Kanz, A. Reinders, J. May, and K. Ding, “Environmental Impacts of Integrated Photovoltaic Modules in Light Utility Electric Vehicles,” *Energies*, vol. 13, no. 19, Art. no. 19, Jan. 2020, doi: 10.3390/en13195120.

[224]Ł. Sobol and A. Dyjakon, “The Influence of Power Sources for Charging the Batteries of Electric Cars on CO2 Emissions during Daily Driving: A Case Study from Poland,” *Energies*, vol. 13, no. 16, Art. no. 16, Jan. 2020, doi: 10.3390/en13164267.

[225]A. Lajunen, K. Kivekäs, J. Vepsäläinen, and K. Tammi, “Influence of Increasing Electrification of Passenger Vehicle Fleet on Carbon Dioxide Emissions in Finland,” *Sustainability*, vol. 12, no. 12, Art. no. 12, Jan. 2020, doi: 10.3390/su12125032.

[226]Y. Li, N. Ha, and T. Li, “Research on Carbon Emissions of Electric Vehicles throughout the Life Cycle Assessment Taking into Vehicle Weight and Grid Mix Composition,” *Energies*, vol. 12, no. 19, Art. no. 19, Jan. 2019, doi: 10.3390/en12193612.

[227]A. Burnham, Z. Lu, M. Wang, and A. Elgowainy, “Regional Emissions Analysis of Light-Duty Battery Electric Vehicles,” *Atmosphere*, vol. 12, no. 11, Art. no. 11, Nov. 2021, doi: 10.3390/atmos12111482.

[228]K. Petrauskienė, A. Galinis, D. Kliaugaitė, and J. Dvarionienė, “Comparative Environmental Life Cycle and Cost Assessment of Electric, Hybrid, and Conventional Vehicles in Lithuania,” *Sustainability*, vol. 13, no. 2, Art. no. 2, Jan. 2021, doi: 10.3390/su13020957.

[229]T. Peng, X. Ou, and X. Yan, “Development and application of an electric vehicles life-cycle energy consumption and greenhouse gas emissions analysis model,” *Chemical Engineering Research and Design*, vol. 131, pp. 699–708, Mar. 2018, doi: 10.1016/j.cherd.2017.12.018.

[230]Q. Qiao *et al.*, “Life cycle cost and GHG emission benefits of electric vehicles in China,” *Transportation Research Part D: Transport and Environment*, vol. 86, p. 102418, Sep. 2020, doi: 10.1016/j.trd.2020.102418.

[231]M. Kannangara, F. Bensebaa, and M. Vasudev, “An adaptable life cycle greenhouse gas emissions assessment framework for electric, hybrid, fuel cell and conventional vehicles: Effect of electricity mix, mileage, battery capacity and battery chemistry in the context of Canada,” *Journal of Cleaner Production*, vol. 317, p. 128394, Oct. 2021, doi: 10.1016/j.jclepro.2021.128394.

[232] Y. Tang, T. T. Cockerill, A. J. Pimm, and X. Yuan, “Reducing the life cycle environmental impact of electric vehicles through emissions-responsive charging,” *iScience*, vol. 24, no. 12, p. 103499, Dec. 2021, doi: 10.1016/j.isci.2021.103499.

[233] E. Zhao, E. May, P. D. Walker, and N. C. Surawski, “Emissions life cycle assessment of charging infrastructures for electric buses,” *Sustainable Energy Technologies and Assessments*, vol. 48, p. 101605, Dec. 2021, doi: 10.1016/j.seta.2021.101605.

[234] M. Shafique and X. Luo, “Environmental life cycle assessment of battery electric vehicles from the current and future energy mix perspective,” *Journal of Environmental Management*, vol. 303, p. 114050, Feb. 2022, doi: 10.1016/j.jenvman.2021.114050.

[235] A. Sierra, C. Gercek, K. Geurs, and A. Reinders, “Technical, Financial, and Environmental Feasibility Analysis of Photovoltaic EV Charging Stations With Energy Storage in China and the United States,” *IEEE Journal of Photovoltaics*, vol. 10, no. 6, pp. 1892–1899, Nov. 2020, doi: 10.1109/JPHOTOV.2020.3019955.

[236] 14:00-17:00, “ISO 14067:2018,” *ISO*. https://www.iso.org/cms/render/live/fr/sites/isoorg/contents/data/standard/07/12/71206.html (accessed Jul. 20, 2021).

[237] “Photovoltaique.info - Analyse du Cycle de Vie.” https://www.photovoltaique.info/fr/info-ou-intox/les-enjeux-environnementaux/analyse-du-cycle-de-vie/#tab-content (accessed May 03, 2021).

[238] “Access the Database – ecoinvent.” https://www.ecoinvent.org/database/access-the-database/access-the-database.html (accessed Jul. 20, 2021).

[239] M. Romare and L. Dahllöf, “The Life Cycle Energy Consumption and Greenhouse Gas Emissions from Lithium-Ion Batteries,” p. 58.

[240] “The Recycling of Lithium-Ion Batteries: A Strategic Pillar for the European Battery Alliance.” https://www.ifri.org/en/publications/etudes-de-lifri/recycling-lithium-ion-batteries-strategic-pillar-european-battery (accessed May 03, 2021).

[241] “EVH3S22P04K - EVlink Wallbox Plus - T2S socket outlet with shutters - 3 phase - 32A/22kW | Schneider Electric Global.” https://www.se.com/ww/en/product/EVH3S22P04K/evlink-wallbox-plus---t2s-socket-outlet-with-shutters---3-phase---32a-22kw/ (accessed May 03, 2021).

[242]“EVC1S22P4E4ERF - EVlink City - borne - 22kW - 2xT2S tri 32A + 2x2P+T - RFID - Professionnels | Schneider Electric France.” https://www.se.com/fr/fr/product/EVC1S22P4E4ERF/evlink-city---borne---22kw---2xt2s-tri-32a-%2B-2x2p%2Bt---rfid/ (accessed May 03, 2021).

[243]“Produire une énergie respectueuse du climat,” *EDF France*. https://www.edf.fr/groupe-edf/produire-une-energie-respectueuse-du-climat (accessed May 03, 2021).

[244]“Live CO_2 emissions of electricity consumption.” http://electricitymap.tmrow.co (accessed Jul. 21, 2021).

[245]“Life Cycle Assessment Harmonization.” https://www.nrel.gov/analysis/life-cycle-assessment.html (accessed May 04, 2022).

[246]“ADEME - Site Bilans GES.” https://www.bilans-ges.ademe.fr/fr/accueil (accessed May 03, 2021).

[247]A. Louwen, W. G. J. H. M. V. Sark, A. P. C. Faaij, and R. E. I. Schropp, “Re-assessment of net energy production and greenhouse gas emissions avoidance after 40 years of photovoltaics development,” *Nature Communications*, vol. 7, p. 13728, Dec. 2016, doi: 10.1038/ncomms13728.